RADIOANALYTICAL MULTI-ELEMENTAL ANALYSIS: NEW METHODOLOGY AND ARCHAEOMETRIC APPLICATIONS

A Dissertation

presented to

the Faculty of the Graduate Committee
University of Missouri-Columbia

In Partial Fulfillment
of the Requirements for the Degree

Doctor of Philosophy

---

by

Magen E. Coleman

Dr. J. David Robertson, Dissertation Supervisor

MAY 2010

The undersigned, appointed by the dean of the Graduate School, have examined the dissertation entitled:

RADIOANALYTICAL MULTI-ELEMENTAL ANALYSIS: NEW METHODOLOGY AND ARCHAEOMETRIC APPLICATIONS

Presented by Magen E. Coleman,

a candidate for the degree of Doctor of Philosophy,

and hereby certify that, in their opinion, it is worthy of acceptance.

Dr. J. David Robertson

Dr. Michael Glasscock

Dr. Silvia S. Jurisson

Dr. C. Michael Greenlief

For my parents

who always supported me no matter what I wanted to do;

For my professors

who believed that I could accomplish great things;

For my friends, fellow graduate students,

who helped me survive with my sanity (relatively) intact;

And for Beau,

who was always there to help, support, listen, and just love me.

ACKNOWLEDGEMENTS

First and foremost, I would like to thank my advisor, Dr. J. David Robertson. He took a chance on a student with no background in radiochemistry and challenged me to never accept mediocrity in my research. Without his patience and support, I would not have been able to achieve what I have: a Ph.D. in chemistry and a postdoctoral position at a national lab. His support of interdisciplinary research is remarkable and his teaching style is always inspiring.

Secondly, I would like to thank Dr. Michael Glascock for introducing me to the field of archaeometry. He showed me a way to combine two of my greatest interests, history and chemistry, into one research project. His support was most helpful during my pursuit of this degree.

I would also like to thank my other committee members, Dr. Silvia Jurisson and Dr. C. Michael Greenlief, for their time and patience these past four years. Dr. Jurisson helped me gain a firm understanding of the basics of radiochemistry in her course and helped me greatly when it came to being a teaching assistant for that class for the first time. Dr. Greenlief helped me gain a greater understanding of spectroscopy and its applications in his analytical courses.

In addition to my committee members, there were many who helped me during the course of my research to gain a greater understanding of all of its aspects. First, I would like to thank Dr. John Simpson. He helped me better understand multivariate statistics and all the information I could get out of it. I would also like to thank Dr. Jeffrey Ferguson (MURR) and Dr. Stanley Ambrose (University of Illinois) for allowing me to not only work on the Kenyan obsidian samples, but also to go to Kenya and

participate in the sample collection. That was truly a once-in-a-lifetime experience. I would also like to thank Dr. James Harrell of the University of Toledo for supplying the Egyptian limestone samples. Dr. Ellery Frahm of the University of Minnesota-Twin Cities performed electron microprobe analysis on several Mesoamerican obsidian samples for me and also helped me gain a better understanding of the analysis technique. The Archaeometry Group at MURR, both past and present members, provided a lot of help and support when working in the lab, especially for sample preparation and the actual analysis of the samples. The Robertson research group in the Chemistry Department was a constant source of support during these four years. It is truly inspiring to work with so many amazing chemists.

Lastly I would like to thank the Chemistry Department and the National Science Foundation for the financial support needed in order to complete these studies.

Table of Contents

List of Figures

List of Tables

Abstract

Several projects are covered in this dissertation: the application of instrumental neutron activation analysis (INAA) and rigorous statistical analyses to the sourcing of Egyptian limestone and Kenyan obsidian, and the development of a method to determine titanium, barium, and arsenic concentrations in obsidian using epithermal neutron activation.

INAA, when coupled with rigorous statistical methods, including principal component analysis and clustering techniques, can provide the precision and confidence needed to accurately determine the source of material. However, this technique has not been fully explored for the provenancing of Egyptian limestone sculpture. A combination of the elemental concentration data and rigorous statistical methods is used to study the compositional differences between known ancient quarries. Preliminary results show that INAA has the potential to be effective for limestone provenance studies.

Obsidian is an important component of East African artifacts. Although compositional studies of obsidian from East Africa conducted in the 1980s showed great potential, a comprehensive database has not been developed. Here, samples from Kenya were examined via X-ray fluorescence (XRF) and INAA. The results indicate that there is a clear correlation between geographic proximity and chemical composition. Using more rigorous statistical methods, including principal component analysis, subgroups can be classified and better correlation to geographical groups is observed.

Titanium and barium are often used for characterizing obsidian, especially in areas in Africa. A method has been developed to analyze for these elements using epithermal neutron activation analysis, which takes advantage of larger natural abundances of parent nuclides and a higher probability for epithermal neutron reactions. It produces results with improved accuracy and precision for titanium and barium analyses in obsidian. It is also now possible to analyze for arsenic, which has not previously been reported in obsidian studies.

Archaeology provides a link to the history of man and, through the application of rigorous analytical techniques, insight into the procurement, distribution, and exchange of resources can be achieved. The use of chemical and radiochemical signatures to distinguish artifacts in an accurate and precise manner brings the histories locked in these pieces closer to becoming clear.

CHAPTER 1:

MULTI-ELEMENTAL ANALYSIS AND ARCHAEOMETRY

1.1 Introduction

Elemental studies of artifacts have been an important part of chemistry and archaeology since the 1800s.[1-3] Many different analytical techniques have been used over the years, from simple gravimetric techniques to determine the concentration of a single element to more complex spectroscopic methods used for multi-elemental analysis.[1-2] The application of these techniques to artifacts also served various purposes. In many cases, it began with an archaeological question about the source, the age, the manufacturing technology, or the authenticity. In a few cases, though, artifacts were used as a convenient sample set for new or improved techniques. Whatever the original motive, this type of work has demonstrated the ability of analytical chemistry to aid in answering archaeological questions.[3]

Archaeological artifacts provide a unique challenge for the analytical chemist.[3] These are precious samples that cannot be duplicated. Often, archaeologists and museums are hesitant to give up samples for destructive analysis, so non-destructive methods or methods that are minimally destructive have to be employed. The archaeologist also wants to get as much information as possible out of each sample to aid

in the studies of ancient peoples. In addition, there is the issue of weathering and other chemical changes that may occur over time that may interfere with the measurement or the final analysis of the results. Artifacts usually have complex matrices that can present a myriad of challenges on their own. These are all things that the analyst must keep in mind when choosing an analytical technique for elemental analysis of archaeological samples.

Different definitions of the idea of destructive analysis have been used throughout the years as archaeologists and chemists work to find a good balance between getting enough information out of an artifact with the smallest amount of destruction possible.[3] Some believe that the artifact must remain completely unchanged in order for the technique to be considered nondestructive, while others believe that a small amount removed from the sample that does not detract from an understanding of its purpose or form is perfectly acceptable. For some techniques, especially extremely sensitive ones such as inductively-coupled plasma mass spectrometry (ICP-MS) and neutron activation analysis (NAA), only milligram amounts of samples are needed for the analysis. In these cases, a small hole can be drilled into the artifact or a small chip broken off, so that the damage is almost imperceptible. There are also techniques, such as x-ray fluorescence and electron microprobe analysis, which can provide elemental analysis without any damage to the artifact at all. These techniques tend to be less sensitive than NAA and ICP-MS, but can still provide valuable information about the sample.[3-4]

One major area of research in archaeology that has benefited from multi-elemental analysis is the sourcing of raw materials.[3, 5] The most common materials that have been applied to these studies are ceramics, lithics, and building materials. In order

to accurately determine the source for a material, the chemical composition needs to act as a fingerprint for the source. Neutron activation analysis (NAA) and x-ray fluorescence (XRF) are the most common techniques applied to sourcing studies because they both offer multi-elemental analysis with good sensitivity for many of the elements of interest. The trace elements in the composition of the samples are usually used to discriminate among sources. These elements are mostly the rare earth elements, though other elements can be used. Both XRF and NAA offer sensitivity down to the part-per-million level for many of the rare earth elements.

This chapter will describe both the techniques of XRF and NAA and how they have been applied to the analysis of obsidian and limestone in this dissertation. The advantages and disadvantages of each will be presented. Also, the choice of NAA for the examination of the sources will be explained in more detail.

1.2 X-ray fluorescence

X-ray fluorescence (XRF) analysis is a nondestructive technique that uses secondary x-rays to characterize the chemical composition of a sample. In XRF analysis, a primary beam of x-rays strikes the sample, interacting with the atoms and ejecting inner-shell electrons. This puts the atom in an excited state, and electrons from the outer shells are quickly transferred to fill the vacancies, giving off an x-ray in the process. These secondary x-rays are characteristic of the element and their energy is equal to the difference in binding energy between the shell initially occupied by the electron and the shell it occupies after filling the vacancy.[6] A diagram of this process is shown in Figure 1.1.

Figure 1.1: Illustration of X-ray Fluorescence

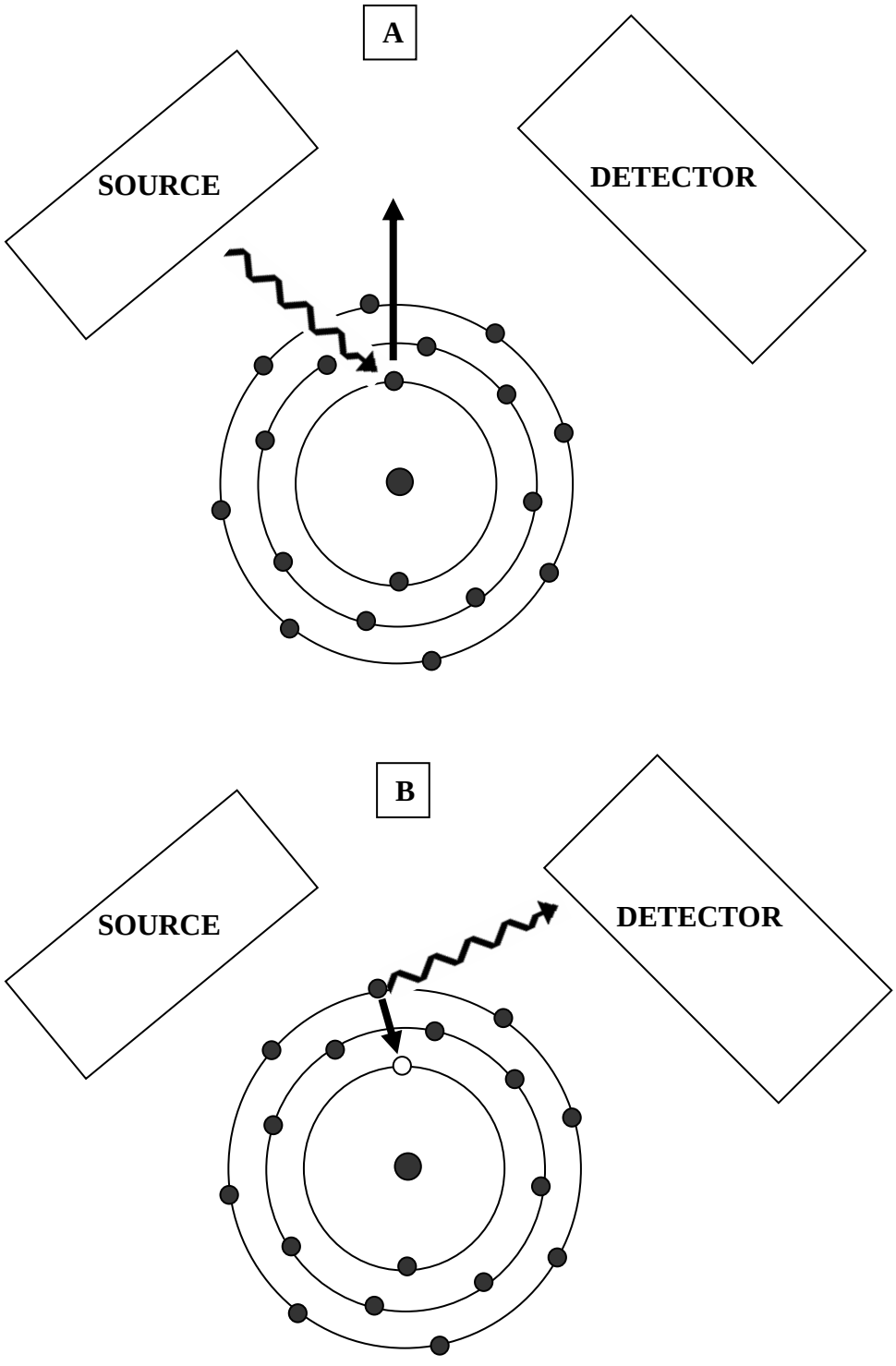

XRF analysis can be used for both qualitative and quantitative analysis. The energy (and wavelength) of the secondary x-rays are characteristic for a particular element and the number of x-rays of a certain energy is proportional to the amount of that element in a sample.[7]

XRF analysis offers several advantages for archaeological applications. First and foremost, it is completely nondestructive. With the trend of XRF instruments toward the completely portable, the size of an artifact is becoming less of an issue, since it does not need to fit in a small sample chamber. Portable instruments also allow the analysis to be performed on site instead of requiring the sample to be brought to a laboratory. For lab-based instruments, as long as the sample fits inside the sample chamber, the analysis is nondestructive. In addition, very little sample preparation is needed. The sample needs to have a clean surface and, in the case of bulk analysis, the spot for analysis should be representative of the whole object. XRF also offers simultaneous multi-elemental analysis that is very rapid, usually on the order of several minutes per sample. Along with the improvements in technology allowing for portable instruments, with similar sensitivities as the larger lab-based instruments for many elements, the instruments are also relatively inexpensive and accessible.

XRF analysis also has several disadvantages. Because of the limited penetrating power of both the primary x-ray beam and the secondary x-rays emitted from the sample, the analysis is often limited to the first few millimeters of the sample, and the matrix plays a very important role in the analysis. XRF analysis is also not applicable to all elements. Most instruments only work well for elements with atomic numbers greater than 13, though better sensitivity for low-Z elements can be achieved by analyzing under

vacuum. XRF analysis tends not to be as sensitive as semi-destructive analytical techniques such as ICP-MS and NAA, and the limits of detection tend to be higher.

1.2.1 XRF instruments

XRF instruments consist of four basic components: an excitation source, a means of separating and isolating characteristic x-ray lines, a detection system, and a data collection and processing system. The excitation source is usually a sealed x-ray tube with a rhodium, tungsten, or silver anode, but radioisotopes such as ^{241}Am, ^{109}Cd, and ^{155}Eu can be used as γ-sources, especially for the excitation of high-Z elements. The detection system can vary depending on the type of XRF analysis being done. Most commonly, either solid-state scintillation detectors or semiconductor detectors are used.[7,8]

XRF analysis can be divided into two general categories, based on the means of separating the characteristic x-rays. Wavelength-dispersive XRF (WDXRF) was the first type of XRF to be regularly used in the lab. Here, the signal from the sample is separated by Bragg diffraction from a single crystal.[6] Then each wavelength is detected by two detectors in sequence: a proportional counter for low energy x-rays and a scintillation detector for high energy x-rays. Multielemental analysis can either be done sequentially, using a single appropriate crystal set to the appropriate angle, or simultaneously. If the analysis is to be done simultaneously, several spectrometers are set out around the sample, each with a crystal tuned to the appropriate angle for the analyte.[6] The major advantage of WDXRF is the resolution that can be achieved; modern instruments can have resolutions of about 5 eV.

Most XRF instruments used in laboratories today are energy-dispersive XRF (EDXRF) instruments. EDXRF differs from WDXRF in that the detector, usually a semiconductor or solid-state scintillation detector, operates as both a means to separate out the characteristic x-rays and a detector for the intensity of the peaks. EDXRF instruments are relatively simple compared to WDXRF instruments, and though they do not have as good a resolution (usually about 100-300 eV), they have the ability to quickly and simultaneously analyze many elements accurately.[6, 8] Because of the simplicity of the instrument and advances in technology, portable EDXRF units are becoming more widely available.

1.2.2 Basic principles of XRF analysis

When using XRF analysis to determine the chemical composition of a sample, several factors must be considered. First is the interaction of x-rays with the sample matrix. As an x-ray beam passes through matter, the intensity of that beam is attenuated as it interacts with the sample. Two basic interaction processes tend to dominate: either the x-ray is scattered or the x-ray transfers its energy to an electron and ejects it from the atom in the sample (photoelectric effect).[6] Though important information can be achieved through x-ray scattering (i.e., x-ray diffraction), this discussion will focus on the photoelectric effect. When an inner-shell electron is ejected, the atom is left in an excited state. This atom can then de-excite by filling the vacancy with an electron from an outer shell. During this process, either an x-ray is emitted that has an energy equal to the difference between the two energy levels or an Auger electron is emitted.[6, 8]

In XRF analysis, the secondary x-rays are detected for qualitative and quantitative analysis of the sample. Each element has a series of characteristic x-ray lines whose energy is dependent on the shell from which the electron was ejected. The relationship between the wavelength of the x-ray (λ) and the atomic number (Z) of the excited element can be described by Equation 1.1, which was established by Moseley.[7]

$$\frac{1}{\lambda} = K[Z - \sigma^2] \qquad \textit{Equation 1.1}$$

where K is a constant for each spectral series and σ is a shielding constant with a value usually just less than 1.

The first, and usually most intense, set of lines is the K-lines, which are emitted when an electron from a higher energy shell fills a vacancy in the innermost shell (the K-shell) (Figure 1.2).[6] The K-lines offer the highest-energy x-rays emitted from an element and are most often used in quantitative analysis. Next come the L-lines (due to a vacancy in the L-shell). These lines are lower in energy than the K-lines and, while there may be a few K-lines for a particular element, there can be several L-lines, often forming multiplets. The L-lines are usually only used for analysis when the K-lines of a particular element are too high in energy to be excited by the x-ray source and cannot be detected. The last major set of x-ray lines are the M-lines (due to a vacancy in the M-shell). These are the lowest in energy and are often overlapping with K-lines and L-lines from other elements, making quantification difficult.

Figure 1.2 Electronic transitions in the atom for characteristic x-ray lines.

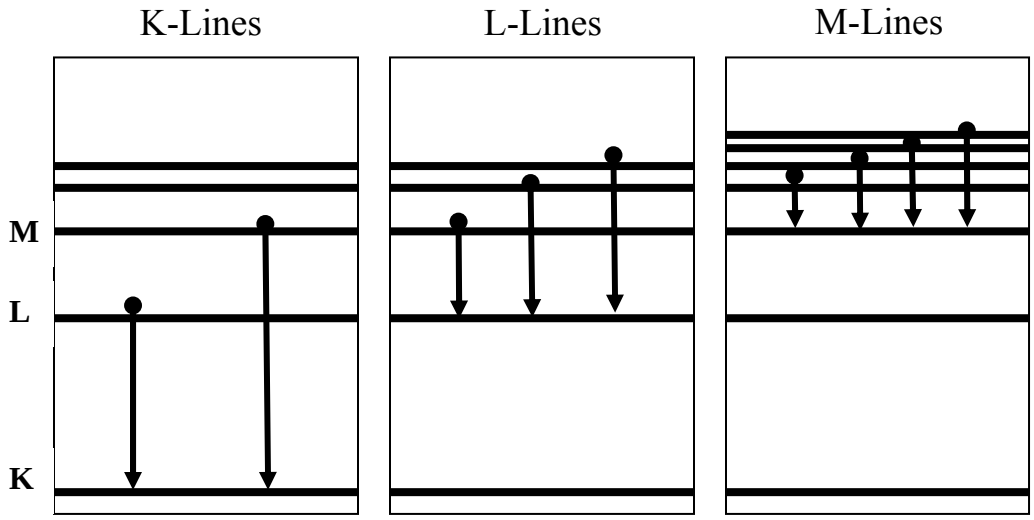

The intensity of the x-ray fluorescence of the sample is dependant on two major factors: the excitation yield and the fluorescence yield.[8] The excitation yield describes the probability of photoelectric absorption of the incoming radiation by the sample. This is dependent on the energy of the incoming radiation (hν), the binding energy of the electron (related to the Coulomb interaction between the electron and the nucleus), and atomic number. This relationship can be easily seen in Equation 1.2:[8]

$$\tau_{ph} = a\frac{Z^5}{(h\nu)^3} \qquad \textit{Equation 1.2}$$

where Z is the atomic number and *a* is a proportionality constant. τ_{ph} is the cross-section, or probability of photon absorption for an individual atom.[8] When working with larger samples, the probability can also be expressed in terms of a mass (photoelectric) absorption coefficient, μ_{ph}, which describes the probability of photon absorption per unit mass of the absorber (Equation 1.3):[8]

$$\mu_{ph} = a\frac{Z^5}{(h\nu)^3}\frac{N_A}{A} \qquad \textit{Equation 1.3}$$

where N_A is Avogadro's number and A is the atomic mass of the sample. Based on these equations, the probability of photoelectric absorption increases with atomic number, and therefore binding energy, assuming everything else remains constant. However, because the excitation yield is also dependent on the mass number, A, which also increases as Z increases, the effect is somewhat modified.[8] The dependence of excitation yield on the energy of the incoming radiation (hν) also plays a strong role.

The excitation yield is also strongly dependent on the energy of the incoming radiation. However, this relationship for a particular atomic number, Z, is not a continuous function, which might be thought considering the above equations. Instead, there are discontinuities when the energy of the incoming radiation is exactly the binding energy of the electron. For example, when hν is just below the binding energy of an electron in the K-shell, there is a sharp decrease in the excitation yield for K electrons. Resonance behavior is also seen in the relationship between hν and the excitation yield. When the energy of the incoming radiation is just above the binding energy of the electron, there is a sharp increase in the excitation yield. The discontinuities are due simply to the fact that a vacancy can only be created when the energy of the photon (hν) is greater than or equal to the binding energy of the electron. This, as mentioned above, greatly affects the excitation yield for elements of high Z. Not only is the atomic mass, A, greater, reducing the excitation yield slightly, but higher energies of incoming radiation are needed in order to excite the sample. This means that for high Z elements, the probability of photoelectric absorption (μ_{ph}) is several orders of magnitudes lower than for low Z elements. This most strongly affects the K-lines for high Z elements, though

the L-lines and M-lines follow the same trend. This also means that for high Z elements, the excitation yield is often higher for L-shell electrons than for K-shell electrons.[8]

The fluorescence yield is the ratio of x-ray photons emitted from the sample to the number of vacancies caused by the excitation. This ratio describes the relative efficiency of the two opposing de-excitation processes that can occur after excitation: emission of an x-ray photon or emission of an Auger electron. The fluorescence yield (ω) is defined for each emission series as the number of x-ray photons (n) of that series emitted divided by the total number of vacancies (N), shown in Equation 1.4 for the K series.[6]

$$\omega_K = \frac{\Sigma(n)_K}{N_K} = \frac{n(K\alpha_1) + n(K\alpha_2) + n(K\beta_1) + n(K\beta_2) + \cdots}{N_K} \qquad \textit{Equation 1.4}$$

The fluorescence yield is always less than one. As the atomic number increases, the probability of the emission of an Auger electron decreases, making the fluorescence yield increase. In addition, the fluorescence yield for K series x-rays is always larger than that for the L series.[8]

X-ray lines chosen for quantitative analysis are based on optimizing and balancing both the excitation yield and the fluorescence yield. The excitation yield is dependant on the energy of the incoming radiation, as well as the composition of the sample, so the energy of the incoming radiation can be chosen to optimize the analysis for a particular set of elements or can be high enough to induce excitation in the majority of the elements of interest. The fluorescence yield, however, is not affected by any of the experimental parameters. Thus, based on the combination of the excitation yield and the fluorescence yield, the K series x-ray lines are often the best for quantification for lower Z elements, while the L series x-ray lines are more sensitive for the higher Z elements.[8]

Because x-rays can be easily scattered and absorbed in a sample, the sample matrix and size play an important role in XRF analysis. Firstly, the incident x-ray beam does not penetrate very far into samples, usually on the order of a few millimeters.[7] For bulk analyses, it is crucial that the spot on the sample being analyzed is characteristic of the entire piece. Differences in composition at different depths, as well as different spots, may exist. Secondly, once the secondary x-rays are emitted, they then can be absorbed by other atoms in the sample and not make it out of the sample at all.[7] If the secondary x-rays have enough energy, they can excite another atom in the sample, which will then emit its own x-ray. Lastly, the matrix can scatter the x-rays so that they are not detected by the instrument.[7-8] These challenges are usually taken into account by using matrix-matched standards for calibration of the instrument and by analyzing the sample at various locations to ensure homogeneity. When possible, thin samples can be used to ensure a reduction in the self-absorption of secondary x-rays.

Figure 1.3 is an example of an x-ray spectrum from a sample of obsidian analyzed by EDXRF. As stated before, the energies of the peaks in the spectra can be used to identify the elements in the sample. The intensities of the peaks are used in quantitative analysis.

Figure 1.3: XRF spectrum of obsidian

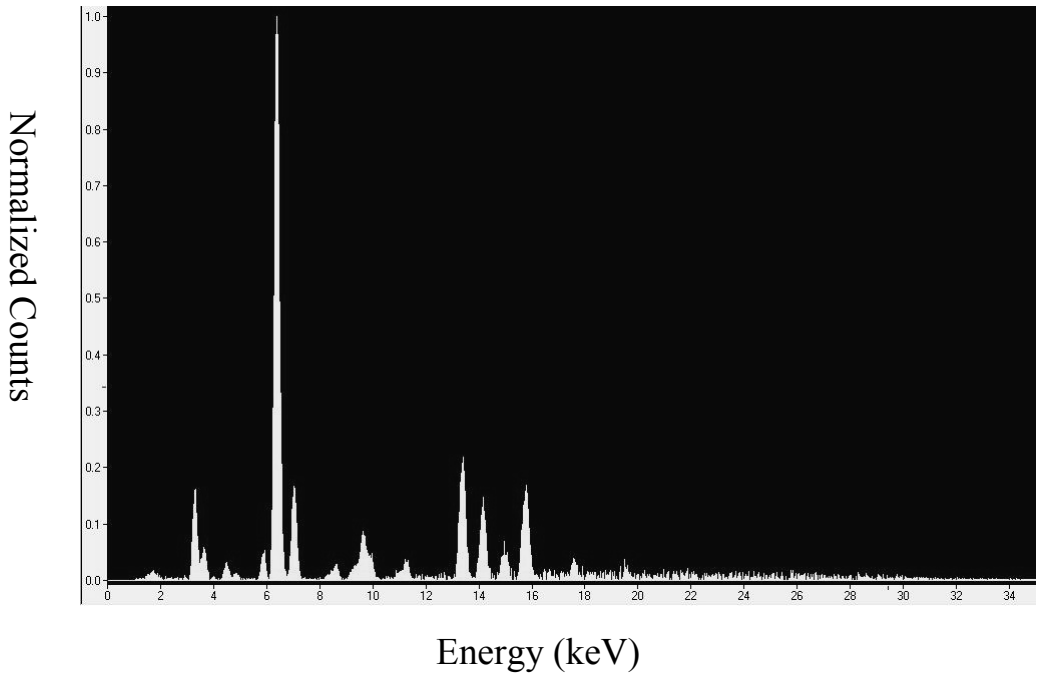

For accurate quantitative analysis, matrix-matched standards are analyzed under the same conditions to be used for the unknown sample and calibration curves are created for the elements of interest. Most XRF instrument software comes with a quantification program to create calibration curves and allow for quick, quantitative, multi-elemental analysis of the unknowns. Sample preparation is very simple; usually a clean, flat surface is the only requirement.

1.2.3 XRF analysis at MURR

In the Archaeometry group at MURR, there are two XRF instruments that are used regularly for analysis: an Elva-X benchtop XRF spectrometer and a Bruker handheld XRF spectrometer. Both of these instruments have energy-dispersive detection

systems. The Elva-X uses a tungsten anode for the x-ray source, while the Bruker uses a rhodium anode.

The concentrations of ten elements (K, Mn, Fe, Zn, Ga, Rb, Sr, Y, Zr, and Nb) are typically determined, though other elements are occasionally added depending on the sample. In order to relate the intensity of the peak seen in the spectrum for each element, a calibration is created using well-characterized obsidian source standards. Since both the standards and the unknowns are run under the same conditions and have very similar matrices, factors that affect the intensity of each peak, such as instrumentation parameters and matrix effects, can be assumed to be the same for both. A linear regression model is then used to create the calibration curve to which unknown samples are compared, directly correlating intensity to concentration. Samples are typically analyzed for three to five minutes on the detector, set to aim for a dead time on the detector of about 10-15%.

Because of the quick, nondestructive capabilities of XRF, it is a common choice of archaeologists and museums for the analysis of artifacts. Though fewer elements are determined at higher levels than with other techniques, the results are usually adequate for most purposes. In sourcing studies for lithics (which usually have the relatively homogenous composition needed for bulk analysis by XRF), usually a few elements are identified as important for analysis and source determination.

1.3 Neutron activation analysis

Neutron activation analysis (NAA) has become a prominent technique in archaeometric studies requiring precise, multi-elemental analysis. With the long list of elements that can be quantified and sensitivity (limited artifact destruction needed for

analysis), NAA has many qualities desired in a technique being applied to archaeological studies. This section will describe the theory of this technique and the current procedures in place at MURR.

1.3.1 A brief overview of NAA

Neutron activation analysis (NAA) is an analytical method that uses nuclear reactions to form radioactive products or excited states of the target nucleus, followed by the use of gamma spectroscopy for identification and quantification.[4, 9-10] NAA is the most common form of activation analysis and uses neutrons to induce radioactivity. Then, gamma rays emitted from the sample as the radioactive products decay are detected (Figure 1.4).

Figure 1.4 Neutron Activation Analysis

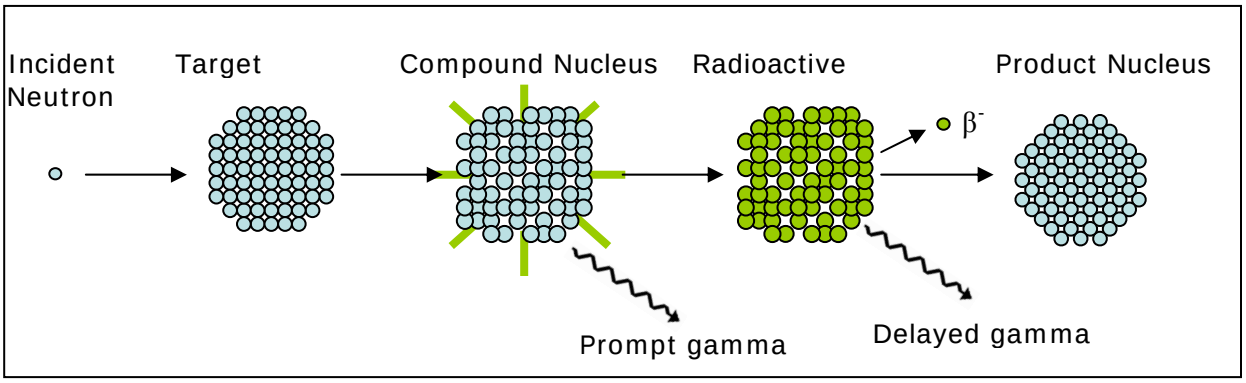

NAA has many advantages that make it a very useful technique for the multi-elemental analysis of archaeological artifacts. First are the very high sensitivities for the majority of the elements in the periodic table. These sensitivities can be on the same order as those for techniques such as ICP-MS.[9] In addition, NAA provides simultaneous

multi-elemental analysis, so most of the elements of interest can be determined at one time. Many of the experimental parameters can be adjusted to provide a very accurate and precise measurement. Unlike methods such as ICP-MS, NAA requires very little sample manipulation, meaning that the method is unsusceptible to contamination. The analysis is also independent of matrix, so complex matrices can be analyzed without the extensive wet chemistry often required to remove matrix interferents. The matrix can contribute significantly to the background in the gamma ray spectrum if it contains significant quantities of elements that easily activate and have half-lives similar to or longer than the analytes of interest. If the elements of interest produce short-lived product isotopes, then the analysis can be very rapid, often completed in minutes. Also, if a large number of samples are being analyzed, there can be a low unit cost.[9]

Some of the disadvantages of NAA include the lack of information on chemical form and difficulty measuring some elements, especially the low-Z elements. In addition, NAA is only semi-nondestructive. While small samples can be placed whole in the vials and are not completely destroyed in the process, the analysis leaves the samples radioactive. Depending on the composition of the sample, it can remain radioactive for many years and may not be returned to the archaeologist or museum for that time. Another drawback is the limited access to neutron facilities, though many research facilities have programs to provide neutron activation analysis to archaeologists.[11-14]

1.3.2 Types of NAA

There are several types of NAA that can be performed. The most common that is applied to archaeometric studies is instrumental neutron activation analysis (INAA).

Here, the sample is simply irradiated and the delayed gamma rays counted, without any additional sample processing. Other types of NAA include radiochemical NAA (RNAA), where the analyte of interest is separated from the matrix after irradiation and before the sample is counted, and prompt gamma NAA (PGNAA), where the prompt gamma rays emitted from the sample during irradiation are detected.[9] For the studies described later in this dissertation, INAA was used for the analyses.

NAA can also be divided by the energy of the neutrons being used for the irradiation. Thermal NAA (TNAA) is the most common and offers the best sensitivity for most elements in the period table.[9] In TNAA, reactions involving thermal neutrons with a mean energy of about 0.025 eV are used for the analysis. High fluxes of thermal neutrons are typically generated from a fission reactor and moderation of the fission spectrum neutrons. Most of the reactions that occur with thermal neutrons are called (n,γ) reactions, where a neutron is absorbed by the target nucleus, followed by the emission of a prompt gamma ray. Because slower neutrons are more likely to interact with the nucleus of the atom, (n,γ) reactions tend to have very high probabilities (cross sections).

Epithermal NAA uses reactions involving the epithermal (also called epicadmium) neutrons that have energies between 0.1 eV and 1 keV.[9] For ENAA, a cadmium or boron shield around the samples is used to reduce the flux of thermal neutrons from the reactor interacting with the samples, but allows the higher-energy neutrons to pass through. ENAA is mostly used to increase the sensitivity for elements that have larger cross sections for reactions with epithermal neutrons compared to thermal neutrons and to reduce the background due to elements that are high in abundance and have large thermal cross sections.

The last type is fast NAA (FNAA), where fast neutrons of energies greater than 0.5 MeV interact with the sample.[9] These fast neutrons have the ability to cause different reactions other than (n,γ). An (n,p) reaction involves a neutron being absorbed, followed by the emission of a proton; (n,α) emits an alpha particle after the absorption of the neutron; and (n,2n) emits two neutrons as a result. These reactions are less probable than thermal and epithermal neutrons due to the reduced wavelength of the neutron, and the barriers (Coulomb and angular momentum) associated with particle emission from the compound nucleus. FNAA can be performed using a cadmium shield around the samples, just as in ENAA, or by using a reactor neutron source that provides high energy neutrons. One common form is 14-MeV INAA, where a small accelerator known as a neutron generator is used to produce 14-MeV neutrons from the reaction of a deuterium beam with a tritium target. FNAA works best for lighter elements and can provide better sensitivity than typical TNAA.

1.3.3 Basic principles of NAA

As stated before, NAA offers the ability to fine-tune the analysis for the desired analyte(s) while offering the ability to determine the concentrations of many elements simultaneously. This is because the activity produced during the irradiation of the sample is dependant on variables such as the number of target nuclei (n), the cross-section (σ, measured in barns or 10^{-24} cm^2) and the decay constant (λ) of the target, the neutron flux (φ, neutrons/cm^2/s), and the irradiation time (t), according to the following equation:[9-10]

$$A = n\phi\sigma\left(1 - e^{-\lambda t}\right) \qquad \textit{Equation 1.5}$$

Isotopes of the elements of interest are usually chosen to maximize the amount of activity that can be detected. Thus, isotopes that have larger abundances (so a larger n) and higher cross sections, with appropriate decay constants, are usually chosen. The irradiation time can be adjusted as well to maximize the sensitivity for the isotope.

The neutron flux in a light-water reactor, such as MURR, contains mostly thermal neutrons. Epithermal and fast neutron fluxes are usually about 2-3% and 7-10% of the thermal neutron flux, respectively.[5] Thus, most of the neutrons interacting with the sample are thermal neutrons. Depending on the type of reaction that is of interest (using thermal, epithermal, or fast neutrons), the flux can also be adjusted with the use of cadmium or boron shields to reduce the thermal flux.[9-10] This can be useful in that some isotopes have larger cross sections for epithermal neutrons than thermal neutrons. Fast neutron reactions tend to have smaller cross sections than either thermal or epithermal neutron reactions. For example, fast neutron reactions tend to have cross sections on the order of millibarns, while thermal and epithermal neutron reactions are usually on the order of barns. However, fast neutron reactions can still provide better sensitivity for lighter elements, especially when the thermal neutron flux has been reduced using cadmium or boron shields.[10]

The choice of irradiation time is based on several factors. If the isotopes of interest are short-lived with larger cross-sections, then short irradiation times are usually chosen so as to reduce the amount of longer-lived isotopes produced which might interfere with the measurement of the short-lived species.[5, 10] However, if the isotopes have smaller cross sections, then longer irradiation times are chosen to maximize the

amount of the radioactive species that is produced. Irradiation times can be anywhere from seconds to days.

Other factors that can be adjusted to increase the sensitivity for the analytes are the decay and count times. Once the radioactive species is produced, then it will immediately begin to spontaneously and randomly decay. The overall rate of decay is described by the following equation:

$$A_t = A_0 e^{-\lambda t} \qquad \textit{Equation 1.6}$$

where λ is the decay constant, which can be calculated from the known half-life of the isotope:

$$t_{1/2} = \frac{\ln(2)}{\lambda} \qquad \textit{Equation 1.7}$$

This decay can be used to the advantage of the analyst. If the isotope is short-lived, then the sample can either be counted immediately, or is allowed to decay a short amount of time, usually to make the sample less hazardous to handle and to reduce the amount of dead time in the detector. However, if the isotope of interest is long-lived, then the short-lived isotopes can be allowed to decay away before counting, reducing the overall activity of the sample, the background in the gamma-ray spectrum, and the amount of potential interferents in the sample.[5] The count time is also chosen accordingly. For short-lived isotopes that are decaying rapidly, shorter count times are used. However, for isotopes that are decaying more slowly, longer count times are needed to achieve good statistics for the counts.

1.3.4 Gamma spectroscopy and quantitative analysis

Delayed gamma rays emitted from the activated sample are detected for identification and quantification of the components. Gamma rays are high-energy photons that are emitted from the nucleus. Because they have no mass or charge, they tend to interact with matter in an all-or-nothing way. Denser materials, like lead, are needed to increase the probability of interaction.[9] Common detectors for gamma rays are scintillation detectors such as sodium iodide (NaI) and semiconductor detectors such as high-purity germanium (HPGe).[4] Because so many elements are being analyzed simultaneously in NAA, the HPGe detectors are most often used because of their high resolution (typically around 1-2 keV).[4] An example gamma ray spectrum achieved from a sample of obsidian is shown in Figure 1.5 below.

Figure 1.5 Gamma spectrum acquired from NIST SRM 278 (obsidian)

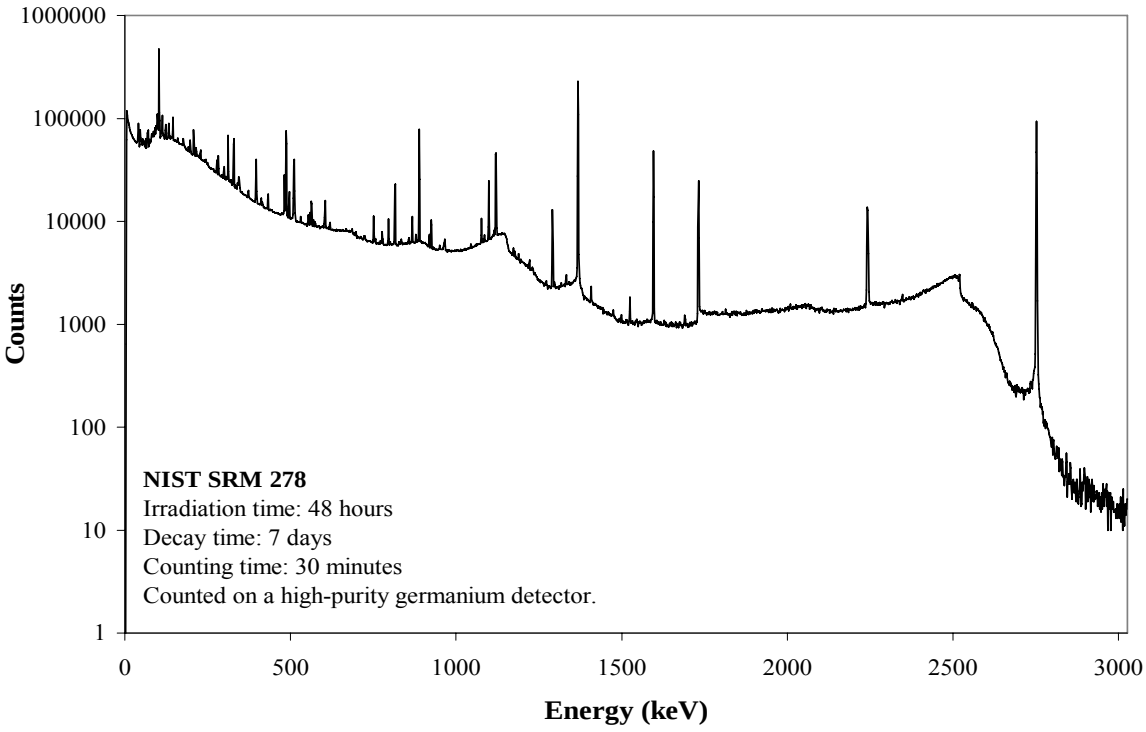

Because the gamma rays are characteristic of the isotopes that emitted them, they can be used to qualitatively determine the composition of the sample.[9-10] Typically, a peak search is performed on the spectrum and then the energies of those peaks are compared to a table of gamma ray energies for the identification of the isotopes. The gamma rays are chosen for the analysis based on their abundance (branching ratio, BR) and energy.[10] Because of the background due to the Compton scattering of all the gamma rays emitted from the sample, gamma rays with low energy are sometimes difficult to see above background and yield a less sensitive signal, even though they typically have a higher efficiency than higher energy gamma rays. The number of counts in the photopeak (R) is dependent on the activity produced during the irradiation (A, calculated using Equation 1.1), the efficiency of the detector (ε), the abundance of the gamma ray (BR), and the count time (t), according to Equation 1.8.[9-10]

$$R = A_0 \varepsilon (BR) \int_{t1}^{t2} e^{-\lambda t} \qquad \textit{Equation 1.8}$$

For quantitative analysis using the gamma spectrum, the total area under the peak is calculated, and then the background is subtracted to find the total counts due to the sample (R_{tot}). The intensity of the observed signal is directly proportional to the quantity of that isotope in the sample, which can then be related back to elemental concentration. However, since quantities such as the neutron flux are difficult to measure with good accuracy and to account for uncertainties in the cross section for the isotope, the comparator method is typically used for quantification rather than Equation 1.4. In the comparator method, a standard of a similar matrix and known concentrations of the

analytes is irradiated under the same conditions as the unknown sample. Then, the mass of the analyte in the unknown can be determined using the following equation:[4, 9]

$$\frac{R_{std}}{R_{sam}} = \frac{W_{std}\left(e^{-\lambda t}\right)_{std}}{W_{sam}\left(e^{-\lambda t}\right)_{sam}} \qquad \textit{Equation 1.9}$$

where R is the count rate for either the standard (std) or the sample (sam), W is the mass of the element, and t is the decay time. If the decay time and the count time are identical for the standard and the sample, then a slightly different form of the equation can be used:[5]

$$c_{sam} = c_{std}\frac{m_{std}R_{sam}}{m_{sam}R_{std}} \qquad \textit{Equation 1.10}$$

where c is the concentration of the element, m is the mass of the sample, and R is the count rate.

As stated before, NAA can offer very high sensitivities for many elements in the periodic table. Detection limits for NAA can be in the nanogram range for single elements in simple matrices. Detection limits calculated as three times the standard deviation of the background, which is the probability that a signal can be observed above background with 95% confidence.[5] Several standards are usually analyzed along with the samples: one is used as a standard for the quantification of the element concentrations and the others are used as quality controls.

1.3.5 Potential interferences

As in any analytical method, the problem of interferences must be considered. For NAA, there are several different types of interferences. Primary interferences are when the desired product radionuclide can be produced in more than one way.[4, 9] For

example, scandium-46 can be produced via an (n,γ) reaction from Sc-45 or from an (n,p) reaction from Ti-46 with fast neutrons. Secondary interferences are when the desired product radionuclide is produced by the decay of another product nuclide.[4, 9] So, for example, Sc-47 can be produced from an (n,p) reaction from Ti-47 and fast neutrons, but it is also produced from the beta decay of Ca-47, a product of an (n.γ) reaction from Ca-46. These two types of interferences are mostly avoided by choosing products that can only be produced via the desired reaction from the target nuclide. A third type of interference can occur in the gamma spectroscopy.[9] Two radionuclides may emit gamma rays of the same energy or of similar energies that cannot be resolved. This can be resolved by using other gamma rays that are emitted from that same radionuclide for quantification. For example, mercury can be measured via NAA using the Hg-202 (n,γ) Hg-203 reaction (σ (thermal) = 4.89 barns). Hg-203 then decays with a half-life of 46.6 days and emits a single gamma ray of 279.2 keV (81%). At the same time, selenium is often measured via NAA using the Se-74 (n,γ) Se-75 reaction (σ (thermal)=51.8 b, $t_{½}$ (Se-75) = 119.78 days). Se-75 emits a gamma ray of 279.54 keV that has a 24.99% abundance, which cannot be resolved from the Hg-203 peak. For the measurement of selenium, the other gamma rays emitted, particularly one at 264.66 keV (58.90%), need to be used for the analysis. For the measurement of mercury in the presence of selenium, another reaction altogether needs to be considered, even though the sensitivity will be lowered.

1.3.6 NAA at MURR

The Archaeometry Group at MURR handles hundreds of samples on a regular basis that have been submitted for elemental analysis via NAA. This section will describe the standard procedures used for NAA for these samples from preparation to analysis, focusing on the procedures for obsidian and limestone.[5] The concentrations of 28 elements are typically determined during the common NAA procedure.

Sample preparation is relatively simple. For obsidian, clean samples that are free of cortex (the weathering that can appear on the outside of the obsidian) are broken into pieces that can fit inside the irradiation vials. For limestone, the outside of the sample piece is cleaned by removing the outer layer using a dremmel tool, then the sample is crushed into a powder, using an agate mortar and pestle, and the powder is then weighed into the irradiation vials. Sample weights for analysis usually range between 50-100 mg for short irradiations and 100-200 mg for long irradiations.

The analysis of samples is divided up into two parts: a procedure for the analysis of the short-lived isotopes that uses the pneumatic tube system in place at the reactor and a procedure for the analysis of longer-lived isotopes which involves placing the samples inside an aluminum can in the flux trap of the reactor. For the short irradiation, samples are weighed into polyvials that are then placed inside a rabbit. The sample is irradiated in the reactor for five seconds, allowed to decay for 25 minutes, and then counted on an HPGe detector for 12 minutes. The elements determined from the short irradiations are aluminum (^{28}Al, $t_{1/2}$ = 2.24 min), barium (^{139}Ba, $t_{½}$ = 83.06 min), dysprosium (^{165}Dy, $t_{1/2}$ = 2.33 h), potassium (^{42}K, $t_{1/2}$ = 12.36 h), manganese (^{56}Mn, $t_{1/2}$ = 2.58 h), sodium (^{24}Na, $t_{1/2}$ = 14.96 h), and vanadium (^{52}V, $t_{1/2}$ = 3.74 min).

For the long irradiation, samples are weighed out into high purity quartz vials. Samples are placed in the reactor for a 48-hour irradiation. After this, the samples are counted twice: once for 30 minutes after a 7-day decay, and again for 168 minutes after a 28-day decay. The first count determines elements that have a mid-range half-life [including lanthanum (^{140}La, $t_{1/2}$ = 40.27 h), lutetium (^{177}Lu, $t_{1/2}$ = 6.73 d), neodymium (^{147}Nd, $t_{1/2}$ = 10.98 d), samarium (^{153}Sm, $t_{1/2}$ = 46.28 h), uranium (^{239}Np, $t_{1/2}$ = 2.36 d) and ytterbium (^{175}Yb, $t_{1/2}$ = 4.185 d)] and the second count determines the elements that produce long-lived isotopes [cerium (^{141}Ce, $t_{1/2}$ = 32.5 d), cobalt (^{60}Co, $t_{1/2}$ = 5.27 y), cesium (^{134}Cs, $t_{1/2}$ = 2.06 y), europium (^{152}Eu, $t_{1/2}$ = 13.54 y), iron (^{59}Fe, $t_{1/2}$ = 44.5 d), hafnium (^{181}Hf, $t_{1/2}$ = 42.39 d), rubidium (^{86}Rb, $t_{1/2}$ = 18.63 d), antimony (^{124}Sb, $t_{1/2}$ = 60.2 d), scandium (^{46}Sc, $t_{1/2}$ = 83.79 d), strontium (^{85}Sr, $t_{1/2}$ = 64.84 d), tantalum (^{182}Ta, $t_{1/2}$ = 114.43 d), terbium (^{160}Tb, $t_{1/2}$ = 72.3 d), thorium (^{233}Pa, $t_{1/2}$ = 27.0 d), zinc (^{65}Zn, $t_{1/2}$ = 244.26 d) and zirconium (^{95}Zr, $t_{1/2}$ = 64.02 d)].

A peak search and quantification is performed using commercial software (Canberra), which detects the presence of a peak and then determines the area of the peak by fitting a Gaussian curve to it. In situations where several peaks seem to overlap, the program deconvolutes the multiplet and fits Gaussian curves to each of the contributing peaks. This program also calculates the peak areas and their uncertainties, the background that has been subtracted, and constants using the data from the standards for the calculation of concentrations of the analytes in the unknowns.

Several standards are analyzed along with each batch of samples. For obsidian, three standards are run with each set of samples, including one fly ash standard (SRM 1633a), one obsidian standard reference material (SRM 278), and one obsidian source

standard (JJO, from the Alca source in Peru), which is used for quality control. For limestone, the same standards are used, except instead of the JJO obsidian standard, the Ohio Red clay standard is used. The precision obtained using this method for obsidian and limestone is usually about 5% RSD or less for most elements. The limits of detection for the elements usually determined in obsidian are listed in Table 1.1.

NAA offers may advantages for the multi-elemental analysis of archaeological samples. The small sample size needed, the high sensitivity for many of the elements of interest, the small chance for contamination due to the limited sample preparation, and the ability to analyze many elements simultaneously offers a large amount of accurate and precise data that can be used for the characterization of the samples. In sourcing studies, data for a large number of elements allows for more discrimination among sources. This can lead to a stronger ability to differentiate between source groups, which can allow archaeologists to better answer questions about the movement of raw materials during prehistory.

Table 1.1 95% confidence level detection limits for elements analyzed in obsidian

ELEMENT	TYPICAL DETECTION LIMIT
Na	100 ppm
Al	500 ppm
Cl	25 ppm
K	700 ppm
Sc	0.001 ppm
Mn	1 ppm
Fe	50 ppm
Co	0.02 ppm
Zn	1 ppm
Rb	1 ppm
Sr	10 ppm
Zr	15 ppm
Sb	0.02 ppm
Cs	0.02 ppm
Ba	10 ppm
La	0.5 ppm
Ce	0.1 ppm
Nd	1 ppm
Sm	0.02 ppm
Eu	0.005 ppm
Tb	0.05 ppm
Dy	0.5 ppm
Yb	0.1 ppm
Lu	0.1 ppm
Hf	0.01 ppm
Ta	0.03 ppm
Th	0.05 ppm
U	0.5 ppm

1.4 Comparison of XRF and NAA

Though XRF analysis and NAA can offer similar information about the elemental composition of artifacts, these techniques can also serve different purposes. For sourcing studies, it is important to have the source thoroughly characterized and to have as much information as possible about the source. This is where the advantages of NAA become useful. NAA can offer results for more elements with better accuracy and precision than XRF analysis. The results from NAA can then be examined to find which elements are important for distinguishing between two sources (most often by using multivariate analysis, discussed in the next chapter). In some cases, the differences in composition are so slight that more precise data are crucial. This especially applies when new sources or new regions are being characterized. In addition, the sources are usually geological samples, which are not as precious as archaeological artifacts, so destructive analysis is easier to perform.

XRF has is better suited for the analysis of artifacts as it requires less preparation and alteration of the samples. Once the composition of a source has been characterized by NAA, then the source samples can be analyzed by XRF to provide a comparative database for artifacts. The elements of interest for each source become the focus for the analysis. XRF can also be useful for the initial screening of artifacts. If an artifact has a similar chemical composition to two sources that are very similar, then those samples can undergo NAA at a later time. Since portable XRF units have become so widely available, the instrument can then be taken to the sample, rather than the sample needing to be transported to the lab.

In the research described in later chapters, NAA was used to characterize the sources of Egyptian limestone and Kenyan obsidian. Since only geological samples were considered in these studies, the semi-destructive nature of NAA was not a problem. In addition, it has been shown that limestone can be very difficult to source unless very precise data is used (discussed in detail in Chapter 3). Obsidian from many parts of the world has been found to work almost equally well with both XRF and NAA, but NAA was used here since the new sources investigated in this work are not as well characterized as obsidian sources from North, Central and South America, in order to fully examine the differences between the sources.

References

1. E. R. Caley, *Journal of Chemical Education*, 1967, **44**, 120.
2. E. R. Caley, *Journal of Chemical Education*, 1951, **28**, 64.
3. M. Pollard, C. Batt, B. Stern and S. M. M. Young, *Analytical Chemistry in Archaeology*, Cambridge University Press, Cambridge, UK, 2007.
4. S. J. Parry, *Activation Spectrometry in Chemical Analysis*, John Wiley & Sons, Inc., New York, 1991.
5. M. D. Glascock and H. Neff, *Measurement Science and Technology*, 2003, **14**, 1516-1526.
6. R. Jenkins, *X-Ray Fluorescence Spectrometry*, John Wiley & Sons, Inc., New York, 1999.
7. R. Jenkins, R. W. Gould and D. Gedcke, *Quantitative X-ray Spectrometry*, Marcel Dekker, Inc., New York, 1995.
8. B. Dziunikowski, *Energy Dispersive X-ray Fluorescence Analysis*, Elsevier Science Publishing Co., Inc., New York, 1989.
9. W. Ehmann, D. and D. E. Vance, *Radiochemistry and Nuclear Methods of Analysis*, John Wiley & Sons, Inc., New York, 1991.
10. D. De Soete, R. Gijbels and J. Hoste, *Neutron Activation Analysis*, Wiley-Interscience, New York, 1972.
11. F. Asaro and D. Adan-Bayewitz, *Archaeometry*, 2007, **49**, 201-214.
12. M. J. Blackman and R. L. Bishop, *Archaeometry*, 2007, **49**, 321-341.
13. M. D. Glascock, R. J. Speakman and H. Neff, *Archaeometry*, 2007, **49**, 343-357.
14. G. Harbottle and L. Holmes, *Archaeometry*, 2007, **49**, 185-199.

CHAPTER 2:

STATISTICAL METHODS OF DATA ANALYSIS AND THEIR APPLICATION TO PROVENANCE STUDIES

2.1 Introduction

Data analysis is a critical part of the analysis process. When working with analytical techniques that produce large amounts of data, statistical techniques can help determine and clearly quantify relationships between different independent and dependent variables including subtle underlying relationships between several variables. In this chapter, several statistical methods will be described, as well as examples given of their use. The methods used include cluster analysis and principal component analysis. These methods have been applied to the various projects described throughout this dissertation.

2.2 Statistics in archaeometry

The use of statistical techniques applied to archaeological and chemical analysis is so diverse that it would prove difficult to discuss every application individually here. Thus, this section will focus on the applications relevant to later chapters of this work, especially those methods with application to sourcing archaeological materials.

Since their infancy, provenancing studies have relied on rigorous statistical methods to help distinguish source groups and characterize samples.[1] The goal of these studies is to characterize samples in order to tell one group from another and how these groups relate to each other. This is often achieved through the use of statistical methods that look for the variance within a data set, as well as the similarities and differences between samples in that data set.[1-2] Multivariate techniques, such as principal component analysis (PCA) and clustering analysis have proved especially useful. A wide variety of materials have been studied in this way including metals, ceramics, obsidian, limestone, chert, and other lithic materials.[3] These materials range from being relatively easily sourced, such as obsidian[2], to those more difficult due to the potential for chemical changes between the source and the artifact, such as ceramics.[3]

In order to be sourced, a material must follow the provenance postulate, which states that the variance within a source must be significantly less than the variance between different sources.[1] If the variance within the source is too large or the variance between two sources is too small, then the exact source of a sample cannot be accurately or precisely determined with a good degree of confidence. Materials such as obsidian and ceramics have been found to follow the provenance postulate in many parts of the world.[1-2]

Generally, sourcing studies focus on the variation of the elemental composition of the material being studied, though other traits, such as color in the case of obsidian, have also been examined. In order to use the elemental composition, very accurate and precise multi-elemental techniques must be applied to the sample, such as x-ray fluorescence and neutron activation analysis (discussed more thoroughly in Chapter 1). Routine multi-

elemental analysis of samples can produce large amounts of data. For example, a standard NAA protocol can determine the concentrations for over 30 elements. Multiply that by the hundreds of samples being analyzed, and thousands of individual data points are created. The large amount of data can prove difficult to examine thoroughly, especially when some variables are correlated. In these cases, multivariate techniques, such as PCA have proved invaluable.

As stated before, obsidian has been proven to follow the provenance postulate and is relatively easily sourced. This is due to the fact that the artifact is chemically unchanged and so its composition should match that of the source very closely. In addition, simple scatter plots of the concentration of one element versus another can be used to distinguish source groups.[2] Then distance calculations, such as the Euclidean distance calculations described later, are used to group samples with a 90% confidence.[2] Here, the usefulness of multivariate techniques comes in pinpointing which elements will be able to best characterize the source groups and in further examining possible subgroups.

Limestone is quite different from obsidian in that it has been shown that simple scatter plots cannot distinguish source groups on their own.[4] The nature of the matrix, a porous calcium carbonate whose general composition can change over time due to weathering, presents more difficulty in looking at the variance within each source and between different sources. In this case, clustering techniques, both hierarchical and nonhierarchical, and PCA allow the entire data set to be examined as each variable in relation to the others is considered. With a larger amount of information being utilized, the differences between sources can be more thoroughly characterized.

2.3 Standardization of data

When applying statistical techniques to large data sets where the data points may have a large variance in their magnitudes, the question of standardization or transformation becomes important.[5] There are several possibilities for standardization and transformation and each has its advantages and disadvantages. Some of the most common are[5]:

1) centering, ($y_{ij} = x_{ij} - \bar{x}_j$), where x_{ij} is any data point of sample *i* and variable *j* and $\bar{x}_j$ is the mean of variable *j*.

2) standardizing, ($y_{ij} = (x_{ij} - \bar{x}_j) / s_j$), where s_j is the standard deviation for variable j.

3) taking the $\log_{10}$, ($y_{ij} = \log x_{ij}$)

4) ratio-transforming the data, ($y_{ij} = x_{ij} / x_{ip}$)

These can also be combined; for example, standardizing logged data.

Most statistical techniques applied to archaeometric data are looking for the variance within the data. Thus the results will be dominated by variables that have a large variance. Variables measured in different units or that have widely different magnitudes have a potential to skew the results. In these cases, standardization or transformation using $\log_{10}$ is usual. Centered data still presents the same problem where variables with large variances will dominate. Standardization will scale the data so that each variable has an equal variance and allows each to play an equal role in the analysis. Taking the $\log_{10}$ of the data will make the data be of a similar magnitude and comparable variance. The data is then said to be lognormal. This has been the typical choice for archaeometric data, though variables that have a large variance may still dominate.[5-6]

Standardization has often been discounted on the basis that is arbitrarily reweights the variables. This is not necessarily true, as standardization actually converts the data to units of standard deviation, and it has been shown that using standardized data still gets comparable results to that of log transformed data.[5-6] For most of the work discussed in later chapters, standardized data was used for statistical analysis. This choice was made to reduce the effect of variance due to the wide range of concentration values, from tens of ppm to thousands of ppm.

2.4 Multivariate statistics

For the following discussions of multivariate statistics, a small data set containing five variables measured for 10 samples will be used as an illustration. The data set was standardized by dividing the difference between each datum and the mean of that variable by the standard deviation for that variable. The standardized data appears in the table below.

Table 2.1: Standardized Sample Data Set

Sample	Al	K	Mn	Na	Fe
A	0.60145	0.72825	-0.80663	-0.15716	-0.77335
B	-0.09115	-0.49447	-0.86184	-0.53460	-0.89564
C	0.72148	-1.20404	-0.91608	-0.34513	-0.94371
D	-1.12247	-1.01227	1.47751	1.04605	1.42670
E	1.62583	2.32687	1.49388	-2.06958	1.26339
F	0.39939	0.36260	-0.90497	-0.20627	-0.92529
G	0.32126	-0.22046	0.00096	0.03172	0.00073
H	-1.70333	-0.20859	0.68397	1.29877	0.77857
I	-0.99226	-0.33157	0.64183	1.18377	0.93233
J	0.23981	0.05367	-0.80865	-0.24758	-0.86371

2.4.1 Variance, covariance, and correlation

Multivariate statistical methods are designed to group and classify objects as well as model relationships between the different variables in the data set. In doing so, common trends between variables become clear. Within the large data sets generated by multi-elemental analysis on archaeological artifacts are several variables that are positively correlated with each other. This is particularly prominent in geological samples, such as obsidian, for the rare earth elements (REEs).[2] Thus, it is quite useful to calculate both the variance and the covariance in the data set.

Variance is defined as the spread of the samples around the mean for that variable and is calculated as the square of the standard deviation according to the following equation:

$$\sigma_{ij}^2 = \frac{\sum_{i=1}^{n}(x_{ij} - \bar{x}_j)^2}{n-1} \qquad \textit{Equation 2.1}$$

where n is the number of samples and $j = 1 \ldots p$ for a matrix of p variables.[7] The measured sample variance (σ_m^2) is the sum of the natural variance in composition (σ_n^2) and the variance due to sampling and analytical errors (σ_a^2).[2]

$$\sigma_m^2 = \sigma_n^2 + \sigma_a^2 \qquad \textit{Equation 2.2}$$

Covariance, like variance, describes the spread of samples around a mean, except here it is the shared variability between two variables around a common mean. This can be calculated for two variables, j and k, according to the following equation[7]:

$$\mathrm{cov}(j,k) = \frac{\sum_{i=1}^{n}(x_{ij} - \bar{x}_j)(x_{ik} - \bar{x}_k)}{n-1} \qquad \textit{Equation 2.3}$$

When working with a large matrix of data that has *p* variables, a variance-covariance matrix (C) can be calculated for all pairs of variables.[7]

$$C = \begin{bmatrix} \sigma_{11}^2 & \text{cov}(1,2) & \dots & \text{cov}(1,p) \\ \text{cov}(2,1) & \sigma_{22}^2 & \dots & \text{cov}(2,p) \\ \vdots & \vdots & & \vdots \\ \text{cov}(p,1) & \text{cov}(p,2) & \dots & \sigma_{pp}^2 \end{bmatrix} \qquad \textit{Equation 2.4}$$

The correlation between two variables can also be calculated. Correlation coefficients are calculated for each pair of variables according to the following equation:

$$r_{jk} = \frac{\text{cov}(j,k)}{\sigma_j \sigma_k} \qquad \textit{Equation 2.5}$$

where σ_j and σ_k are the standard deviations of variables j and k. Values for the correlation coefficient range from -1 to +1, where -1 indicates an inverse relationship, 0 means no relationship, and +1 is perfect correlation.[2, 7] In geological samples, coefficients for the REEs can be as high as 0.9.[2] When the data has been standardized, the covariance matrix and the correlation matrix are equivalent.[7] The covariance and correlation matrices also form the basis for many multivariate statistical techniques such as principal component analysis (PCA), discussed in depth later.

2.4.2 Distance measurements and clustering methods

While covariance and correlation matrices provide information on the relationship between different variables in the dataset, other methods need to be used for initial studies of the relationship between samples. Measurement of the distance between samples in multidimensional space is often a first step in determining their similarity.[2, 6] There are

several distance measures commonly used: city-block (or Manhattan), Euclidean, and Mahalanobis.[7] The city-block distance is calculated by

$$d_{ij} = \sum_{k=1}^{n} \left| x_{ik} - x_{jk} \right| \qquad \textit{Equation 2.6}$$

where n is the number of variables and *i* and *j* are the indices for samples *i* and *j*. Graphically, this distance can be represented in two dimensions as the following:

Figure 2.1: City-block distance

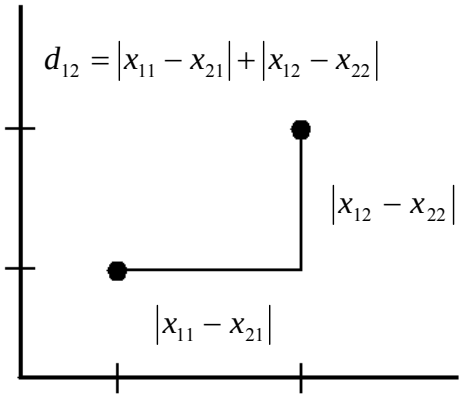

One of the most useful distance measurements is the Euclidean distance. This is the straight-line distance between the two objects (the shortest distance between the two points). The Euclidean distance[7] for a pair of objects in multidimensional space is:

$$d_{ij} = \left[\sum_{k=1}^{n} (x_{ik} - x_{jk})^2 \right]^{1/2} \qquad \textit{Equation 2.7}$$

and can be graphically represented in two dimensions by:

Figure 2.2: Euclidean Distance

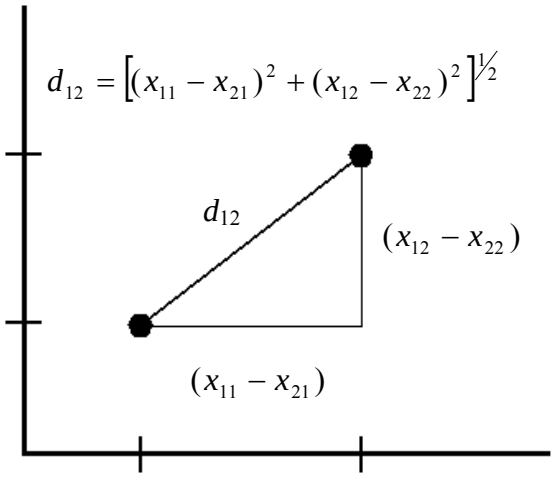

Many clustering methods (discussed in detail later) use either the Euclidean distance or the squared-mean Euclidean distance as a way of hierarchically grouping samples. The squared-mean Euclidean distance (SMED)[2, 5] is calculated by the following equation:

$$d_{ij}^2 = \frac{\sum_{k=1}^{n} (x_{ik} - x_{jk})^2}{n} \qquad \textit{Equation 2.8}$$

The Mahalanobis distance is defined as the squared Euclidean distance between a sample and a group centroid, divided by the group standard deviation in that direction.[2, 6,7] Here, instead of looking at the relationship between two individual samples, the relationship between a cluster of samples and an individual sample is elucidated. Mahalanobis distance between the centroid of group X and sample *k* is calculated as shown below.

$$D_{kX}^2 = \sum_{i=1}^{n} \sum_{j=1}^{n} \left[x_{ik} - \bar{x}_i\right] \cdot \mathrm{C}_{ij} \cdot \left[x_{jk} - \bar{x}_j\right] \qquad \textit{Equation 2.9}$$

where $\bar{x}_i$ and $\bar{x}_j$ are the means of variables *i* and *j*, and C_{ij} is the *ij*th element in the covariance matrix. The Mahalanobis distance is calculated using the covariance matrix, so any covariance between variables is taken into account. This distance measurement is especially useful when assigning samples to already existing groups (i.e., assigning artifacts to source groups).[2] Other common uses of the Mahalanobis distance are to test the distance between two neighboring groups and to create confidence ellipses for clusters, typically at 90% or 95% confidence.[2]

As mentioned before, distance measurements are often used in cluster analysis. Cluster analysis endeavors to place samples in groups based on their similarity and distance measures are used as a way to calculate that similarity.[7] The two major types of cluster analysis are hierarchical and nonhierarchical.[7] Hierarchical cluster analysis is usually agglomerative and starts with individual samples, grouping them one at a time according to their distances. This can be graphically represented in dendrograms. Nonhierarchical cluster analysis partitions the samples independently of each other and does so without ordering them hierarchically. Here, the number of groups is determined initially and each sample is mathematically tested to prove its membership in the group.

Hierarchical cluster analysis is the more common in archaeological applications.[2, 6] Samples are grouped together based on similarity, then those groups are linked to other groups, and the iterations continue until all the samples are related to each other. This is often depicted as a dendrogram, with the samples on the x-axis and the distance between those samples plotted on the y-axis.[7] In most common clustering routines, the Euclidean or squared-mean Euclidean distance is used to determine similarity between two samples.[2, 7]

To mathematically determine if the samples are similar enough to be linked, one of several different linkage methods can be used. These linkage methods, or clustering algorithms, each have their own advantages and disadvantages and can often produce different results for the clustering of the same data set. Several examples of the different linkage methods are given in Table C for linking groups A and B into a new cluster *k* by comparing them to object *i*.[7]

Table 2.2: Linkage methods[7]

Method	***Equation***	***Description***
Single Linkage	$d_{ki} = \frac{d_{Ai} + d_{Bi}}{2} - \frac{\lvert d_{Ai} - d_{Bi} \rvert}{2} = \min(d_{Ai}, d_{Bi})$	The shortest distance between opposite clusters is calculated.
Complete Linkage	$d_{ki} = \frac{d_{Ai} + d_{Bi}}{2} + \frac{\lvert d_{Ai} - d_{Bi} \rvert}{2} = \max(d_{Ai}, d_{Bi})$	The largest distance between opposite clusters is calculated.
Unweighted Average Linkage	$d_{ki} = \frac{d_{Ai} + d_{Bi}}{2}$	Average distance from objects A and B is calculated.
Weighted Average Linkage	$d_{ki} = \frac{n_A}{n} d_{Ai} + \frac{n_B}{n} d_{Bi}$ with $n = n_A + n_B$	The number of objects (n) in the clusters is used for weighting the cluster distances.
Centroid Linkage	$d_{ki} = \frac{n_A}{n} d_{Ai} + \frac{n_B}{n} d_{Bi} - \frac{n_A n_B}{n^2} d_{AB}$	The distance between the centroids of the clusters is calculated.
Median Linkage	$d_{ki} = \frac{d_{Ai}}{2} + \frac{d_{Bi}}{2} - \frac{d_{AB}}{4}$	The median instead of the centroid of each cluster is used for calculation.
Ward's Method	$d_{ki} = \frac{n_A + n_i}{n + n_i} d_{Ai} + \frac{n_B + n_i}{n + n_i} d_{Bi} - \frac{n_i}{n + n_i} d_{AB}$	Clusters are combined based on a minimum increase in the within-group variance from the centroid.

Each of these linkage methods can produce different results because they stress different characteristics in the strategy for grouping samples. For example, single linkage can produce loosely-bound clusters, while complete linkage tends to form small, well-separated clusters.[7]

The sample data set described above is used as an example of hierarchical clustering using the clustering routines in Matlab©. Distances between samples were determined using the Euclidean distance measures and then two different linkage methods were applied, the average linkage and Ward's linkage. The resulting dendrograms for both are shown below.

Figure 2.3: Dendrogram of standardized sample data set (Table 2.1) using average linkage

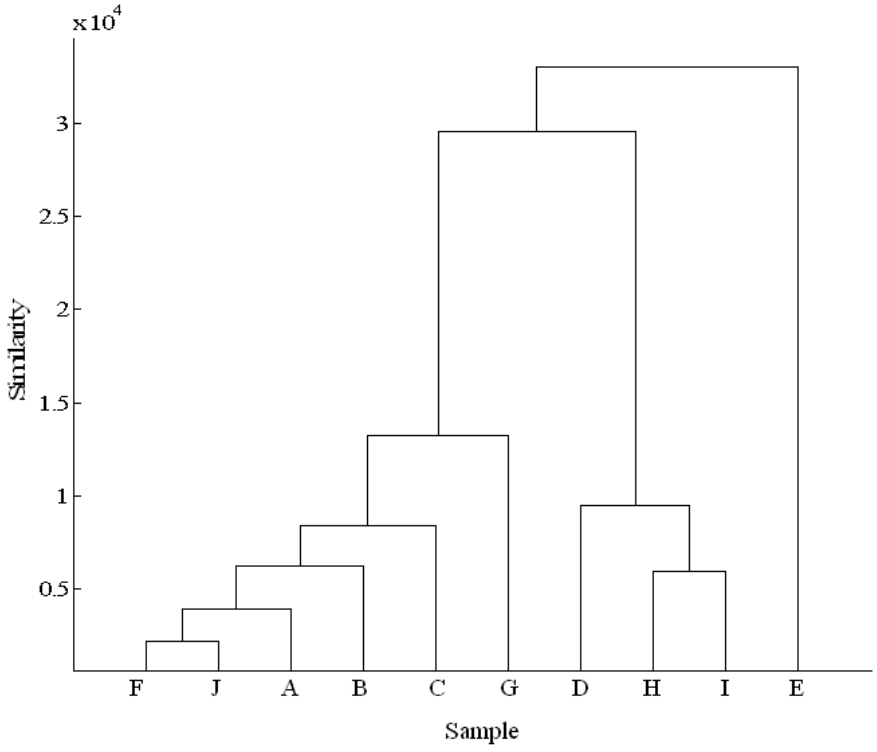

Figure 2.4: Dendrogram of standardized sample data (Table 2.1) using Ward's linkage

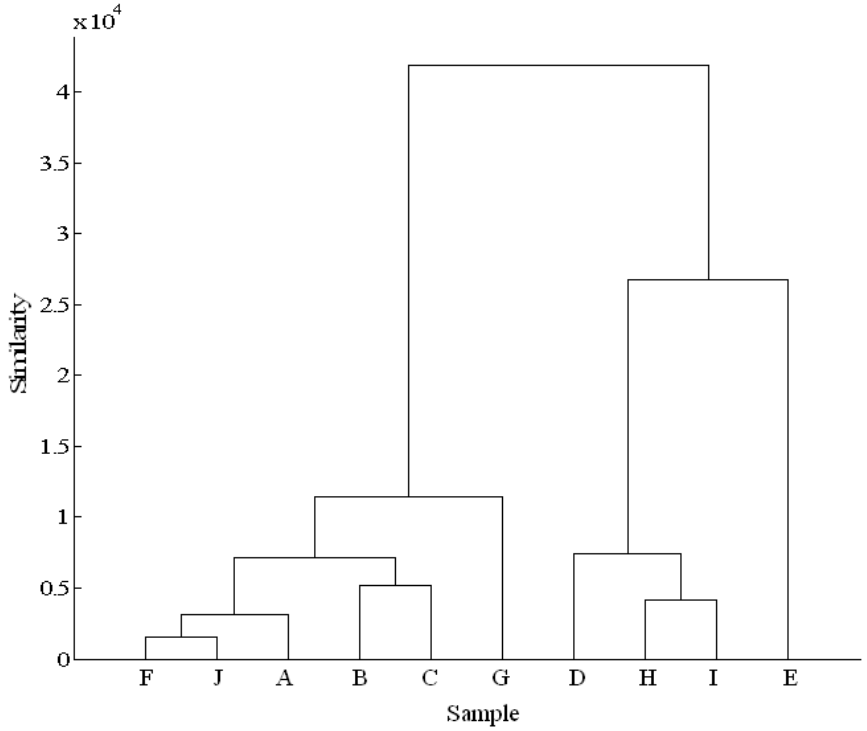

In both of these figures, similar groups are seen in the higher clustering levels, while differences between the two methods are more visible in the initial clusters formed. However, both methods suggest the presence of at least two clusters, with one or two outliers. The first cluster is made up of samples A, B, C, F, and J (and possibly G), while the second includes samples D, H, and I, with sample E as an outlier in that group.

Nonhierarchical clustering is another way to view potential groups within the data. One method for nonhierarchical clustering is K-means clustering.[6] This method works as a partitioning method, where samples are placed within clusters that are mutually exclusive based on their similarities, rather than on proximities. Rather than creating structure in the data to represent the levels of similarity (as in a dendrogram), a single level of clusters is formed. The method defines each cluster by the samples belonging to

it and the centroid of the cluster. Samples are then added to the clusters so that the sum of the distance measures to the centroid in that cluster is minimized. Usually this is done iteratively, moving samples from cluster to cluster until all the distances from sample to centroid cannot be minimized any further. While this can be useful for clustering large amounts of data (since a large, complicated dendrogram is not produced), the number of clusters, K, must be determined beforehand. This means that using a different number of clusters to begin with can change the results of the clustering, sometimes dramatically.[6]

Again, the sample data set is used as an illustration. Here, K-means clustering was performed using the *kmeans* function in Matlab©. This function uses squared Euclidean distances to determine the distance from each point to the centroid of the cluster. The output is a vector that contains the cluster indices for each sample. Below are three tables showing the results of the K-means clustering when K (the number of clusters) is three, four, and five, respectively.

Table 2.3: Results of K-means clustering for standardized sample data set (Table 2.1)

A) K=3

Sample	***Cluster***
D	1
H	1
I	1
A	2
B	2
C	2
F	2
G	2
J	2
E	3

B) K=4

Sample	***Cluster***
D	1
H	1
I	1
A	2
B	2
C	2
F	2
J	2
G	3
E	4

C) K=5

Sample	***Cluster***
D	1
H	1
I	1
A	2
F	2
J	2
B	3
C	3
G	4
E	5

It is apparent that all three analyses get similar results for some samples. Samples D, H, and I form one cluster that remains the same in all three approaches, while sample E is placed in a group on its own. K-means clustering with K = 4 seems to get results that most closely match those from the hierarchical clustering methods. When K = 5, further division is seen between samples A, F, and J, and samples B and C.

Though it is useful as a starting point in distinguishing groups, cluster analysis cannot be used alone as a quantitative measure for the differentiation of groups.[2] Cluster analysis assumes that the variables in the data are uncorrelated, which is known not to be the case with archaeological data sets.[2] If the data were truly uncorrelated, then the dendrograms might accurately represent the similarities between samples. However, when sourcing geological materials, it has been shown that many elements, such as the REEs, are correlated. Thus, cluster analysis can only be used as an initial step and should not be taken as faithfully representing differences between groups of samples. For truly accurate distinction between groups, other statistical techniques, such as principal component analysis, should be used.

2.4.3 Principal component analysis

Principal component analysis (PCA) is a statistical method which reduces the amount of variables needed to describe a data set when there is correlation present.[7-10] It allows data from a high dimensional space to be projected into fewer dimensions (typically either two or three dimensional space) while maintaining the distances between each point. In addition, while the number of dimensions needed to graphically represent the data are reduced, the data points still include all of the original data. PCA does this by

finding the principal components (PCs), linear combinations of the original variables, which account for the variation in the data set.[7] This technique is especially useful when looking at archaeometric data. Since there are so many variables, it is quite useful to be able to reduce the number of variables to a few that can describe the majority of the variance in the data set. It is also then important to relate these new variables to the original ones to understand how they affect the variance between groups within the data.

PCA takes a large data set with *p* variables that may be correlated and linearly transforms it into *p* uncorrelated variables so that the best clustering of groups within the data is achieved.[5-7, 10] The standardized data set is then projected onto the new set of axes created, where the first axis (principal component), PC1, accounts for most of the variation, the second (PC2) accounts for the next greatest amount of variation and is orthogonal to PC1, and so forth. The same number of PCs is produced as there were original variables. The linear transformation is done using the following equation for each principal component:

$P1 = a_{11}X_1 + a_{12}X_2 + a_{13}X_3 + \ldots a_{1n}X_n$ for PC1, *Equation 2.10*

$P2 = a_{21}X_1 + a_{22}X_2 + a_{23}X_3 + \ldots a_{2n}X_n$ for PC2,

etc, where a is the score for each variable and X is the standardized data.[2, 6, 9]

When PCA is performed on a particular data set, three matrices are typically returned.[7-8] The first is the set of eigenvalues, which describe the amount of variance described by each principal component. The second is the loadings matrix which describes the influence of each variable on each principal component. The last is the scores matrix, which is the projection of the data set into principal component space.

PCA was performed on the sample data set above (Table 2.1) and will be used to illustrate the results of a PC analysis.

The eigenvalues, or the variance described by each PC, provide useful information about how the principal components describe the variance in the sample and they allow an informed number of principal components to be chosen for examination.[8-9] The eigenvalues are the sum of the variances for each principal component. When the data is standardized, the total variance in the data set equals the sum of the variances of each PC.[8] So, for the data set containing 5 standardized variables, $\sigma_i^2=1$ for $i = 1$ to 5 for each variable. When PCA was performed on the sample data set described above (Table 2.1), the following eigenvalues were obtained (Table 2.4).

Table 2.4: Eigenvalues of standardized sample data set (Table 2.1)

Principal Component	Eigenvalue	% Variance explained by each PC	% Cumulative variance
PC1	2.6555	53.11	53.11
PC2	1.9976	39.95	93.06
PC3	0.2824	5.648	98.71
PC4	0.06191	1.238	99.95
PC5	0.00252	0.05048	100

Here, the sum of the eigenvalues also adds up to 5.

The eigenvalues are particularly useful for determining the number of principal components that are appropriate for consideration for the analysis of the data set. Here, several factors are considered. First, the amount of variance explained by each PC is calculated by dividing each eigenvalue by the total variance (here, 5) and multiplying by 100% (Table 2.4). The cumulative variance is also calculated. Usually a fixed

percentage of variance is specified, for example 90%, and the number of PCs needed to reach that cumulative variance are chosen.[7] In this data set, the first two PCs explain about 93% of the variance, so only the first two PCs would be considered for further analysis. In addition, a Scree plot can also be used to determine the number of PCs.[7-8] The Scree plot can either be created by plotting the eigenvalues for each PC (Figure 2.5a) or by plotting the percent variance explained for each PC (Figure 2.5b).

Figure 2.5: Scree plots from PCA of standardized sample data set (Table 2.1)

A) Eigenvalues vs. PCs

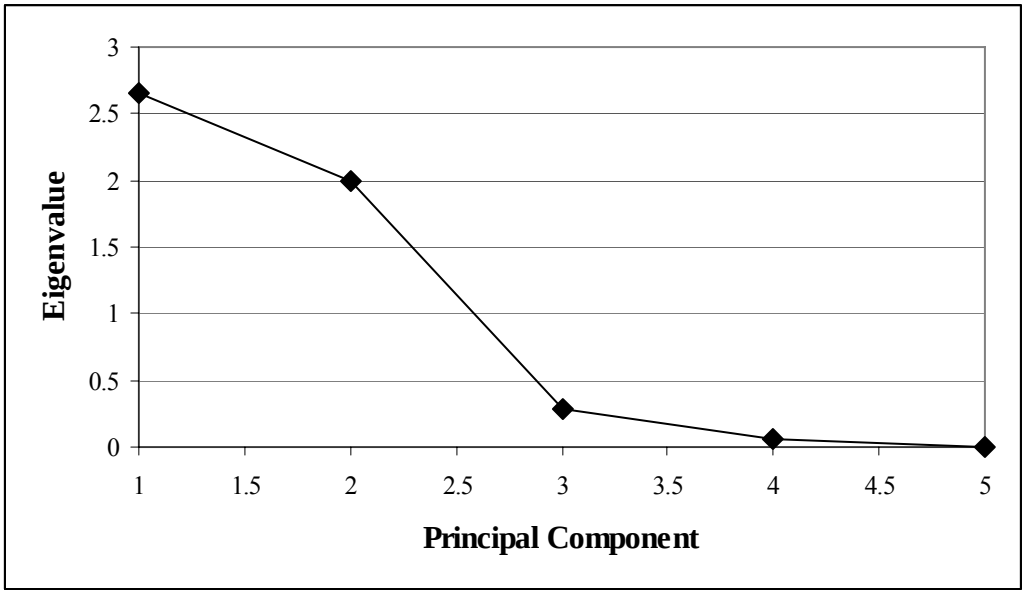

B) % Variance vs. PCs

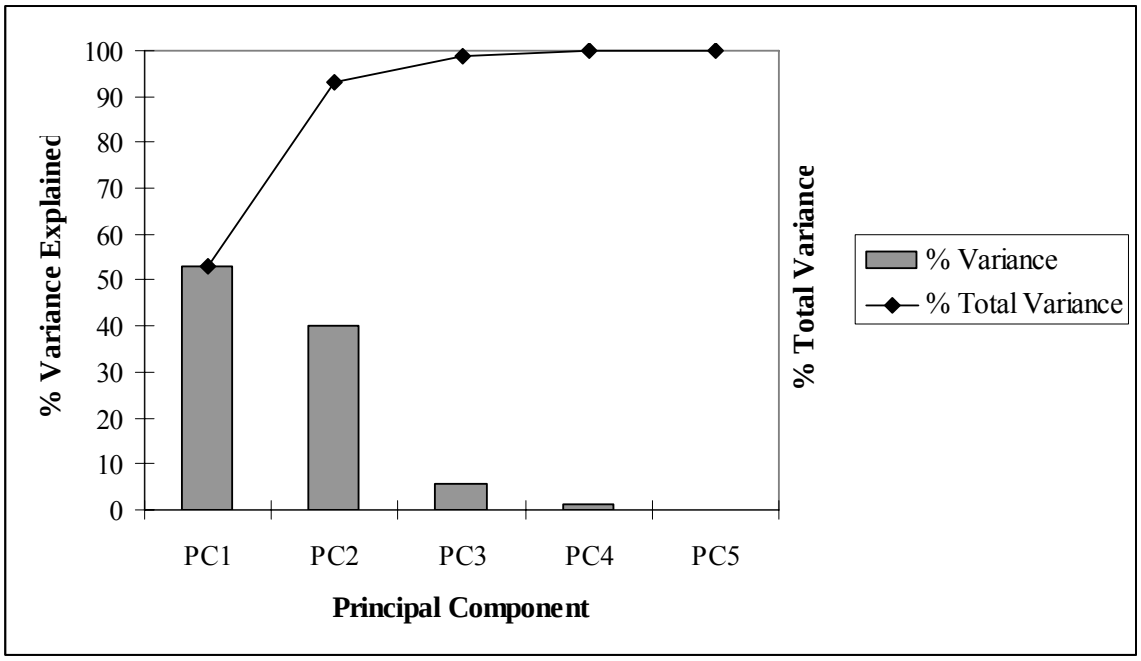

In each of these plots, the amount of variance levels off when the appropriate number of PCs has been reached. These justify the choice of the first two principal components to describe the majority of the variance in the data set.

The loadings matrix describes how each of the variables contributes to the variance in the data set and thus to each PC.[5, 7-8] It also shows the correlations between each variable within the data set. The loadings are the coefficients (a_{ij}) shown in equation 2.10 above. These coefficients weight the original variables to project them into principal component space. Shown below is a plot of the loadings values for each variable in the first two PCs.

Figure 2.6: Loadings plot from PCA of standardized sample data set (Table 2.1)

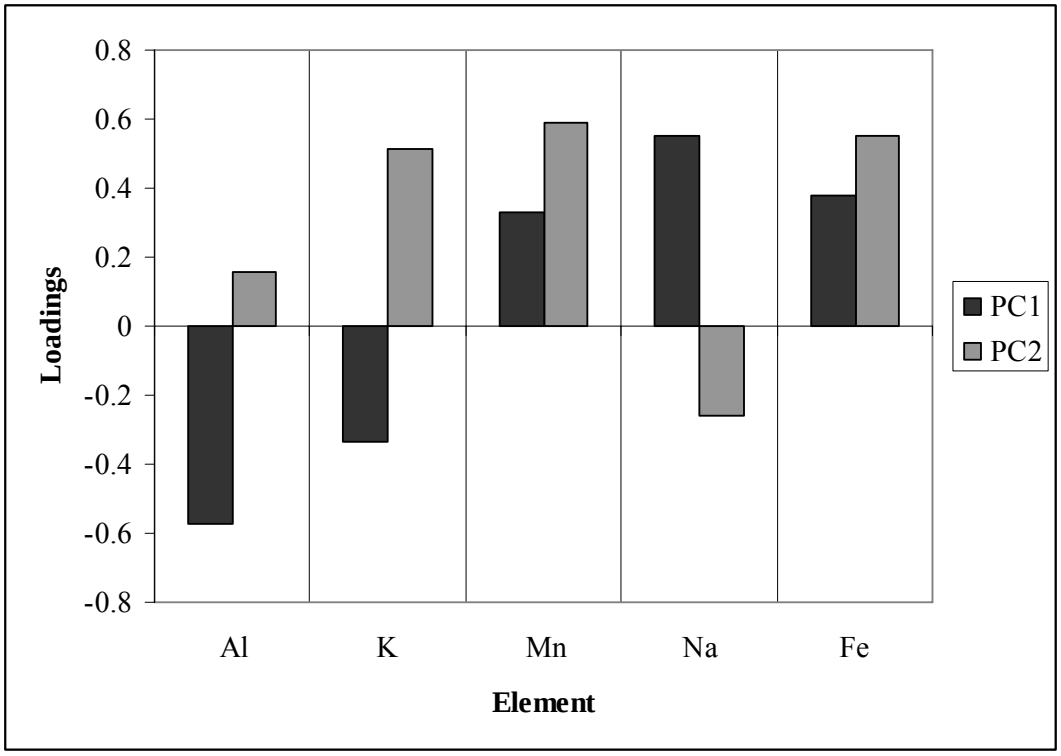

In this plot, the size of the value reflects the contribution to each PC and the direction (positive or negative) can give information on the relationship between variables. For example, aluminum and sodium both strongly contribute to the variance explained by PC1 but they are inversely correlated to each other. Thus it seems possible that sodium and aluminum can be used to differentiate between groups within this data set. Meanwhile, the second principle component is driven by variance from potassium, manganese, and iron, all of which are strongly intercorrelated with each other in this dimension. Another way of plotting the loadings is shown in Figure 2.7.[7] Here, the strong correlation between manganese and iron is clearly visible as is the negative correlation between aluminum and sodium.

Figure 2.7: Loadings vector plot from PCA of standardized sample data set (Table 2.1)

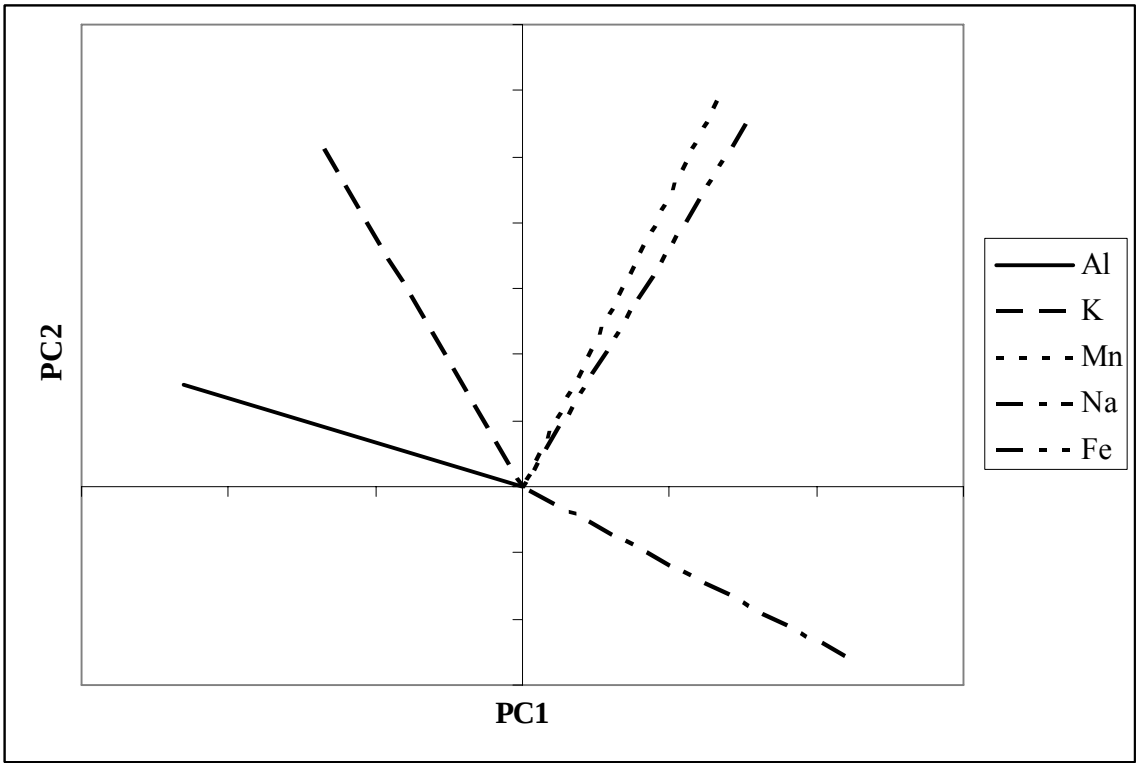

The last matrix that results from PCA is the scores matrix. This matrix is the projection of the data onto the new axes defined by the principal components.[7, 9-10] PCA maintains the distance between each data point in multidimensional space, so the scores represent the same data as before, just with a redefined origin and set of axes. The scores are the new coordinates of the data. Figure 2.8 is a plot showing the scores values for PC2 plotted versus those from PC1 for the sample data set. These principal components were proven above to describe over 90% of the variance in the data set.

Figure 2.8: Scores plot from PCA of standardized sample data set (Table 2.1)

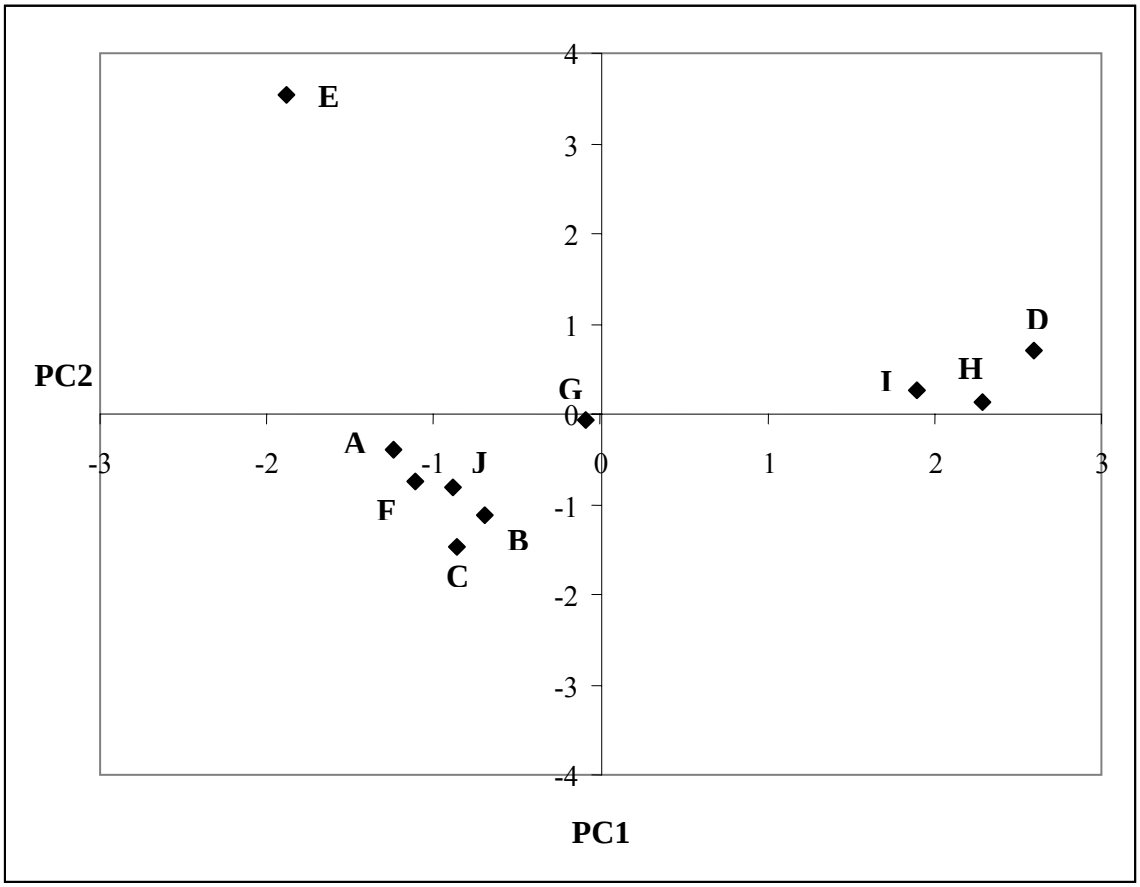

As can be seen in the plot, there are several distinct groups formed by the samples. For samples to have similar scores values, they must have similar values in the original data set. In this data set, samples A, B, C, F, and J form one group while D, H, and I for another. Samples E and G seem to be outliers in the data set. If the loadings vectors and the scores are plotted on the same graph, then the relationship between the samples and the principal components becomes even clearer (Figure 2.9). In this plot, the loadings vectors have been scaled up for clarity.

Figure 2.9: Plot of scores and loadings vectors from PCA of standardized sample data set (Table 2.1)

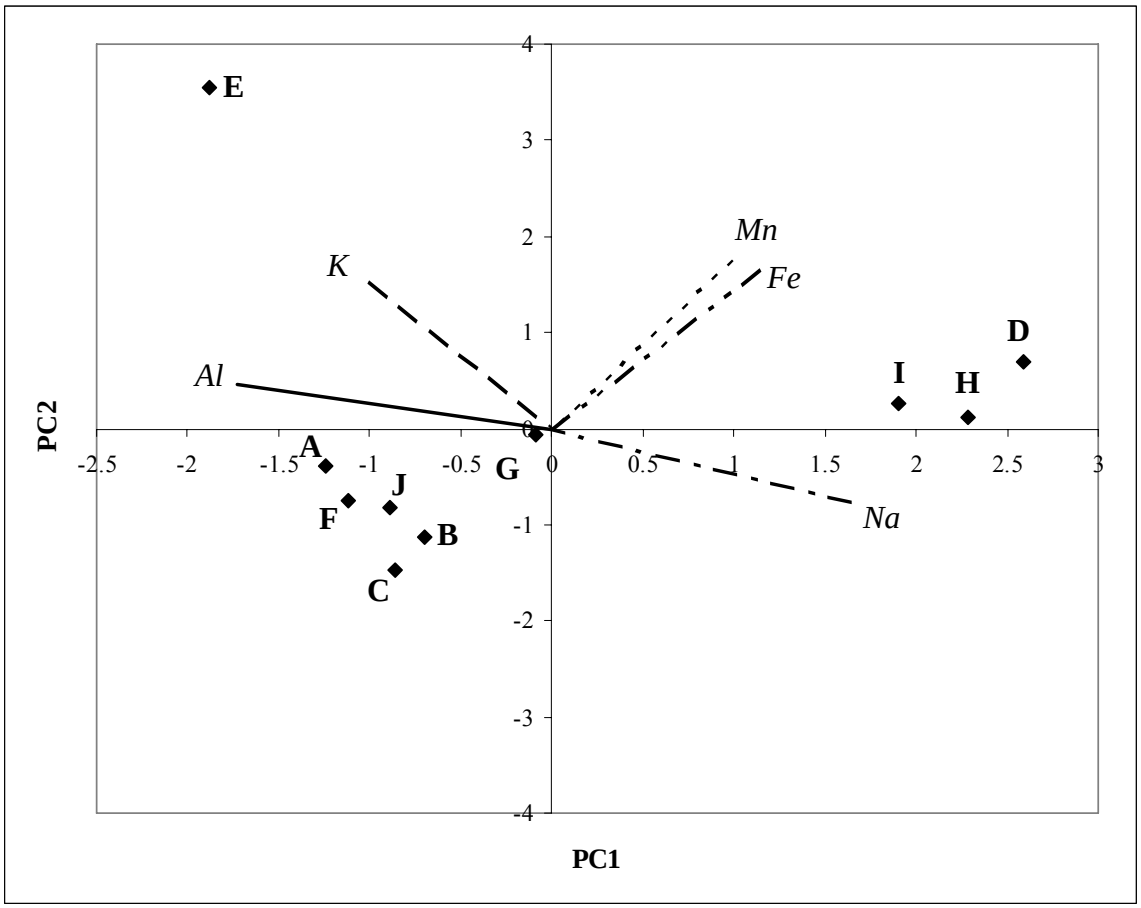

In this plot, it is clearly seen how aluminum and sodium drive the separation of the (A,B,C,F,J) group and the (D,H,I) group. The latter also has relatively high levels of iron and magnesium. High levels of potassium distinguish sample E from the rest of the samples, while moderate levels of all the measured elements separates sample G. Thus, not only are the differences between groups and similarities within groups more evident using the results from PCA but also these results can be related back to the original variables.[7-9]

PCA is applied to sourcing studies because the focus of those studies is to distinguish groups of similar elemental composition and to determine what elements

actually drive the variance between source groups. By applying PCA, large data sets can be reduced to much fewer variables, through analysis of the eigenvalues, which can then be used to study the variance within the data set. Plots of the loadings and the scores then describe how the original variables (the elemental concentrations) drive the variance and can be used on their own to distinguish between compositional groups. Finally, the scores plot itself shows how the samples in the data set are related to each other and the most probable compositional groups are formed.

2.5 Conclusion

The goal of studies involving the sourcing of geological materials is to accurately describe the chemical composition of the source so that the source of samples of unknown origin might be determined with confidence. In order to accomplish this, multivariate statistical techniques can be used on the large data sets that result from multi-elemental analysis to decipher the variations within source groups and between different source groups.[2] Initial analysis using covariance matrices and cluster analysis can be used to determine the relationship between the measured variables and the individual samples, respectively. More rigorous statistical methods, such as principal component analysis, can then be used to accurately model the groups within the data. This allows for a complete characterization of the data set, using all the information available from the multi-elemental analysis.

References

1. L. Wilson, Pollard, A.M., in *Handbook of Archaeological Science*, eds. D. R. Brothwell and A. M. Pollard, John Wiley & Sons, Ltd., New York, 2001, ch. 41, pp. 507-517.
2. M. D. Glascock, G. E. Braswell and R. H. Cobean, in *Archaeological Obsidian Studies*, ed. M. S. Shackley, Plenum Press, New York, 1998, ch. 2, pp. 15-65.
3. G. Harbottle, in *Chemical Applications of Nuclear Probes*, ed. K. Yoshihara, Harbottle, G., Springer-Verlag, Berlin, 1990, vol. 157, ch. 3, pp. 59-91.
4. L. L. Holmes, Harbottle, G., *Archaeometry*, 1994, **36**, 25-39.
5. M. Baxter, *Statistics in Archaeology*, Oxford University Press, New York, 2003.
6. M. Baxter, *Exploratory Multivariate Analysis in Archaeology*, Edinburgh Univeristy Press, Edinburgh, 1994.
7. M. Otto, *Chemometrics: Statistics and Computer Application in Analytical Chemistry*, Wiley-VCH, New York, 1999.
8. G. H. Dunteman, *Principal Components Analysis*, Sage Publications, Newbury Park, CA, 1989.
9. I. T. Jolliffe, *Principal Component Analysis*, Springer-Verlag, New York, 1986.
10. P. Gemperline, in *Practical Guide to Chemometrics*, ed. P. Gemperline, Boca Raton : CRC/Taylor & Francis, 2nd edn., 2006, ch. 4, pp. 70-104.

CHAPTER 3:

SOURCING EGYPTIAN LIMESTONE

3.1 Introduction

Neutron activation analysis (NAA) has performed an important role in sourcing ancient artifacts including ceramics and a wide variety of lithic materials, including flint, basalt and obsidian. When coupled with rigorous statistical methods, including principal component analysis and various clustering techniques, it can provide the precision needed to determine the source of the material with high confidence. However, this technique has not been fully exploited for the provenancing of Egyptian limestone sculpture. Limestone has played an important role in the building and sculpting history of many cultures all over the world, but sourcing studies have been mostly limited to France and other regions in Europe.[1-3] A plethora of ancient Egyptian monuments and sculptures has been made from limestone and the Egyptian people have continued to use limestone as a building material since antiquity. Most Egyptian provenance studies have focused on the use of petrology rather than the chemical composition.[4-5] This study examines the use of elemental analysis by INAA as a complementary method for sourcing Egyptian limestone. Here, a combination of the elemental concentration data and statistical methods is used to study the compositional differences between known ancient quarries.

3.1.1 The geology of limestone

Limestone is a sedimentary rock that is mostly calcium carbonate in the form of calcite.[6] Most limestone is formed from the remains of microscopic marine species which have been compressed into the solid rock. The calcite needed to form limestone can also be deposited by evaporation of a solution rich in calcium carbonate. Limestone is a relatively porous and soft rock, making it easily carved. It is also widely available all over the world. These last two qualities are what made limestone a popular choice as a building material and for sculptures.

Because limestone is mostly made from the remains of small marine species, especially those with calcite shells, the mineral and fossil composition of limestone can vary from location to location. Different species in limestone can be identified through optical and scanning electron microscopy. These differences are often used to source the limestone, though analysis of the trace elemental composition has also been proven useful in sourcing studies involving limestone.[3, 6-7]

The chemical composition of the limestone is dependent on its formation and weathering history, just like the petrology of the sample. Over time, limestone that contains easily dissolved minerals will become more porous and wear away, while limestone that is more "weather-resistant" will remain behind. The more resistant limestone was frequently chosen by ancient people as being good building material.[6] This deliberate choice limits the number of limestone formations that were actively used as quarries. However, each of these still has a unique formation and weathering history,

which supports the hypothesis that the chemical composition of these sources can act like a fingerprint.

3.1.2 Limestone sourcing studies

Sourcing studies for limestone began as a way to assign a provenance to limestone sculptures that have been moved or "lost their histories".[1] Initial studies used a combination of petrological and compositional techniques to characterize and assign the unknown samples. Extensive research has been done in sourcing limestone from France and other areas of Europe using NAA. These studies, mostly performed at Brookhaven National Laboratory (BNL) by Holmes and colleagues,[1-2, 7-10] have shown that using the elemental composition and rigorous statistical techniques, including cluster analysis and multivariate analysis, the limestone sources can be distinguished. This has been especially useful in determining not only the limestone quarries used but also in tracing sculptures back to their original locations.[2, 11]

In contrast to Europe, very little has been done on sourcing Egyptian limestone. Only three major papers have been published on the subject in the last 20 years. In addition, two out of the three papers focus mostly on the petrological analysis rather than elemental composition. The first major study done was by Meyers and van Zelst[3] in 1977. Their work describes the analysis of limestone artifacts from Egypt and Spain. The Egyptian artifacts were from a variety of locations and it was assumed that each was made from local limestone deposits. However, it was found that the Egyptian limestone seemed to be relatively inhomogeneous in composition, since the variation between samples that came from the same location was about the same as the variation between

samples from different locations. Cluster analysis was applied to the samples and they found that only one small group of artifacts from Thebes seemed to be distinguishable from the rest of the samples. The other limestone artifacts were indistinguishable from each other compositionally and there was no consistent relationship between composition and geographic origin. However, one of the drawbacks of this study was that quarry samples were not analyzed along with the artifacts. Therefore it is possible that these artifacts were made from limestone from the same quarry or quarries close together that are similar in composition. A compositional study of the quarries is needed to confirm that there is no distinction between geographical sources and chemical composition. In addition, more rigorous statistical methods need to be applied and reported in order for statistical confirmation of these results.

The second major study of Egyptian limestone artifacts was published by Middleton and Bradley in 1989.[5] In this study, a combination of petrographic examination using both optical and scanning electron microscopes (SEM) and mineralogical analysis using x-ray diffraction was used to characterize three major groups of Egyptian limestone. Again, mostly artifacts were studied and grouped according to their similar composition. However, this paper showed promising results: the sources were distinguishable from each other by the petrological analysis. Finer distinctions could also be made using the elemental composition determined using the energy-dispersive x-ray spectrometer attached to the SEM instrument. The three regions that could be distinguished were centered around Cairo, El Bersha, and the Thebes/Abydos region. However, very few geological source samples were analyzed and the few that had been sampled were painted reliefs. Quarry samples from geological

sources need to be analyzed in order for these results to be confirmed and to begin applying this method to unknown artifacts.

More recent work done on sourcing Egyptian limestone is that by Dr. Harrell of the University of Toledo. In his 1992 paper,[4] Harrell describes a combination of thin-section petrography and x-ray fluorescence spectrometry for the analysis of quarry samples. These methods were applied to samples of limestone from 23 known quarries in Egypt, with a total of 28 samples analyzed. These known quarries are located in six main limestone formations in Egypt: Tarawan, Serai, Drunka, Minia, Salamut, and Mokattam formations (listed in order from north to south), all along the Nile. The main results of this study centered around distinguishing between these six major limestone formations. In a few instances, Harrell reports being able to distinguish specific quarries, but for the most part, only the general region can be determined for the limited number of limestone samples. The geochemical results were used mostly to confirm the petrological results, since there was not much variation seen between quarries for the elements analyzed.

At about the same time, a book by Rosemarie Klemm and Dietrich D. Klemm also considers the idea of sourcing limestone from Egypt.[6] In the chapter on limestone, most of the emphasis is placed on using the petrology of the sample to determine the origin. However, a smaller section described the use of elemental analysis, performed by x-ray fluorescence, atomic absorption, and inductively-coupled plasma spectrometry, to also aid in distinguishing sources. The elements chosen to distinguish between sources were magnesium and strontium, which provided satisfactory results. These elements are rather mobile in the environment, but because of insufficient limits of detection for the

less mobile trace elements, they provided the best possible results. The authors also caution that in order to achieve the best possible separation between source groups, a large number of samples from each quarry location need to be analyzed. Analyzing many samples from each location provides information not just on the variation between source groups, but also characterizes the intra-source variation.

3.1.3 The current project

As a combination of neutron activation analysis and rigorous statistical methods have been proven useful in determining the source of limestone from other areas of the world, a similar technique is applied to quarry samples of Egyptian limestone. Since x-ray fluorescence was shown to be a useful complementary technique to the petrological analysis, NAA should also provide complementary information about the samples. In addition, NAA has the ability to precisely measure more elements, especially the rare-earth trace metals that have been useful in sourcing studies of other lithic materials.

3.2 Methodology

Two sets of samples were used in this study. The first is a set of 75 samples that were inherited by the Archaeometry Group at MURR from BNL. These samples had little identification other than the list of the regions from which they came and they were already in powder form. Some limited data had been collected on the elemental composition using INAA at BNL. To make up for the missing elements, these samples were reanalyzed using standard INAA procedures (as described in Chapter 1) at MURR.

The second group of samples is a set of 65 samples acquired from Dr. Harrell at the University of Toledo. These samples were taken from many known ancient quarries along the Nile and had more detailed geographical information, including geospatial coordinates for the specific locations. About half of these samples came in powder form, while the other half were rock fragments. The fragments where cleaned by burring off the surface and rinsing in DI water. After drying in an oven overnight, they were then crushed into a powder using an agate mortar and pestle. The powders were placed overnight in an oven at 110 ^{0}C to dry the samples.

Samples of about 150 milligrams (for the short irradiation procedure) and 200 milligrams (for the long irradiation procedure) were weighed out into high-density polyethylene vials (shorts) and quartz tubes (longs). The samples were then analyzed via INAA according to standard procedures for limestone (as described in Chapter 1). Standards used in the analysis included SRM1633a (fly ash), SRM 278 (obsidian), and Ohio Red clay, which acted as a QC sample for the analyses. Once the data was collected, several multivariate statistical techniques were used to characterize the samples in the data set. Each set of samples was treated separately for the statistical analysis.

3.3 Statistical results and interpretation

3.3.1 The BNL samples

The Egyptian limestone samples from BNL came to the Archaeometry Group at MURR as part of a large collection of limestone samples, mostly from France, which had been previously analyzed by Lore Holmes and colleagues. However, among the plethora of information that came with the samples, there was very little about these particular

samples. There are 75 samples in total from five different quarry locations in Egypt: Beni Hasaan (BH), Deir Abu Hennis (DAH), Maasara (M), Quseir el Amarna(QA), and Tura (T). Very little else is known about these samples. A map of the locations of these five quarries is shown in Figure 3.1.

Figure 3.1: Map of sampled quarry locations in Egypt (BNL samples)

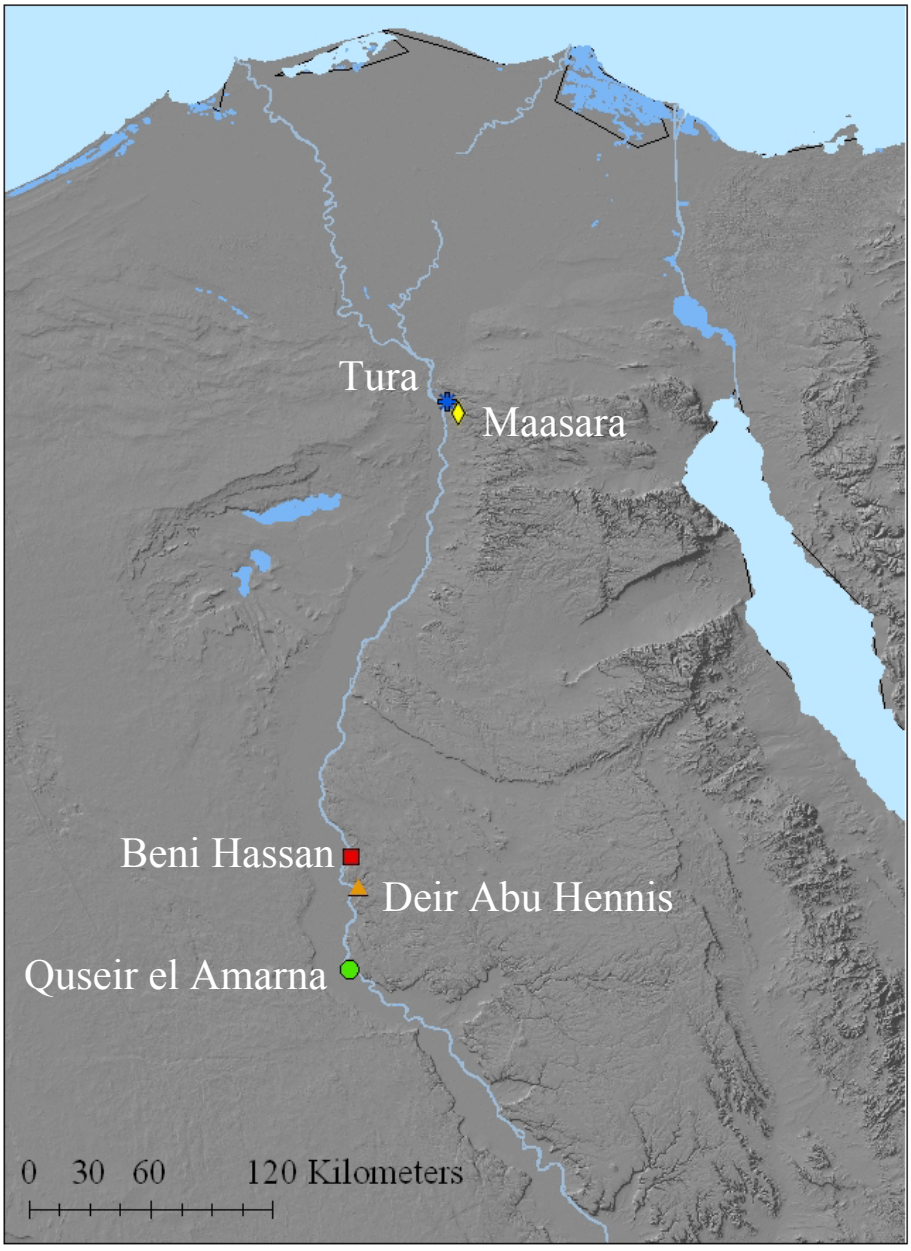

As stated before, there were many missing values for certain elements, such as manganese, so these samples were reanalyzed at MURR. Then data (given in Appendix 2) were subjected to several multivariate statistical techniques. First, cluster analysis was performed on the data set, using Euclidean distances and single linkages. The resulting dendrogram is shown in Figure 3.2. From this, it can be seen that the samples form two main groups, along with a few outliers. In addition, samples from the same source tend to cluster together more than those from different sources.

Figure 3.2: Dendrogram resulting from hierarchical cluster analysis of Egyptian limestone samples (BNL samples)

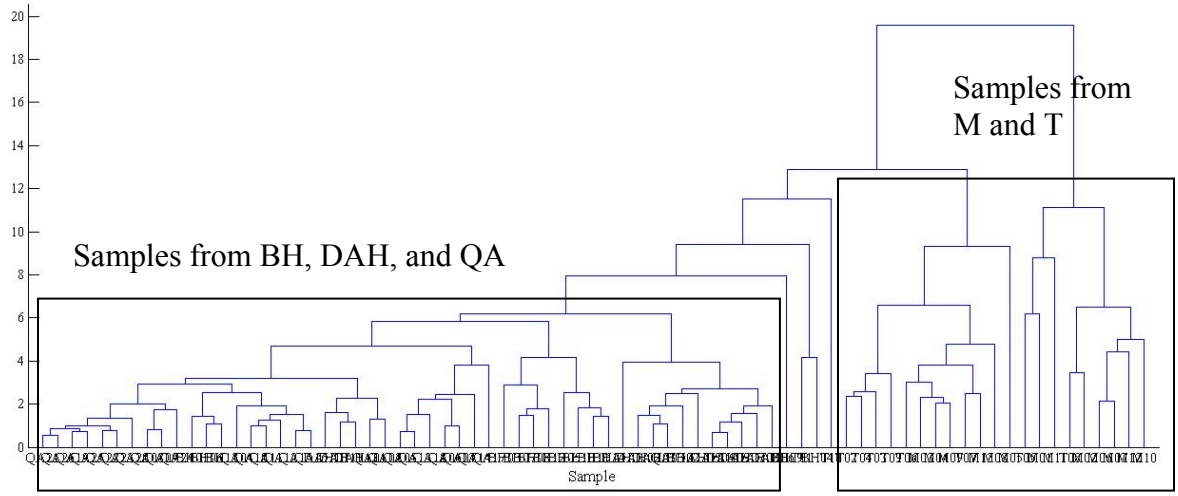

K-means clustering was also performed on the data set, with k = 2, 3, and 5. The results from this analysis for k = 3 are shown in Table 3.1. Here the samples are still grouping in similar ways as before. When k=3, the results almost perfectly match those achieved with hierarchical clustering, if groups 1 and 3 are combined. The separation between groups 1 and 3 is most likely due to a large intra-source variation.

Table 3.1: Results from k-means clustering of Egyptian limestone samples (BNL samples)

anid	Group	IDX3
EB0102	M	1
EB0103	M	1
EB0104	M	1
EB0107	M	1
EB0108	M	1
EB0112	M	1
EB0078	T	1
EB0079	T	1
EB0080	T	1
EB0082	T	1
EB0083	T	1
EB0084	T	1
EB0085	T	1
EB0100	M	3
EB0101	M	3
EB0105	M	3
EB0106	M	3
EB0109	M	3
EB0110	M	3
EB0111	M	3
EB0081	T	3
EB0038	BH	2
EB0051	BH	2
EB0052	BH	2
EB0053	BH	2
EB0054	BH	2
EB0055	BH	2
EB0056	BH	2
EB0057	BH	2
EB0058	BH	2
EB0059	BH	2
EB0060	BH	2
EB0061	BH	2
EB0062	BH	2
EB0063	BH	2
EB0037	T	2
EB0086	T	2

anid	Group	IDX3
EB0039	DAH	2
EB0040	DAH	2
EB0041	DAH	2
EB0042	DAH	2
EB0043	DAH	2
EB0044	DAH	2
EB0045	DAH	2
EB0046	DAH	2
EB0047	DAH	2
EB0048	DAH	2
EB0049	DAH	2
EB0050	DAH	2
EB0064	QA	2
EB0065	QA	2
EB0066	QA	2
EB0067	QA	2
EB0068	QA	2
EB0069	QA	2
EB0070	QA	2
EB0071	QA	2
EB0072	QA	2
EB0073	QA	2
EB0074	QA	2
EB0075	QA	2
EB0076	QA	2
EB0087	QA	2
EB0088	QA	2
EB0089	QA	2
EB0090	QA	2
EB0091	QA	2
EB0092	QA	2
EB0093	QA	2
EB0094	QA	2
EB0095	QA	2
EB0096	QA	2
EB0097	QA	2
EB0098	QA	2
EB0099	QA	2

From the clustering results, it appears as though the samples from these five locations are actually from two different limestone formations. This is supported by the geographical locations of the quarries. BH, DAH, and QA are quarries that are very close in proximity and tend to group together in the data set. The same goes for quarries M and T. These quarries are located farther north on the Nile than the other three.

Principal component analysis was also performed on the data set. The concentrations of the elements in each sample were standardized by dividing by the standard deviation. Then Matlab® was used to calculate the loadings, scores, and eigenvalues. A plot of the loadings for the first three principal components (Figure 3.3) shows that almost every element plays a role in the first PC, indicating that there is a lot of variance among the samples. PC2 provides more useful information. PC2 is more strongly driven by fewer elements which could prove useful in distinguishing between sources.

A plot of the scores for PC1 and PC2 (Figure 3.4) shows similar results to the cluster analysis. The data seems to be forming two groups, though those groups are very spread out. The more tightly-bound group is made up of the samples from BH, DAH, and QA, while the samples from M and T are much more spread out. In comparing these two groups, it seems as though there is much less intra-source variation in the samples from BH, DAH, and QA than there is in the samples from M and T.

Figure 3.3a: Loadings bar plot for Egyptian limestone samples (BNL samples)

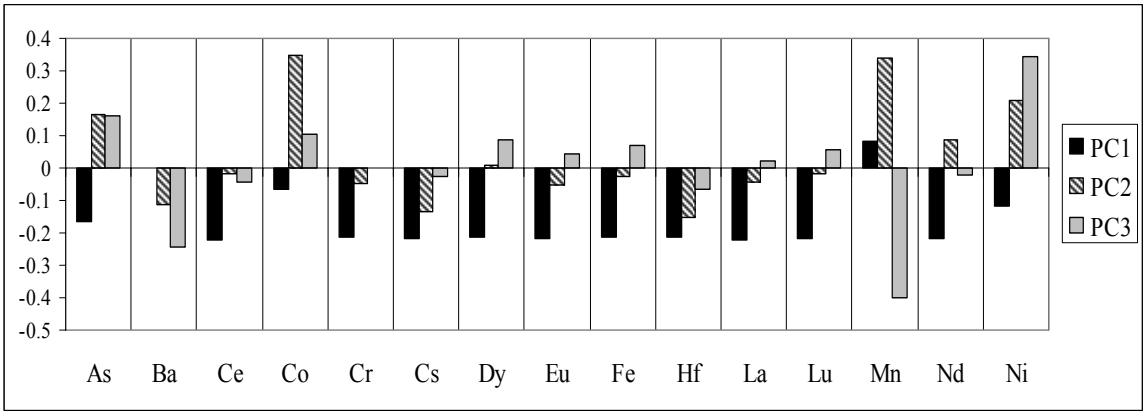

Figure 3.3b: Loadings bar plot for Egyptian limestone samples (BNL samples)

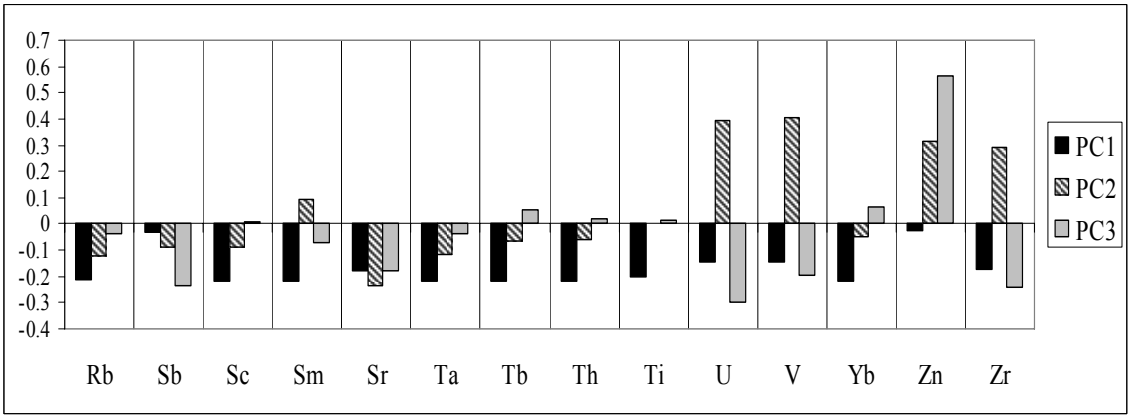

Figure 3.4: Plot of PC2 vs. PC1 for the BNL Egyptian limestone samples

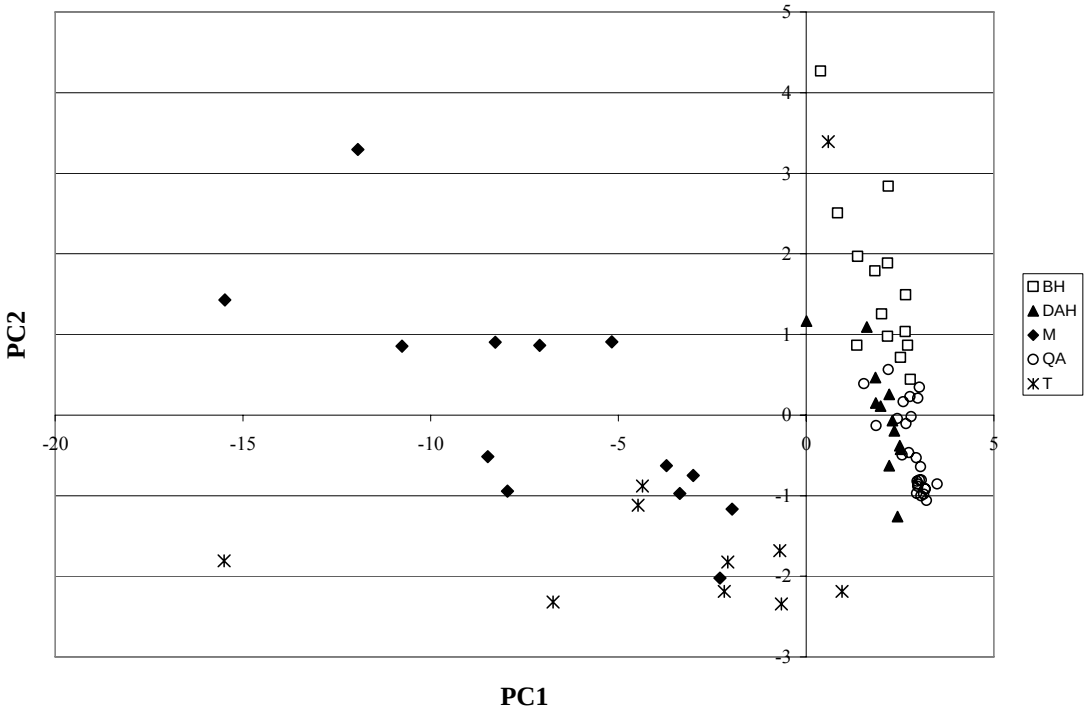

Since the groups in the scores plot were so spread out, bivariate plots were tried in order to refine the grouping of the samples. In examining the loadings, several elements were chosen for this analysis, including manganese, iron, and strontium. Figure 3.5 is a plot of the standardized concentrations of iron versus those of strontium. Figure 3.6 is a similar plot using the standardized concentrations of manganese versus strontium. In both plots, the two groups of samples are easily seen, with one group being more spread out in each plot than the other. In Figure 3.5, quarries BH, DAH, and QA form a very tightly-packed group. In Figure 3.6, quarries M and T are the more tightly-packed group, but still show significant variance within the group.

Figure 3.5: Plot of strontium versus iron using the standardized concentrations (BNL samples)

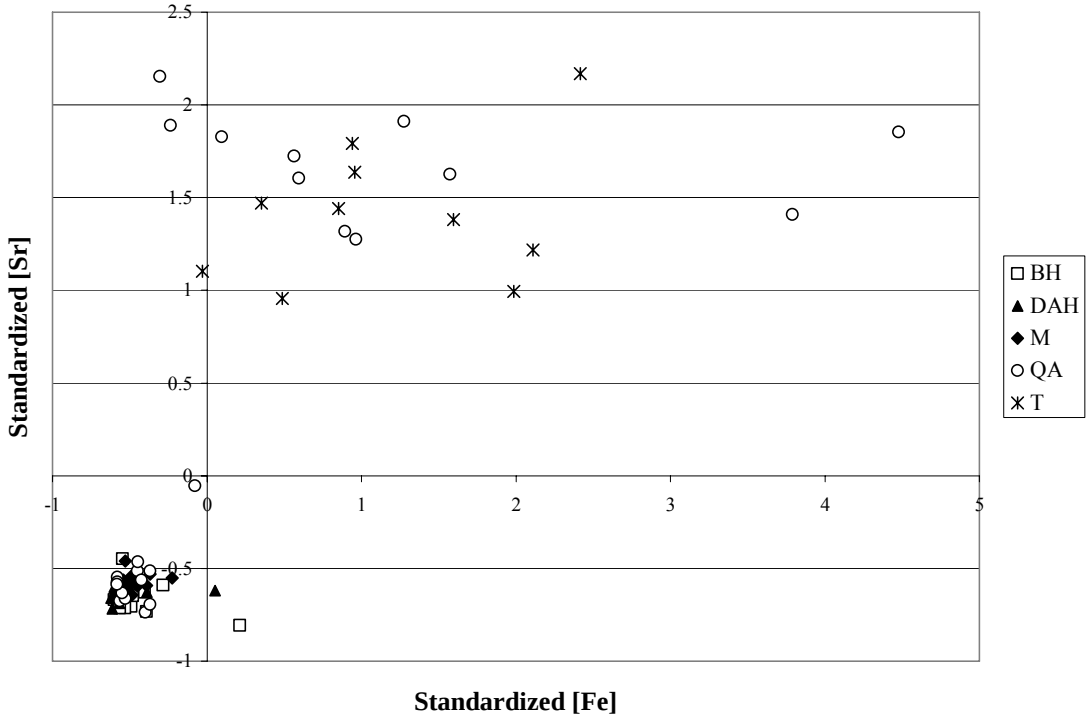

Figure 3.6: Plot of strontium versus manganese using the standardized concentrations (BNL samples)

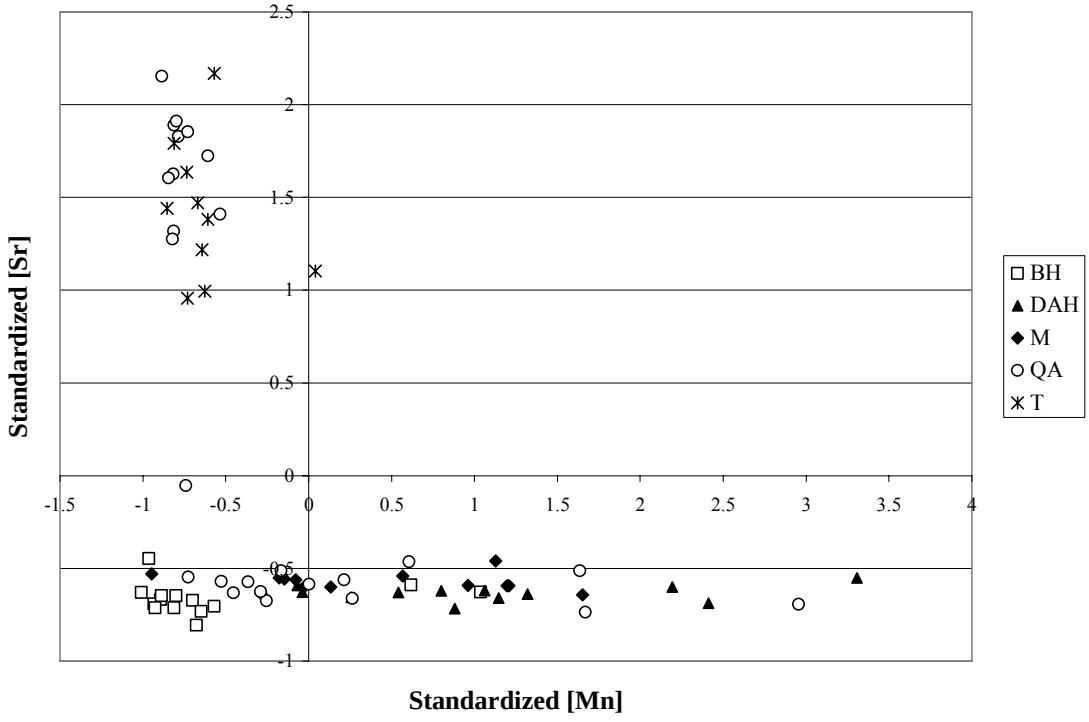

The elements chosen here are more mobile in the environment, so the variation seen between the two groups is subject to the extent of weathering; however, substitution of rare earth elements which have similar loadings values for the elements used in these plots shows very similar results.

The results from this set of limestone samples are promising for using elemental composition as a complementary method to sourcing Egyptian limestone. Though the intra-source variance for some sources may be large, like that of the samples from quarries M and T, it still is possible to distinguish between source groups. The large variation contained in source groups for limestone is often seen in other limestone data sets from Europe.[3, 11] The large variation within a source is often attributed to the weathering of the limestone over time, which can leach more mobile elements from the rock. However, a combination of cluster analysis, PCA, and simple bivariate plots allows the extraction of the most information possible from the samples and aids in accurately interpreting the results.

3.3.2 Samples from Dr. Harrell

As the samples from BNL's collection seemed to be representative of only two sources of limestone, additional samples from other locations were acquired from Dr. Harrell of the University of Toledo. Dr. Harrell had previously reported the usefulness of petrological analysis for sourcing Egyptian limestone, but also examined the use of elemental analysis as an aid in characterizing the source more thoroughly. It was hoped that using the elemental composition might enable distinction between limestone samples with similar petrology. To this end, 62 samples from 42 locations were acquired from Dr.

Harrell and analyzed by INAA at MURR. The source locations are shown in Figure 3.8 below (listed in Appendix 3).

As for the BNL samples described above, the results from the chemical analysis of these samples, listed in Appendix 4, were subjected to several multivariate techniques, including clustering techniques and principal component analysis. Hierarchical cluster analysis was first performed several times, using both Euclidean and standardized Euclidean distances and using both complete and Ward's linkage methods. Figure 3.8 is a dendrogram resulting from cluster analysis using the standardized Euclidean distance and Ward's linkage method.

Figure 3.7: Map showing the sampled locations in Egypt for the limestone from Dr. Harrell

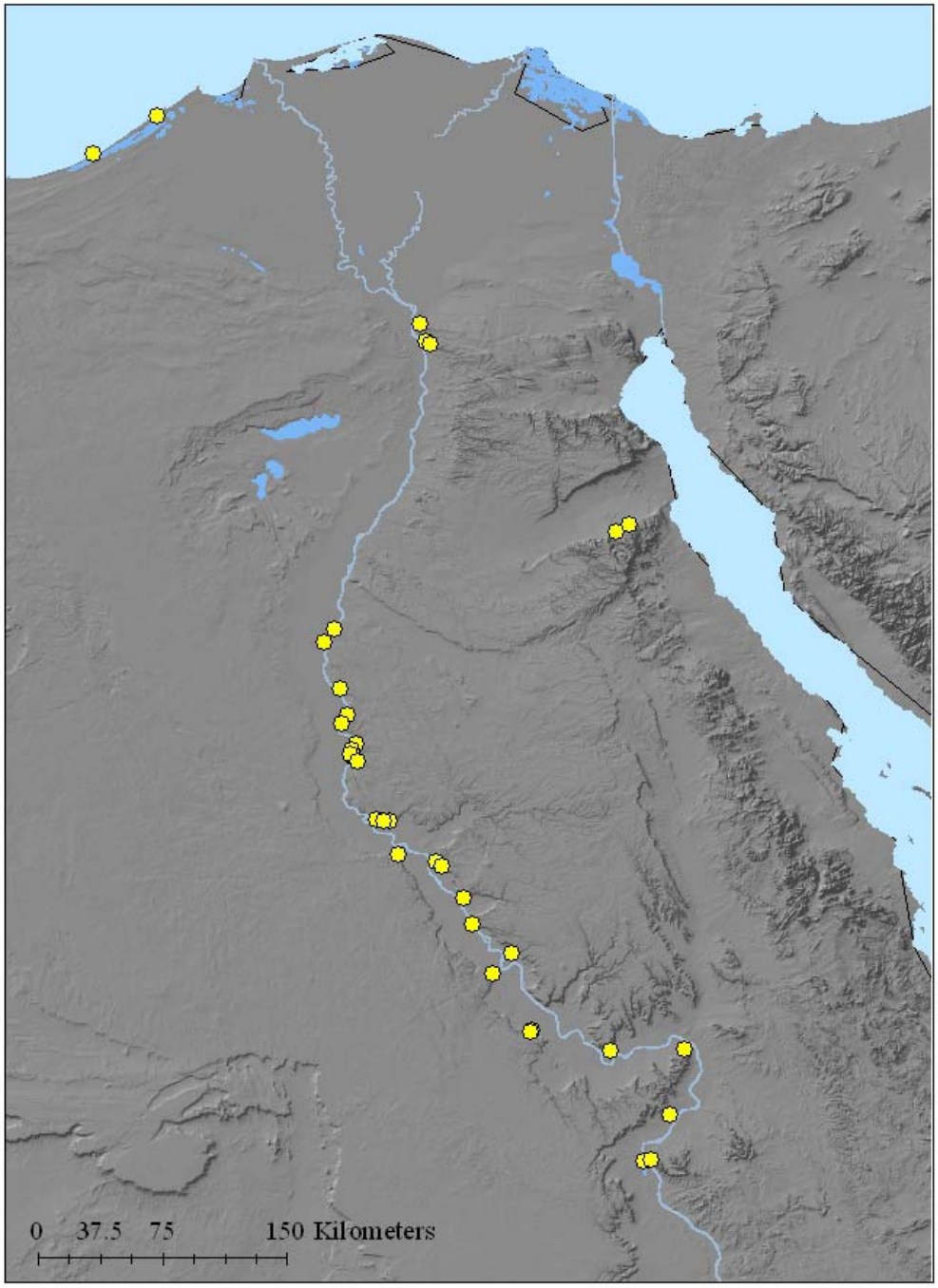

Figure 3.8 Results from cluster analysis using Euclidean distances and Ward's linkages for the Harrell limestone samples

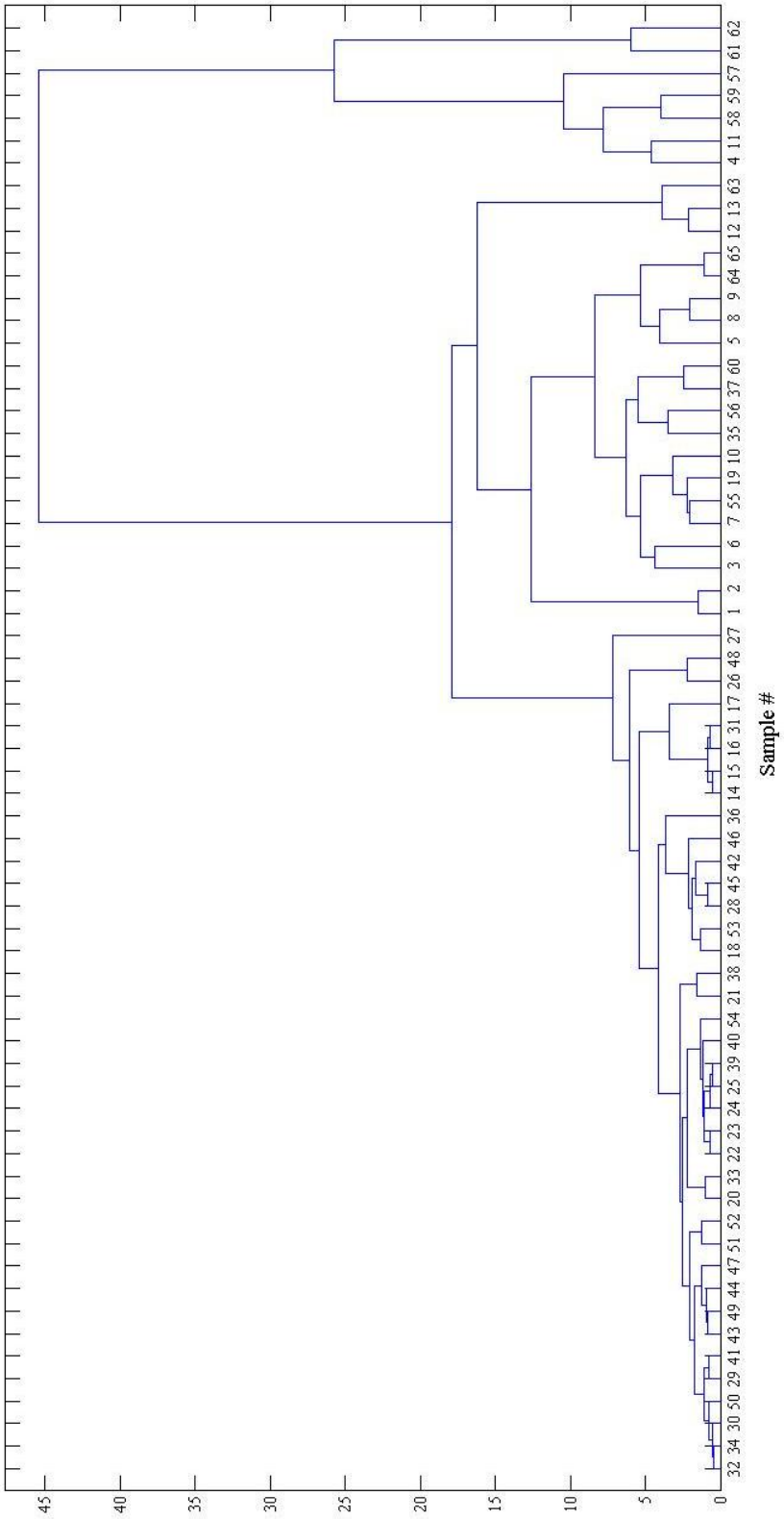

While there are some small groups that are seen in the dendrogram that do accurately represent samples from about the same location, such as the group of samples 1 and 2, 12 and 13, 22-25, and 61 and 62, few of the rest of the clusters correlate with geographic location. Since cluster analysis does not always accurately predict groups of similar samples, principal component analysis was performed on the data set. (k_{means} clustering was also performed, but the results also did not show much promise in distinguishing groups of samples.)

Before PCA was performed, the data was standardized as described in Chapter 2 and then PCA was performed using Matlab® as previously described. In examining the eigenvalues resulting from the analysis, the first three principal components described about 85% of the variance in the data set. The loadings for the first three principal components were then plotted (Figure 3.9).

Figure 3.9: Loadings bar plot for Egyptian limestone samples (Harrell)

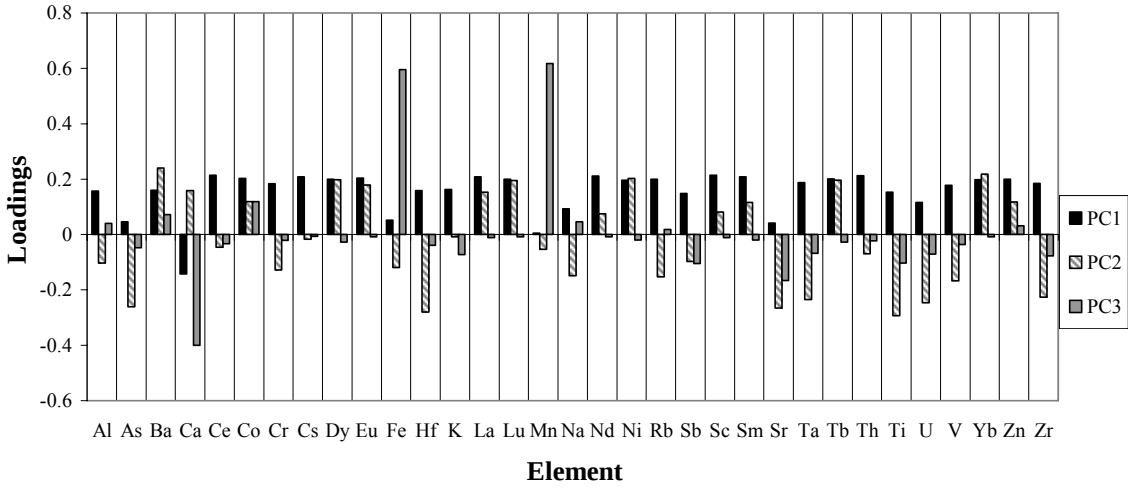

In the first PC, the majority of the elements is correlated and appears to have the same contribution to the variance and only calcium is inversely correlated. As the concentration of minor and trace elements increases, this reflects an increase of impurities in the limestone, the amount of pure calcium carbonate decreases. More useful information can be extracted from the second and third principal components. Here, elements such as strontium (which has been previously shown useful in the elemental analysis of limestone),[6] hafnium, iron, and manganese play important roles. A biplot of the loadings projected on the scores was created to see how the variation caused by these elements affected the differentiation between source groups. Figure 3.10 depicts PC2 plotted against PC1, while Figure 3.11 shows PC3 versus PC2.

Figure 3.10 Biplot of PC2 vs. PC1 for the Harrell Egyptian limestone samples

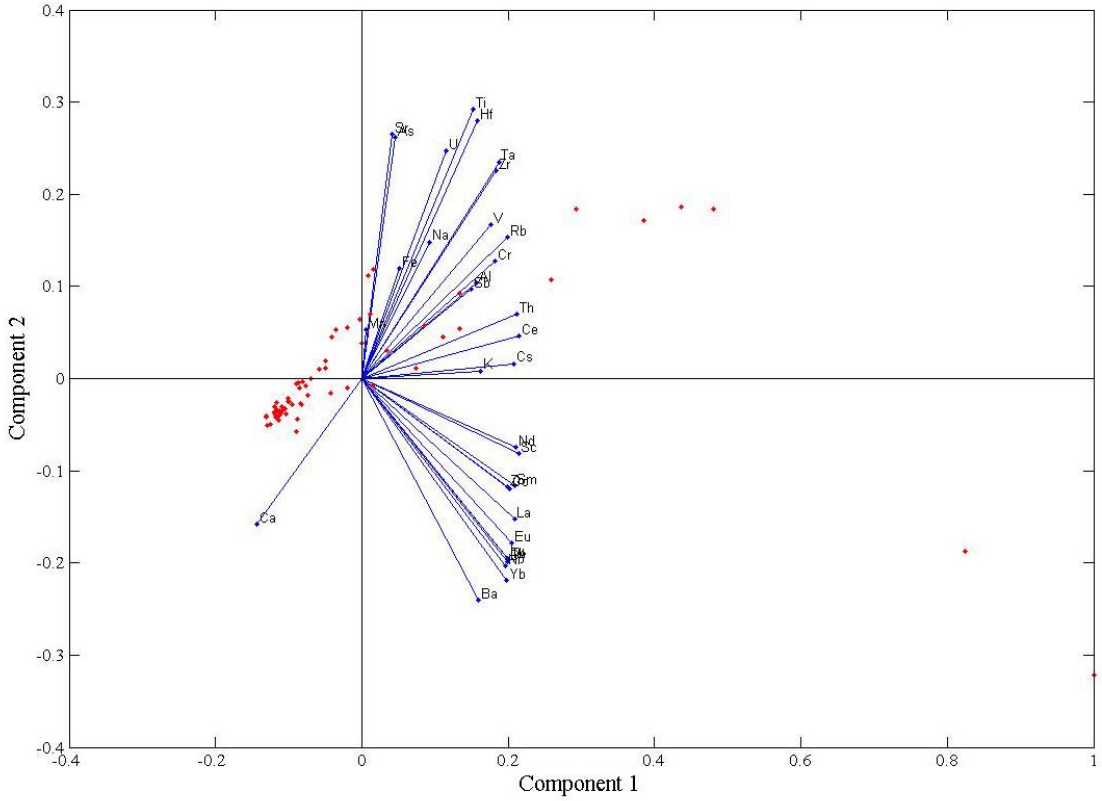

Figure 3.11 Biplot of PC3 vs. PC2 for the Harrell Egyptian limestone samples

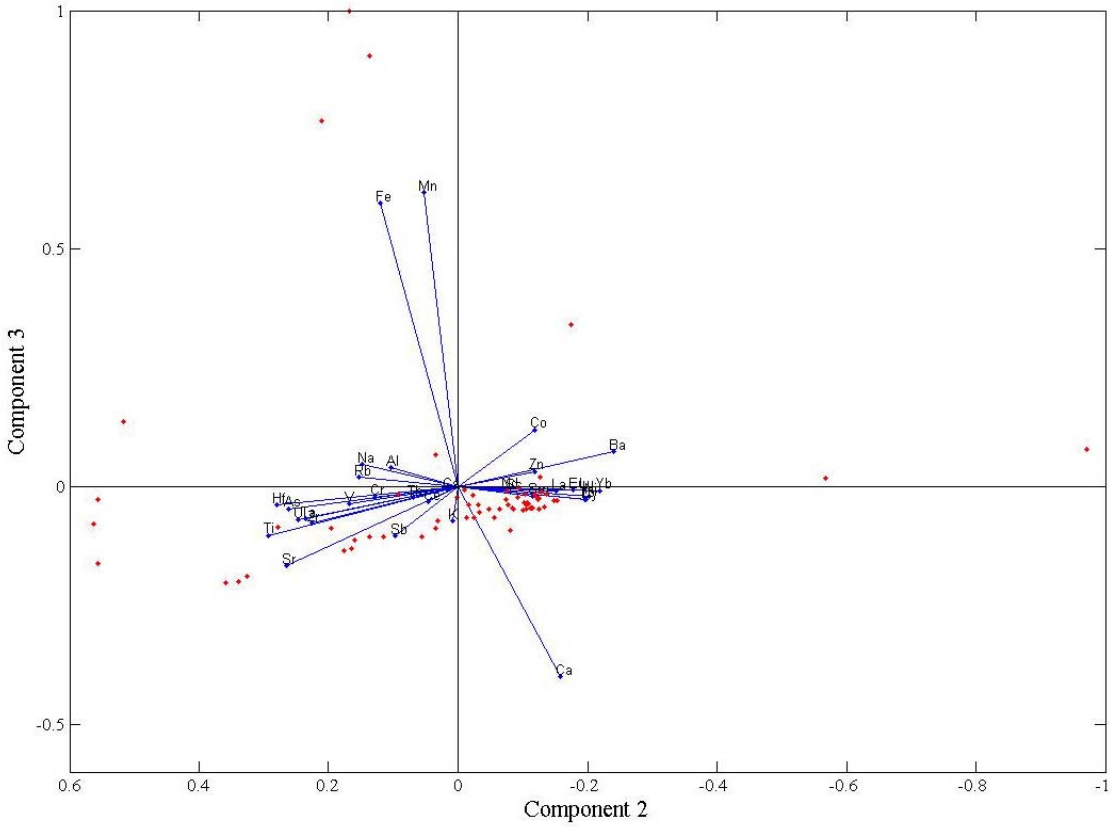

Figures 3.9 and 3.10 show that only a few samples from some of the sampled locations seem to separate out, while the rest form an oblong cluster in the center. The samples that do separate seem to reflect the geographical locations. For example, Figure 3.12 shows a plot of just the scores for the data, PC3 versus PC2. Figure 3.13 shows the groups of samples highlighted in Figure 3.12 plotted on a map.

Figure 3.12 PC2 versus PC3 for the Egyptian limestone samples (Harrell)

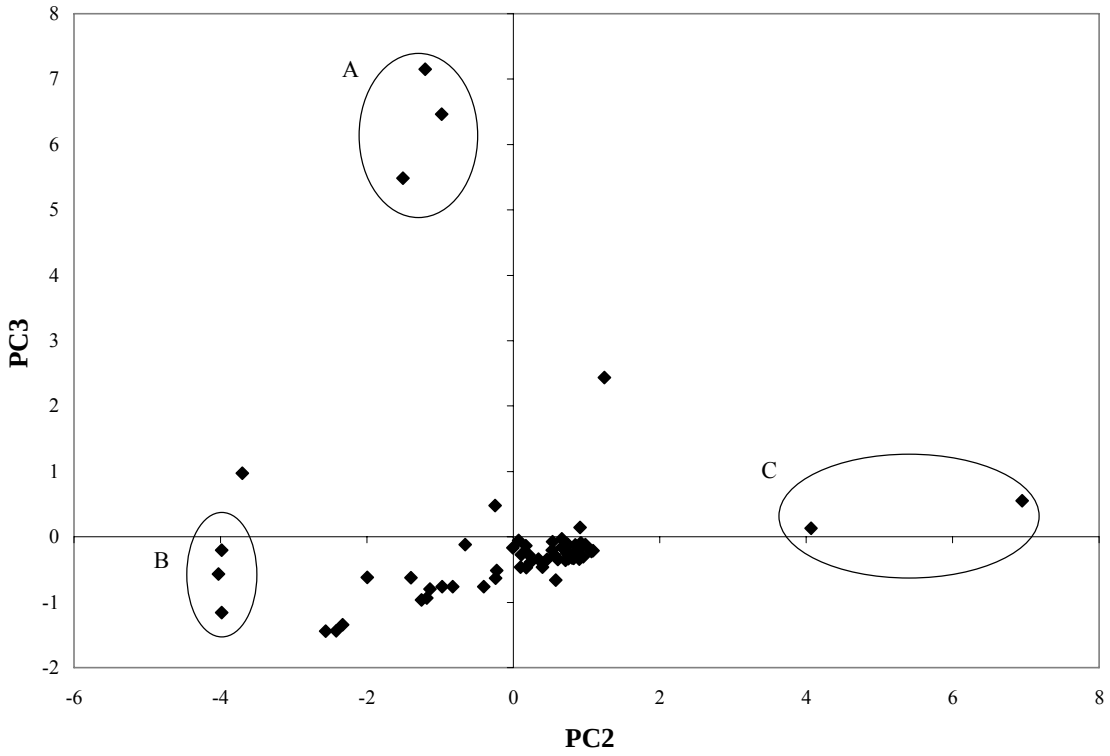

Figure 3.13 Map of three chemical groups of Egyptian limestone samples (Harrell)

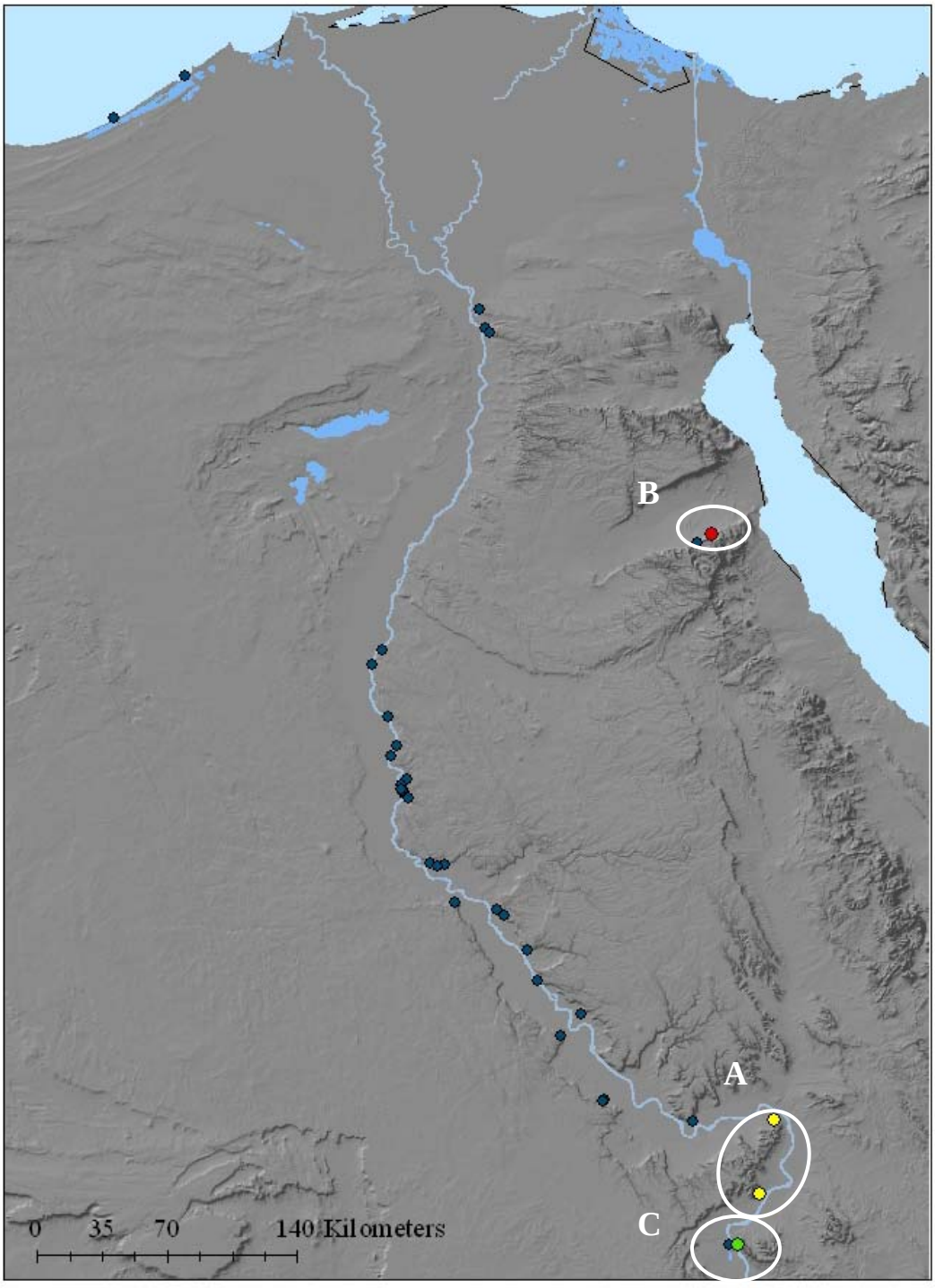

In addition to examining the scores plots, several bivariate plots were created using the elements of interest from the loadings matrix, such as strontium, iron, manganese, hafnium, and cobalt. However, the bivariate plots only echoed the results of the scores plots above. The same samples could be separated out to form groups, while the rest of the data set formed one large group with a few outliers. From these results, it seems like the intra-source variation is large enough in many cases to overshadow the inter-source variation.

Though these results are not as promising as those achieved from the BNL data set, there is one major difference between the two that could be a part of the problem. In performing studies of this sort, it is assumed that the composition of a source is relatively homogenous and that the within-source variation is small. However, with the small samples from Dr. Harrell that were used in this analysis, it is possible that the within-source variation was not characterized well enough to prove this assumption true. With only one or two samples from most of the sources, it is difficult to distinguish the within-source variation from the variation between sources. In the BNL data set, there were at least ten samples from each quarry site, which allowed the intra-source variation to be characterized more completely. The more samples from each site that can be characterized, the more accurate statistical analysis will be.[6, 9-11] Since limestone is a material that can undergo many changes in composition both during its formation and the natural weathering process, the stone itself can have quite high variations in composition, especially for the more mobile elements like magnesium, sodium, potassium, and iron.[6] More samples from each source would need to be analyzed in order to better examine the potential of INAA for the characterization of Egyptian limestone sources. However,

based on the results using the BNL data set, it is possible that this could be a powerful technique, especially when used in conjunction with petrological studies.

3.4 Conclusions and future work

Using elemental analysis alone to source Egyptian limestone is challenging. The most important of these is the potential for high intra-source variation, which requires the analysis of many samples from each source location. Limestone has been shown to follow the provenance postulate in other parts of the world, but it has not been proven in Egypt, mostly due to the lack of source analyses. With more samples from each known source being analyzed, the intra-source variation can be examined and compared to the inter-source variation. With this variation taken into account, more useful information can be extracted from the samples. As seen with the BNL samples, where the 75 samples were representative of only two source groups, it is possible to distinguish between source groups if the source is well characterized. This information can then be used alongside traditional petrology techniques to provide accurate sourcing of limestone artifacts.

References

1. L. Holmes, G. Harbottle and A. Blanc, *Archaeometry*, 1994, **36**, 25-39.
2. L. Holmes, G. Harbottle and E. V. Sayre, *Journal of Field Archaeology*, 1986, **13**, 419-438.
3. P. Meyers and L. van Zelst, *Radiochimica Acta*, 1977, **24**, 197-204.
4. J. A. Harrell, *Archaeometry*, 1992, **34**, 195-211.
5. A. P. Middleton and S. M. Bradley, *Journal of Archaeological Sciences*, 1989, **16**, 475-488.
6. R. Klemm and D. D. Klemm, *Stones and Quarries in Ancient Egypt*, The British Museum Press, London, 2008.
7. L. Holmes, G. Harbottle and A. Blanc, *Gesta*, 1994, **33**, 10-18.
8. G. Harbottle and L. Holmes, *Archaeometry*, 2007, **49**, 185-199.
9. L. Holmes and G. Harbottle, *Journal of Radioanalytical and Nuclear Chemistry*, 2001, **248**, 75-79.
10. L. Holmes and G. Harbottle, *Archaeometry*, 2003, **45**, 199-220.
11. C. T. Little, *Gesta*, 1994, **33**, 29-37.

CHAPTER 4:
SOURCING OBSIDIAN FROM KENYA USING NEUTRON ACTIVATION ANALYSIS

4.1 Introduction

Obsidian, a volcanic stone that is easily chemically characterized and the source of which can be determined with great accuracy, is relatively common in East African artifact assemblages. Although compositional studies of obsidian from East Africa conducted during the 1980s showed great potential, a comprehensive database has not been developed. Instead, many smaller studies have been performed focusing on specific sites and surrounding sources. Similar databases have proven critical to the interpretation of obsidian compositional data in other areas around the world. African archaeology is vital to an understanding of the origins of modern humans, and such a database would be useful to study the movements and interactions of the peoples who lived in this region by studying the distance from recovery sites to the sources to understand the past procurement and exchange systems.

4.1.1 Obsidian: a brief overview

Obsidian is a volcanic glass formed when viscous molten lava is cooled too quickly to crystallize. It has many characteristics that make it easy to source.[1] First, the

sources are limited. Second, the chemical composition of these sources is relatively homogenous within a source, but quite variable between sources. Third, the composition of an artifact made from obsidian is unchanged from that of the source, since the artifact is made simply by flaking the obsidian to create the sharp cutting edges desired. Obsidian does absorb water slowly over time, so hydration layers can form on the outside of the piece, but this crust on the outside is usually avoided for analysis.

4.1.1.1 Formation of obsidian

Not every volcano can produce obsidian-forming lava and not every eruption occurs under the right conditions to form obsidian. The lava must have certain characteristics in order to form obsidian.[2] Specifically, it must be viscous enough to slow the mobility of ions within the lava. Since obsidian forms under unique conditions, the presence of obsidian is limited to those volcanoes, which produce lava that has the opportunity to be quickly cooled, often near a source of water such as a river or lake.

4.1.1.2 Composition of obsidian

The chemical composition of obsidian is relatively homogenous within a source, but quite variable between sources. Because of this, obsidian has been found to follow the provenance postulate, which states that in order to be able to determine the source of a sample, the intra-source variations must be statistically less than the inter-source variations.[3] In some cases, the composition of a particular magma can even be variable over time, making it possible, not only to distinguish between obsidian from different volcanoes, but also to distinguish between obsidian produced from different eruptions of

the same volcano.[4] Typically, obsidian is primarily silicon dioxide (SiO_2; 70-75%), but also includes significant amounts of aluminum oxide (Al_2O_3; 10-15%), sodium oxide (Na_2O; 2-5%), potassium oxide (K_2O; 1-5%) and iron oxide (FeO and Fe_2O_3; 1-5%).[1] These concentrations are representative of the typical rhyolitic obsidian. Peralkaline obsidian, which has higher iron concentrations, is also found. Other elements are usually below 1% w/w in concentration. Obsidian also contains a small amount of water, usually 0.1-0.5%. Over time, the concentration of water increases to approximately 3.5%, as the obsidian slowly becomes perlite.[4]

The concentrations of trace elements are used to separate source samples into groups. The best elements are those incompatible with the solid phase due to large ion size or high ionic charges.[4] The large-ion lithophile elements (LILE) include potassium, rubidium, cesium, strontium, barium, the light rare earth elements (LREEs, La to Sm), thorium, and uranium. The high field-strength elements (HFSE) include yttrium, zirconium, hafnium, niobium, tantalum, and the heavy rare earth elements (HREEs, Eu to Lu).[1] Because lava must cool quickly in order to form obsidian, the incompatible elements are unable to fractionate between solid, crystallizing phases and the rest of the melt.[2] This gives the obsidian formed a relatively homogenous composition relative to the trace elements. In this way, the incompatible elements tend to have higher and more variable concentrations in obsidian than in other volcanic rocks, such as granite. Many of these elements can be measured with excellent precision and accuracy using either XRF or NAA.

4.1.2 African obsidian and anthropological implications

Obsidian use has a long history in East Africa, which is generally considered the region in which modern human behavior originated. The transition to modern behavior can be observed in the patterns of raw material procurement seen in the artifacts left behind. Typically, procurement of raw materials follows a distance-decay pattern, i.e. as the distance between a site and the source increases, the relative abundance of that source decreases.[5] However, as the interaction between socio-political groups increases, the slope of the typical distance-decay curve becomes shallower, as more artifacts from non-local materials are found at greater distances. In some cases, the distance-decay curve may even be the opposite of what is expected, with some of the more-distant sources having greater abundances, though this is more often seen in later sites.[5-6]

Very few studies have been done on obsidian sources in this region of the world, and most have stemmed from the work of Merrick and Brown in 1984.[7-8] Their work using electron microprobe in addition to x-ray fluorescence spectrometry provides a good start toward the development of a database for Kenya and Tanzania. As a result, they were able to identify at least 35 chemically distinct sources from 54 geographically distinct source localities, based on the more well-known locations of obsidian-bearing localities. In addition, the analyses of artifacts indicated the presence of possibly 22 more unknown sources. Merrick and Brown noticed that they were able to distinguish most groups using major and minor elements (iron, titanium, and calcium), unlike obsidian from other parts of the world which rely on trace elements to characterize sources. They do state that trace element analysis would still be needed to distinguish between chemically similar sources or outcrops of the same source, depending on the precision of

source assignment needed. Their work proved that provenance studies in Kenya and Tanzania had a great potential for studying raw material procurement patterns and interaction patterns of ancient peoples living in this region.

Negash, Shackley, and coworkers have also studied obsidian in Africa, focusing on Ethiopian sites and sources.[9-11] Their work stems from the preliminary studies done by Muir and Hivernel[12] in 1976 which showed the potential for sourcing obsidian from the Melka-Konture site in Ethiopia, a site occupied by ancient peoples from the Early Stone Age (ESA) through the Late Stone Age (LSA). Negash *et al.* have taken this work and expanded it by more extensively sampling known sources of obsidian in Ethiopia and by examining more archaeological sites, including Porc Epic[10-11], Melka Konture[10-11], and Beseka[9], which range from the ESA through to the Holocene (1.6 million years ago to 3500 years ago). Similar to the Merrick and Brown studies, they found that the obsidians from sources around Beseka were well-characterized using major and minor elements (iron, titanium, aluminum, and manganese).[9] Obsidian sources near the other sites, though still using iron as one of the best elements for characterization, used trace elements such as rubidium, zirconium, and zinc to distinguish sources. However, the presence of artifacts from these sites with no known source gives compelling evidence that further study into sourcing obsidian from this region is needed.

Currently, more and more anthropologists are gaining interest in building a database of obsidian sources for this part of the world. More recent work is being done by Ambrose[13-14], who is expanding on the work of Merrick and Brown in Kenya. His work is currently focused on the Central Rift Valley area of Kenya, which is well-known for its obsidian sources. The Rift Valley sources were commonly used sources because

of their high quality and abundance.[14] Other researchers are beginning to expand into other parts of Ethiopia and Tanzania and are interested in examining long-distance procurement patterns, which would require consulting a comprehensive database to source artifacts coming from sources quite distant from the site.

Though initial steps have been taken toward studying the geochemistry of the obsidian from this region, the work has mostly been focused on specific archaeological sites or has only brushed the surface of studying all the possible obsidian sources in East Africa. Though many of the known sources are located within the Rift Valley, even these large sources show the possibility of being further divided into smaller subsources, all distinguishable from the chemical data. In addition, one of the major difficulties anthropologists have faced is the large number of artifacts coming from as yet unidentified sources.[13, 15] The presence of unknown sources limits the ability to study procurement patterns and thus limits evaluation of how ancient peoples interacted with their environment and with each other. This can be quite a difficult problem to solve because it is possible that the sources no longer exist or no longer exist in a similar state as when the ancient people were using the source. Because of this, more work needs to be done in this area, first in expanding our geochemical knowledge of currently known sources and subsources, then by extensive fieldwork in collaboration with anthropologists to attempt to discover previously unknown sources, and, lastly, in compiling the work done in previous studies to make it accessible to archaeologists and anthropologists working in this region today.

4.1.3 Current project

In this study, geological samples from Kenya were collected and examined via neutron activation analysis to test our ability to distinguish between individual sources and to begin creating a database for future use. The preliminary results indicate that there is a clear correlation between geographic proximity and chemical composition. Most of the source groups can be distinguished by using simple bivariate plots, but a few groups, including possible subgroups, require three-dimensional plots using three elements to show clear separation. Thus far, the results have shown the potential for characterizing Kenyan obsidian based on the major and minor elements rather than trace elements, which has been demonstrated in previous studies.

4.2 Experimental methods

Samples of obsidian from the Central Rift Valley in Kenya were acquired over a period of several field seasons. Initially, one hundred samples from sources mostly centering around Lake Naivasha were obtained from Dr. Stanley Ambrose at the University of Illinois, which he had collected over several previous field seasons. An additional 405 samples were collected during eight-week field seasons in Kenya by Dr. Ambrose and two of his students in summer 2008 and 2009. I participated in collecting field samples in the 2008 field session. A total of 505 samples from various parts of the Central Rift Valley have been analyzed. A map showing the locations of the sources of these samples is shown in Figure 4.1.

Figure 4.1: Map of sampled locations of obsidian in the Central Rift Valley of Kenya

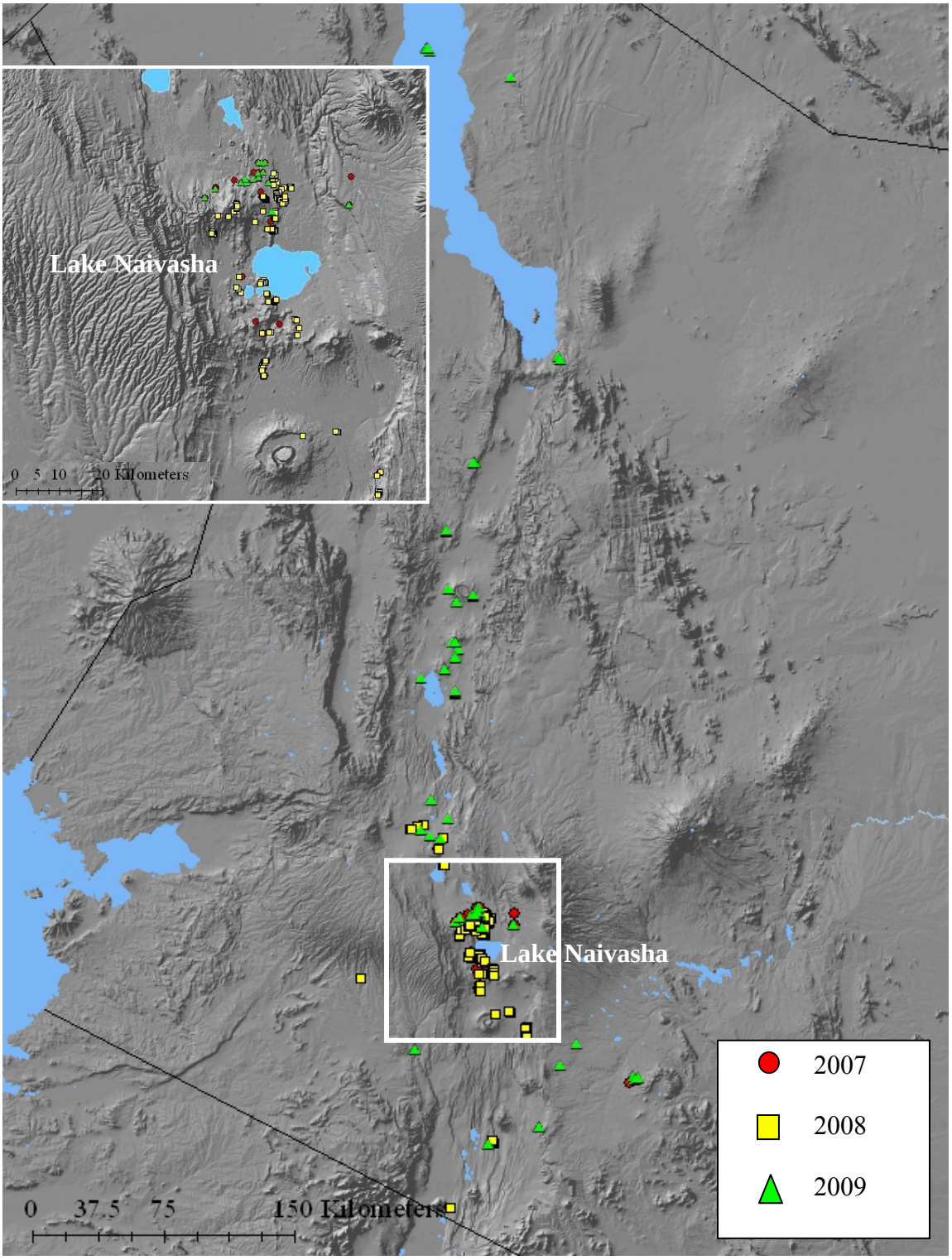

Neutron activation analysis was performed at the University of Missouri Research Reactor under the guidance of Dr. Michael Glascock. For the analysis of the source samples, previously developed procedures were used for sample preparation and analysis for both short and long irradiations. The relative concentrations of twenty-eight elements (Al, Ba, Ce, Co, Cs, Cl, Dy, Eu, Fe, Hf, K, La, Lu, Mn, Nd, Na, Rb, Sb, Sc, Sr, Sm, Ta, Tb, Th, U, Yb, Zn, and Zr) were determined by INAA at MURR. Concentrations of each element are determined by the comparator method. The standards used included NIST standards SRM-278 (obsidian) and SRM-1633a (fly ash). An additional standard, JJO, an obsidian source sample from the Alca source in Peru, was used as a quality control sample.

For short irradiation samples, samples of between 50 and 100 milligrams were weighed out into polyethylene vials. The vials were then subjected to a five-second irradiation, followed by a 25-minute decay and a 12-minute count. The elements determined from the short irradiations are aluminum, barium, calcium, dysprosium, potassium, manganese, sodium, titanium and vanadium.

Samples of between 100 and 200 milligrams were weighed out into quartz vials and sealed for the long irradiation and were placed into the reactor for a 70-hour irradiation. These samples are counted twice, once after a seven-day decay followed by a 33-minute count and again after a 28-day decay and a 168-minute count. The first count determines elements that have a mid-range half-life (including lanthanum, lutetium, neodymium, samarium, uranium and ytterbium) and the second count determines the elements that produce long-lived isotopes (cerium, cobalt, chromium, cesium, europium, iron, hafnium, nickel, rubidium, antimony, scandium, strontium, tantalum, terbium,

thorium, zinc and zirconium). All concentration data for the samples can be found in the Appendix 6.

Following data acquisition, the concentration values were standardized as described in Chapter 2. Then principal component analysis was applied to the standardized data set, using the Matlab© program. Results of the chemical analysis were then compared with the geographical locations for the characterization of geographical source groups.

4.3 PCA results

As described in earlier chapters, sourcing studies rely on being able to characterize the variance between source groups. In this study, data for over 30 elements was acquired for 505 samples and PCA was applied to this data set in order to extract the most information possible without having to go through each element and each sample individually. As discussed in Chapter 2, PCA can be used to determine how the variance is driven by each variable and how this can be used to distinguish between groups in the data set.

The eigenvalues vector was first examined to see which principal components described the most variance in the data set, which would focus the rest of the interpretation. As seen in Figure 4.2 below, the first three principal components describe almost 90% of the variance in the data. The Scree plot also starts to level off after the second PC. Hence, we concluded that the first three PCs can be used for examining the variance in the data set.

Figure 4.2 Scree plot from PCA results of the standardized Kenyan obsidian data

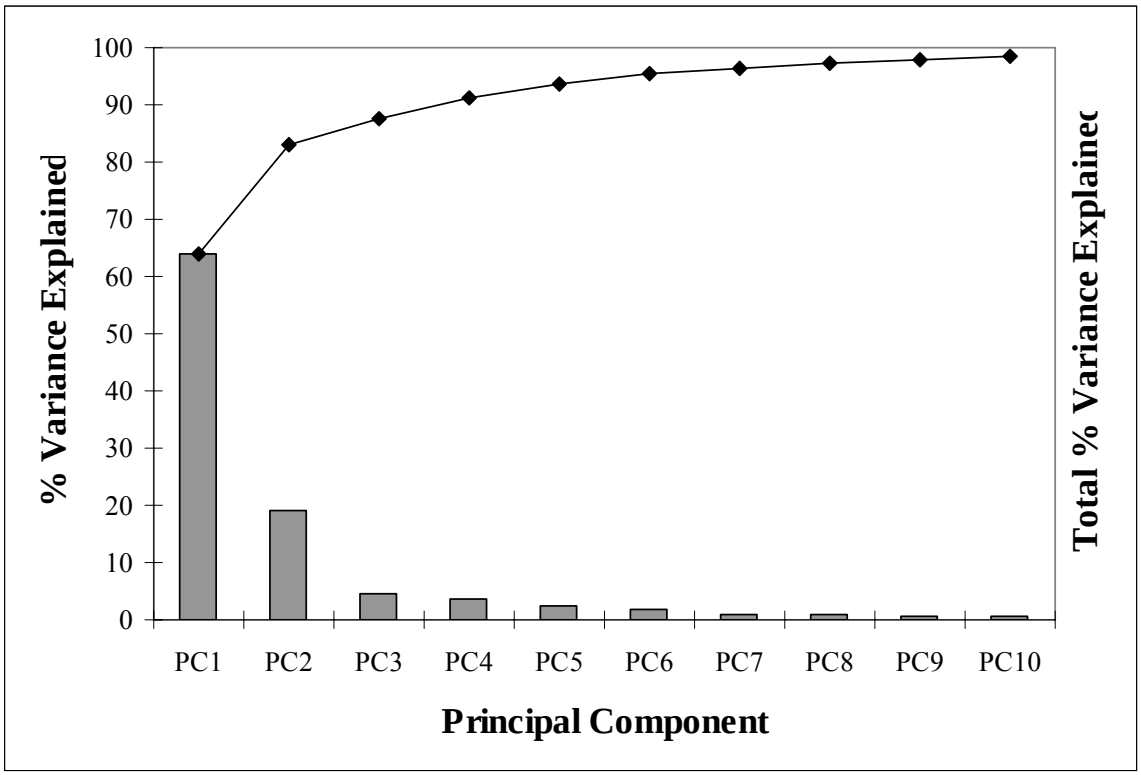

Next, a bar plot of the loadings was created to determine the influence of each element on the first three principal components (Figure 4.3). From this plot it can be seen that there is significant covariance among the rare earth elements, which drives the variance explained by PC1, while PC2 is more strongly influenced by many of the minor elements, such as iron, sodium, and manganese, as well as a few trace elements. As discussed earlier, Merrick and Brown had found with their analyses that the minor elements could be used to distinguish source groups and these results are consistent with their findings. Bivariate plots of elements that are not correlated but have a strong influence on either of the first two PCs might be enough to distinguish between source groups, since these elements drive the variance in the data set. For example, plotting iron

versus cesium has been found useful in separating most of the major groups in the data set (discussed in detail later). PC3 is influenced mostly by two of the major elements, aluminum and potassium, and to a smaller extent scandium.

Figure 4.3 Bar plot of loadings from PCA results of the standardized Kenyan obsidian data

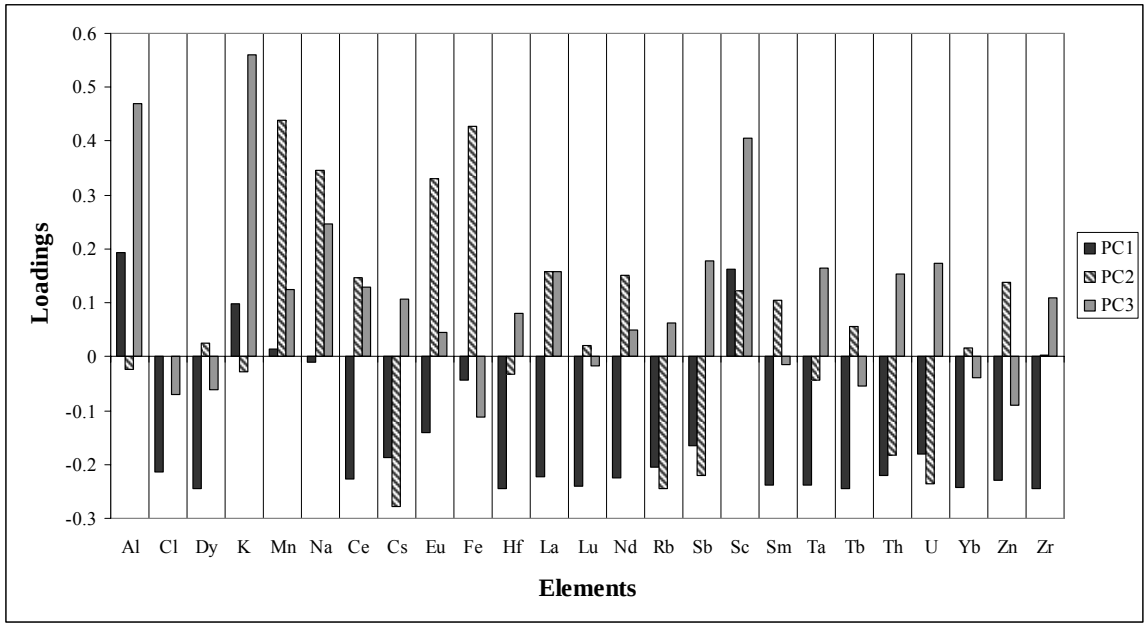

Since PC1 and PC2 seem to describe the majority of the variance in the data set, the scores for PC1 and PC2 were plotted to see if groups were discernible (Figure 4.4). Several large groups were quite noticeable in this evaluation. Other smaller groups were then distinguished on closer inspection of the plot. These groups represent samples that are similar to each other in multidimensional space and so have similar compositional patterns, which ideally are linked to geographical location. In addition, a few outliers were identified.

Figure 4.4 Scores plot from PCA results of the standardized Kenyan obsidian data

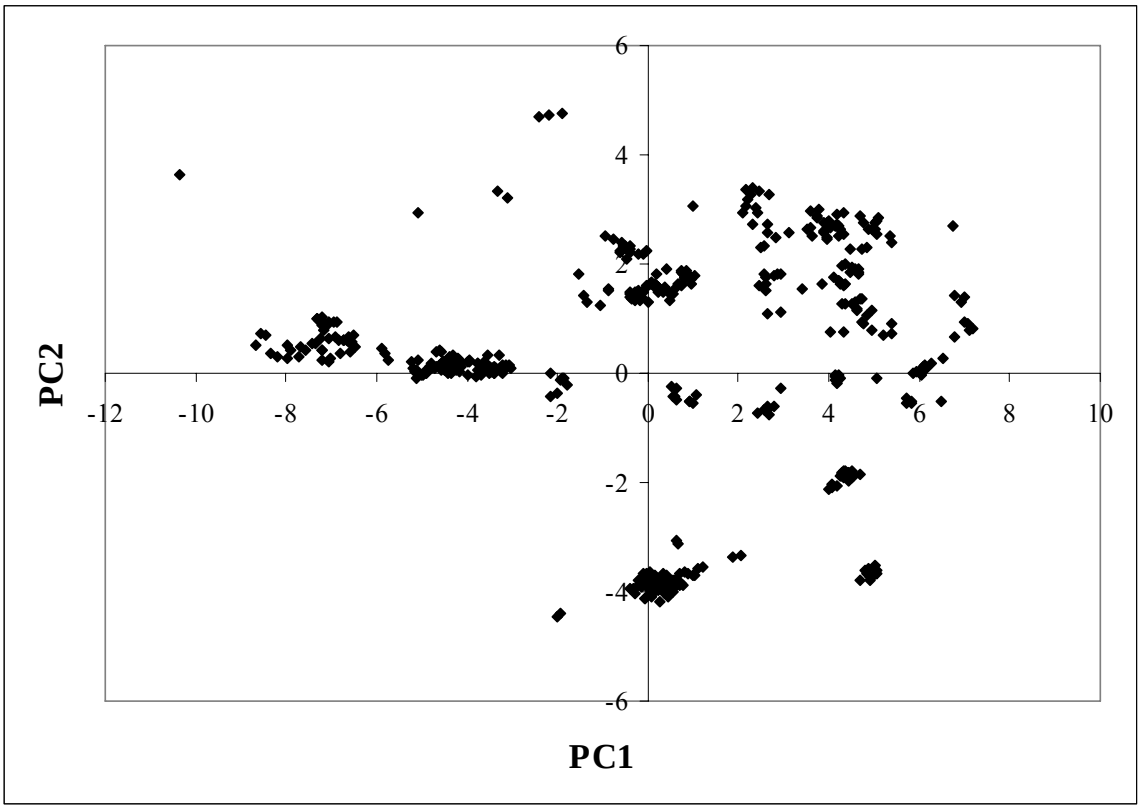

In order to transition to examining simple bivariate plots, which are most often used with artifacts to simplify the analysis, the loadings for PC1 and PC2 were projected onto the scores plot to determine which pairs of elements might be most useful in distinguishing source groups (Figure 4.5). This plot reiterates how many of the rare earth elements covary with each other and have a strong influence on PC1. It also shows more clearly the relationship between pairs of elements. Pairs of elements that have the potential to aid in distinguishing source groups are usually those that have little correlation between them. So, a plot of iron versus cesium (shown in the following section) would do well in distinguishing groups while a plot of iron versus manganese would not. Other pairs of elements that were considered were dysprosium versus iron,

thorium versus iron, cesium versus scandium, sodium versus scandium, and europium versus thorium.

Figure 4.5 Biplot of scores and loading vectors from PCA results of the standardized Kenyan obsidian data

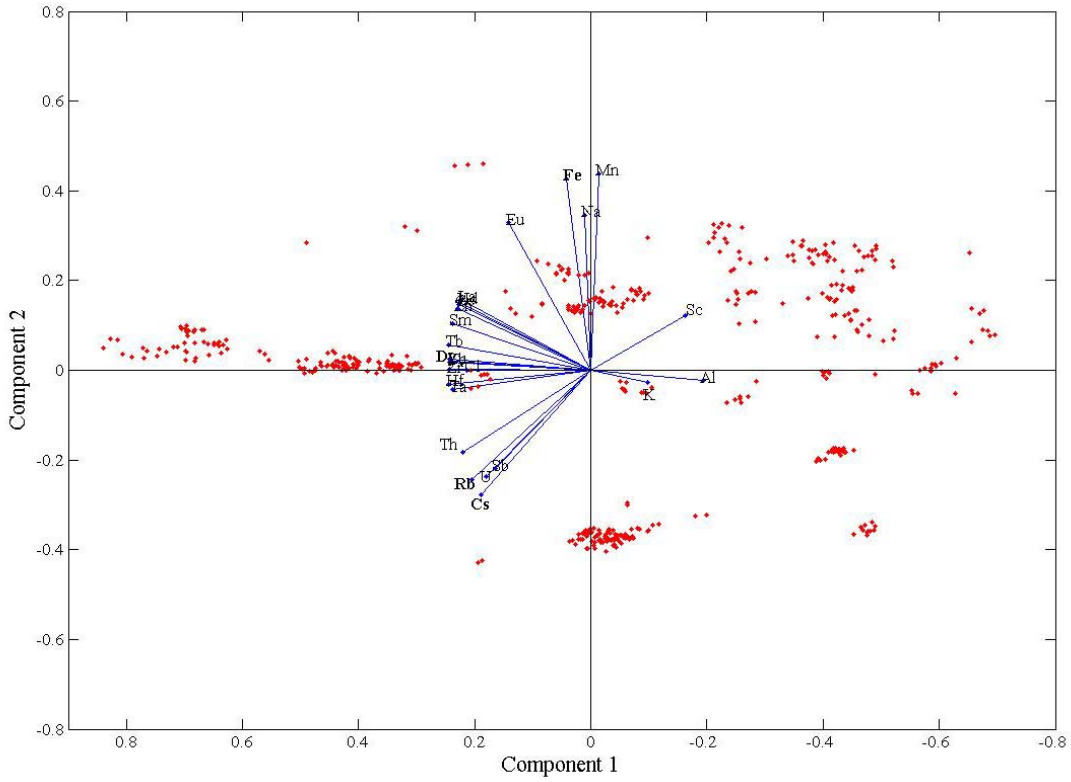

4.4 Characterizing geological source groups using elemental bivariate plots

From the results of the principal component analysis, an initial set of chemical source groups were created based on the samples that were similar to each other in multidimensional space. These initial groups, shown in the scores plot, Figure 4.6, were used as a starting point to characterize the geological sources of obsidian. The locations of these groups were then plotted on a map to examine the results when compared with the different geographical locations of the sources (Figure 4.7). As can be seen in Figure

4.7, several of the geological sources seem to have very similar compositions, even though they are in very different locations, while other sources that exist in close proximity are quite different in composition.

Figure 4.6: Initial groups, using scores plot from PCA results of the standardized Kenyan obsidian data

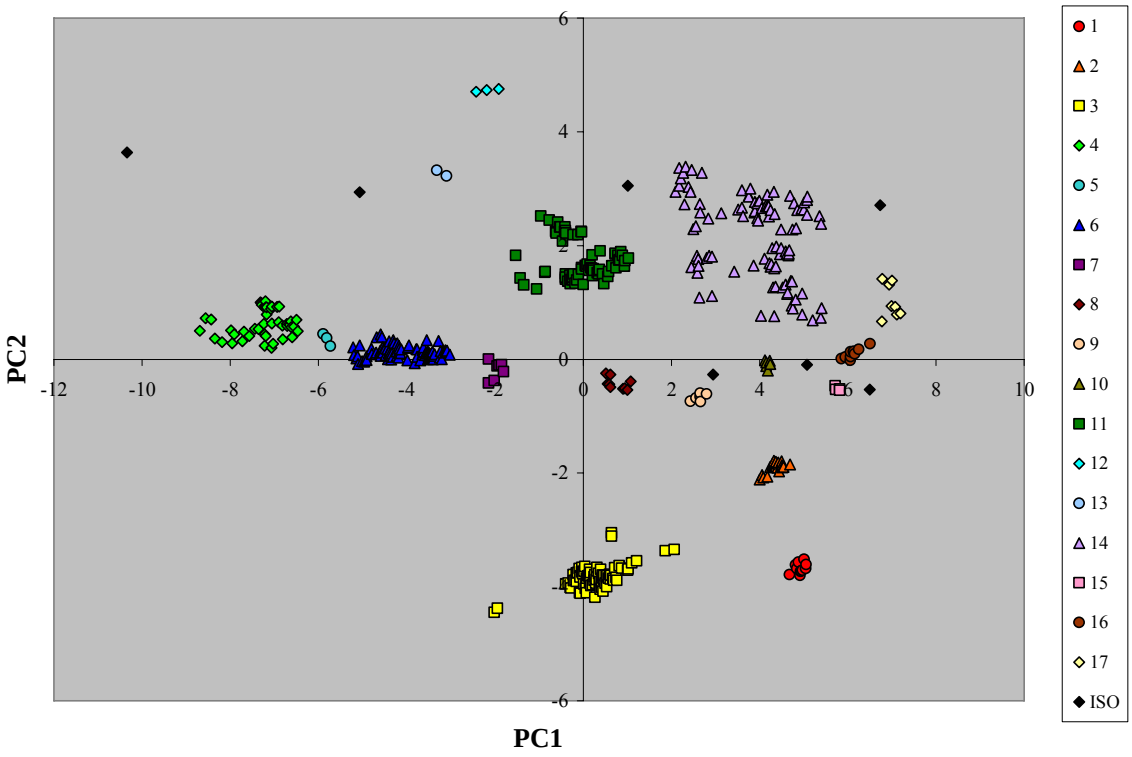

Figure 4.7 Map showing locations in Kenya of the initial chemical groups

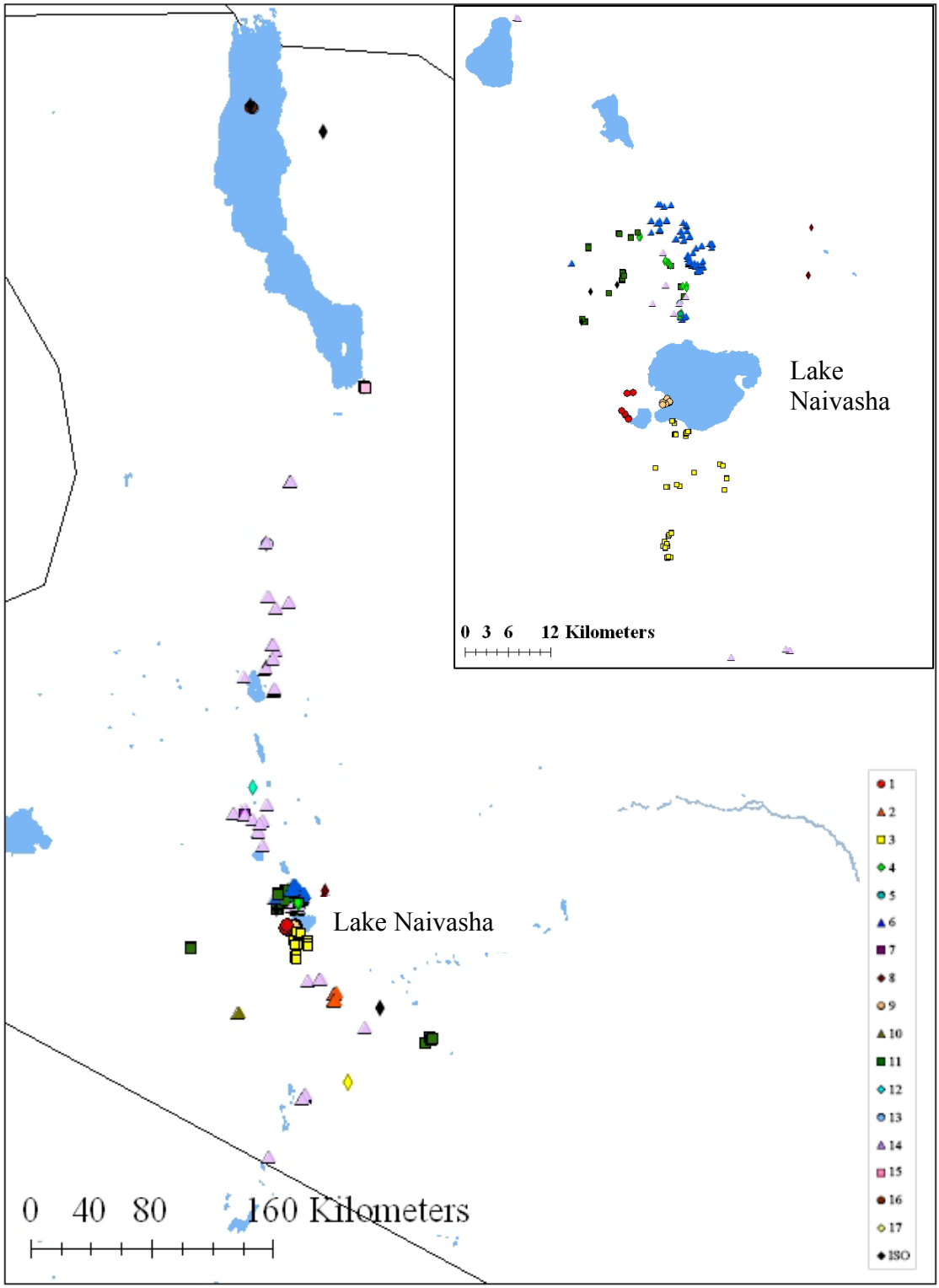

For finer separations of the geological source groups, several bivariate plots were used to distinguish between sources. In some cases, the difference in the composition of two source groups, even if they are quite distant from each other, can be only one or two elements. Starting with the groups found in the initial scores plot, the source groups were refined with each bivariate plot and the results were compared to the geographical locations of the sources. As soon as a group could be reliably distinguished from the rest of the samples, it was removed from the subsequent plots for clarity. In this way, some groups can be characterized using only one plot, while other groups take several bivariate plots to accurately characterize.

Elements for each bivariate plot were chosen based on the results of the PCA performed on the entire data set. The two-dimensional biplot shown above (Figure 4.5) was used to choose the best elements for the separation of each source group. Elements such as iron, cesium, thorium, and many of the rare earth elements have the potential to distinguish between groups, since they contribute significantly to the variance in the data set. The use of iron to distinguish between source groups was also supported by the literature, as many researchers working in this region found iron and other minor elements useful for characterization.[7-11, 15]

The following bivariate plots demonstrate the characterization of the groups using this method of analysis. The first of these is a plot of the standardized values for cesium versus those for iron (Figure 4.8). As seen in the plot, many of the original groups found in the plot of PC2 versus PC1 (shown in the same colors as above) are still visible and distinguishable. In fact, this plot can distinguish between many of the geographical source locations and finer separations can be made between source groups that previously

seemed very similar. For example, group 6 appeared in the scores plot to be one larger group. In Figure 4.8, however, three small groups are distinguishable. These finer separations were plotted on the map and confirmed the separation between source groups. However, there are still groups that are geographically distinct and cannot be distinguished using this elemental bivariate plot.

Figure 4.8: Plot of cesium versus iron using the standardized concentrations for the entire Kenyan obsidian data set

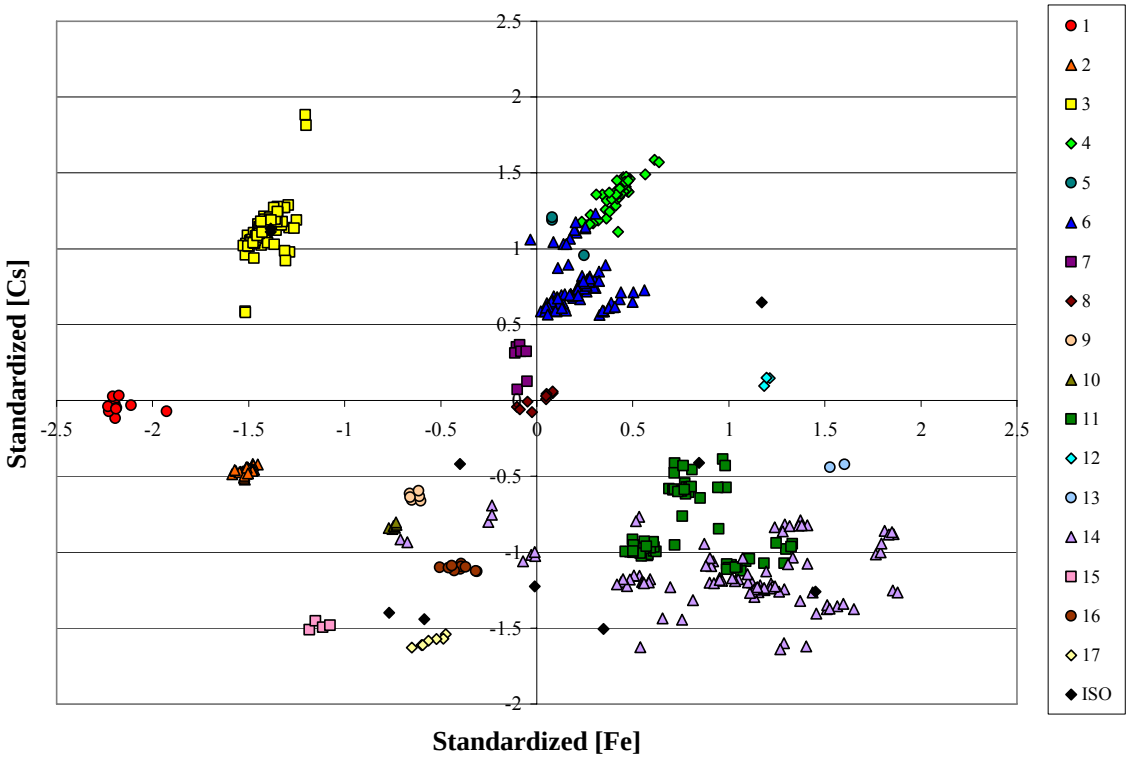

In order to better separate the geographical source groups contained in groups 11 and 14, additional bivariate plots are needed.

Groups 11 and 14, shown in Figure 4.8, overlap quite a bit, even though they are completely separated in the scores plot. Another bivariate was made using the

standardized concentrations of dysprosium versus cesium (Figure 4.9). In this plot, groups 11 and 14 are well separated and subgroups within each group are more easily visible. In group 11, there appear to be three subgroups (11, 18, 19). When plotted on a map, these three chemical subgroups appear as distinct geological sources (Figure 4.10). Subgroup 19 does seem to characterize two different geological sources, but it is possible that these two sources were formed during the same geological event. The samples would then have very similar compositions, as seen here, even though the sources are several kilometers apart.

Figure 4.9: Plot of dysprosium versus cesium, using standardized concentrations, showing the separation of group 11 into subgroups

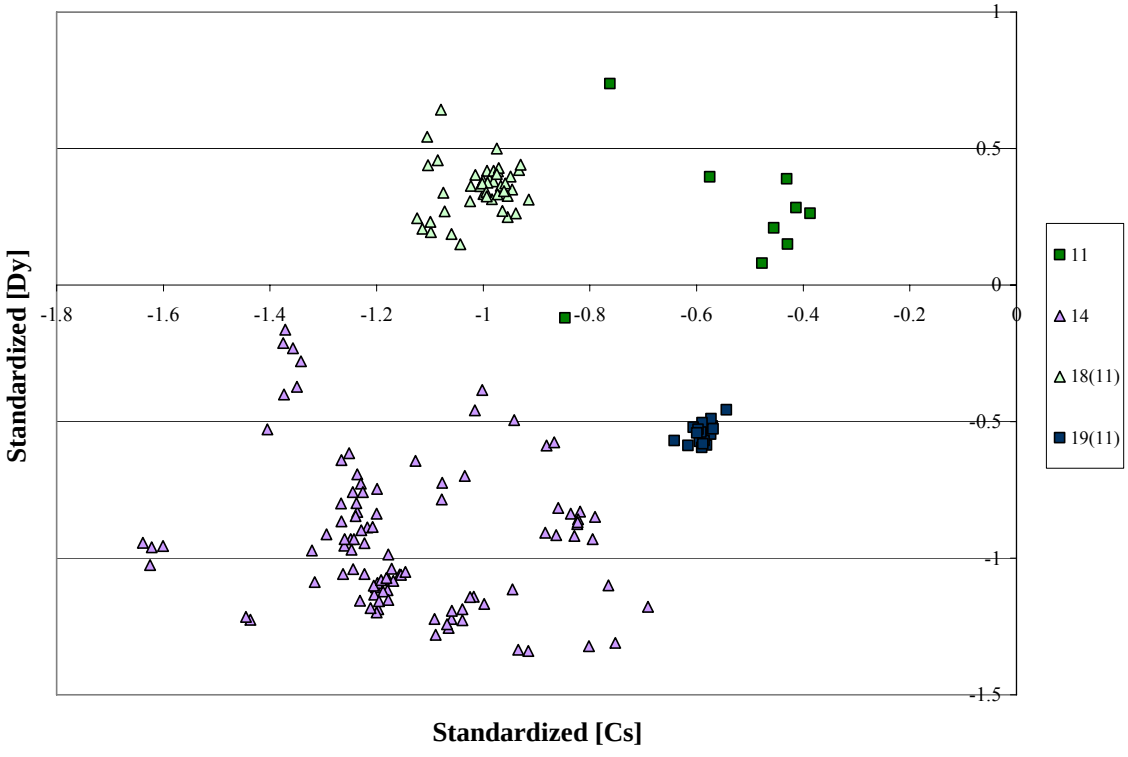

Figure 4.10: Map of the locations of chemical group 11 subgroups, identified on Figure 4.9.

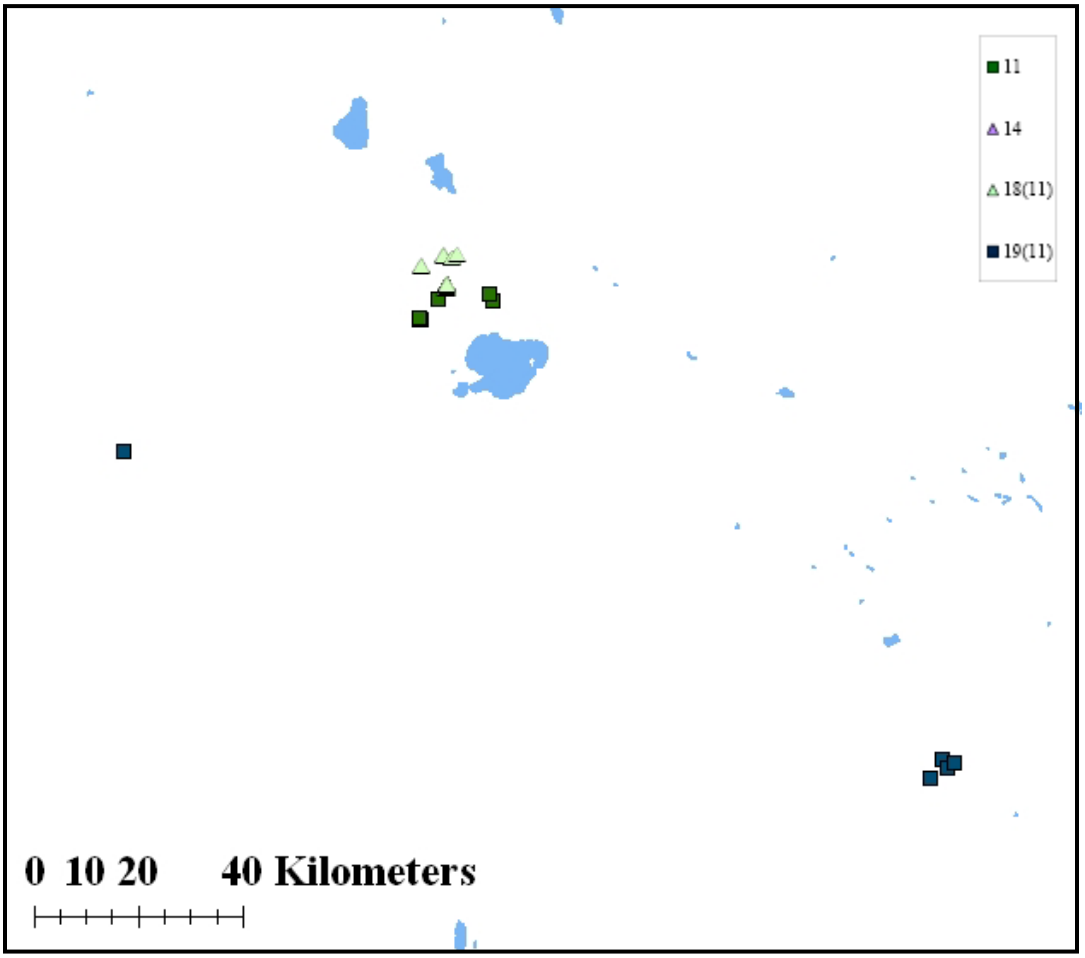

The last group to be characterized is group 14, seen in Figure 4.9 above. This group is spread out in many of the bivariate plots without forming distinct subgroups. Geographically, this group covers a large area and overlaps many of the other sources described above. To further examine this "source group", PCA was performed on this subset of samples which contained 110 samples. While one must exercise caution in employing PCA on small sample sets, this analysis provided information about which elements contribute most to the variance in this small subset. From the results of the loadings plot (Figure 4.11), it seems that antimony and scandium play more of a role in the variance described by the first two principal components for this set of samples than in the entire data set. Other elements that had played a larger role before, such as cesium and dysprosium, play a much smaller role here, which is why good separation was not achieved with the previous bivariate plots. A plot of antimony versus iron shows good separation between subgroups within group 14 (Figure 4.12) and these groups match up relatively well geographically (Figure 4.13).

Figure 4.11: Loadings plot for group 14 of the Kenyan obsidian data set

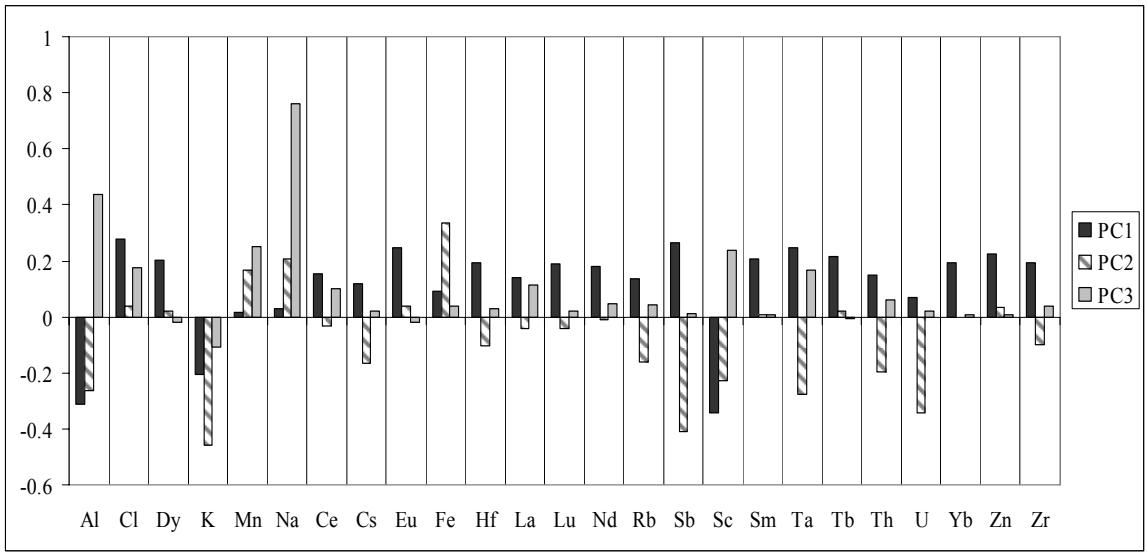

Figure 4.12: Plot of antimony versus iron, using standardized concentrations, for group 14 of the Kenyan obsidian data set

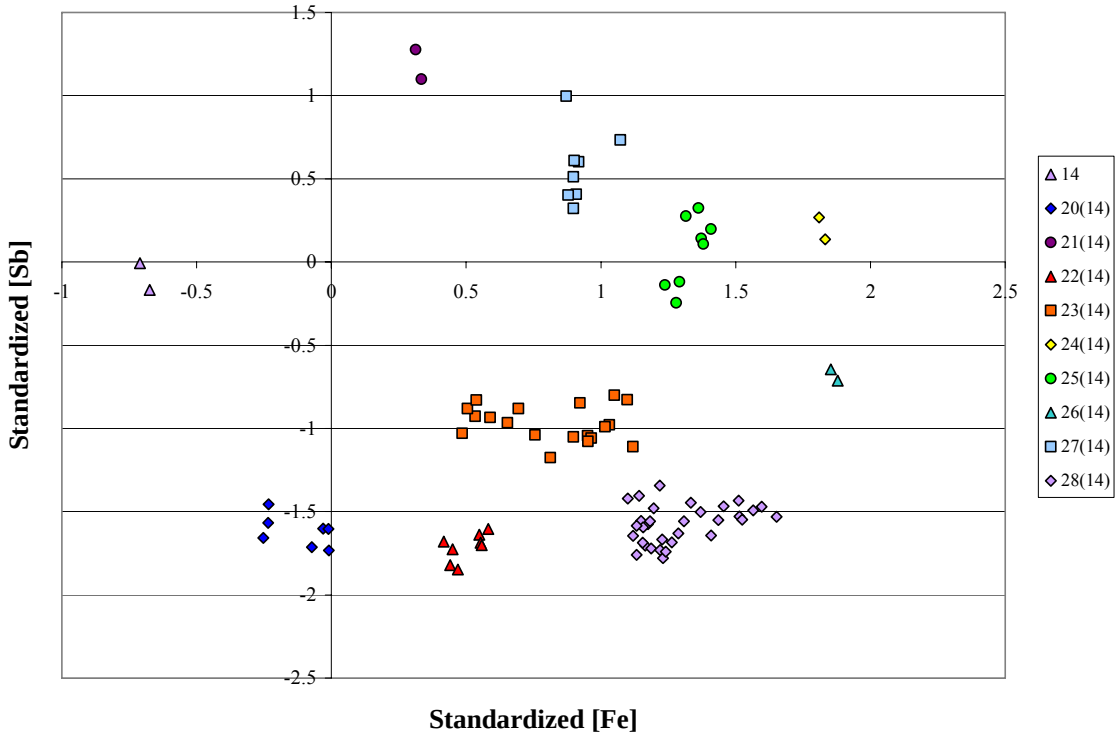

Figure 4.13: Map of subgroups of group 14 identified in Figure 4.12

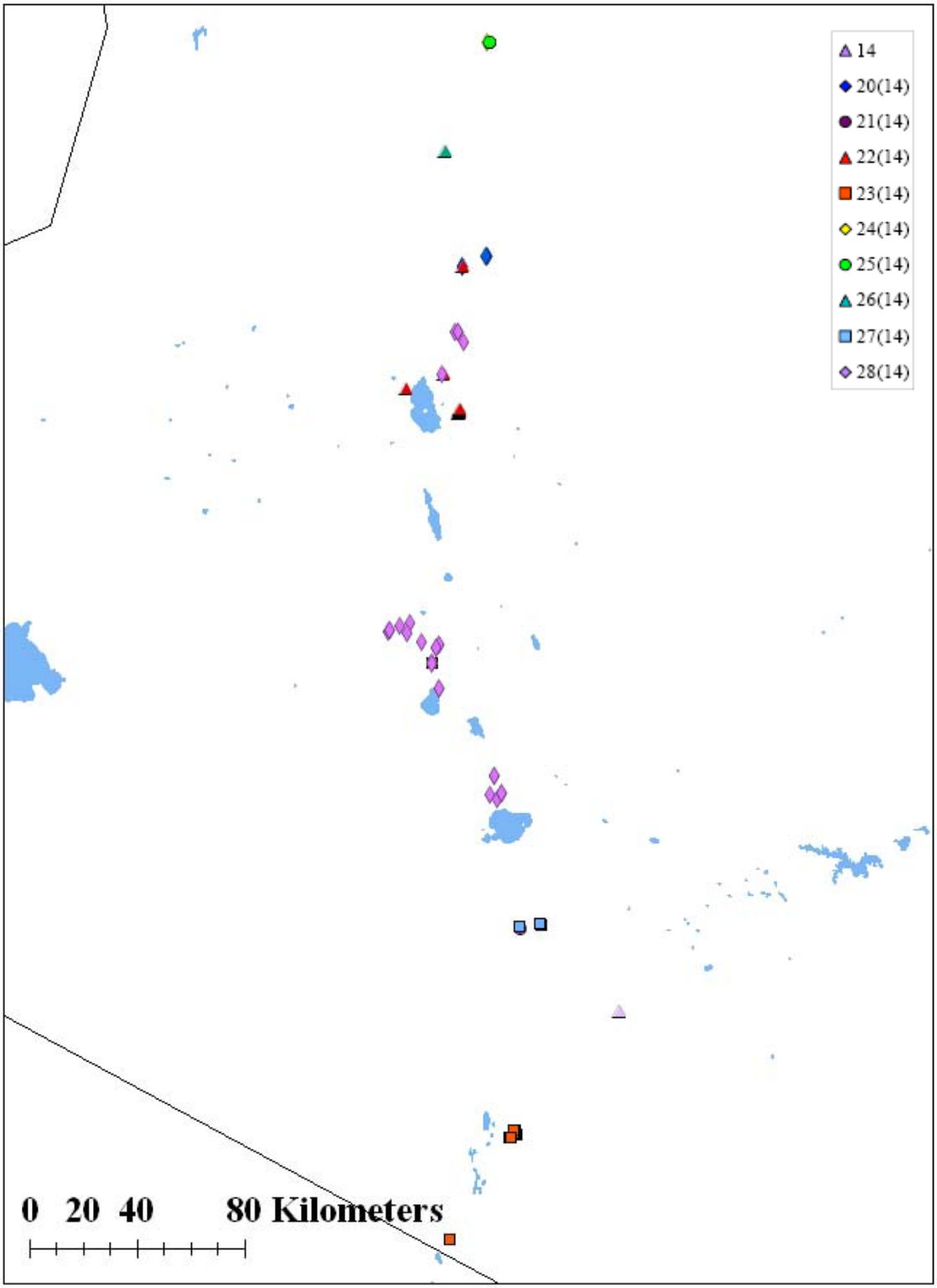

Though Figure 4.12 shows good separation between most of the subgroups, there is still one subgroup, 28(14), that seems to represent three geographically distinct source groups. This subgroup can be further divided into three groups using a plot of uranium versus thorium, two additional elements that play a large role in the first two principal components (Figure 4.14). These smaller groups match up well with the geographical locations (Figure 4.15).

Figure 4.14: Plot of uranium versus thorium, using standardized concentrations for group 14, subgroup 28

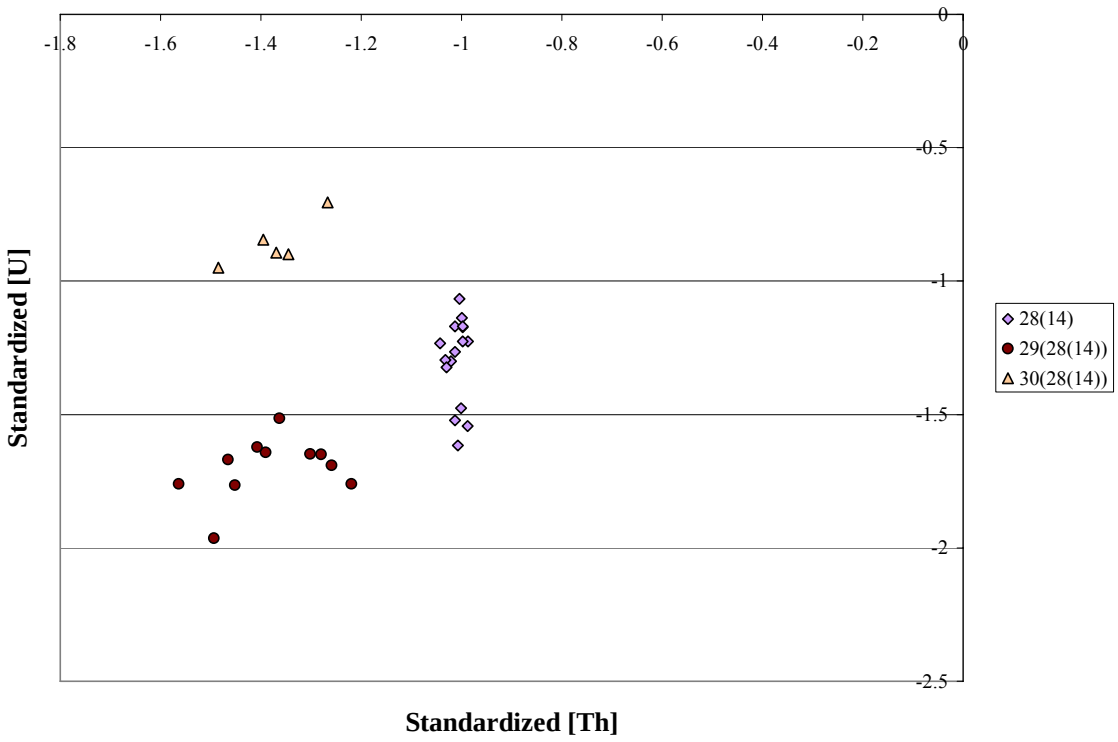

Figure 4.15: Map of subgroup 28 for group 14, identified in Figure 4.14

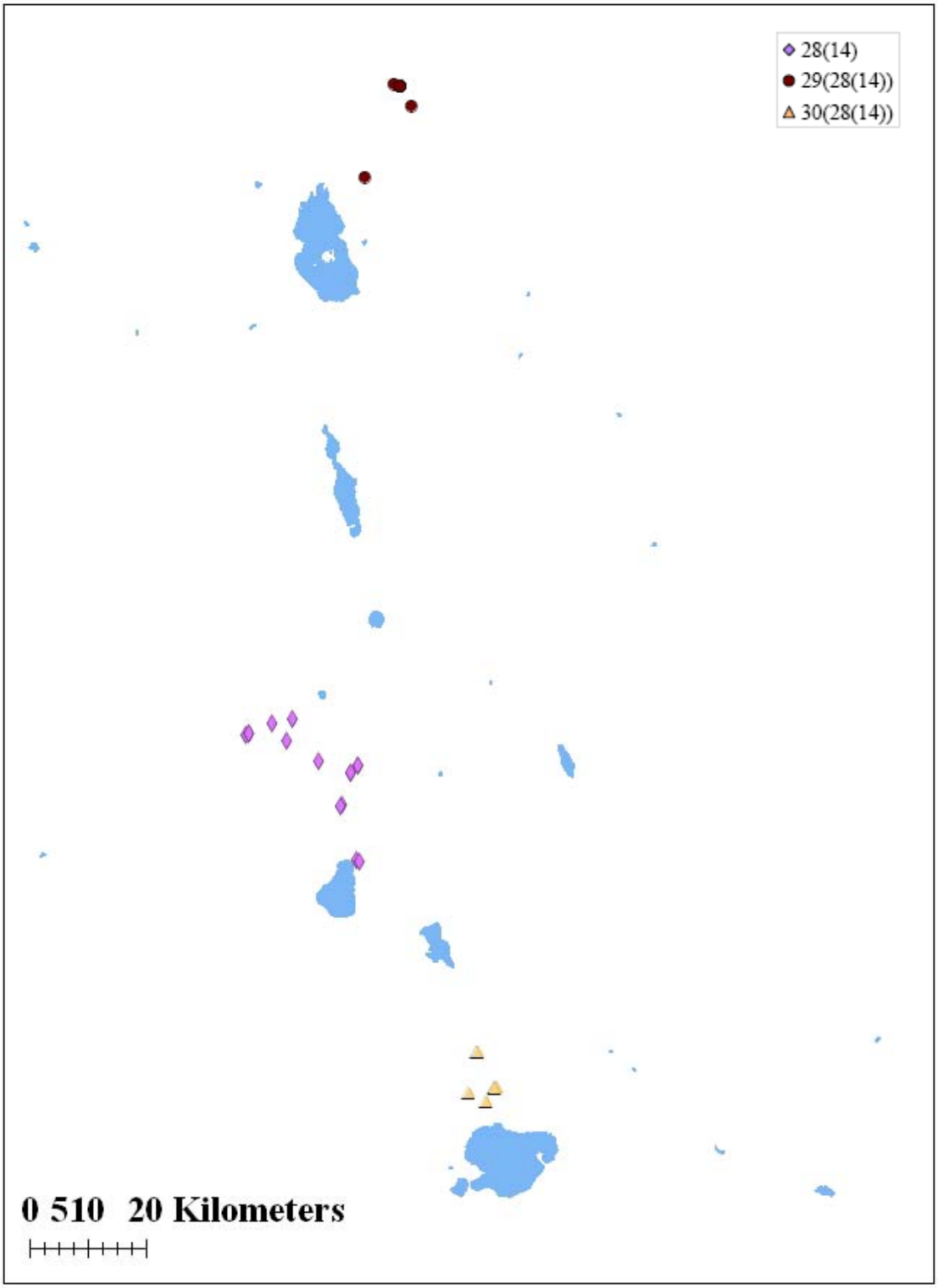

4.5 Conclusion

Through this study, it has been demonstrated that obsidian from the Central Rift Valley in Kenya follows the provenance postulate. Over 25 chemically-distinct sources were characterized from over 40 geographically-distinct sources. Many of the major source groups can be distinguished using one elemental bivariate plot, but a few sources, including several subgroups within those sources, require a series of bivariate plots to characterize them completely. As work on obsidian from this region continues, more samples will allow for additional refinement of known source groups as well as provide information on "new" sources. As this data set is continually added to and refined through collaboration with researchers working in this region, the results can be applied to archaeological and anthropological research to answer questions about the origin of modern humans and their interactions with each other and the environment.

References

1. M. D. Glascock, G. E. Braswell and R. H. Cobean, in *Archaeological Obsidian Studies*, ed. M. S. Shackley, Plenum Press, New York, 1998, ch. 2, pp. 15-65.
2. V. Bouska, *Natural Glasses*, Ellis Horwood, New York, 1993.
3. L. Wilson, Pollard, A.M., in *Handbook of Archaeological Science*, eds. D. R. Brothwell and A. M. Pollard, John Wiley & Sons, Ltd., New York, 2001, ch. 41, pp. 507-517.
4. M. S. Shackley, *Obsidian: Geology and Archaeology in the North American Southwest*, The University of Arizona Press, Tucson, 2005.
5. C. Renfrew, in *Exchange Systems in Prehistory*, eds. T. Earle and J. Ericson, Academic Press, New York, 1977, ch. 4, pp. 71-90.
6. S. H. Ambrose, *Journal of Human Evolution*, 2006, **50**, 365-369.
7. H. V. Merrick and F. H. Brown, *Archaeometry*, 1984, **26**, 230-236.
8. H. V. Merrick and F. H. Brown, *The African Archaeological Review*, 1984, **2**, 129-152.
9. A. Negash, M. Alene, F. H. Brown, B. P. Nash and M. S. Shackley, *Journal of Archaeological Science*, 2007, **34**, 1205-1210.
10. A. Negash and M. S. Shackley, *Archaeometry*, 2006, **48**, 1-12.
11. A. Negash, M. Steven Shackley and M. Alene, *Journal of Archaeological Science*, 2006, **33**, 1647-1650.
12. I. D. Muir, F. Hivernel and J. H. Scoon, *Journal of Archaeological Science*, 1976, **3**, 211-217.
13. S. H. Ambrose, in *Settlement Dynamics of the Middle Paleolithic and Middle Stone Age*, ed. N. J. Conrad, Kerns Verlag, Tubingen, 2001, ch. 2, pp. 21-43.
14. S. H. Ambrose, in *The Dating and Provenance of Obsidian and Ancient Manufactured Glasses*, eds. C. Stevenson, W. R. Ambrose and I. Liritzis, University of New Mexico Press, Albuquerque, In Press.
15. H. V. Merrick, F. H. Brown and W. P. Nash, in *Society, Culture, and Technology in Africa*, ed. S. T. Childs, MASCA, Philadelphia, 1994, pp. 29-44.

CHAPTER 5:

A NEW EPITHERMAL NEUTRON ACTIVATION ANALYSIS METHOD FOR TITANIUM AND BARIUM ANALYSIS IN OBSIDIAN

5.1 Introduction

Though NAA and XRF have been the most common analytical techniques used in sourcing studies for obsidian, other techniques, such as electron microprobe analysis, have been used. Each of these techniques varies with the elements that can be determined and the sensitivity for those elements. Even though standard thermal NAA is sensitive for many of the elements used for obsidian analyses, there are some elements that require a different analysis procedure in order to achieve accurate and precise results. By examining alternate neutron-induced reactions for the analysis, not only can better results be achieved for currently measured elements, but the list of measurable elements can be expanded to include those that are usually more difficult to quantify.

5.1.1 The challenge

Previous work has described the use of such elements as titanium and barium to distinguish between chemical source groups of obsidian in several areas of the world, including Kenya. The two most common techniques used for these studies have been

electron microprobe analysis (EMPA) and x-ray fluorescence (XRF). In many cases, a combination of the two has been used, such as in Merrick and Brown's work.[1-2]

However, a concern arises about the use of these two techniques for the analysis of titanium and barium. Both of these methods are based on the emission of secondary x-rays from the sample to characterize the chemical composition. The typical x-ray line used for titanium analyses is the K-line at 4.51 keV. This falls very close to the x-ray line normally used for barium analysis, the most intense L-line at 4.47 keV. A resolution of better than 40 eV is needed in order to clearly separate these peaks. Many XRF and EMPA instruments use energy-dispersive detection systems which have resolutions of several hundred eV, which means that the peaks would be overlapping, as seen in Figure 5.1.

Figure 5.1: Titanium (K) and barium (L) lines in a typical EDXRF spectrum.

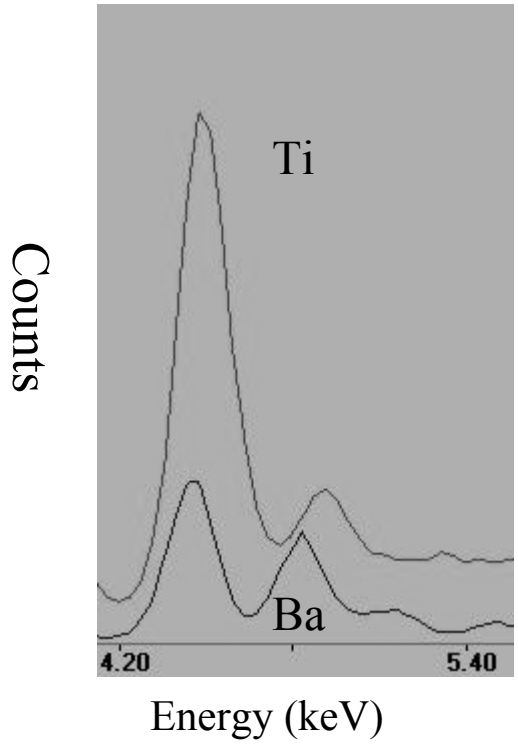

However, there are also many instruments for both techniques that use wavelength-dispersive detection systems, where the resolution can be on the order of 5-10 eV. This would easily separate the two peaks and greatly simplify the quantification of barium and titanium. Because concentrations of barium in obsidian can range up to several hundred parts per million, the overlap of the peaks becomes an important consideration. If the peaks cannot be resolved, then there would be a contribution of barium to the titanium peak, causing an inflated value for titanium.

In many of the previous studies, however, the type of instrument is not mentioned.[1-2] In addition, any calculations used to take this interference into account are not described and a list of which elements were determined by which technique is not given. It cannot be assumed that wavelength-dispersive instruments were used, so a way of independently verifying the previous results is needed to ensure the accuracy of the values included in a large database.

Neutron activation analysis (NAA) is a good candidate as a verification method. Since it is based on nuclear reactions (as described in Chapter 1), there is no interference experienced between the titanium and the barium in the analysis. It is matrix-independent and has many tunable parameters that can be utilized to get the best results possible. A method using NAA to determine the titanium and barium concentrations in obsidian would work well to verify the results previously attained, especially in Kenyan obsidian. These results could then also be used in conjunction with the results achieved from the standard NAA procedure to allow us to make direct comparison to previous studies.

Currently there is no method in place at MURR for the analysis of titanium in obsidian and the current method for barium suffers from poor precision over much of the concentration range observed. New methods need to be developed to determine titanium and barium with good accuracy and precision. In this chapter, the new methodology that has been developed will be described. For each element, the limits of detection have been calculated and the precision is evaluated using the relative standard deviation. This new methodology offers better precision and low detection limits for the analysis of barium and titanium and also provides a way to expand the current list of elements that can be determined in obsidian.

5.2 Development of the new methodology

To obtain better results for barium and titanium in obsidian than is achievable with the current method, alternate neutron-induced reactions need to be considered, in particular those using epithermal or fast neutrons. These reactions are typically not used because they are usually masked by the activity generated from the thermal neutron reactions. In most cases, the thermal neutron cross sections are larger than the fast and resonance reactions and thermal neutrons dominate the spectrum; they make up about 90% of the neutron flux in the graphite moderated irradiation positions. The number of these reactions can cause a large background in the gamma spectrum that overwhelms the peaks from isotopes formed via epithermal and fast neutron activation.

However, using a boron or cadmium shield around the samples can reduce the thermal neutron flux reaching the samples and thus reduce the number of thermal neutron reactions taking place. At MURR, a boron shield is often used for short irradiations,

while a cadmium can is used for longer irradiations. Boron and cadmium both have large cross sections for thermal neutrons and much smaller cross sections for the higher-energy neutrons. Cadmium, in particular, is very efficient at absorbing neutrons with energies lower than 0.5 eV.[3-4] At greater energies, the ability for cadmium to absorb the neutrons drops off precipitously. This makes cadmium a good choice for specifically filtering thermal neutrons while allowing the epithermal and fast neutron fluxes to remain relatively high. For cadmium-covered irradiations, a standard aluminum canister (3.35 in x 10 in) has been lined with 40 mils (0.040 in or 1.016 mm) of cadmium.[5]

Epithermal and fast neutron activation analysis has been shown to greatly increase the sensitivity for the analysis of many elements in geological materials.[3, 6-9] By reducing the thermal flux, and thus reducing the Compton due to the many abundant isotopes that react via thermal (n,γ) reactions, the sensitivity for many of the trace elements can be improved usually by factors of 2-5.[7] Here, methods for the analysis of titanium and barium using epithermal neutron activation analysis (ENAA) will be considered as well as the standard thermal NAA procedures for the best sensitivity.

5.2.1 Titanium

For titanium, several reactions can be considered. First, the only (n,γ) reaction to result in a radioactive isotope of titanium was examined. Here, Ti-50, which has a natural abundance of 5.18%, reacts with thermal neutrons to produce Ti-51 ($t_{½}$ = 5.76 min, Eγ = 320.1 keV).[10] If this reaction was used for the measurement of titanium, it could be incorporated into the current short-irradiation procedure, since the half-life of Ti-51 is relatively short. However, the cross section for Ti-50 for thermal neutrons is

0.1795 barns.[10] This is relatively small, meaning that not much activity is produced during the irradiation. In fact, in examining the spectrum for an obsidian standard, NIST SRM-278, which has a titanium concentration of 1470 ppm, the peak for Ti-51 is barely visible above background. If the concentration of titanium was smaller than this, as for another standard, JR-1 ([Ti] = 660 ppm), then a peak would not be distinguishable from background. Thus, other reactions and methodologies must be considered.

Titanium can also undergo several different reactions when the isotopes react with fast neutrons. One potential reaction is the (n,p) reaction on Ti-46 to produce Sc-46. Ti-46 has a natural abundance of 8.25% and a fast reaction cross section of 12.5 millibarns.[10] Sc-46 has a half-life of 83.79 days, which would make it a good candidate for a long-irradiation procedure that is followed by a longer count time. However, Sc-46 is also produced via an (n,γ) reaction from Sc-45 (100% abundant, $\sigma_{thermal}$ = 17.4 b, $\sigma_{epithermal}$ = 7.0 b).[10] Since there is usually some scandium present in obsidian and other geological samples, there is no way to distinguish the activity from scandium from the activity due to the reaction with titanium.

Another fast neutron reaction is the (n,p) reaction on Ti-47 to form Sc-47. Ti-47 has a natural abundance of 7.44% and a fast neutron cross section of 20.0 mb.[10] Sc-47 has a half-life of 3.35 days, which would work well for a long irradiation followed by a longer count time. The only concern with this reaction is that Sc-47 is also produced via the beta decay of Ca-47, which decays at a similar rate as Sc-47 ($t_{½}$ = 4.54 days for Ca-47).[10] Ca-47 is produced via an (n,γ) reaction on Ca-46, which has a 0.004% abundance and a thermal cross section of 0.74 b. Ca-47 also emits several gamma rays, the most abundant of which is at 1297.09 keV (71.00%). However, since calcium concentrations

in obsidian are usually less than 0.5% and the abundance of Ca-46 is so low, this interference should be minimal. However, peaks in the gamma spectrum due to the decay of Ca-47 can be monitored for their presence or absence.

The last option for a fast-neutron reaction is an (n,p) reaction on Ti-48 to make Sc-48. Titanium-48 is the most abundant isotope of titanium at 73.72%. The product, Sc-48, has a half-life of 43.67 hours, and has two gamma rays that are 100% abundant at 983.52 keV and 1312.10 keV. However, the cross section for the (n,p) reaction with fast neutrons on Ti-48 is only 0.315 millibarns.[10]

Production rates for all three (n,p) reactions were calculated to quantitatively compare them. Table 5.1 shows a summary of these calculations. As can be seen in the table, the reaction Ti-47 (n,p) Sc-47 produces the greatest amount of activity, mostly due to the larger cross section. This reaction was chosen as the best to use for the quantification of titanium using this method, but the Ti-48 (n,p) Sc-48 was also monitored in the spectrum.

Table 5.1: Production rates for fast neutron reactions of titanium using 200 mg of SRM 278 ([Ti]=1470 ppm), a fast neutron flux of 1.50 x 10^{12} n $cm^{-2}s^{-1}$, and an irradiation time of 48 hours[10]

	Ti-46 (n,p) Sc-46	**Ti-47 (n,p) Sc-47**	**Ti-48 (n,p) Sc-48**
Target Abundance	8.25 %	7.44 %	73.72 %
Target cross section	12.5 mb	20 mb	0.315 mb
Half-life	83.79 days	3.35 days	43.67 hours
Saturation Activity	5.74 x 10^3 Bq	8.28 x 10^3 Bq	1.29 x 10^3 Bq
Activity at end of irradiation	94.1 Bq	2.8 x 10^3 Bq	689 Bq

5.2.2 Barium

Currently, the standard procedure to measure barium in the Archaeometry Group at MURR uses the thermal neutron Ba-138 (n,γ) Ba-139 reaction. Ba-138 is the most abundant isotope of barium (71.69%) and has a thermal neutron cross section of 0.36 barns.[10] Ba-139 has a half-life of 83.06 minutes and emits a gamma ray at 165.85 keV (23.70%). The current procedure determines the concentration of barium as part of the short-irradiation procedure, where the samples are irradiated for 5 seconds, allowed to decay for 25 minutes, and then counted for 12 minutes. However, because Ba-138 has such a low cross section, not much Ba-139 is produced during the short irradiation. In addition, the half-life of Ba-139 is so long compared to the counting time and the gamma ray emitted has a low abundance that very little is detectable above background. This method suffers from poor precision, especially when the concentration of barium in the sample is low. This method could be improved by irradiating the sample for a longer period of time as well as counting it for longer as well. Alternate methods using a Cd covered irradiation were explored.

One reaction that was of great interest was Ba-130 (n,γ) Ba-131. Ba-130 is a less abundant isotope of barium (0.106%) but has a thermal cross section of 8.8 barns and a resonance cross section of 184. barns.[10] Ba-131 has a half-life of 11.5 days, making it suitable for a procedure using a longer counting time, and the most abundant gamma ray has an energy of 496.33 keV (47.00%). With a cadmium can reducing the thermal flux reaching the samples, the large resonance cross section can be utilized to produce a strong signal for Ba-131. So, even though the abundance of the target isotope is low, this

reaction can produce results at least ten times better than the reaction using Ba-138 as the target.

5.3 Initial experiments

The initial experiments to test this new methodology used a cadmium can to reduce the thermal neutron flux and take advantage of the larger cross sections for the epithermal and fast neutron reactions. Several standards and samples were analyzed to explore a wide range of concentrations for titanium and barium. A procedure resembling the standard long-irradiation procedure was used to provide the longer irradiation times and longer counting times necessary. From the results, the accuracy and precision were evaluated for each method and the limits of detection were calculated.

5.3.1 Standards and samples

In order to demonstrate the new methods for a wide range of concentrations of barium and titanium, several different standards and samples were prepared. The standards included NIST SRM 278 (obsidian), USGS AGV-1 (andesite), JGS JA-1 (andesite), JGS JB-2 (basalt), JGS JR-1 (rhyolite), and NIST SRM1633a (fly ash). The concentrations of titanium and barium in these standards are found in Table 5.2.

Table 5.2: Concentrations of titanium and barium in NIST, USGS, and JGS standards[10]

Standard	Titanium (ppm)	Barium (ppm)
NIST SRM 278 (obsidian)	1470	881.
USGS AGV-1 (andesite)	6340	1221
JGS JA-1 (andesite)	5100	311
JGS JB-2 (basalt)	7100	222
JGS JR-1 (rhyolite)	660	50.3
NIST SRM 1633a (fly ash)	8230	1320

As well as the standards, obsidian samples from well-characterized sources in Central and South American were also analyzed to examine the ranges of barium and titanium concentrations found in obsidian. These included samples from Guadalupe Victoria, Otumba, Paredon, El Paraiso, and Pico de Orizaba. In addition, several flux wires were placed inside the cadmium can with the samples to measure the thermal and fast neutron fluxes. For the analyses, two hundred milligrams of each sample was weighed out and sealed into a high-purity quartz vial.

5.3.2 Irradiation, decay, and counting procedures

In order to achieve the best possible results for these analyses, a modified long-irradiation procedure was used. Samples were irradiated in a cadmium can in the reactor for 48 hours. Then, because the final total activity of the samples after irradiation was unknown, the samples were allowed to decay for 7 days. Because the samples were not as radioactive from this cadmium-covered irradiation as they would be after a typical long irradiation, subsequent analyses allowed the samples to decay for only 5 days. Then the samples were counted on an HPGe detector to acquire the gamma spectra. The samples were counted for 30 minutes each, 5 inches away from the detector. Dead times for the detectors were kept below 15%, usually ranging between 5 and 10%.

5.3.3 Gamma spectra and determination of precision and limits of detection

The results from the first experiment showed marked improvement over traditional NAA methodologies. The cadmium can reduced the thermal flux by about a factor of 10, which allowed the peaks emitted from isotopes resulting from epithermal

and fast neutron reactions to be observed. Limits of detection were lowered and precision was greatly improved. Figure 5.2 shows the comparison between the gamma spectrum acquired during a standard NAA procedure and one acquired after irradiation in the cadmium can for NIST SRM 278 (obsidian). As seen in the spectrum, the activity due to thermal neutron reactions was significantly reduced and allowed gamma peaks resulting from epithermal and fast neutron reactions to be detectable.

Figure 5.2: Comparison of the gamma ray spectrum from the standard NAA procedure and the epithermal NAA procedure

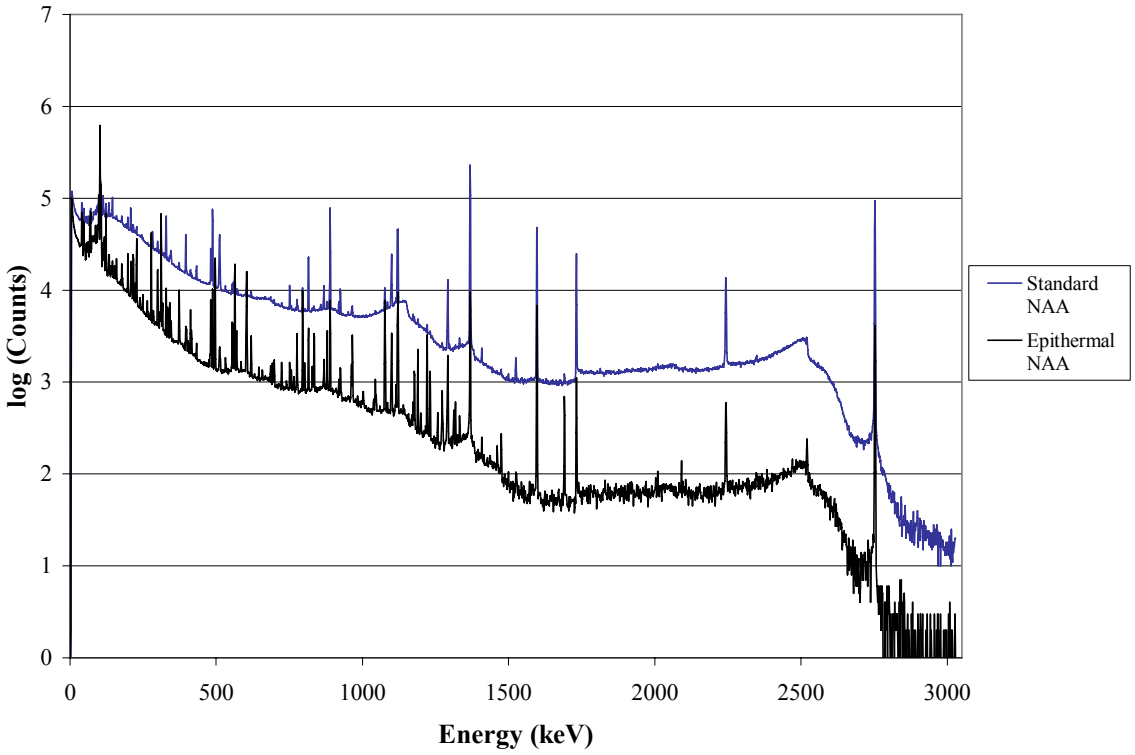

5.3.3.1 Titanium results

After examining the results from this initial analysis, the Ti-47 (n,p) Sc-47 reaction was chosen for the analysis of titanium in the sample. As expected, the lower cross section of Ti-48 caused less Sc-48 to be produced, so the peak was not visible above the background. A clear peak was, however, seen for Sc-47 in all the samples analyzed, even those with lower titanium concentrations.

One concern, as stated above, is that Sc-47 is also produced from the beta decay of Ca-47. To examine this potential interference, the gamma peak for Ca-47 at 1297.09 keV was followed in the spectrum. However, because of the small abundance and low cross section of the target isotope, Ca-46, very little Ca-47 activity is produced. The gamma-ray peak due to Ca-47 was not observed in any of the standards or samples. However, this energy was monitored for all samples. If a peak had appeared at 1297 keV, the contribution of the Ca-47 decay to the Sc-47 peak would be taken into account in the calculations.

Figure 5.3 shows two gamma spectra of NIST SRM 278 (obsidian), one resulting from a typical short irradiation analysis and the other from the cadmium-covered, long irradiation. These spectra highlight the contrast between the results for titanium for each irradiation. In the typical short irradiation analysis, the peak for Ti-51 is barely visible above background. Since this standard has one of the higher concentrations of titanium (1470 ppm), it is unlikely that a peak would be detectable above background for samples with lower concentrations. On the other hand, the spectrum resulting from the cadmium-

covered long irradiation shows a distinct peak from Sc-47, which can be used to calculate the concentration of titanium in the sample.

Figure 5.3: Gamma spectra of SRM 278 (obsidian) depicting peaks for titanium analysis

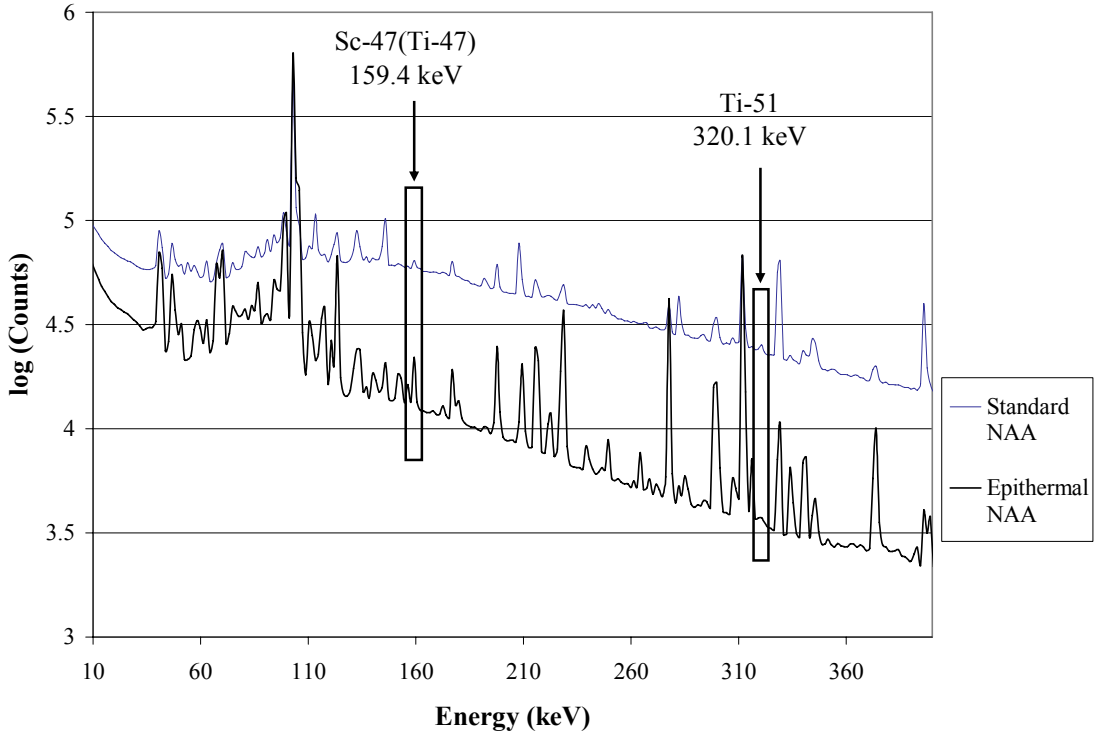

Since each standard was a different matrix, the estimated limit of detection for titanium, percent relative standard deviation, and the signal to noise ratio were calculated for each, for both the typical short irradiation and the cadmium-covered long irradiation analysis. The limit of detection was calculated by estimating the background under the peak and then calculating three times the square root of the background counts. The results of these calculations are shown in Table 5.3. For all matrices, the cadmium-covered irradiation procedure showed a marked improvement in the limit of detection of

titanium and the precision of the measurements. The accuracy of the results also improved significantly.

Table 5.3: Titanium analysis results: comparison of thermal NAA and fast NAA (Concentrations were calculated using NIST SRM 278 as a primary standard)

	Literature Concentrations[10]	**Ti-51 (thermal NAA)**	**Sc-47 (Ti-47) (fast NAA)**
SRM 278 (primary standard)	1470 ppm ± 40	N/A	N/A
Signal to Noise Ratio		0.062	0.47
LOD		436 ppm	58.1 ppm
SRM 1633a (n=3)			
[Ti] ± Std. Dev	8230 ppm ± 390	11530 ± 1430	7973 ± 23
% RSD		12.44%	0.28%
Signal to Noise Ratio		0.97	0.78
LOD		151 ppm	124 ppm
AGV-1 (n=3)			
[Ti] ± Std. Dev	6340 ppm ± 300	5751 ppm ± 257	6461 ppm ± 94
% RSD		4.47%	1.45%
Signal to Noise Ratio		0.16	2.01
LOD		314 ppm	53.5 ppm
JA-1 (n=3)			
[Ti] ± Std. Dev	5100 ppm	4440. ppm ± 197	5239 ppm ± 71
% RSD		4.44%	1.36%
Signal to Noise Ratio		0.11	2.59
LOD		365 ppm	34.4 ppm
JB-2 (n=3)			
[Ti] ± Std. Dev	7100 ppm	4807 ppm ± 604	7482 ppm ± 118
% RSD		12.55%	1.58%
Signal to Noise Ratio		0.12	2.14
LOD		505 ppm	40.9 ppm
JR-1 (n=3)			
[Ti] ± Std. Dev	660 ppm	486.2 ppm ± 430.2	678.2 ppm ± 56.7
% RSD		88.48%	8.36%
Signal to Noise Ratio		0.024	0.12
LOD		462 ppm	69.1 ppm

5.3.3.2 Barium results

Using the Ba-130 (n,γ) Ba-131 reaction for the analysis of barium results in great improvement in the precision of the analysis, especially at the low concentrations. Figure 5.4 shows the two comparison spectra for NIST SRM 278, with the peaks due to Ba-139 and Ba-131 highlighted. Whereas the peak due to Ba-139 is hardly visible above background in the traditional irradiation, the peak from Ba-131 (496.3 keV) is strong.

Figure 5.4: Gamma spectra of SRM 278 (obsidian) depicting peaks for barium analysis

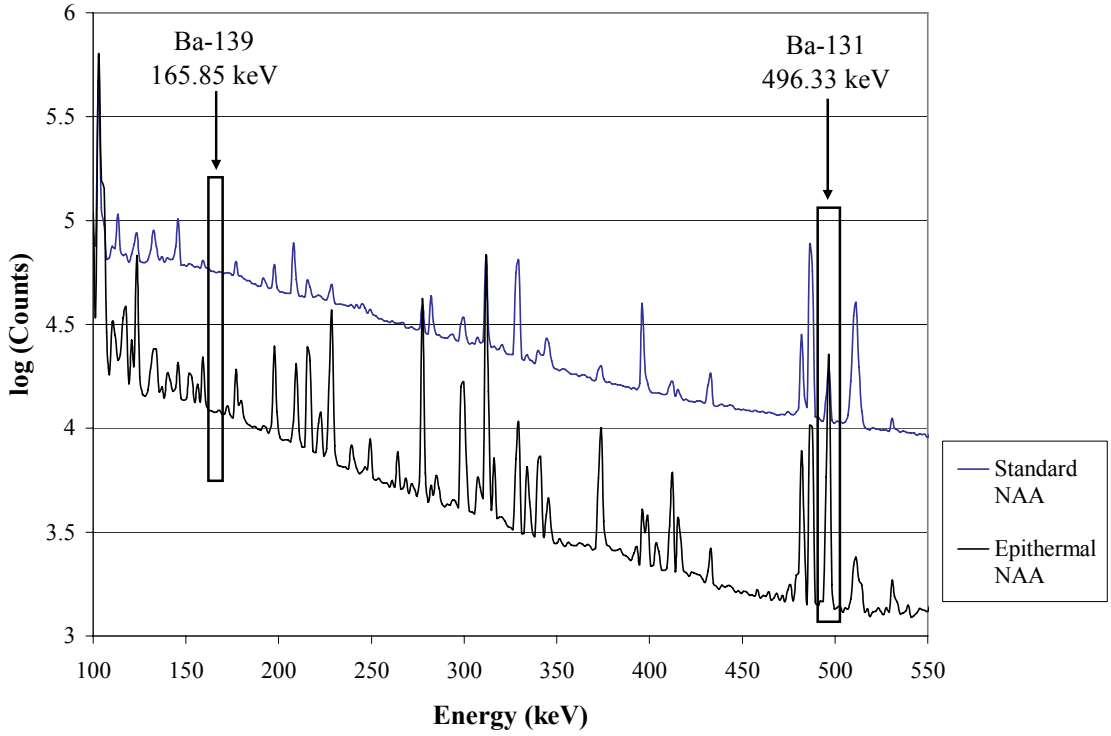

As for the titanium analysis, the limit of detection, precision, and signal-to-noise ratio were calculated for each standard for both the standard irradiation procedure and the cadmium-covered irradiation. The results of these calculations can be found in Table 5.4. The limit of detection for barium improves by a factor of ten, while the precision (%RSD) improves by a factor of 100. The accuracy of the measurement also improves greatly.

Table 5.4: Barium analysis results: comparison of thermal NAA and epithermal NAA (Concentrations were calculated using NIST SRM 278 as a primary standard)

	Literature concentrations[10]	**Ba-139 (thermal NAA)**	**Ba-131 (epithermal NAA)**
SRM 278 (primary standard)	880 ± 40	N/A	N/A
Signal to Noise Ratio		0.226	5.07
LOD		26.2 ppm	4.26 ppm
SRM 1633a (n=3)			
[Ba] ± Std. Dev	1320 ± 40	1509 ppm ± 144	1279 ± 19
% RSD		9.57%	1.49%
Signal to Noise Ratio		0.79	2.68
LOD		161 ppm	124 ppm
AGV-1 (n=3)			
[Ba] ± Std. Dev	1221 ± 16	858 ppm ± 31	1194 ppm ± 8
% RSD		3.65%	0.65%
Signal to Noise Ratio		0.21	5.26
LOD		35.4 ppm	4.70 ppm
JA-1 (n=3)			
[Ba] ± Std. Dev	311	161.1 ppm ± 21.7	293.6 ppm ± 2.4
% RSD		13.46%	0.80%
Signal to Noise Ratio		0.049	1.68
LOD		54.2 ppm	4.74 ppm
JB-2 (n=3)			
[Ba] ± Std. Dev	222	96.7 ppm ± 23.4	216 ppm ± 6
% RSD		24.44%	2.72%
Signal to Noise Ratio		0.031	0.85
LOD		70.8 ppm	6.41 ppm
JR-1 (n=3)			
[Ba] ± Std. Dev	50.3	Not detected in spectrum; below detection limit	53.8 ppm ± 0.4
% RSD			0.68%
Signal to Noise Ratio			0.29
LOD			4.84 ppm

5.4 Other elements of interest

In examining the spectra further, other isotopes of interest were identified. Two in particular, As-76 and Br-82, showed clear peaks in the spectra and have presented the opportunity to study the affect of these elements on the sourcing of obsidian. Arsenic has

never before been applied to obsidian studies, mostly because of the difficulty in measurement due to such low concentrations. Bromine has been occasionally examined, but has only been thought useful in the sourcing of obsidian in Turkey.

5.4.1 Arsenic Analysis

Arsenic is a trace element in obsidian that is usually only present in levels ranging from a few parts-per-million to low tens of parts-per-million. Because it has been difficult to measure via traditional NAA methods, where it usually is barely above background if the peak appears at all, it has not been applied to obsidian sourcing studies. Since the cadmium-covered irradiation appears to offer an alternative way of measuring arsenic, the presence of the arsenic peak in the spectrum has been examined further, both to confirm that the peak is due to arsenic in the sample and to determine the sensitivity of this method for its analysis.

5.4.1.1 Neutron capture of arsenic

Arsenic has only one naturally-abundant isotope, As-75. As-75 can undergo a neutron capture reaction with both thermal and epithermal neutrons to form As-76, which has a half-life of 26.3 hours. The typical reaction examined for NAA is the thermal neutron reaction. As-75 has a thermal neutron capture cross section of 4.5 barns. Even though the abundance of the target isotope is high and the thermal cross section is moderately high, very little activity due to As-76 is detectable during either the typical long or short irradiation analysis. However, As-75 also has a resonance cross section of 61 barns. With the use of the cadmium can to reduce the thermal neutron flux, the

background due to activity from other thermal neutron reactions is reduced and the probability of observing an epithermal neutron reaction increases. Thus, a strong peak at 559.1 keV (44.60%) is visible and quantifiable. Figure 5.5 shows the comparison of the 599.1-keV arsenic peak in both a standard irradiation and the cadmium-covered irradiation.

Figure 5.5: Gamma spectra of SRM 278 (obsidian) depicting peak for arsenic analysis

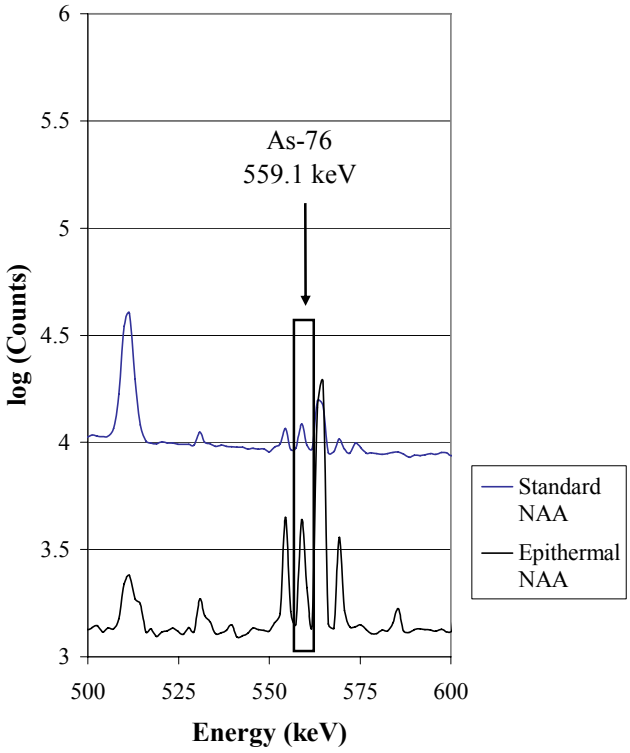

5.4.1.2 Is the peak really due to arsenic?

One concern about this peak was that the half-life of As-76 was short compared to the time the samples were allowed to decay (seven days for the initial experiments). By the time of counting, the As-76 had already been through about 6.5 half-lives. It seemed unlikely that such an intense peak would still be present after that period of time,

especially since the concentrations of arsenic are usually low in obsidian. To confirm that the peak was due to arsenic, two tests were performed. First, the theoretical activity due to As-76 was estimated using the measured thermal and epithermal neutron fluxes and compared to the activity seen in the spectrum for NIST SRM 278 (obsidian). These calculations showed that the intensity of the peak was consistent with the activity produced due to the As-75 (n,γ) As-76 reaction. A value of 3590 counts was calculated as a combination of the thermal and resonance neutron reactions and a value of 3827 counts was observed.

An additional test was to follow the decay of the peak over a period of several days and determine if the decay matched that of As-76. This would prove that the peak was due to As-76 and that it was due to As-76 produced during the irradiation (i.e., not being produced from any other decay after the irradiation). Several standards including the NIST SRM 278 (obsidian), SRM 1633a (fly ash), and JGS JR-1 (rhyolite) and two obsidian samples were irradiated for 48 hours, allowed to decay for about 4.5 days, and then counted several times over the next 5 days. Each count was for 30 minutes and each sample was counted about four times during the course of one day. A total of 17 counts were performed for each of the samples. The decay curve achieved from the analysis of the 559-keV peak in SRM 1633a (fly ash) is shown in Figure 5.6 below.

Figure 5.6: Decay of the 559.1-keV gamma peak in SRM 1633a (fly ash)

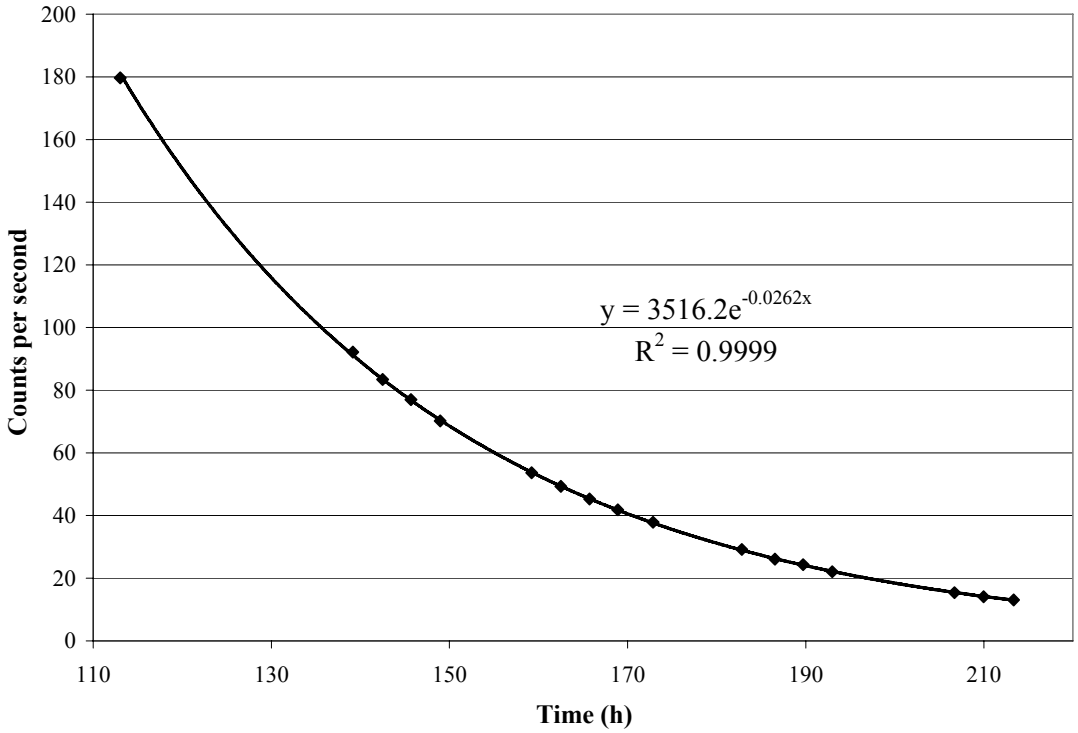

The exponential fit gave an R^2 value of 0.9999 and a decay constant of 0.0262 h^-, which gives a half-life of 26.408 ± 0.053 hours, a 0.41% difference from the literature value of 26.3 hours. The results and uncertainties for all standards are listed in Table 5.5. The results calculated from the SRM278 standard have a greater error than the other two, but this is most likely due to this standard containing the smallest concentration of arsenic. Since less activity due to arsenic was produced, the counting statistics were not as good for this sample. However, the calculated half-life is still very close to the true value. These results confirm that the 559-keV peak is due to the decay of As-76 produced during the cadmium-covered irradiation.

Table 5.5 Results from the decay experiment for As-76

Standard	**Decay constant (λ)**	σ_λ	**Half-life ($t_{1/2}$)**	$\sigma_{1/2}$
SRM-278 *(n=3)*	0.025560 h^-	0.00036 h^-	27.1 h	0.38 h
SRM-1633a *(n=3)*	0.026247 h^-	0.000052 h^-	26.4 h	0.053 h
JR-1 *(n=3)*	0.026043 h^-	0.00017 h^-	26.6 h	0.17 h

5.4.1.3 Arsenic results

As for titanium and barium, the limit of detection, relative standard deviation, and the signal-to-noise ratios were calculated for each standard analyzed in the initial experiment. The results of these calculations are found in Table 5.6 below. In addition, these were also calculated for several of these standards after an analysis involving a 4.5-day decay instead of a 7-day decay (also shown in Table 5.6).

This procedure for the analysis of arsenic in geological samples proves to have good results with low limits of detection and good precision for the measurements. The 5-day decay allowed even better precision and a better detection limit to be achieved.

Several of the standards had not been analyzed with the second set of samples for the 5-day decay because the concentration of arsenic was so low in these materials. The main goal of this second set had been to follow the decay, and since space inside the cadmium can is limited, standards with larger concentrations, which would still have a signal after several days of counting for good counting statistics, were chosen for analysis.

Table 5.6: Arsenic analysis results: comparison of results after a 7-day or 5-day decay (Concentrations were calculated using NIST SRM 278 as a primary standard)

	Literature concentrations[10]	**As-76 (7-day decay)**	**As-76 (5-day decay)**
SRM 278 (primary standard)	4.7 ppm	N/A	N/A
Signal to Noise Ratio		0.75	1.18
LOD		0.2 ppm	0.09 ppm
SRM 1633a (n=3)			
[As] ± Std. Dev	145 ppm	150.4 ppm ± 1.8	141.8 ppm ± 1.2
% RSD		1.20%	0.83%
Signal to Noise Ratio		9.70	34.25
LOD		0.497 ppm	0.109 ppm
AGV-1 (n=3)			
[As] ± Std. Dev	0.84 ppm	1.22 ppm ± 0.28	Not analyzed
% RSD		22.70%	
Signal to Noise Ratio		0.18	
LOD		0.147 ppm	
JA-1 (n=3)			
[As] ± Std. Dev	2.78 ppm	3.09 ppm ± 0.17	Not analyzed
% RSD		5.60%	
Signal to Noise Ratio		0.48	
LOD		0.214 ppm	
JB-2 (n=3)			
[As] ± Std. Dev	2.87 ppm	3.63 ppm ± 0.37	Not analyzed
% RSD		10.15%	
Signal to Noise Ratio		0.28	
LOD		0.252 ppm	
JR-1 (n=3)			
[As] ± Std. Dev	16.3 ppm	15.9 ppm ± 0.34	16.43 ppm ± 0.21
% RSD		2.13%	1.28%
Signal to Noise Ratio		2.08	4.82
LOD		0.253 ppm	0.0912 ppm

5.4.2 Bromine analysis

Bromine is an element not often used for obsidian studies. However, it is thought to be useful in distinguishing between two Turkish obsidian sources, Bingol and Nemrut, that are otherwise almost identical.[11] However, it is not usually determined during the

typical NAA procedure because of the low concentration in the standards and the assumed low concentration in the samples. Using epithermal neutron activation, however, the bromine can be more easily quantified as the signal is improved with the lower background.

5.4.2.1 Neutron capture reactions of bromine

For the analysis of bromine, there are two naturally abundant isotopes that can undergo reactions by capturing neutrons. The first, Br-79 (50.69%), can react via an (n,γ) reaction to form Br-80. Br-79 has a thermal neutron cross section of 8.60 barns and Br-80 has a half-life of 17.68 minutes, which would make it perfect for a short-irradiation analysis procedure. However, the gamma rays emitted during the decay of Br-80 are so low in abundance (616.60 keV is the most abundant peak at 6.70%), that it is difficult to see the peak above background unless the concentration of bromine in the sample is high. Br-79 can also capture a neutron to form Br-80m ($t_{½}$ = 4.42 hours) with a thermal cross section of 2.40 barns, but the only gamma ray emitted from the decay of Br-80m to Br-80 is 37.05 keV. Such a low energy peak can be difficult to distinguish in a complex gamma spectrum.

The other naturally-occurring isotope of bromine is Br-81 (49.31% abundant). Br-81 can undergo an (n,γ) reaction to form Br-82 ($t_{½}$ = 35.3 hours) with a thermal cross section of 0.26 barns and a resonance cross section of 17 barns. Br-81 can also react to form Br-82m ($t_{½}$ = 6.13 minutes) with a thermal cross section of 2.43 barns and a resonance cross section of 34 barns. Br-82m then decays 99.6% of the time to Br-82. When Br-82 decays, there are several gamma rays emitted; the most abundant are 776.5

keV (83.54%) and 554.35 keV (70.76%). When the cadmium can is used for the analysis, these peaks due to Br-82 are clearly visible in the spectrum (Figure 5.7).

Figure 5.7: Gamma spectra of SRM 278 (obsidian) depicting peaks for bromine analysis

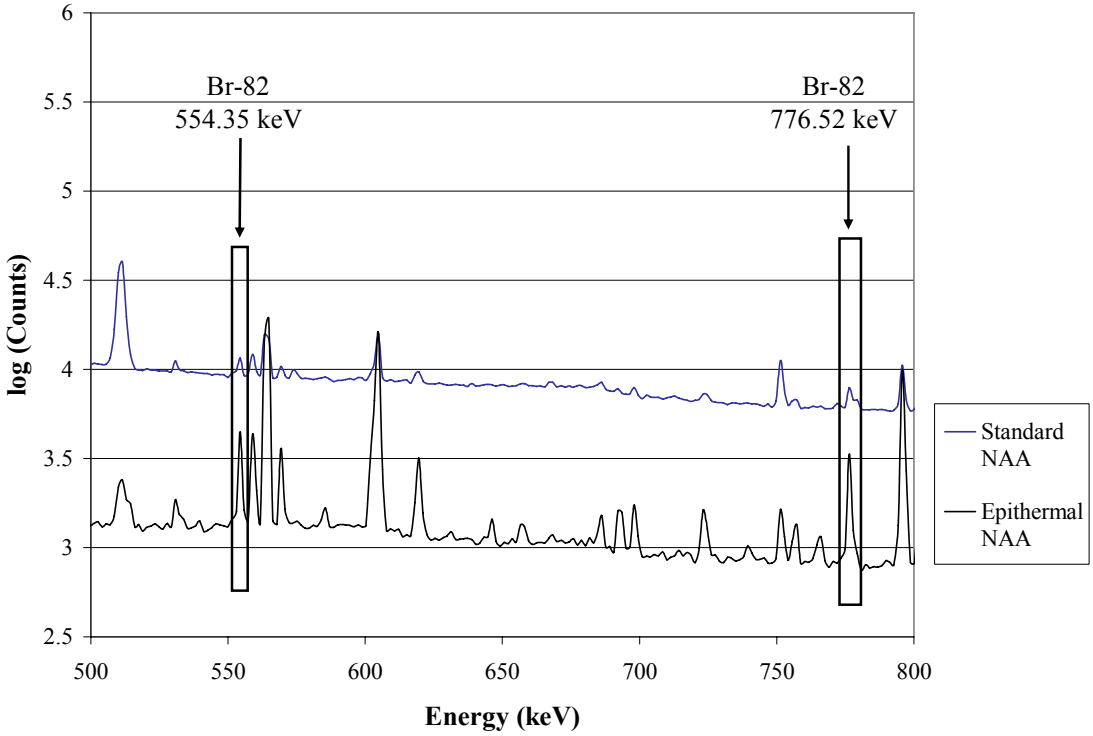

5.4.2.2 Br-82 decay test

Even though the half-life for Br-82 is longer than that of the arsenic isotope tested before, the decay of the 776-keV peak in the gamma spectrum was followed over the course of several days under the same conditions described for the arsenic peak above. Figure 5.8 shows the decay curve of the peak.

Though the results are not quite as precise as those for the arsenic peak, an R-squared value of 0.9918 indicates a good fit for the trendline. The half-life calculated

from the decay constant (0.0197 h^{-}) is 35.19 hours, a 0.32% difference from the literature value of 35.3 hours. This peak is definitely due to the decay of Br-82 and it is unlikely that anything is significantly interfering with it.

Figure 5.8: Decay of the 776-keV gamma peak in SRM 278 (obsidian)

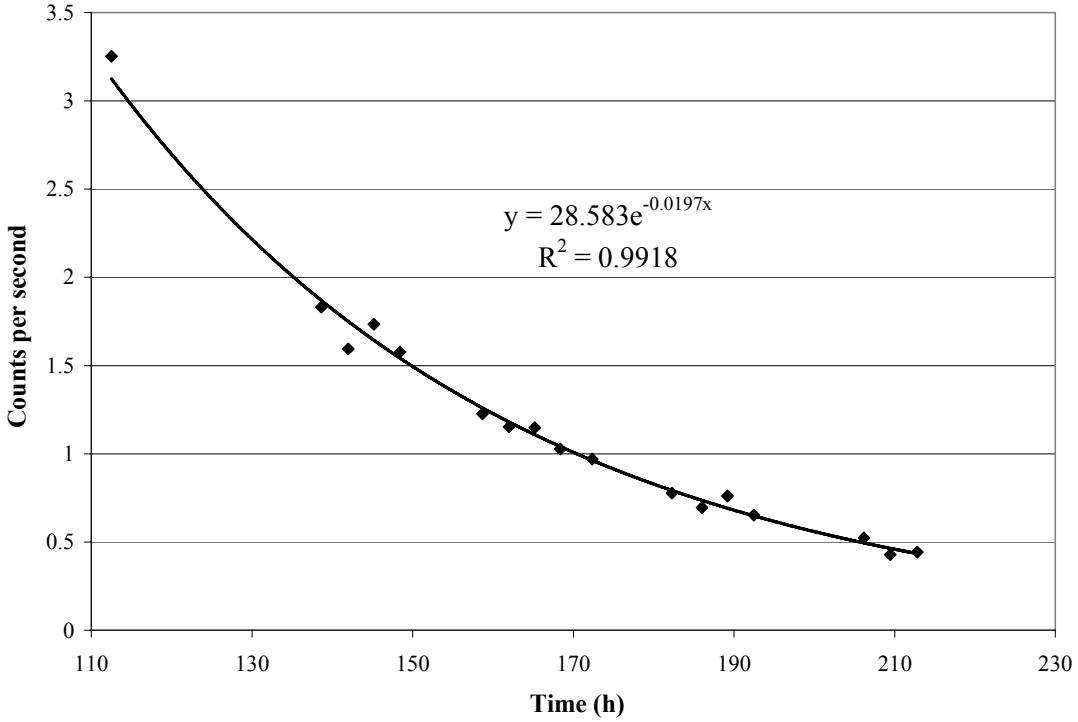

5.4.2.3 Bromine results

Because several of the standards analyzed during these irradiations did not have published values for bromine, and those that are known have large uncertainties, the accuracy and limits of detection could not be calculated. With the proper standards with known concentrations of bromine, the determination of bromine in obsidian could be quite accurate.

Two samples of obsidian from each of the two Turkish sources were analyzed as part of the second set of samples in the cadmium-covered irradiation. The samples from one source, Bingol, showed a strong bromine signal (over 10,000 counts for both samples); while the samples from the other source were much lower (only a few hundred counts in the peak). There seems to be a clear difference between the two sources, though more samples would need to be analyzed to confirm this.

5.5 Comparison of results from ENAA and x-ray methods

As stated in the introduction, one of the main goals of creating this new methodology was to verify previous results by Merrick and Brown for the sourcing of African obsidian.[1-2] Since these results were analyzed using both x-ray fluorescence and electron microprobe analysis, it is necessary to be able to directly compare those results for the concentration of titanium to those achieved with this new method. This comparison is made more difficult by the lack of detailed information about the analysis procedure used for both the XRF and EMPA and the lack of a published table of data. Even though a perfect comparison cannot be made between these two data sets, trends in the data can be studied. To achieve this, the same set of Mesoamerican obsidian included in the initial experiments with the cadmium can was sent to be analyzed via EMPA. This allowed a more direct comparison of the two methods, since more information about the instrument and the analysis method was available. These experiments also provided a way to compare the results using x-ray methods from previous studies for the African obsidian and examine the trends between the data sets.

5.5.1 Results from the Mesoamerican obsidian samples

A selection of the Mesoamerican samples described above were sent to Ellery Frahm, Electron Microprobe Lab at the University of Minnesota-Twin Cities, to be analyzed via EMPA. The instrument used was a JEOL JXA-8900R "SuperProbe" electron probe microanalyzer, with a wavelength-dispersive detection system, giving this instrument a resolution of 5 eV. Use of a wavelength-dispersive instrument provided a comparison under the most ideal circumstances. The peaks due to barium and titanium are easily resolved with this instrument, allowing for more accurate results from the x-ray method. Figure 5.9 below shows the results from both methods for the concentration of titanium (in parts per million) plotted against each other.

Figure 5.9: Comparison of the results from EMPA versus those from ENAA for Mesoamerican obsidian

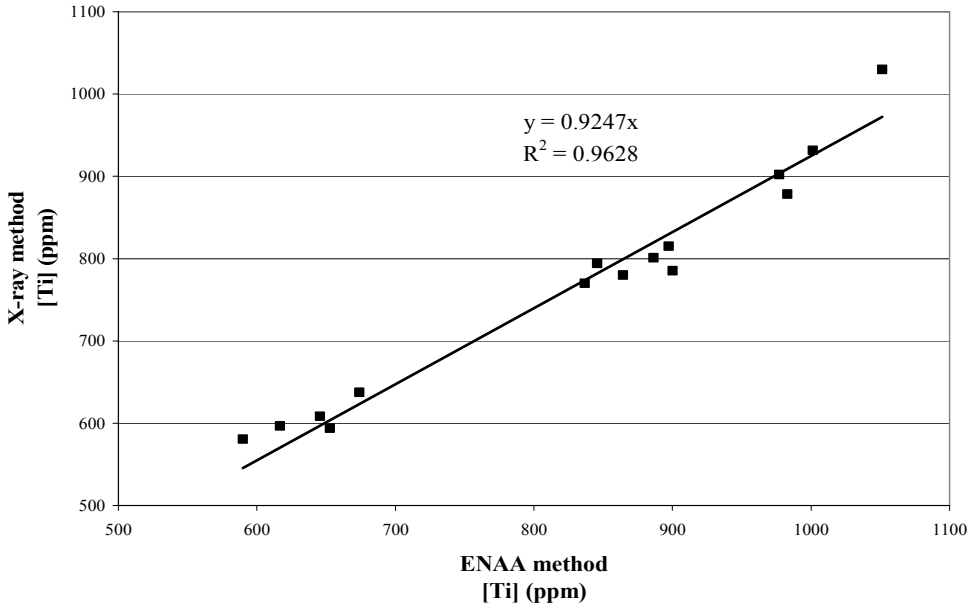

The relationship between the results from both methods is very close to one-to-one, and considering the relative standard deviation for the EMPA results (about 10% for each sample), the differences between the two data sets is minimal. To be sure that the differences were minimal statistically, an ANOVA analysis was performed on the two data sets.[12] The results of that analysis proved that the two data sets were not significantly different ($p=0.42$).

From these results, it can be seen that, if a wavelength-dispersive detection system is used and the barium and titanium peaks can be resolved, then both the x-ray method and the ENAA method yield identical results. This hypothesis can then be extended to the African obsidian results: if the x-ray peaks for titanium and barium were well-resolved, then the results from the x-ray method and the ENAA method should be very similar.

5.5.2 Results from the African obsidian samples

Before any comparison between the ENAA method for titanium and the results from previous studies can be discussed, a few major challenges need to be addressed. There is the lack of published tables of the calculated values for the titanium concentrations for the previous studies. However, though tables of numbers are not given, the concentration of titanium is used in many plots to demonstrate its ability to distinguish source samples. The values used here, in contrast to those obtained by ENAA, have been estimated from these plots.

Secondly, the same exact samples as in previous studies were not available for analysis using the ENAA method. Instead, samples from the same or similar locations

were used for comparison. In most cases, three or four samples from each location (where available) were analyzed to account for any intra-source variation in the titanium concentration. Because of this limitation, only a subset of the localities listed in the published works was analyzed. The sample localities were chosen for the availability of samples from the same region for a better comparison.

Shown below in Figure 5.10 is the comparison of the results from each method, just as in Figure 5.9. Here, the results for the African obsidian samples have been added to the same plot for a more direct comparison. The slope of the trendline for the African obsidian data is greater than 1, showing that the concentrations estimated for the previous studies are generally greater than those determined using the ENAA method. The fit of the data to the trendline, shown in the R-squared value, is also not as good, though this could mostly be due to intra-source variation and error introduced in the estimation of the concentrations. The larger concentrations from the x-ray methods used in previous works could be due to some contribution of barium to the peak intensity.

Figure 5.10: Comparison of the results from EMPA versus those from ENAA for Mesoamerican obsidian and African obsidian

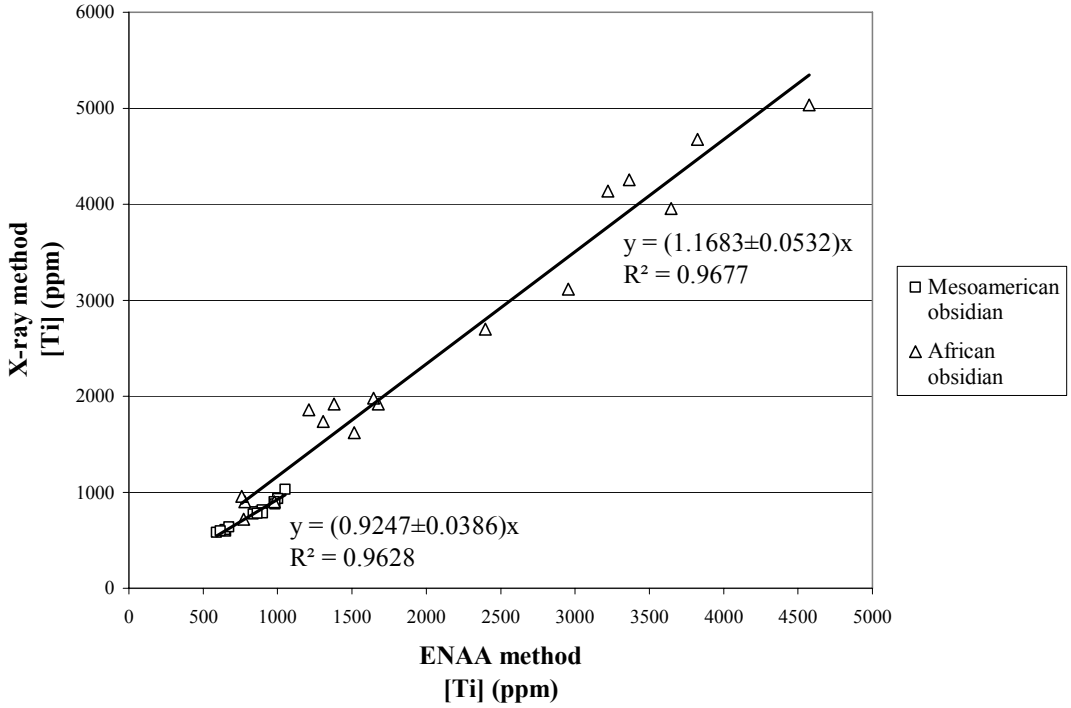

5.6 Future work and conclusions

Here a method using epithermal neutron activation analysis for the determination of titanium, barium, arsenic, and bromine concentrations in obsidian has been presented. This method not only provides better limits of detection, precision, and signal-to-noise ratio for each of these elements in obsidian, but also has the potential to be applied to other materials. Future directions for this project include the application of this method to biological materials for the analysis of arsenic and evaluating the potential of this method as an alternative to the current long irradiation procedure.

5.6.1 Analysis of arsenic in biological samples

Arsenic is often an element of interest in biological materials, but it is difficult to measure using standard thermal INAA.[13] Since NAA sample preparation procedures are usually minimal, sample preparation for analysis via NAA would greatly reduce the potential of contamination as compared to other analytical techniques. A small set of biological samples was analyzed using the ENAA method described here. Fifty milligrams of NIST SRM1577 bovine liver were weighed out into quartz vials and sealed under slight vacuum. Unfortunately, the heating of the samples caused the sealed quartz vials to burst, as the sample degraded and released carbon dioxide, oxygen, and other gases. Two potential solutions to the heating problem are reducing the irradiation time or by using larger vials. Reducing the irradiation time does decrease the amount of activity produced during the irradiation, but this would also allow for shorter decay times for the sample before counting and has the potential to prevent the pressure from released gasses reaching the point of rupturing the vial. Using larger vials simply gives the gases more room to expand, thus slowing the buildup of pressure. If the heating problem could be solved, then this method could be used to accurately and precisely measure the concentrations of arsenic in biological samples.

5.6.2 An alternative method for standard INAA procedures

ENAA can also be considered for the detection of other elements in the obsidian sample. Many of the rare earth elements that are of interest in sourcing studies have large resonance cross sections. These larger cross sections in addition to the reduction in thermal background can improve the signal-to-noise ratio significantly, leading to better precision and limits of detection for these elements. As described earlier, ENAA has

been demonstrated to increase the sensitivity for many trace elements of interest in geological samples.[3, 6-7] Table 5.7 below lists many of the elements currently analyzed during the long irradiation procedure for obsidian, along with their thermal and resonance cross sections. Theoretical advantage factors (F) were calculated using the Brune[14] definition (Equation 5.1)

$$F_a = \frac{R_i}{R} \qquad \text{Equation 5.1}$$

where R and R_i are the cadmium ratios for the radionuclide and the interferent (in obsidian, usually ^{30}Si and ^{24}Na). The cadmium ratios were calculated using Equation 5.2[15]

$$R = \frac{\phi_{th}\sigma_{th} + \phi_{epi}I}{\phi_{epi}I} \qquad \text{Equation 5.2}$$

where φ is the thermal (th) and epithermal (epi) neutron flux, σ is the thermal cross section, and I is the resonance integral.

Table 5.7: Elements of interest for the ENAA procedure

Target Isotope	**Thermal σ (b)[10]**	**Resonance I (b)[10]**	**F (i = Na-24)**	**F (i = Si-30)**
Fe-58	1.28	1.7	2.25	1.99
Co-59	17.1	34.3	3.37	2.98
Zn-64	0.76	1.45	3.21	2.84
Sr-84	0.35	6.72	27.61	24.44
Rb-85	0.427	7.31	25.06	22.17
Zr-94	0.05	0.23	7.54	6.67
Sb-123	4.1	118	38.31	33.90
Cs-133	26.4	390	22.06	19.53
La-139	8.93	11.8	2.24	1.98
Ce-140	0.57	0.47	1.40	1.24
Nd-146	1.4	3.2	3.83	3.39
Sm-152	206	2970	21.60	19.12
Tb-159	23.4	418	25.98	22.99
Hf-180	13.04	35	4.48	3.97
Ta-181	20.5	660	41.75	36.95

These advantage factors provide a way of evaluating the potential increase in sensitivity for these elements. Other isotopes measured during the standard long irradiation procedure, such as Sc-45 (Sc-46), Eu-151 (Eu-152), Yb-174 (Yb-175), and Lu-176 (Lu-177), show a decrease in the sensitivity because their resonance integrals are much smaller than the thermal cross section. However, for these same isotopes, the thermal cross section is so large (i.e., Eu-151 has a thermal cross section of 5900 b) that the reduction in thermal flux may only have a minor impact on the activity produced during the irradiation.

5.6.3 Conclusions

The results described in this section have shown the versatility of ENAA toward analyzing archeological samples, and also provide greater data per analysis for each sample. These methods allow for geologists and archeologists to obtain greater amounts of data, with better precision and accuracy, while only analyzing small samples. As described in Chapter 1, NAA methods are minimally destructive and would lend to application to samples of artifacts or for use in creation of standards for development of an x-ray based analysis.

References

1. H. V. Merrick and F. H. Brown, *Archaeometry*, 1984, **26**, 230-236.
2. H. V. Merrick and F. H. Brown, *The African Archaeological Review*, 1984, **2**, 129-152.
3. W. Ehmann, J. Brückner and D. McKown, *Journal of Radioanalytical and Nuclear Chemistry*, 1980, **57**, 491-502.
4. W. Ehmann, D. and D. E. Vance, *Radiochemistry and Nuclear Methods of Analysis*, John Wiley & Sons, Inc., New York, 1991.
5. K. Riggle, Ph.D., Univeristy of Missouri, 1992.
6. P. Baedecker, J. Rowe and E. Steinnes, *Journal of Radioanalytical and Nuclear Chemistry*, 1977, **40**, 115-146.
7. S. J. Parry, *Journal of Radioanalytical and Nuclear Chemistry*, 1982, **72**, 195-207.
8. R. E. Williams, P. K. Hopke and R. A. Meyer, *Journal of Radioanalytical and Nuclear Chemistry*, 1981, **63**, 187-199.
9. R. E. Williams, P. K. Hopke and R. A. Meyer, *Journal of Radioanalytical and Nuclear Chemistry*, 1982, **72**, 183-194.
10. M. D. Glascock, *Tables for Neutron Activation Analysis*, Univeristy of Missouri, Columbia, 2006.
11. J. Blackman, Department of Anthropology, Smithsonian National Museum of Natural History, Washington D.C., personal communication, February 2010.
12. J. C. M. J. N. Miller, *Statistics for analytical chemistry*, New York, Chichester : E. Horwood, 1984.
13. R. Zeisler, E. A. Mackey, G. P. Lamaze, T. E. Stover, R. O. Spatz and R. R. Greenberg, *J. Radioanal. Nucl. Chem. FIELD Full Journal Title:Journal of Radioanalytical and Nuclear Chemistry*, 2006, **269**, 291-296.
14. W.-Z. Tian and W. D. Ehmann, *Journal of Radioanalytical and Nuclear Chemistry*, 1984, **84**, 89-102.
15. D. De Soete, R. Gijbels and J. Hoste, *Neutron Activation Analysis*, Wiley-Interscience, New York, 1972.

List of Appendices

Appendix 1 – Limestone quarry information for the BNL Egyptian limestone samples.

Anid	Quarry
EB0037	Tura
EB0038	Beni Hassan
EB0039	Deir Abu Hennis
EB0040	Deir Abu Hennis
EB0041	Deir Abu Hennis
EB0042	Deir Abu Hennis
EB0043	Deir Abu Hennis
EB0044	Deir Abu Hennis
EB0045	Deir Abu Hennis
EB0046	Deir Abu Hennis
EB0047	Deir Abu Hennis
EB0048	Deir Abu Hennis
EB0049	Deir Abu Hennis
EB0050	Deir Abu Hennis
EB0051	Beni Hassan
EB0052	Beni Hassan
EB0053	Beni Hassan
EB0054	Beni Hassan
EB0055	Beni Hassan
EB0056	Beni Hassan
EB0057	Beni Hassan
EB0058	Beni Hassan
EB0059	Beni Hassan
EB0060	Beni Hassan
EB0061	Beni Hassan
EB0062	Beni Hassan
EB0063	Beni Hassan
EB0064	Quseir el Amarna
EB0065	Quseir el Amarna
EB0066	Quseir el Amarna
EB0067	Quseir el Amarna
EB0068	Quseir el Amarna
EB0069	Quseir el Amarna
EB0070	Quseir el Amarna
EB0071	Quseir el Amarna
EB0072	Quseir el Amarna
EB0073	Quseir el Amarna
EB0074	Quseir el Amarna
EB0075	Quseir el Amarna
EB0076	Quseir el Amarna
EB0078	Tura
EB0079	Tura

Appendix 1 – Limestone quarry information for the BNL Egyptian limestone samples, continued.

Anid	Quarry
EB0080	Tura
EB0081	Tura
EB0082	Tura
EB0083	Tura
EB0084	Tura
EB0085	Tura
EB0086	Tura
EB0087	Quseir el Amarna
EB0088	Quseir el Amarna
EB0089	Quseir el Amarna
EB0090	Quseir el Amarna
EB0091	Quseir el Amarna
EB0092	Quseir el Amarna
EB0093	Quseir el Amarna
EB0094	Quseir el Amarna
EB0095	Quseir el Amarna
EB0096	Quseir el Amarna
EB0097	Quseir el Amarna
EB0098	Quseir el Amarna
EB0099	Quseir el Amarna
EB0100	Maasara
EB0101	Maasara
EB0102	Maasara
EB0103	Maasara
EB0104	Maasara
EB0105	Maasara
EB0106	Maasara
EB0107	Maasara
EB0108	Maasara
EB0109	Maasara
EB0110	Maasara
EB0111	Maasara
EB0112	Maasara

Appendix 2 – Concentration data from NAA for limestone from Egypt (BNL samples). All concentrations are in parts per million (ppm)

Sample ID	Al	As	Ba	Ca	Ce	Co	Cr
EB0037	0.0	0.5455	12.3	418583.8	1.3434	2.6209	6.4077
EB0038	0.0	0.2333	8.4	412720.7	0.3843	0.1550	6.5697
EB0039	0.0	1.5955	0.0	415623.6	1.0475	0.4255	6.4056
EB0040	0.0	0.1288	0.0	416673.1	0.6742	0.1300	8.5082
EB0041	420.7	0.2155	0.0	414381.7	0.6485	0.1212	8.1787
EB0042	0.0	0.1708	8.2	415773.8	0.5301	0.2197	7.0762
EB0043	506.8	0.3500	0.0	415378.6	0.7300	0.3476	7.9735
EB0044	0.0	0.1834	0.0	410863.2	0.4060	0.1015	9.4522
EB0045	0.0	0.2249	6.3	409493.2	0.5205	0.3309	8.8425
EB0046	0.0	0.3627	0.0	419790.8	0.7873	0.2548	5.1872
EB0047	0.0	0.2306	0.0	414061.5	0.4985	0.1297	5.9179
EB0048	0.0	0.1144	0.0	427300.2	0.4954	0.0652	11.0820
EB0049	0.0	0.1885	0.0	416124.9	0.4955	0.0733	6.6187
EB0050	0.0	0.2078	8.7	419983.0	0.5685	0.0711	12.4380
EB0051	0.0	0.3490	18.5	421036.0	1.2756	0.3489	5.6239
EB0052	0.0	0.2230	29.9	422701.8	0.8143	0.4683	4.9293
EB0053	0.0	0.3917	17.3	419393.7	1.2765	1.4716	8.3478
EB0054	0.0	0.0000	23.6	417692.0	1.1292	0.2967	6.7502
EB0055	0.0	0.3975	9.1	419510.0	0.4598	0.1281	6.6555
EB0056	0.0	0.0000	25.6	419910.9	0.6907	0.1059	6.1519
EB0057	0.0	0.0000	40.8	421021.7	0.8343	0.1508	8.0770
EB0058	0.0	0.2227	34.8	413957.1	2.0175	0.2066	6.6609
EB0059	0.0	0.0000	13.3	431619.2	0.7433	0.2261	5.2167
EB0060	0.0	0.0000	21.6	424844.3	0.8892	0.1179	5.9596
EB0061	0.0	0.2885	19.2	423992.4	0.4810	0.1155	6.7758
EB0062	0.0	0.0000	11.5	420263.3	0.5378	0.1126	4.9102
EB0063	0.0	0.2247	25.1	416502.9	0.9440	0.1238	6.3768
EB0064	903.5	0.2642	15.6	412956.8	0.7134	0.1740	9.5427
EB0065	0.0	0.2446	26.2	411792.6	0.4699	0.1441	7.6373
EB0066	0.0	0.1961	11.7	422219.4	0.6991	0.1156	10.7338
EB0067	0.0	0.3618	0.0	411831.3	0.6619	0.0974	3.1013
EB0068	0.0	0.0000	7.5	426331.6	0.3750	0.1455	3.7835
EB0069	0.0	0.3348	12.8	420313.6	0.2123	0.1366	2.1585
EB0070	0.0	0.3614	22.1	416647.2	0.3693	0.1119	4.0702
EB0071	0.0	0.4705	0.0	413524.0	0.3503	0.1532	3.3583
EB0072	0.0	0.0000	0.0	427257.3	0.3818	0.0889	3.6055
EB0073	0.0	0.0000	0.0	417463.5	0.3464	0.0393	3.2798
EB0074	1047.0	0.3009	0.0	419326.7	0.3881	0.0823	2.7328
EB0075	0.0	0.0000	10.5	416278.0	0.3911	0.1567	3.5608
EB0076	0.0	0.0000	10.0	416840.5	0.5929	0.1492	4.0360
EB0078	3583.0	0.7841	6.6	388883.9	2.7446	0.1394	13.1269
EB0079	0.0	0.0000	10.9	374084.0	2.1905	0.1616	12.6403
EB0080	878.9	0.0000	10.7	385504.9	3.2841	0.0849	14.0466
EB0081	7500.2	0.9092	0.0	316533.2	9.6137	0.3675	35.3593
EB0082	4063.1	1.2900	127.6	398910.1	3.8534	0.2664	16.8637

Appendix 2, continued

Sample ID	Al	As	Ba	Ca	Ce	Co	Cr
EB0083	4038.5	0.7987	12.1	381362.8	4.0728	0.3398	17.2407
EB0084	0.0	0.9044	0.0	334532.1	5.8749	0.3678	27.5630
EB0085	0.0	0.9240	13.1	406625.8	2.8517	0.1786	6.1525
EB0086	0.0	0.0000	916.6	401046.4	1.1430	0.6990	5.9964
EB0087	3071.0	0.1262	21.7	411073.7	0.5129	0.4038	5.9343
EB0088	0.0	0.2465	0.0	417227.7	0.4259	0.4238	4.7781
EB0089	0.0	0.2977	14.2	411580.3	0.3442	0.2936	5.2674
EB0090	0.0	1.9382	14.5	405657.9	0.6172	0.1849	3.1207
EB0091	0.0	0.1682	14.7	403082.3	0.3236	0.2595	3.9388
EB0092	0.0	0.5488	15.1	409432.2	0.1724	0.1548	2.7042
EB0093	0.0	0.3847	23.5	406409.1	0.3175	0.1829	3.2048
EB0094	0.0	0.0000	9.0	412418.4	0.2551	0.1520	2.6628
EB0095	0.0	0.1070	11.1	410423.5	0.2388	0.1922	2.4222
EB0096	0.0	0.3281	11.3	414472.7	0.3016	0.1689	2.7161
EB0097	0.0	0.4340	12.9	415494.5	0.4710	0.1530	4.4192
EB0098	0.0	0.4275	13.2	407936.4	0.3964	0.1219	3.8574
EB0099	0.0	0.1410	14.9	405628.3	0.2857	0.1015	3.3788
EB0100	5616.4	3.0085	25.1	326187.1	9.8801	0.6885	26.9994
EB0101	5298.6	1.1799	21.7	357753.9	6.0426	0.2638	25.7383
EB0102	1574.8	0.5324	0.0	371152.4	2.7821	0.2047	14.7879
EB0103	2760.6	0.5463	0.0	385744.1	3.2425	0.1791	14.9198
EB0104	2003.5	0.0000	20.5	390019.9	3.4290	0.2088	14.4129
EB0105	3255.3	0.8447	16.6	380537.9	5.0678	0.4850	21.7251
EB0106	3460.0	1.4293	18.7	377277.2	6.1509	0.4128	21.2248
EB0107	3191.3	2.1156	19.1	395556.6	4.0286	0.2561	19.7098
EB0108	3905.6	0.9570	14.7	387576.4	3.5170	0.2698	14.7060
EB0109	4310.5	2.5183	28.2	365227.3	7.7105	0.4060	25.8313
EB0110	5556.8	3.8984	25.8	372107.7	7.2016	1.4240	28.3854
EB0111	4495.3	0.3488	28.3	368428.1	6.8337	0.2191	28.8855
EB0112	2955.7	1.1889	10.3	375009.0	3.4182	0.2247	15.4478

Appendix 2, continued

Sample ID	Cs	Dy	Eu	Fe	Hf	K	La
EB0037	0.0000	0.1556	0.0411	338.5	0.0101	0.0	0.6476
EB0038	0.0092	0.0000	0.0044	235.7	0.0053	0.0	0.1713
EB0039	0.0268	0.2372	0.0433	769.3	0.0242	0.0	1.1441
EB0040	0.0000	0.0813	0.0122	64.4	0.0000	0.0	0.4115
EB0041	0.0209	0.1071	0.0148	131.9	0.0119	0.0	0.4904
EB0042	0.0300	0.0000	0.0136	131.8	0.0097	0.0	0.4396
EB0043	0.0296	0.0802	0.0164	160.5	0.0157	0.0	0.5109
EB0044	0.0135	0.0000	0.0108	101.0	0.0072	0.0	0.3631
EB0045	0.0000	0.0000	0.0112	125.2	0.0080	0.0	0.4018
EB0046	0.0176	0.1023	0.0258	246.5	0.0090	0.0	0.5264
EB0047	0.0109	0.0000	0.0114	168.4	0.0097	0.0	0.3999
EB0048	0.0207	0.0000	0.0113	101.3	0.0057	0.0	0.4099
EB0049	0.0083	0.0000	0.0078	96.4	0.0083	0.0	0.3020
EB0050	0.0169	0.0000	0.0078	111.3	0.0106	0.0	0.3379
EB0051	0.0136	0.0000	0.0364	246.9	0.0109	0.0	0.5944
EB0052	0.0000	0.0000	0.0052	178.8	0.0000	0.0	0.2804
EB0053	0.0393	0.0656	0.0166	629.7	0.0794	0.0	0.5856
EB0054	0.0150	0.0000	0.0086	114.1	0.0115	0.0	0.4313
EB0055	0.0000	0.0000	0.0045	140.5	0.0000	0.0	0.1625
EB0056	0.0000	0.0000	0.0023	73.4	0.0000	231.0	0.1839
EB0057	0.0000	0.0000	0.0060	64.8	0.0067	0.0	0.3055
EB0058	0.0000	0.0000	0.0039	130.6	0.0031	0.0	0.4607
EB0059	0.0000	0.0000	0.0000	58.8	0.0000	0.0	0.2116
EB0060	0.0000	0.0000	0.0062	53.9	0.0148	0.0	0.3235
EB0061	0.0000	0.0000	0.0045	93.2	0.0000	0.0	0.1787
EB0062	0.0000	0.0000	0.0035	47.8	0.0000	0.0	0.1766
EB0063	0.0000	0.0000	0.0080	195.8	0.0070	0.0	0.2887
EB0064	0.0389	0.0000	0.0112	388.5	0.0199	0.0	0.4677
EB0065	0.0217	0.0000	0.0090	157.3	0.0167	0.0	0.3206
EB0066	0.0335	0.0500	0.0155	265.0	0.0213	0.0	0.4821
EB0067	0.0151	0.0000	0.0085	245.1	0.0916	0.0	0.2985
EB0068	0.0089	0.0000	0.0113	164.4	0.0120	0.0	0.2767
EB0069	0.0000	0.0000	0.0021	149.4	0.0119	0.0	0.0799
EB0070	0.0124	0.0000	0.0052	127.2	0.0076	0.0	0.1539
EB0071	0.0184	0.0000	0.0050	137.7	0.0154	0.0	0.1626
EB0072	0.0138	0.0000	0.0051	116.4	0.0111	0.0	0.1624
EB0073	0.0200	0.0000	0.0043	115.3	0.0140	0.0	0.1704
EB0074	0.0174	0.0000	0.0051	87.8	0.0127	0.0	0.1555
EB0075	0.0165	0.0000	0.0054	162.6	0.0110	0.0	0.1308
EB0076	0.0335	0.0000	0.0090	238.0	0.0284	0.0	0.2329
EB0078	0.1628	0.2925	0.0570	1358.2	0.2227	0.0	1.5065
EB0079	0.1637	0.0000	0.0447	666.4	0.1933	0.0	1.1657
EB0080	0.1278	0.2652	0.0779	380.0	0.2013	0.0	1.7598
EB0081	0.5563	0.5851	0.2223	4464.1	0.6474	1949.4	5.2131
EB0082	0.2129	0.2952	0.0736	1689.9	0.3003	168.2	1.9644

Appendix 2, continued

Sample ID	Cs	Dy	Eu	Fe	Hf	K	La
EB0083	0.2321	0.3679	0.0820	1073.8	0.2695	0.0	2.1546
EB0084	0.3315	0.2126	0.1168	1948.2	0.3915	0.0	2.9454
EB0085	0.0481	0.1965	0.0639	516.6	0.3125	0.0	1.2717
EB0086	0.0510	0.0883	0.0286	320.6	0.1392	555.6	0.5361
EB0087	0.0235	0.0000	0.0071	264.7	0.0143	510.5	0.1837
EB0088	0.0000	0.0000	0.0081	193.9	0.0053	0.0	0.1319
EB0089	0.0000	0.0000	0.0042	217.3	0.0000	0.0	0.0893
EB0090	0.0192	0.0000	0.0079	196.7	0.0179	0.0	0.1830
EB0091	0.0092	0.0000	0.0047	266.5	0.0000	0.0	0.0903
EB0092	0.0000	0.0000	0.0039	95.9	0.0000	0.0	0.1137
EB0093	0.0099	0.0000	0.0037	126.6	0.0000	1061.9	0.1396
EB0094	0.0149	0.0000	0.0051	107.4	0.0124	391.1	0.1406
EB0095	0.0152	0.0000	0.0049	109.0	0.0088	0.0	0.1400
EB0096	0.0000	0.0000	0.0058	82.7	0.0058	457.5	0.1492
EB0097	0.0118	0.0000	0.0038	83.3	0.0066	0.0	0.1757
EB0098	0.0180	0.0000	0.0062	82.9	0.0000	0.0	0.1667
EB0099	0.0000	0.0000	0.0035	79.1	0.0000	0.0	0.1611
EB0100	0.4357	0.9859	0.2293	3867.2	0.5617	1612.9	5.1436
EB0101	0.3759	0.3572	0.0959	1419.6	0.4542	880.5	2.8577
EB0102	0.1539	0.1887	0.0472	1100.1	0.1890	247.7	1.3621
EB0103	0.1791	0.2560	0.0615	1008.1	0.2364	0.0	1.6657
EB0104	0.1760	0.1775	0.0562	560.1	0.2141	0.0	1.6123
EB0105	0.2263	0.3786	0.1008	1966.1	0.2802	0.0	2.6163
EB0106	0.2689	0.4798	0.1235	2305.8	0.3247	0.0	3.1575
EB0107	0.1884	0.1993	0.0664	1323.0	0.2921	0.0	1.7701
EB0108	0.1597	0.2411	0.0634	1413.5	0.2645	0.0	1.6249
EB0109	0.3039	0.5946	0.1739	2413.2	0.3419	0.0	3.9933
EB0110	0.3274	0.5760	0.1366	2678.1	0.3908	0.0	3.5189
EB0111	0.3048	0.4444	0.1435	890.7	0.3574	0.0	3.5007
EB0112	0.1860	0.2997	0.0588	1399.2	0.2670	0.0	1.6453

Appendix 2, continued

Sample ID	Lu	Mn	Na	Nd	Ni	Rb	Sb
EB0037	0.0367	88.37	414.5	0.9719	0.00	0.00	0.1518
EB0038	0.0000	110.57	196.8	0.4344	0.00	0.00	0.0262
EB0039	0.0221	20.14	164.6	1.1452	5.79	0.30	0.1836
EB0040	0.0000	8.71	799.3	1.1090	4.70	0.00	0.0353
EB0041	0.0211	18.85	445.4	0.0000	5.26	0.00	0.0769
EB0042	0.0056	6.65	182.6	0.0000	2.71	0.00	0.0514
EB0043	0.0069	25.84	459.0	0.5587	8.62	0.00	0.1201
EB0044	0.0167	9.02	526.3	0.0000	0.00	0.00	0.0263
EB0045	0.0146	13.02	192.8	0.0000	6.44	0.00	0.0518
EB0046	0.0186	21.61	667.2	0.7584	5.51	0.00	0.1514
EB0047	0.0056	13.60	240.9	0.4871	4.34	0.00	0.0867
EB0048	0.0196	2.58	505.6	0.0000	0.00	0.00	0.0350
EB0049	0.0047	7.03	1185.8	0.0000	0.00	0.00	0.0819
EB0050	0.0250	5.01	427.3	0.0000	0.00	0.00	0.0084
EB0051	0.0113	53.81	370.1	1.1584	4.61	0.00	0.1299
EB0052	0.0000	230.38	824.6	0.5981	0.00	0.00	0.0429
EB0053	0.0293	111.84	283.0	0.8905	0.00	0.00	0.0502
EB0054	0.0000	52.27	349.0	0.7899	6.79	0.00	0.0259
EB0055	0.0000	84.36	225.8	0.6269	4.58	0.00	0.0269
EB0056	0.0000	125.54	337.1	0.0000	0.00	0.00	0.0095
EB0057	0.0000	171.63	174.2	1.0679	0.00	0.00	0.0215
EB0058	0.0000	98.07	510.0	1.7305	4.17	0.00	0.0473
EB0059	0.0000	69.34	225.0	0.7260	0.00	0.00	0.0119
EB0060	0.0000	102.36	470.0	0.9733	2.96	0.00	0.0184
EB0061	0.0000	183.10	345.1	0.5279	3.31	0.00	0.0218
EB0062	0.0000	116.35	348.3	0.0000	3.44	0.00	0.0089
EB0063	0.0000	119.66	916.1	1.7987	0.00	0.00	0.0139
EB0064	0.0195	46.50	401.0	0.6612	4.38	0.45	0.0351
EB0065	0.0142	48.10	688.0	0.0000	3.48	0.00	0.0171
EB0066	0.0060	5.86	434.3	1.0591	6.16	0.00	0.1768
EB0067	0.0038	106.61	1694.4	0.0000	0.00	0.00	0.0580
EB0068	0.0059	143.07	209.2	0.0000	3.00	0.00	0.0224
EB0069	0.0000	119.04	348.6	0.0000	0.00	0.00	0.0256
EB0070	0.0112	115.31	259.8	0.0000	2.78	0.00	0.0242
EB0071	0.0000	62.84	508.5	0.0000	5.27	0.00	0.0178
EB0072	0.0000	54.13	194.5	0.0000	6.06	0.21	0.0176
EB0073	0.0000	51.77	384.9	0.0000	0.00	0.00	0.0177
EB0074	0.0000	40.73	233.2	0.0000	2.87	0.00	0.0201
EB0075	0.0000	85.78	257.8	0.6253	3.17	0.00	0.0374
EB0076	0.0102	143.97	267.3	0.0000	4.36	0.54	0.0299
EB0078	0.0471	12.85	9085.6	1.5552	0.00	2.60	0.0541
EB0079	0.0294	14.38	10481.0	1.3701	0.00	2.25	0.0242
EB0080	0.0286	13.01	1666.1	1.8233	0.00	2.32	0.0140
EB0081	0.1435	17.42	4907.0	6.2906	8.43	7.23	0.0922
EB0082	0.0609	13.82	1277.5	2.2272	7.58	3.49	0.0887

Appendix 2, continued

Sample ID	Lu	Mn	Na	Nd	Ni	Rb	Sb
EB0083	0.0641	23.85	2245.0	1.9171	0.00	3.67	0.1413
EB0084	0.0657	12.77	22297.5	2.8973	0.00	4.31	0.0837
EB0085	0.0365	16.72	383.5	1.4651	0.00	0.69	0.0713
EB0086	0.0000	9.08	1001.9	0.0000	0.00	0.00	0.0161
EB0087	0.0000	211.77	214.4	0.0000	3.66	0.00	0.0282
EB0088	0.0000	47.08	184.2	0.0000	2.74	0.00	0.0256
EB0089	0.0000	67.18	566.4	0.0000	2.67	0.12	0.0444
EB0090	0.0000	87.79	630.0	0.0000	4.15	0.00	0.0355
EB0091	0.0000	142.22	216.7	0.0000	6.17	0.00	0.0323
EB0092	0.0000	42.42	198.0	0.0000	3.81	0.00	0.0154
EB0093	0.0113	69.72	435.3	0.0000	0.00	0.54	0.0170
EB0094	0.0000	40.55	273.4	0.0000	3.51	0.00	0.0117
EB0095	0.0000	31.94	172.0	0.0000	2.43	0.00	0.0116
EB0096	0.0085	28.10	352.3	0.0000	2.51	0.00	0.0181
EB0097	0.0000	17.47	294.9	0.0000	4.21	0.00	0.0150
EB0098	0.0000	36.56	219.8	0.0000	2.57	0.00	0.0086
EB0099	0.0000	55.95	214.4	0.0000	2.89	0.00	0.0137
EB0100	0.1386	27.65	1741.2	7.1610	20.08	6.36	0.1175
EB0101	0.0780	12.49	2175.2	3.4926	5.06	5.83	0.0695
EB0102	0.0387	11.31	872.7	1.7301	6.16	2.54	0.0325
EB0103	0.0401	17.25	856.9	2.7155	10.01	2.69	0.0989
EB0104	0.0497	58.04	742.0	2.6825	0.00	2.31	3.1663
EB0105	0.0852	23.78	1089.3	4.7546	10.29	3.51	0.0927
EB0106	0.1020	22.80	1597.9	4.2258	12.13	3.77	0.0755
EB0107	0.0760	10.76	1263.6	2.5174	7.78	3.05	0.4289
EB0108	0.0569	17.02	1161.7	2.2573	5.94	3.02	0.0465
EB0109	0.1102	21.91	1243.8	5.7588	4.09	3.68	0.1427
EB0110	0.1275	25.74	1872.7	5.5558	16.01	5.21	0.2753
EB0111	0.1110	20.56	1592.2	4.4125	0.00	4.66	0.0331
EB0112	0.0414	13.04	740.7	1.3530	0.00	2.70	0.0889

Appendix 2, continued

Sample ID	Sc	Sm	Sr	Ta	Tb	Th	Ti
EB0037	0.0610	0.3051	272.59	0.0220	0.0246	0.1058	0.0
EB0038	0.0315	0.1152	238.68	0.0000	0.0000	0.0150	0.0
EB0039	0.1874	0.2716	78.81	0.0087	0.0307	0.0791	0.0
EB0040	0.0507	0.2094	202.08	0.0000	0.0106	0.0290	0.0
EB0041	0.0466	0.1471	199.62	0.0000	0.0100	0.0359	0.0
EB0042	0.0656	0.1171	180.91	0.0000	0.0104	0.0420	0.0
EB0043	0.0654	0.1458	169.44	0.0035	0.0154	0.0526	0.0
EB0044	0.0476	0.0880	220.67	0.0000	0.0108	0.0297	0.0
EB0045	0.0473	0.1049	162.60	0.0000	0.0081	0.0347	0.0
EB0046	0.0561	0.1519	146.23	0.0000	0.0198	0.0700	0.0
EB0047	0.0450	0.1087	221.70	0.0000	0.0127	0.0301	0.0
EB0048	0.0710	0.1312	236.84	0.0000	0.0096	0.0350	0.0
EB0049	0.0403	0.1176	161.86	0.0000	0.0085	0.0289	0.0
EB0050	0.0589	0.1457	399.86	0.0000	0.0043	0.0326	0.0
EB0051	0.0599	0.2876	239.43	0.0000	0.0239	0.0971	0.0
EB0052	0.0243	0.2591	306.30	0.0000	0.0000	0.0190	0.0
EB0053	0.1134	0.2573	245.59	0.0102	0.0148	0.1140	0.0
EB0054	0.0449	0.3391	271.78	0.0000	0.0048	0.0281	0.0
EB0055	0.0165	0.1356	237.23	0.0000	0.0000	0.0114	0.0
EB0056	0.0163	0.2162	228.44	0.0000	0.0000	0.0080	0.0
EB0057	0.0267	0.2643	262.90	0.0000	0.0000	0.0143	0.0
EB0058	0.0190	0.6130	245.28	0.0000	0.0000	0.0091	0.0
EB0059	0.0215	0.2325	214.71	0.0000	0.0000	0.0133	111.3
EB0060	0.0412	0.2795	159.59	0.0000	0.0000	0.0125	0.0
EB0061	0.0202	0.1681	186.18	0.0000	0.0000	0.0113	0.0
EB0062	0.0148	0.1837	210.82	0.0000	0.0000	0.0111	0.0
EB0063	0.0342	0.2880	269.57	0.0000	0.0000	0.0139	0.0
EB0064	0.0936	0.1340	308.09	0.0076	0.0090	0.0619	0.0
EB0065	0.0572	0.0967	301.68	0.0000	0.0057	0.0351	0.0
EB0066	0.1034	0.1839	326.05	0.0023	0.0106	0.0622	0.0
EB0067	0.0589	0.1380	271.71	0.0051	0.0089	0.0545	0.0
EB0068	0.0422	0.0987	225.04	0.0000	0.0084	0.0183	14.4
EB0069	0.0160	0.0444	269.23	0.0000	0.0000	0.0112	0.0
EB0070	0.0318	0.0925	389.34	0.0000	0.0000	0.0253	0.0
EB0071	0.0362	0.0723	263.18	0.0000	0.0000	0.0355	0.0
EB0072	0.0373	0.0817	258.96	0.0000	0.0058	0.0337	0.0
EB0073	0.0341	0.0814	298.44	0.0000	0.0000	0.0326	0.0
EB0074	0.0297	0.0963	230.94	0.0000	0.0000	0.0293	0.0
EB0075	0.0301	0.0893	316.48	0.0032	0.0000	0.0256	0.0
EB0076	0.0703	0.1389	140.98	0.0000	0.0048	0.0505	0.0
EB0078	0.4055	0.3886	1980.76	0.0493	0.0447	0.2832	0.0
EB0079	0.3402	0.3084	2437.61	0.0440	0.0237	0.2368	0.0
EB0080	0.4368	0.4633	2493.54	0.0435	0.0518	0.2550	0.0
EB0081	1.7643	1.4085	2461.96	0.1793	0.1554	1.0645	575.1
EB0082	0.5384	0.6099	2513.42	0.0637	0.0506	0.3835	0.0

Appendix 2, continued

Sample ID	Sc	Sm	Sr	Ta	Tb	Th	Ti
EB0083	0.5711	0.5641	2345.70	0.0691	0.0673	0.3911	193.4
EB0084	0.8708	0.7401	2257.66	0.0983	0.0777	0.5863	271.4
EB0085	0.2183	0.4103	752.81	0.0330	0.0462	0.2683	0.0
EB0086	0.1198	0.1905	2729.96	0.0165	0.0254	0.1169	0.0
EB0087	0.0454	0.1263	178.97	0.0000	0.0000	0.0310	0.0
EB0088	0.0327	0.1094	341.47	0.0000	0.0067	0.0282	0.0
EB0089	0.0197	0.0882	297.54	0.0000	0.0000	0.0164	0.0
EB0090	0.0423	0.1651	385.64	0.0000	0.0000	0.0317	0.0
EB0091	0.0242	0.0908	342.00	0.0000	0.0000	0.0173	0.0
EB0092	0.0190	0.0473	196.53	0.0000	0.0000	0.0081	0.0
EB0093	0.0234	0.0778	208.92	0.0000	0.0000	0.0136	0.0
EB0094	0.0371	0.0627	240.21	0.0000	0.0000	0.0242	0.0
EB0095	0.0343	0.0656	235.72	0.0000	0.0048	0.0212	0.0
EB0096	0.0210	0.0767	290.71	0.0000	0.0041	0.0147	0.0
EB0097	0.0292	0.1395	311.93	0.0000	0.0000	0.0256	0.0
EB0098	0.0250	0.1103	287.33	0.0000	0.0000	0.0152	0.0
EB0099	0.0203	0.0654	276.46	0.0031	0.0000	0.0159	0.0
EB0100	1.4699	1.4844	2063.63	0.1354	0.1547	1.1618	305.6
EB0101	0.8876	0.7977	1943.60	0.1184	0.0789	0.6997	285.4
EB0102	0.3647	0.4024	2239.04	0.0460	0.0361	0.2688	0.0
EB0103	0.4495	0.4394	1658.31	0.0516	0.0414	0.3067	140.0
EB0104	0.3991	0.4684	1789.00	0.0526	0.0472	0.2549	0.0
EB0105	0.6849	0.8617	2037.57	0.0734	0.0759	0.4951	266.9
EB0106	0.7767	1.0326	1691.17	0.0857	0.0898	0.6694	193.7
EB0107	0.4919	0.7098	2091.72	0.0565	0.0383	0.3575	221.4
EB0108	0.4609	0.6033	2267.89	0.0480	0.0466	0.3532	163.8
EB0109	1.0176	1.2870	1891.93	0.0935	0.1227	0.8044	323.0
EB0110	0.9605	1.2135	2743.73	0.1025	0.0931	0.6942	368.7
EB0111	0.9606	1.1650	2118.64	0.1013	0.0911	0.6620	160.1
EB0112	0.4632	0.4645	2406.64	0.0570	0.0351	0.3336	167.8

Appendix 2, continued

Sample ID	U	V	Yb	Zn	Zr
EB0037	1.7877	7.16	0.0900	19.67	12.59
EB0038	1.0477	7.93	0.0163	10.94	8.20
EB0039	1.0868	12.02	0.1936	16.79	9.83
EB0040	1.6712	4.82	0.0582	12.23	8.79
EB0041	1.0906	8.32	0.0480	16.35	11.20
EB0042	0.7391	4.65	0.0494	15.11	7.84
EB0043	1.0220	7.91	0.0766	21.69	7.33
EB0044	0.5983	3.29	0.0445	18.39	6.71
EB0045	0.7218	5.91	0.0620	15.89	5.66
EB0046	0.7522	1.74	0.0566	18.78	6.01
EB0047	0.7935	5.43	0.0606	14.85	6.96
EB0048	0.8378	0.00	0.0651	8.79	6.29
EB0049	1.0684	8.05	0.0304	8.36	10.97
EB0050	1.1568	6.83	0.0388	9.64	7.04
EB0051	1.8814	5.70	0.1092	14.13	12.72
EB0052	2.7909	18.67	0.0213	7.58	18.05
EB0053	2.0703	16.03	0.0392	10.27	15.40
EB0054	3.6179	11.90	0.0444	8.70	26.38
EB0055	1.5230	6.97	0.0000	10.24	11.30
EB0056	2.3671	7.98	0.0117	9.40	16.75
EB0057	2.7721	9.31	0.0515	12.74	19.99
EB0058	7.2064	16.43	0.0217	8.43	47.41
EB0059	2.5222	9.58	0.0270	9.22	16.64
EB0060	2.9984	9.56	0.0584	5.36	20.74
EB0061	1.5616	8.16	0.0174	12.31	12.26
EB0062	1.8156	7.01	0.0208	9.36	13.97
EB0063	3.0818	13.12	0.0335	9.11	21.15
EB0064	0.9466	1.25	0.0391	13.55	11.02
EB0065	0.7539	2.97	0.0282	9.78	4.75
EB0066	1.2604	8.43	0.0399	16.20	10.74
EB0067	1.0316	9.20	0.0344	3.85	11.63
EB0068	0.6457	11.39	0.0387	2.58	6.94
EB0069	0.4443	0.00	0.0000	3.04	2.78
EB0070	0.8544	0.00	0.0000	2.39	5.58
EB0071	0.6297	0.00	0.0142	2.05	3.99
EB0072	0.6919	0.00	0.0171	2.46	6.17
EB0073	0.8866	6.74	0.0000	2.21	8.39
EB0074	0.6735	5.07	0.0000	1.76	5.90
EB0075	0.8543	5.08	0.0000	1.49	5.79
EB0076	0.8665	9.47	0.0195	1.87	7.22
EB0078	1.4831	0.00	0.2156	4.69	15.50
EB0079	1.1536	0.00	0.1086	5.61	14.16
EB0080	1.3919	8.56	0.1963	4.84	18.11
EB0081	3.0537	13.14	0.5444	10.10	36.14
EB0082	2.3058	9.47	0.1909	8.60	18.88

Appendix 2, continued

Sample ID	U	V	Yb	Zn	Zr
EB0083	1.8923	10.36	0.2054	11.93	17.29
EB0084	2.7780	0.00	0.2932	7.03	19.96
EB0085	1.1819	0.00	0.1476	2.30	15.02
EB0086	0.8936	9.98	0.0910	3.35	7.33
EB0087	1.1258	0.00	0.0203	1.63	6.94
EB0088	1.0052	9.27	0.0150	3.42	4.67
EB0089	0.8651	12.15	0.0000	2.60	4.00
EB0090	1.5668	8.39	0.0000	2.15	9.93
EB0091	0.9695	4.85	0.0000	2.72	5.49
EB0092	0.4397	0.00	0.0129	5.30	2.57
EB0093	0.7411	0.00	0.0246	6.69	3.98
EB0094	0.4001	0.00	0.0118	6.49	2.22
EB0095	0.5033	3.01	0.0201	6.20	0.00
EB0096	0.6374	0.00	0.0339	8.07	0.00
EB0097	1.4795	0.00	0.0000	8.06	7.78
EB0098	0.8921	0.00	0.0157	6.34	5.63
EB0099	0.5902	0.00	0.0302	6.15	4.22
EB0100	3.4031	21.58	0.5030	16.33	36.63
EB0101	2.8603	14.93	0.2291	7.03	29.49
EB0102	1.8627	8.79	0.1108	5.08	11.89
EB0103	1.6503	12.09	0.1593	6.06	11.10
EB0104	2.2385	8.06	0.1427	2.42	15.33
EB0105	3.5176	18.63	0.2908	9.96	26.24
EB0106	3.8345	15.57	0.2891	10.63	30.30
EB0107	3.9895	20.08	0.1727	6.68	26.36
EB0108	2.6062	10.27	0.1672	5.54	18.36
EB0109	4.0877	25.12	0.3929	7.53	29.71
EB0110	5.2673	25.44	0.3436	11.71	35.32
EB0111	4.4226	18.03	0.3417	5.46	31.74
EB0112	1.7936	13.84	0.1341	5.37	23.07

Appendix 3 - Limestone source information for the Harrell Egyptian limestone samples.

ID	Formation	Location	Coordinates	
			°N	°E
EL-01	Alexandria	Abu Sir	30.9467	29.5000
EL-02	Alexandria	Abu Sir	30.9467	29.5000
EL-03	Alexandria	Mex village	31.1542	29.8433
EL-04	Mokattam	Zawyet on Gebel Mokattam near Citadel	30.0267	31.2700
EL-05	Mokattam	Gebel Tura near Tura village	29.9333	31.2987
EL-06	Mokattam	Gebel Hof near el-Masara village	29.9150	31.3200
EL-07	Mokattam	Gebel Hof near el-Masara village	29.9150	31.3200
EL-08	Mokattam	Wadi Abu Mu'aymil near St. Antony Monastery	28.8983	32.3250
EL-09	Mokattam	Wadi Abu Mu'aymil near St. Antony Monastery	28.8983	32.3250
EL-10	Mokattam	Wadi Abu Mu'aymil near St. Antony Monastery	28.8983	32.3250
EL-11	Mokattam	Wadi Abu Mu'aymil near St. Antony Monastery	28.8983	32.3250
EL-12	Mokattam	Wadi Umm Zanatir near St. Antony Monastery	28.9383	32.3950
EL-13	Mokattam	Wadi Umm Zanatir near St. Antony Monastery	28.9383	32.3950
EL-14	Samalut	near el-Sawayta village	28.3768	30.8010
EL-15	Samalut	el Babein tomb near Beni Khalid village	28.3047	30.7507
EL-16	Samalut	Zawyet el-Amwat village in Zawyet Sultan district	28.0550	30.8317
EL-17	Minia	Beni Hasan tombs	27.9107	30.8717
EL-18	Minia	Beni Hasan tombs	27.9107	30.8717
EL-19	Minia	el-Sheikh Timay village	27.8617	30.8453
EL-20	Minia	Wadi el-Nakla near Deir el-Bersha village	27.7512	30.9193
EL-21	Minia	Wadi el-Nakla near Deir el-Bersha village	27.7512	30.9193
EL-22	Minia	Wadi el-Nakla near Deir el-Bersha village	27.7512	30.9193
EL-23	Minia	Wadi el-Nakla near Deir el-Bersha village	27.7512	30.9193
EL-24	Minia	Wadi el-Nakla near Deir el-Bersha village	27.7512	30.9193
EL-25	Minia	Wadi el-Nakla near Deir el-Bersha village	27.7512	30.9193
EL-26	Minia	Wadi el-Nakla near Deir el-Bersha village	27.7512	30.9193
EL-27	Minia	el-Bersha village on Gebel Sheikh Said	27.7207	30.8945
EL-28	Minia	eastern Wadi el-Zebeida (Queen Tiy Quarry)	27.6835	30.9022
EL-29	Minia	eastern Wadi el-Zebeida (Queen Tiy Quarry)	27.6835	30.9022
EL-30	Minia	eastern Wadi el-Zebeida (Queen Tiy Quarry)	27.6835	30.9022
EL-31	Minia	eastern Wadi el-Zebeida (Queen Tiy Quarry)	27.6835	30.9022
EL-32	Minia	central Wadi el-Zebeida (Abd el-Azziz Quarry)	27.6895	30.9058
EL-33	Minia	central Wadi el-Zebeida (Abd el-Azziz Quarry)	27.6895	30.9058
EL-34	Minia	western Wadi el-Zebeida	27.6928	30.9017
EL-35	Minia	near Sheikh Said tomb on Gebel Sheikh Said	27.6997	30.8890
EL-36	Minia	near Sheikh Said tomb on Gebel Sheikh Said	27.6997	30.8890
EL-37	Minia	near Sheikh Said tomb on Gebel Sheikh Said	27.6997	30.8890
EL-38	Minia	near Sheikh Said tomb on Gebel Sheikh Said	27.6997	30.8890
EL-39	Minia	Northern Tombs at Amarna ruins	27.6620	30.9297
EL-40	Minia	Northern Tombs at Amarna ruins	27.6620	30.9297
EL-41	Minia	el-Maabda village on Gebel el-Harrana	27.3453	31.0283
EL-42	Minia	Deir el-Gabrawi village on Gebel el-Tawila	27.3388	31.1032
EL-43	Minia	Arab el-Atiat el-Bahariya village on Gebel el-Harrana	27.3345	31.0662
EL-44	Drunka	el-Izam monastery near Assiut city	27.1542	31.1483
EL-45	Drunka	Wadi Emu	27.1195	31.3568

Appendix 3 - Limestone source information for the Harrell Egyptian limestone samples, continued.

ID	Formation	Location	Coordinates	
			N	E
EL-46	Drunka	el-Khawalid village	27.0935	31.3870
EL-47	Drunka	Qaw el-Kebir/Antaeopolis ruins	26.9218	31.5002
EL-48	Drunka	Qaw el-Kebir/Antaeopolis ruins	26.9218	31.5002
EL-49	Drunka	Nazlet el-Haridi village on Gebel el-Haridi	26.7772	31.5518
EL-50	Drunka	el-Salamuni village	26.6178	31.7642
EL-51	Drunka	Nag Hamad village and Athribis ruins	26.5093	31.6627
EL-52	Drunka	Nag Hamad village and Athribis ruins	26.5093	31.6627
EL-53	Drunka	el-Salmuni village and Abydos ruins (mostly destroyed)	26.2042	31.8758
EL-54	Drunka	Wadi Naqb el-Salmuni near Abydos ruins	26.1935	31.8658
EL-55	Drunka	Wadi Naqb el-Salmuni near Abydos ruins	26.1935	31.8658
EL-56	Serai	Nag el-Buza village	26.0950	32.3000
EL-57	Issawia	Gebel el-Gir near Tentyris/Dendara ruins	26.1045	32.6950
EL-58	Serai	Wadi el-Muluk (Valley of Kings) and Qurna	25.7463	32.6225
EL-59	Serai	Wadi el-Muluk (Valley of Kings) and Qurna	25.7463	32.6225
EL-60	Serai	el-Ghrera village in el-Gebelein district (now destroyed)	25.4977	32.4790
EL-61	Tarawan	el-Dibabiya village	25.5013	32.5183
EL-62	Tarawan	el-Dibabiya village	25.5013	32.5183

Appendix 4 – Concentration data from NAA for limestone from Egypt (Harrell samples). All concentrations are in parts per million (ppm)

Sample ID	Al	As	Ba	Ca	Ce	Co	Cr
EL01	723.4373	12.082	38.73553	380778.8	3.3874	0.2964	2.3437
EL02	1632.057	15.0009	23.28542	382987.3	3.7104	0.3575	2.6266
EL03	0	2.0288	17.90644	375440.6	2.0614	0.1109	1.8339
EL04	9204.907	5.2011	24.72878	354192.8	8.9902	0.5688	30.9747
EL05	5482.053	1.8776	43.52981	343062.6	4.8384	0.2821	23.3047
EL06	0	0.9003	91.05511	276624.6	0.8977	0.0829	9.5759
EL07	0	0.28	13.51148	384113.3	1.1704	0.0772	12.0844
EL08	4191.739	0.3489	40.35509	379221.8	3.8859	0.2349	23.2527
EL09	3794.588	0.8741	17.77534	371380.5	3.8971	0.2453	18.8732
EL10	2060.192	0.8426	10.53595	383732.3	2.6199	0.1029	14.8273
EL11	6185.242	2.2953	25.413	363021.1	6.8083	0.6473	30.6139
EL12	3507.994	1.074	0	231764.8	1.3711	0.5827	6.0781
EL13	4906.892	1.2019	0	252326.8	1.2592	1.1459	11.0204
EL14	4828.893	0	8.03519	398464	0.4031	0.0665	6.3108
EL15	6041.666	0	0	401336.9	0.4738	0.0265	6.9172
EL16	4697.163	0	0	408532.9	0.3962	0.0471	4.1542
EL17	10260.58	0.113	16.98495	400398	0.7205	0.0777	7.5618
EL18	3300.669	0.2921	19.82584	401567.8	0.7636	0.2297	6.7607
EL19	1828.264	0.4307	0	398113.3	1.5801	0.1906	10.1975
EL20	1420.299	0.227	0	399441.7	0.515	0.1199	7.8936
EL21	3463.952	0	0	401099.4	0.4809	0.0373	11.4205
EL22	508.7635	0.3126	0	409365.5	0.4122	0.0268	9.5965
EL23	0	0.1877	0	405182.7	0.4379	0.0236	15.8539
EL24	665.5685	0	0	400512.3	0.5215	0.0488	8.8138
EL25	0	0	0	396609.8	0.476	0.0421	12.2639
EL26	0	0.298	8.87214	405606.4	0.4892	0.0816	9.3463
EL27	0	0.5053	162.0849	396315.5	0.3118	0.2907	4.8339
EL28	1350.58	0	0	401009.1	0.7505	0.0707	9.4043
EL29	0	0	0	405085.7	0.4243	0.062	6.699
EL30	588.2661	0	0	395176.3	0.307	0.0314	5.9396
EL31	4831.842	0	0	404898.5	0.4354	0.0636	7.1738
EL32	0	0	0	402996.8	0.2404	0.1445	7.14
EL33	0	0	0	395812.5	0.4202	0.1556	4.9878
EL34	0	0	0	395425.9	0.2571	0.0211	5.5698
EL35	0	0.5831	21.56146	389214.6	1.4283	0.0824	7.9978
EL36	0	0	7.70596	392607.5	0.6953	0.0728	5.3599
EL37	1657.535	0.4273	0	359715.3	1.8887	0.2458	38.1255
EL38	0	0	10.75944	386910	0.4404	0.073	6.5269
EL39	0	0	0	402256.8	0.4737	0.1087	5.138
EL40	0	0	0	394662.6	0.4383	0.0522	5.6434
EL41	0	0	0	393214.5	0.2793	0.1534	5.0608
EL42	0	0	13.65086	396275.2	0.8084	0.1809	9.4878
EL43	602.6922	0	13.03092	398985.5	0.5134	0.1955	2.3445
EL44	1453.334	0	13.34118	391381.8	0.271	0.1364	4.6014
EL45							

Appendix 4, continued

Sample ID	Al	As	Ba	Ca	Ce	Co	Cr
EL46	3854.677	0	0	395907.8	0.6739	0.1316	9.2355
EL47	2219.237	0	0	399337.4	0.3482	0.1105	5.6537
EL48	5256.07	0	0	402816.7	0.5301	0.1825	4.1893
EL49	2388.83	0	15.02989	411851	0.2832	0.1311	5.5741
EL50	1222.226	0	0	406193.9	0.2164	0.125	8.285
EL51	0	0.307	44.19081	394167.1	0.2921	0.1201	4.0962
EL52	0	0.2869	39.12222	408888.1	0.5962	0.1748	7.5556
EL53	1079.175	0	27.67321	400048.8	1.052	0.1079	6.6188
EL54	0	0.1522	15.13041	403665.5	1.3008	0.0707	10.8048
EL55	0	0.4066	17.71337	400098	2.1467	0.3903	16.0166
EL56	1800.865	0.4217	31.1739	360483.9	1.8718	0.1406	33.8924
EL57	6748.384	0.9706	40.93084	239055.3	9.2895	1.9224	71.8134
EL58	8046.468	1.8536	22.032	306716.1	10.8423	2.6984	44.0464
EL59	10069.42	1.2169	52.99543	276179.5	11.4837	1.8664	69.4308
EL60	990.9293	0.4342	17.80272	330374.4	1.9206	0.3544	44.7385
EL61	8826.216	1.2488	158.2274	274685.9	15.0968	4.5816	55.134
EL62	10485.34	1.2516	327.1948	270151.5	18.9766	5.0219	57.6346

Appendix 4, continued

Sample ID	Cs	Dy	Eu	Fe	Hf	K	La
EL01	0.0374	0.5396	0.0779	1450.398	0.1835	0	1.3923
EL02	0.0398	0.3387	0.0942	1798.032	0.0979	0	1.6877
EL03	0.0257	0.3751	0.0364	400.3628	0.1322	0	0.776
EL04	0.5289	0.4956	0.1637	4948.203	0.8452	727.2986	4.4866
EL05	0.2894	0.3236	0.1081	2211.933	0.4325	0	2.5929
EL06	0	0.0459	0.0232	479.8501	0.3495	0	0.4953
EL07	0.0258	0.2194	0.0333	249.444	0.4269	0	0.674
EL08	0.1009	0.3608	0.1047	1592.769	0.3797	1179.483	2.6663
EL09	0.105	0.229	0.096	1990.069	0.3966	1086.756	2.2495
EL10	0.0418	0.3328	0.0666	1157.213	0.2506	0	1.6691
EL11	0.192	0.5701	0.1662	3937.007	0.6078	1489.509	3.9003
EL12	0.0552	0	0.0198	33698.04	0.02	0	0.5562
EL13	0.0389	0	0.0248	39265.82	0.0245	0	0.6437
EL14	0	0.137	0.0169	49.2617	0.0338	0	0.5636
EL15	0	0	0.0176	30.6542	0.0595	0	0.5447
EL16	0	0	0.0114	27.5386	0.0436	0	0.481
EL17	0	0	0.0049	62.897	0.0659	0	0.218
EL18	0	0	0.0049	304.612	0.0662	0	0.1896
EL19	0.0162	0.1719	0.0552	345.1442	0.3745	0	1.3838
EL20	0.0126	0	0.009	150.7457	0.0973	0	0.2975
EL21	0.0268	0	0.0079	91.7291	0.0171	0	0.3581
EL22	0.0211	0	0.0073	78.1986	0.0112	0	0.2983
EL23	0.0163	0	0.0096	65.4546	0.0095	77.33	0.4294
EL24	0.013	0.2338	0.01	85.3663	0.0129	0	0.3872
EL25	0.0208	0	0.0092	147.9299	0.0163	0	0.3055
EL26	0.0237	0	0.009	166.9162	0.0169	0	0.3624
EL27	0	0	0.0041	186.1024	0	0	0.1198
EL28	0.027	0	0.0111	150.3192	0.1376	0	0.4736
EL29	0.0147	0.087	0.0076	56.4655	0.0787	0	0.2983
EL30	0	0	0.0063	44.3811	0.0092	0	0.2134
EL31	0.0139	0	0.0082	83.4844	0.0115	0	0.3743
EL32	0	0	0.0045	51.252	0.0043	0	0.1656
EL33	0.0262	0	0.0069	144.9231	0.0073	0	0.2419
EL34	0	0	0.0055	61.8807	0.0066	0	0.1324
EL35	0.0126	0.1094	0.008	116.8608	0	0	0.4666
EL36	0.0238	0	0.0096	241.2478	0.0142	1233.601	0.3292
EL37	0.1551	0.2451	0.041	1166.068	0.1076	697.9789	1.2591
EL38	0.0158	0	0.008	135.8086	0.012	0	0.2203
EL39	0.0142	0	0.0058	89.3379	0.0091	0	0.2033
EL40	0	0	0.0032	37.435	0.0072	0	0.1725
EL41	0	0	0.0043	82.7982	0.18	0	0.1698
EL42	0.0201	0	0.008	157.249	0.1469	0	0.3391
EL43	0.0148	0	0.0075	135.1587	0.1153	0	0.221
EL44	0.009	0	0.0046	71.3161	0.0294	173.2735	0.1336
EL45	0.0264	0	0.0104	202.0459	0.1396	0	0.4223

Appendix 4, continued

Sample ID	Cs	Dy	Eu	Fe	Hf	K	La
EL46	0.0347	0	0.0135	189.9125	0.1258	0	0.4246
EL47	0.0101	0	0.0053	131.3949	0.0269	0	0.1685
EL48	0.0145	0	0.0082	195.4129	0.0234	0	0.2537
EL49	0	0	0.0026	53.22	0.059	0	0.1458
EL50	0	0	0.0047	53.9828	0.0479	0	0.1811
EL51	0.0178	0	0.004	458.5437	0.0696	0	0.1263
EL52	0.0137	0	0.0074	401.6594	0.183	0	0.2404
EL53	0.044	0	0.007	186.1854	0.0492	0	0.3028
EL54	0.0218	0.1013	0.0302	275.3276	0.067	0	0.6393
EL55	0.0474	0.2325	0.0516	741.6682	0.6514	0	1.1757
EL56	0.0845	0.042	0.0272	585.0671	0.0529	0	0.9368
EL57	0.4681	0.8316	0.1684	5694.186	0.8675	0	4.6481
EL58	0.4577	0.575	0.1959	6407.481	1.4812	1158.705	5.3008
EL59	0.5395	0.7299	0.2058	7424.528	1.0799	1609.493	5.4622
EL60	0.0937	0.1402	0.0325	983.686	0.0781	1143.589	1.18
EL61	0.708	2.7671	0.685	7669.845	0.5234	1951.388	15.049
EL62	0.8627	3.7595	0.8822	8556.633	0.6152	1451.53	19.3173

Appendix 4, continued

Sample ID	Lu	Mn	Na	Nd	Ni	Rb	Sb
EL01	0.0301	34.3109	1064.067	1.7869	0	0.9209	0.0825
EL02	0.035	43.5692	1003.023	2.7748	0	0.7298	0.1168
EL03	0.0159	13.015	6456.238	3.5621	0	0.896	0.0309
EL04	0.0544	27.0273	1112.977	3.676	0	7.5503	0.2019
EL05	0.0348	14.1102	3559.249	2.3654	10.2143	4.5842	0.1056
EL06	0.0102	10.7988	1599.525	0	2.3651	0	0.0617
EL07	0.0168	16.9071	848.515	0.9552	0	0.8688	0.0363
EL08	0.0377	57.1585	459.3869	2.8752	6.307	2.3893	0.0477
EL09	0.033	29.0611	434.3038	2.126	3.3955	2.5947	0.1632
EL10	0.0258	29.0441	245.9055	1.3345	0	0.7673	0.0997
EL11	0.0651	40.316	720.0685	4.1882	16.818	4.1427	0.25
EL12	0.0121	1339.166	670.811	1.009	0	0	0.0278
EL13	0	1495.365	696.4515	1.9215	0	2.4554	0.064
EL14	0.0091	8.1181	306.6308	0	0	0	0.011
EL15	0.0136	2.788	344.1302	0	0	0	0.0061
EL16	0.0046	52.6155	457.3216	0.8041	0	0	0
EL17	0.0034	51.2094	361.7356	0.9619	1.6612	0	0.0096
EL18	0.0034	161.3169	1312.553	1.1929	0	0	0.0469
EL19	0.0252	51.7697	3177.694	1.6061	0	0	0.1093
EL20	0.008	8.9752	1176.862	0	3.1257	0	0.1008
EL21	0	2.5637	3058.591	0	0	0	0.0217
EL22	0	2.0483	175.8513	0	2.2136	0	0.0218
EL23	0	2.5053	191.0553	0	0	0	0.0046
EL24	0.006	5.1695	160.2459	0	0	0	0.0449
EL25	0	12.6175	220.3936	0	0	0	0.0637
EL26	0.0158	6.538	345.404	0	0	0	0.3041
EL27	0	1142.789	2634.11	0	0.6276	0	0.0263
EL28	0.0042	7.3827	402.2969	0	0	0	0.0354
EL29	0.0046	5.8379	133.4854	0	0	0	0.0056
EL30	0	3.7516	123.0436	0	0	0	0.0149
EL31	0.0167	6.6473	141.5274	0	0	0	0.0212
EL32	0.013	2.9104	235.5294	0	1.605	0	0
EL33	0	5.9085	143.226	0	0	0	0.1402
EL34	0.0017	3.0269	111.214	0	0	0	0.0088
EL35	0.0064	11.6866	176.8533	1.698	0	0	0.2018
EL36	0	63.4345	354.399	0	2.1257	0.6697	0.0483
EL37	0.0171	30.7654	552.128	1.7245	6.8641	2.3267	0.0504
EL38	0	8.9243	4000.347	0	0	0	0.0049
EL39	0	4.3713	139.7246	0	0	0	0.0574
EL40	0	2.0882	108.7462	0	0	0	0.0118
EL41	0.0028	36.0973	756.6639	0	2.103	0	0.0183
EL42	0.0046	7.0797	247.3509	0	6.4983	0	0.0348
EL43	0	68.0256	192.9405	0	3.4825	0	0.0317
EL44	0.0015	24.5823	217.638	0	4.2704	0	0
EL45	0.0058	11.9245	373.7765	0	0	0	0.0139

Appendix 4, continued

Sample ID	Lu	Mn	Na	Nd	Ni	Rb	Sb
EL46	0.0033	9.5907	158.0595	0	0	0	0.0083
EL47	0	4.2884	175.9028	0	1.809	0	0.0757
EL48	0	11.0106	534.4362	0	4.3701	0.4496	0.2277
EL49	0.0032	52.9297	321.0579	0	3.7417	0	0.0333
EL50	0.0059	5.9865	190.9769	0	2.2595	0	0.0091
EL51	0.0088	126.3166	415.8568	0	0	0	0.013
EL52	0	140.4131	467.0687	0	0	0	0.0189
EL53	0	4.1455	236.125	0	0	0.2931	0.038
EL54	0.0212	16.1386	142.008	0	0	0	0.0121
EL55	0.0394	58.2782	274.9984	2.1373	0	0	0.0464
EL56	0	16.0943	449.1566	1.2677	0	1.6721	0.0523
EL57	0.0472	77.0488	19189.6	6.467	13.1045	7.9769	0.1065
EL58	0.0956	112.0825	1526.814	5.5222	13.0176	6.5001	0.2366
EL59	0.0741	67.9393	2966.074	8.1652	13.3228	10.3911	0.1741
EL60	0.0394	35.1365	2965.087	2.0817	4.4029	1.7252	0.0393
EL61	0.2904	111.385	3460.12	14.7363	46.752	7.8564	0.2725
EL62	0.3843	134.0708	3772.372	18.155	53.8096	9.2892	0.2524

Appendix 4, continued

Sample ID	Sc	Sm	Sr	Ta	Tb	Th	Ti
EL01	0.2433	0.5554	11290.6	0.0193	0.0544	0.176	34.8701
EL02	0.2777	0.6135	10933.83	0.0192	0.0682	0.1948	0
EL03	0.1746	0.3685	7474.351	0.0165	0.0257	0.1094	0
EL04	1.4133	0.9746	1828.375	0.1975	0.1257	1.0202	572.3628
EL05	0.775	0.6597	3563.617	0.0919	0.0738	0.5334	383.6012
EL06	0.118	0.1853	3638.516	0.009	0.0205	0.0871	0
EL07	0.1558	0.2149	2093.064	0.0126	0.0323	0.0956	96.9171
EL08	0.6648	0.5222	2493.24	0.047	0.0726	0.3125	212.6439
EL09	0.67	0.5995	3211.235	0.0422	0.0667	0.4126	319.8443
EL10	0.4781	0.4117	2298.087	0.0285	0.0391	0.1934	339.5098
EL11	1.4061	0.9476	2277.717	0.1023	0.1136	0.6302	621.2758
EL12	0.1427	0.2666	231.459	0	0.0201	0.0798	0
EL13	0.1796	0.2386	246.1732	0	0	0.1136	0
EL14	0.0354	0.0967	260.743	0	0.0109	0.0224	0
EL15	0.0342	0.0925	269.2094	0	0.013	0.0238	0
EL16	0.0219	0.0896	208.0103	0	0.0092	0.012	0
EL17	0.0234	0.2002	229.6062	0	0	0.0137	0
EL18	0.0438	0.2271	280.4822	0	0.0024	0.0212	0
EL19	0.1305	0.2747	292.9138	0.0058	0.051	0.0723	0
EL20	0.0494	0.1176	296.5218	0	0.0092	0.0251	0
EL21	0.0794	0.123	353.4978	0	0.0092	0.034	0
EL22	0.0583	0.0876	201.764	0	0.0091	0.0278	0
EL23	0.0688	0.1056	294.1511	0	0.0127	0.0409	0
EL24	0.0561	0.11	244.1501	0	0.0088	0.0381	0
EL25	0.066	0.1032	321.1066	0	0.0054	0.0331	0
EL26	0.0956	0.0963	256.7806	0.004	0.0078	0.0512	0
EL27	0.0211	0.0602	203.2115	0	0	0.0101	0
EL28	0.0688	0.152	230.861	0.0042	0.0091	0.0448	0
EL29	0.0374	0.1145	189.2319	0.003	0.0063	0.0221	0
EL30	0.0338	0.0599	209.5441	0	0	0.0138	0
EL31	0.0395	0.1273	186.3802	0	0.0092	0.0219	0
EL32	0.0289	0.0671	180.5539	0	0.0057	0.0122	0
EL33	0.0504	0.0958	196.711	0	0.0054	0.0314	0
EL34	0.0186	0.101	235.0531	0	0	0.0098	0
EL35	0.0301	0.3679	442.0373	0	0.0099	0.0187	0
EL36	0.0785	0.1421	313.5757	0	0.008	0.062	0
EL37	0.3937	0.2973	479.3769	0.0304	0.0433	0.2549	0
EL38	0.0461	0.0839	522.1274	0	0	0.0355	0
EL39	0.0406	0.0864	255.1243	0	0.0057	0.026	0
EL40	0.0211	0.1249	238.6739	0	0	0.013	0
EL41	0.0172	0.0751	176.3389	0	0	0.0092	0
EL42	0.0457	0.2141	295.343	0	0	0.0474	124.018
EL43	0.0506	0.1149	155.4796	0.0053	0	0.0378	0
EL44	0.0274	0.0766	128.7726	0	0	0.023	0
EL45	0.0714	0.2061	461.2819	0.0051	0	0.0666	0

Appendix 4, continued

Sample ID	Sc	Sm	Sr	Ta	Tb	Th	Ti
EL46	0.0933	0.1418	466.2859	0.0074	0.0161	0.0607	0
EL47	0.0303	0.0809	255.434	0	0	0.0184	0
EL48	0.0616	0.1373	183.3022	0	0	0.0453	0
EL49	0.0105	0.0102	264.9862	0	0	0.0085	0
EL50	0.0197	0.0521	186.202	0	0.0073	0.0182	0
EL51	0.0356	0.0686	371.202	0	0	0.0397	0
EL52	0.0458	0.1529	226.5613	0	0.0053	0.0329	0
EL53	0.0711	0.2423	515.4393	0	0.0053	0.0661	0
EL54	0.0991	0.2517	291.4455	0	0.0186	0.1114	0
EL55	0.235	0.3519	205.0295	0.0177	0.0404	0.2945	0
EL56	0.1736	0.4344	4278.684	0.0144	0.0155	0.1286	0
EL57	1.7811	0.8381	1450.459	0.1541	0.0994	1.2051	367.3408
EL58	1.9266	1.0331	1858.577	0.1788	0.1205	1.2621	781.2933
EL59	2.0828	1.1204	1950.057	0.1751	0.1252	1.4198	699.3959
EL60	0.2744	0.3335	2124.61	0.0197	0.0249	0.1467	0
EL61	4.0379	2.8899	1248.565	0.1283	0.4862	1.5436	349.8646
EL62	4.9028	3.6965	1120.609	0.1389	0.638	1.9149	224.1217

Appendix 4, continued

Sample ID	U	V	Yb	Zn	Zr
EL01	3.032	7.9294	0.2054	1.3756	22.5537
EL02	2.8863	7.5073	0.2319	1.4084	21.9198
EL03	2.4951	0	0.125	0.8558	21.8603
EL04	2.9	18.7925	0.358	12.2408	41.1845
EL05	2.3815	12.8581	0.2671	8.9789	27.4947
EL06	0.9999	2.8176	0.1064	3.0109	17.4974
EL07	1.0064	6.4402	0.1285	2.5326	19.0856
EL08	1.7332	9.3488	0.2516	13.8195	17.4705
EL09	2.1205	13.7889	0.3115	10.4437	24.2473
EL10	1.8724	16.6078	0.1416	8.1415	18.6158
EL11	3.2001	30.8785	0.3673	19.5619	35.1588
EL12	2.2403	0	0.0502	8.6349	11.9428
EL13	1.5971	12.1595	0.038	7.4144	6.6969
EL14	0.332	0	0.0415	2.4006	3.279
EL15	0.338	0.8985	0.0565	3.7945	3.3155
EL16	0.578	0	0.0334	3.6516	5.0081
EL17	2.0094	11.3434	0	8.1023	14.3838
EL18	2.163	7.5182	0	7.8103	16.5354
EL19	0.7837	7.5216	0.1735	13.7863	16.5669
EL20	0.8816	4.0829	0.0495	10.6507	7.8324
EL21	1.0257	0	0.0478	10.6218	6.5836
EL22	0.7445	4.0603	0.0251	9.5381	5.1326
EL23	0.6838	9.3305	0.0441	10.4029	5.3454
EL24	0.838	8.4779	0.0411	10.0226	7.6276
EL25	0.7143	5.7707	0.0276	8.8814	4.8567
EL26	0.6064	7.8829	0.0342	11.7557	5.7535
EL27	0.3747	17.6844	0	7.3011	3.3687
EL28	1.1327	3.5604	0.0328	6.7768	11.0694
EL29	1.0068	0	0.0366	5.8483	7.8417
EL30	0.5529	3.0444	0.0253	3.6863	2.8913
EL31	0.8298	1.9009	0.0224	5.3279	7.4458
EL32	0.5908	0	0.0211	5.2849	3.2315
EL33	0.7985	7.7772	0.0315	11.5935	5.7069
EL34	0.7805	0	0	6.5919	5.1082
EL35	3.7759	12.0885	0.0492	8.7755	22.4288
EL36	1.1998	9.8503	0.0256	8.7215	7.4088
EL37	1.3496	17.1491	0.1141	19.5972	9.4212
EL38	0.5715	0	0	4.2853	5.6691
EL39	0.8771	7.0999	0.0208	7.4022	6.0646
EL40	1.2748	11.964	0	6.9998	7.9397
EL41	0.6618	0	0	9.4886	7.6919
EL42	1.6895	14.0219	0.0244	9.2345	15.5206
EL43	1.0132	6.0041	0.0222	3.5119	9.6047
EL44	0.7392	4.7171	0.0157	3.0409	4.6871
EL45	1.5446	10.1572	0.0413	5.6344	12.4842

Appendix 4, continued

Sample ID	U	V	Yb	Zn	Zr
EL46	0.9576	23.3888	0.037	6.1448	9.8634
EL47	0.6377	0	0	3.0822	4.2509
EL48	0.9706	9.3313	0	14.0141	7.142
EL49	0.8685	4.3765	0	3.0171	6.808
EL50	0.3305	0	0.0365	6.8323	3.8955
EL51	0.4956	6.499	0	2.1383	5.9543
EL52	1.2156	7.2502	0.0231	6.5661	13.4194
EL53	2.2697	13.3964	0	2.2548	15.5998
EL54	1.0953	4.5943	0.0838	14.4077	9.6091
EL55	0.9622	6.6202	0.1437	15.1188	24.6919
EL56	3.6851	25.4008	0.0902	9.3571	25.9875
EL57	1.768	54.6314	0.3654	31.0637	32.2842
EL58	1.7584	55.2784	0.4872	33.4192	53.2964
EL59	2.5504	62.9306	0.3317	40.1934	37.5222
EL60	2.0311	33.2006	0.1042	14.253	15.7593
EL61	2.6861	42.5034	1.9354	67.3745	49.4551
EL62	2.702	45.6051	2.48	63.6789	41.7665

Appendix 5 – Geographical data for African obsidian samples from Kenya

ANID	Source Name	Coordinates	
		°N or °S	°E
KES001	Kinangop #1	-0.63350	36.48714
KES002	Kinangop #2	-0.57367	36.49033
KES003	Kongoni area Mundui road cut	-0.81272	36.26106
KES004	Sonachi	-0.78047	36.26683
KES005	N. Lake Rd quarry pit	-0.66817	36.32500
KES006	Eburru GsJj53/52 area	-0.62014	36.31361
KES007	Masai Gorge rd quarry	-0.64647	36.33419
KES008	Eburu/GilGil Elmenteita Junction GsJj82	-0.58619	36.26408
KES009	Eburu/GilGil Elmenteita Junction GsJj82	-0.58619	36.26408
KES010	N. Eburu Rd. scree	-0.58619	36.27667
KES011	N. Eburu Rd. scree	-0.58619	36.27667
KES012	Gilgil-Eburu Rd pumice bed	-0.54461	36.29850
KES013	Gilgil-Eburu Rd pumice bed	-0.63450	36.25594
KES014	Lukenya quarry fiame	-1.48006	37.08367
KES015	Lukenya quarry bomb	-1.48006	37.08367
KES016	Upper Kedong rd	-1.23286	36.54603
KES017	Upper Kedong rd	-1.23286	36.54603
KES018	Gicheru	-1.18706	36.54944
KES019	Gicheru	-1.18706	36.54944
KES020	Mid-Kedong Valley	-1.10297	36.46361
KES021	Dawson's Camp	-0.98572	36.31286
KES022	Dawson's Camp	-0.98572	36.31286
KES023	Hell's Gate South Entrance	-0.97489	36.30689
KES024	Hell's Gate South Entrance	-0.97489	36.30689
KES025	Hell's Gate S Upper Hill	-0.97181	36.30992
KES026	Hell's Gate S Upper Hill	-0.97181	36.30992
KES027	Hell's Gate South East Wall	-0.95928	36.31014
KES028	Hell's Gate South East Wall	-0.95928	36.31014
KES029	Obsidian Cave, Hell's Gate Nat. Pk.	-0.88781	36.38375
KES030	Obsidian Cave, Hell's Gate Nat. Pk.	-0.88781	36.38375
KES031	Obsidian Cave, Hell's Gate Nat. Pk.	-0.88781	36.38375
KES032	Obsidian Cave, Upper	-0.88781	36.38375
KES033	Eburu top 100m E Kinogono school	-0.63044	36.25431
KES034	Eburu top 100m E Kinogono school	-0.63044	36.25431
KES035	Eburu top 100m E Kinogono sch	-0.63044	36.25431
KES036	Eburu top 100m E Kinogono sch	-0.63044	36.25431
KES037	Eburu top Kinogono sch	-0.63450	36.25594
KES038	Eburu top Kinogono sch	-0.63450	36.25594
KES039	Eburu top Kinogono sch	-0.63450	36.25594
KES040	Eburu top Kinogono sch	-0.63450	36.25594
KES042	Old Tepesi Rock Shelter	-0.69192	36.20728

Appendix 5 – continued

ANID	Source Name	Coordinates	
		°N or °S	°E
KES043	Eburu Station Rd.	-0.58108	36.24889
KES044	Eburu Station Rd.	-0.58108	36.24889
KES045	Eburu Station Rd. 150 m S	-0.58192	36.24972
KES046	Eburu Station Rd. 150 m S	-0.58192	36.24972
KES047	Hell's Gate main Middle	-0.87978	36.34272
KES048	Hell's Gate Central Tower	-0.89667	36.32436
KES049	Hell's Gate Central Tower	-0.89667	36.32436
KES050	Ol Karia	-0.89819	36.30919
KES051	Ol Karia	-0.89819	36.30919
KES052	Ol Karia II	-0.87436	36.29433
KES053	Ol Karia II	-0.87436	36.29433
KES054	Ol Jorai Quarry base	-0.59700	36.21092
KES055	Ol Jorai Quarry west	-0.60008	36.21108
KES056	Ol Jorai Quarry GsJi59	-0.60008	36.21108
KES057	Menengai lookout	-0.22656	36.09567
KES058	Prospect Farm Upper	-0.61803	36.18994
KES059	GsJj53 Acheulean/MSA	-0.61603	36.30694
KES060	Marula Estate (upper)	-0.62211	36.31333
KES061	Marula Estate (upper)	-0.62211	36.31333
KES062	GsJj84 Gema 1	-0.54556	36.31406
KES063	Gema 2 planar exposure	-0.56433	36.30875
KES064	Gema 2 planar exposure	-0.56433	36.30875
KES065	Marula Valley NE	-0.58756	36.32039
KES066	Ol Doinyo Nyokie (Magadi)	-1.80556	36.37500
KES067	GsJj85 Nagum	-0.57686	36.30044
KES068	GsJj85 Nagum	-0.57686	36.30044
KES069	GsJj85 Nagum	-0.57686	36.30044
KES070	GsJj53 Southwest	-0.61608	36.30856
KES071	GsJj53 Southwest	-0.61608	36.30856
KES072	GsJj53 Southwest	-0.61608	36.30856
KES073	GsJj53 Southwest	-0.61608	36.30856
KES074	GsJj53 Southwest	-0.61608	36.30856
KES075	Fisherman's Camp	-0.82833	36.33589
KES076	Mundui at student outcrop	-0.80911	36.25739
KES077	Mundui at student outcrop	-0.80911	36.25739
KES078	Sonachi Green Crater Lake	-0.78047	36.26683
KES079	N. Lake Rd. Quarry	-0.66817	36.32500
KES080	Eburu Rd N.	-0.66817	36.32500
KES081	GsJj50 Area A	-0.62947	36.25372
KES082	GsJj50 Area A	-0.62947	36.25372
KES083	GsJj50 Area B	-0.62947	36.25372

Appendix 5 – continued

ANID	Source Name	Coordinates	
		°N or °S	°E
KES084	GsJj50 Area B	-0.62947	36.25372
KES085	GsJj50 Area B	-0.62947	36.25372
KES086	GsJj50 Area B	-0.62947	36.25372
KES087	Rd. Quarry above Masai Gorge	-0.64644	36.33411
KES088	Rd. Quarry above Masai Gorge	-0.64644	36.33411
KES089	Marula Valley NW	-0.60522	36.30456
KES090	Marula Valley NW	-0.60522	36.30456
KES091	GilGil Eburu pumice outcrop	-0.56475	36.30022
KES092	GilGil Eburu pumice outcrop	-0.56475	36.30022
KES093	Gilgil Eburu Rd. 2	-0.56769	36.29733
KES094	Gilgil Eburu Rd. 2	-0.56769	36.29733
KES095	Ol Doinyo Njeru Ofisini	-0.56558	36.28917
KES096	Ol Doinyo Njeru Ofisini	-0.56558	36.28917
KES097	Ol Doinyo Njeru Ofisini	-0.56558	36.28917
KES098	Lukenya Rd.	-1.46267	37.11436
KES099	Lukenya Rd.	-1.46267	37.11436
KES100	Lukenya Rd.	-1.46267	37.11436
KES101	Ol Doinyo Alasho	-2.15297	36.15686
KES102	Ol Doinyo Alasho	-2.15297	36.15686
KES103	Ol Doinyo Alasho	-2.15297	36.15686
KES104	Ol Doinyo Alasho	-2.15297	36.15686
KES124	Ol Doinyo Nyokie Loc 1	-1.80508	36.37708
KES125	Ol Doinyo Nyokie Loc 1	-1.80508	36.37708
KES126	Ol Doinyo Nyokie Loc 2	-1.80269	36.37631
KES127	Ol Doinyo Nyokie Loc 3	-1.79767	36.37203
KES128	Ol Doinyo Nyokie Loc 3	-1.79725	36.37147
KES130	Ol Doinyo Nyokie Loc 5	-1.78850	36.37369
KES131	Ol Doinyo Nyokie Loc 6	-1.78875	36.37083
KES132	Ol Doinyo Nyokie Loc 6	-1.78933	36.37131
KES133	Ewuaso-Suswa Road Loc 1	-1.10275	36.46403
KES134	Ewuaso-Suswa Road Loc 1	-1.10283	36.46336
KES135	Ewuaso-Suswa Road Loc 1	-1.10283	36.46336
KES136	Ewuaso-Suswa Road Loc 1	-1.10275	36.46264
KES137	Salasun	-1.11119	36.39047
KES138	Salasun	-1.11119	36.39047
KES139	Salasun	-1.11083	36.38975
KES140	Ewuaso-Suswa Road Loc 2	-1.10047	36.45847
KES141	Ewuaso-Suswa Road Loc 2	-1.10053	36.45811
KES147	Naivasha Top Camp Loc 1	-0.83383	36.33228
KES148	Naivasha Top Camp Loc 1	-0.83392	36.33228
KES149	Naivasha Top Camp Loc 1	-0.83392	36.33228

Appendix 5 – continued

ANID	Source Name	Coordinates	
		°N or °S	°E
KES150	Naivasha Top Camp Loc 1	-0.83417	36.33228
KES151	Naivasha Top Camp Loc 1	-0.83417	36.33228
KES152	Ol Doinyo Oserian	-0.81808	36.31817
KES153	Ol Doinyo Oserian	-0.83211	36.31842
KES154	Ol Doinyo Oserian	-0.83186	36.31853
KES155	Ol Doinyo Oserian	-0.83186	36.31853
KES156	Ol Doinyo Oserian Quarry	-0.83244	36.31972
KES157	Ol Doinyo Oserian Quarry	-0.83244	36.31972
KES158	Ol Doinyo Oserian Quarry	-0.83244	36.31972
KES159	Naivasha Top Camp Loc 2	-0.83206	36.33211
KES160	Naivasha Top Camp Loc 2	-0.83192	36.33194
KES161	Naivasha Top Camp Loc 2	-0.83175	36.33183
KES162	Naivasha Top Camp Loc 3	-0.83014	36.33333
KES163	Naivasha Top Camp Loc 3	-0.83103	36.33339
KES164	Naivasha Top Camp Loc 3	-0.83103	36.33339
KES165	GsJi53 Kiteko Loc 1	-0.69175	36.20717
KES166	GsJi53 Kiteko Loc 1	-0.69175	36.20717
KES167	GsJi53 Kiteko Loc 2	-0.69269	36.20508
KES168	Delamere Dam Loc 1	-0.68811	36.20342
KES169	Delamere Dam Loc 2	-0.69189	36.20211
KES170	Ololerai Loc 1	-0.79294	36.31275
KES171	Ololerai Loc 2	-0.78769	36.30931
KES172	Ololerai Loc 3	-0.79133	36.31256
KES173	Ololerai Loc 4	-0.79428	36.30783
KES174	Ololerai Loc 5	-0.79275	36.30408
KES175	Ololerai Loc 6	-0.79572	36.30339
KES176	Mundui Loc 1	-0.81322	36.26144
KES177	Mundui Loc 2	-0.80722	36.25661
KES178	Mundui Loc 2	-0.80722	36.25661
KES179	Mundui Loc 3	-0.80350	36.25278
KES180	Crater Lake Loc 1	-0.78161	36.25894
KES181	Crater Lake Loc 1	-0.78161	36.25894
KES182	Ilkek Loc 1	-0.59431	36.36619
KES183	Ilkek Loc 2	-0.59386	36.36536
KES184	Ilkek Loc 3	-0.59356	36.36433
KES185	Ilkek Loc 4	-0.59411	36.36300
KES186	Ilkek Loc 5	-0.59842	36.36589
KES187	Ilkek Drift Hill Loc 1	-0.59650	36.35333
KES188	Ilkek Drift Hill Loc 2	-0.59672	36.35236
KES189	Ilkek Drift Hill Loc 3	-0.59925	36.34600
KES190	Ilkek Drift Hill Loc 3	-0.59925	36.34600

Appendix 5 – continued

ANID	Source Name	Coordinates	
		°N or °S	°E
KES191	Waterloo Ridge Loc 1	-0.60519	36.34178
KES192	Waterloo Ridge Loc 2a	-0.58489	36.33775
KES193	Waterloo Ridge Loc 2b	-0.58447	36.33822
KES194	Waterloo Ridge Loc 2c	-0.58553	36.33664
KES195	Waterloo Ridge Loc 3a	-0.60792	36.33542
KES196	Waterloo Ridge Loc 3b	-0.60856	36.33547
KES197	Waterloo Ridge Loc 3c	-0.60844	36.33589
KES198	Waterloo Ridge Loc 3d	-0.60958	36.33647
KES199	Waterloo Ridge Loc 4a	-0.61217	36.33647
KES200	Waterloo Ridge Loc 4b	-0.61264	36.33658
KES201	Waterloo Ridge Loc 4c	-0.61294	36.33661
KES202	Waterloo Ridge Loc 4d	-0.61250	36.33650
KES203	Waterloo Ridge Loc 5a	-0.61558	36.33744
KES204	Waterloo Ridge Loc 5b	-0.61594	36.33753
KES205	Waterloo Ridge Loc 5c	-0.61619	36.33711
KES206	Waterloo Ridge Loc 6a	-0.61883	36.33714
KES207	Waterloo Ridge Loc 6b	-0.61792	36.33719
KES208	Waterloo Ridge Loc 6c	-0.61731	36.33756
KES209	Waterloo Ridge Loc 7a	-0.62050	36.34206
KES210	Waterloo Ridge Loc 7b	-0.62067	36.34153
KES211	Waterloo Ridge Loc 7c	-0.62114	36.34108
KES212	Waterloo Ridge Loc 7d	-0.62111	36.34306
KES213	Waterloo Ridge Loc 8a	-0.61861	36.34406
KES214	Waterloo Ridge Loc 8b	-0.61869	36.34369
KES215	Waterloo Ridge Loc 8c	-0.61886	36.34319
KES216	Waterloo Ridge Loc 9	-0.61936	36.34700
KES217	Waterloo Ridge Loc 10	-0.62172	36.34519
KES218	Elsa Loc 1a	-0.81578	36.31628
KES219	Elsa Loc 1b	-0.81575	36.31564
KES220	Waterloo Ridge Loc 11a	-0.62258	36.35450
KES221	Waterloo Ridge Loc 11b	-0.62297	36.35483
KES222	Waterloo Ridge Loc 12a	-0.62625	36.34875
KES223	Waterloo Ridge Loc 12b	-0.62622	36.34856
KES224	Waterloo Ridge Loc 13a	-0.62822	36.35133
KES225	Waterloo Ridge Loc 13b	-0.62714	36.35147
KES226	Waterloo Ridge Loc 13c	-0.62814	36.34833
KES227	Waterloo Ridge Loc 13d	-0.62731	36.34819
KES228	Waterloo Ridge Loc 13e	-0.62900	36.34825
KES229	Waterloo Ridge Loc 14a	-0.61994	36.35347
KES230	Waterloo Ridge Loc 14b	-0.62003	36.35317
KES231	Waterloo Ridge Loc 15	-0.61525	36.35433

Appendix 5 – continued

ANID	Source Name	Coordinates	
		°N or °S	°E
KES232	Waterloo Ridge Loc 16	-0.57711	36.33433
KES233	Waterloo Ridge Loc 16	-0.57711	36.33433
KES234	Waterloo Ridge Loc 17a	-0.57211	36.33400
KES235	Waterloo Ridge Loc 17b	-0.56972	36.33322
KES236	Waterloo Ridge Loc 18	-0.56675	36.32972
KES237	Waterloo Ridge Loc 19a	-0.57739	36.32672
KES238	Waterloo Ridge Loc 19b	-0.57819	36.32681
KES239	Waterloo Ridge Loc 20a	-0.58219	36.32806
KES240	Waterloo Ridge Loc 20b	-0.58339	36.32833
KES241	Waterloo Ridge Loc 21a	-0.58936	36.33036
KES242	Waterloo Ridge Loc 21b	-0.58972	36.33047
KES243	Njorowa Loc 1a	-0.96578	36.30619
KES244	Njorowa Loc 1b	-0.96578	36.30619
KES245	Njorowa Loc 2a	-0.95925	36.31008
KES246	Njorowa Loc 2b	-0.95936	36.31036
KES247	Njorowa Loc 2c	-0.95925	36.31008
KES248	Njorowa Loc 3a	-0.95758	36.31142
KES249	Njorowa Loc 3b	-0.95758	36.31142
KES250	Njorowa Loc 3c	-0.95778	36.31158
KES251	Njorowa Loc 4	-0.97169	36.30425
KES252	Njorowa Loc 5a	-0.96903	36.30819
KES253	Njorowa Loc 5b	-0.96903	36.30819
KES254	Njorowa Loc 6	-0.97411	36.30631
KES255	Gicheru Loc 1a	-1.18694	36.54944
KES256	Gicheru Loc 1b	-1.18722	36.54931
KES257	Gicheru Loc 1c	-1.18719	36.54961
KES258	Gicheru Loc 1d	-1.18719	36.55008
KES259	Gicheru Loc 1e	-1.18644	36.54931
KES260	Gicheru Loc 2a	-1.18475	36.55072
KES261	Gicheru Loc 2b	-1.18475	36.55072
KES262	Gicheru Loc 2c	-1.18475	36.55072
KES263	Gicheru Loc 2d	-1.18475	36.55072
KES264	Gicheru Loc 3a	-1.19336	36.54500
KES265	Gicheru Loc 3b	-1.19336	36.54500
KES266	Gicheru Loc 3c	-1.19281	36.54506
KES267	Gicheru Loc 3d	-1.19281	36.54506
KES268	Kedong Road Loc 1a	-1.22589	36.54636
KES269	Kedong Road Loc 1b	-1.22589	36.54636
KES270	Kedong Road Loc 1c	-1.22589	36.54636
KES271	Kedong Road Loc 2a	-1.22669	36.54914
KES272	Kedong Road Loc 2b	-1.22669	36.54914

Appendix 5 – continued

ANID	Source Name	Coordinates	
		°N or °S	°E
KES273	Kedong Road Loc 2c	-1.22669	36.54914
KES274	Kedong Road Loc 3a	-1.22850	36.54889
KES275	Kedong Road Loc 3b	-1.22850	36.54889
KES276	Kedong Road Loc 4	-1.23142	36.54836
KES277	Kedong Road Loc 5	-1.23311	36.54669
KES278	Njorowa Loc 7	-0.95528	36.31403
KES279	Njorowa Loc 8	-0.95461	36.31469
KES281	Njorowa Loc 7b	-0.95561	36.31406
KES282	Dawson's Camp Loc 1	-0.98719	36.30922
KES283	Dawson's Camp Loc 2	-0.98578	36.30864
KES284	Dawson's Camp Loc 3	-0.98531	36.31008
KES285	Menengai Loc 1	-0.22583	36.09681
KES286	Menengai Loc 2	-0.22903	36.09483
KES287	Lion Hill Loc 1	-0.31153	36.12078
KES288	Lion Hill Loc 2	-0.31183	36.12389
KES289	Bahati Loc 1a	-0.16661	36.12117
KES290	Bahati Loc 1b	-0.16661	36.12117
KES291	Banwala Loc 1	-0.09403	36.02192
KES292	Lasibil Loc 1	-0.10064	35.99069
KES293	Kampi Ya Moto Loc 3	-0.11953	35.95022
KES294	Kampi Ya Moto Loc 1a	-0.11614	35.95389
KES295	Kampi Ya Moto Loc 1b	-0.11631	35.95381
KES296	Kampi Ya Moto Loc 1c	-0.11631	35.95381
KES297	Naivasha Top Camp Loc 4a	-0.82839	36.33519
KES298	Naivasha Top Camp Loc 4b	-0.82839	36.33519
KES299	Naivasha Top Camp Loc 4c	-0.82833	36.33500
KES300	Orengenai Loc 1a	-0.68425	36.33297
KES301	Orengenai Loc 1b	-0.68489	36.33294
KES302	Orengenai Loc 2a	-0.68608	36.33147
KES303	Orengenai Loc 2b	-0.68550	36.33142
KES304	Orengenai Loc 3a	-0.68842	36.32889
KES305	Orengenai Loc 3b	-0.68853	36.32892
KES306	Orengenai Loc 4a	-0.68539	36.32742
KES307	Orengenai Loc 4b	-0.68469	36.32700
KES308	Orengenai Loc 4c	-0.68581	36.32728
KES309	Orengenai Loc 4d	-0.68322	36.32675
KES310	Orengenai Loc 4e	-0.68289	36.32725
KES311	Orengenai Loc 4f	-0.68161	36.32769
KES312	Orengenai Loc 4g	-0.68067	36.32764
KES313	Orengenai Log 4h	-0.67997	36.32761
KES314	Orengenai Loc 5a	-0.68458	36.32567

Appendix 5 – continued

ANID	Source Name	Coordinates	
		°N or °S	°E
KES315	Orengenai Loc 5b	-0.68442	36.32536
KES316	Orengenai Loc 6a	-0.68181	36.32558
KES317	Orengenai Loc 6b	-0.68181	36.32558
KES318	Baixia Loc 1	-0.68122	36.31814
KES319	Green Park Loc 1	-0.66808	36.29164
KES320	Murwa Loc 1	-0.65472	36.21419
KES321	Murwa Loc 2	-0.65583	36.23617
KES322	Eburru Forest Station Loc 1	-0.64619	36.24703
KES323	Eburru Forest Station Loc 2a	-0.63997	36.25292
KES324	Eburru Condensor Loc 1	-0.64014	36.25336
KES325	Eburru Condensor Loc 2a	-0.63975	36.25353
KES326	Eburru Condensor Loc 2b	-0.63956	36.25356
KES327	Eburru Condensor Loc 2c	-0.63947	36.25353
KES328	Eburru Condensor Loc 3a	-0.63903	36.25361
KES329	Eburru Condensor Loc 3b	-0.63861	36.25381
KES330	Eburru Condensor Loc 3c	-0.63839	36.25350
KES331	Eburru Condensor Loc 3d	-0.63800	36.25375
KES335	GsJj50 Area A	-0.62961	36.25378
KES336	GsJj50 Area B1	-0.63031	36.25431
KES337	GsJj50 Area B2	-0.63019	36.25406
KES338	GsJj50 Area C1	-0.63419	36.25594
KES339	GsJj50 Area C2	-0.63467	36.25589
KES340	GsJj50 Area C3	-0.63436	36.25536
KES341	Masai Gorge Loc 1a	-0.65992	36.33072
KES342	Masai Gorge Loc 1b	-0.65992	36.33072
KES343	Masai Gorge Loc 2a	-0.65975	36.33281
KES344	Masai Gorge Loc 2b	-0.65983	36.33286
KES345	Eburru North Road Loc 1a	-0.64558	36.30847
KES346	Eburru North Road Loc 1b	-0.64569	36.30733
KES347	GsJj52 Loc 2a	-0.62211	36.31308
KES348	GsJj52 Loc 2b	-0.62203	36.31336
KES349	GsJj52 Loc 2c	-0.62208	36.31386
KES350	GsJj52 Loc 3a	-0.62100	36.31419
KES351	GsJj52 Loc 3b	-0.62089	36.31450
KES352	GsJj52 Loc 3c	-0.62142	36.31464
KES353	GsJj52 Loc 3d	-0.62014	36.31353
KES354	GsJj52 Loc 4a	-0.61764	36.31183
KES355	GsJj52 Loc 4b	-0.61778	36.31192
KES356	GsJj52 Loc 4c	-0.61736	36.31153
KES357	GsJj52 Loc 4d	-0.61725	36.30997
KES358	GsJj52 Loc 1c	-0.61636	36.30933

Appendix 5 – continued

ANID	Source Name	Coordinates	
		°N or °S	°E
KES359	GsJj52 Loc 1c	-0.61636	36.30933
KES360	GsJj52 Loc 1b	-0.61594	36.30922
KES361	GsJj52 Loc 1a	-0.61606	36.30850
KES362	GsJj53 Loc 1a	-0.61419	36.30725
KES363	GsJj53 Loc 1b	-0.61428	36.30722
KES364	Masai Gorge Loc 3a	-0.64639	36.33431
KES365	Masai Gorge Loc 3b	-0.64592	36.33406
KES366	Masai Gorge Loc 3b	-0.64592	36.33406
KES367	Masai Gorge Loc 4a	-0.64928	36.33453
KES368	Masai Gorge Loc 4b	-0.64928	36.33453
KES369	Masai Gorge Loc 4c	-0.64928	36.33453
KES370	Entorobonni Loc 1	-0.91739	35.69475
KES371	Entorobonni Loc 1	-0.91739	35.69475
KES372	Entorobonni Loc 2	-0.91844	35.69511
KES373	Entorobonni Loc 2	-0.91844	35.69511
KES374	Hell's Gate Loc 1a (Obsidian Caves track)	-0.86961	36.37453
KES375	Hell's Gate Loc 1b	-0.86961	36.37453
KES376	Hell's Gate Loc 2a	-0.87150	36.37856
KES377	Hell's Gate Loc 2b	-0.87150	36.37856
KES378	Hell's Gate Loc 2b	-0.87150	36.37856
KES379	Hell's Gate Loc 2c	-0.87150	36.37856
KES380	Hell's Gate Loc 3a	-0.88653	36.38347
KES381	Hell's Gate Loc 3b	-0.88653	36.38347
KES382	Hell's Gate Loc 3c	-0.88653	36.38347
KES383	Hell's Gate Loc 4a, upper flow (Obsidian Caves)	-0.88769	36.38378
KES384	Hell's Gate Loc 4a, upper flow (Obsidian Caves)	-0.88769	36.38378
KES385	Hell's Gate Loc 4a, lower flow	-0.88769	36.38378
KES386	Hell's Gate Loc 4b, lower flow	-0.88800	36.38392
KES387	Hell's Gate Loc 4b, middle flow	-0.88800	36.38392
KES388	Hell's Gate Loc 4b, upper flow	-0.88800	36.38392
KES389	Hell's Gate Loc 5a	-0.90192	36.38028
KES390	Hell's Gate Loc 5b	-0.90192	36.38028
KES391	Hell's Gate Loc 5c	-0.90192	36.38028
KES392	Hell's Gate Loc 6 (Fischer's Tower Drift)	-0.89667	36.32433
KES393	Hell's Gate Loc 7 (Fischer's Tower Gorge)	-0.89544	36.32067
KES394	Hell's Gate Loc 8 (Olkaria)	-0.89828	36.30717
KES403	Kalusha Loc 1c (Lukenya)	-1.44781	37.10525
KES404	Lukenya Road Loc 1	-1.46258	37.11436
KES405	Lukenya Road Loc 2a	-1.45539	37.12481
KES406	Lukenya Road Loc 3	-1.45392	37.12608
KES407	Lukenya Road Loc 2b	-1.45528	37.12481

Appendix 5 – continued

ANID	Source Name	Coordinates	
		°N or °S	°E
KES408	Kisanana Loc 1a	0.03417	36.06406
KES409	Kisanana Loc 1b	0.03417	36.06406
KES410	Kisanana Loc 1c	0.03414	36.06433
KES411	Kabazi	-0.06900	36.14786
KES412	Olongai Loc 1	-0.12706	36.01317
KES413	Olongai Loc 2	-0.12669	36.01203
KES414	Olongai Loc 3	-0.12706	36.01317
KES415	Arahuka	-0.15808	36.06094
KES416	NE Menengai Crater Loc 1a	-0.17681	36.10975
KES417	NE Menengai Crater Loc 1b	-0.17681	36.10975
KES418	Lokil	0.84472	36.20244
KES419	Karau Loc 1	0.60475	36.18783
KES420	Karau Loc 2	0.60633	36.18544
KES421	Karau Loc 3	0.61217	36.18772
KES422	Karau Loc 4	0.61708	36.18756
KES423	Karau Loc 5	0.62150	36.18864
KES424	Chepungus (Paka) Loc 1a	0.87758	36.18489
KES425	Chepungus (Paka) Loc 1b	0.87758	36.18489
KES426	Chepungus (Paka) Loc 1c	0.87758	36.18489
KES427	Chepungus (Paka) Loc 1d	0.87758	36.18489
KES428	Chepungus (Paka) Loc 2	0.87819	36.17611
KES429	Lokoritabim	0.68933	36.01178
KES430	Shin	3.91656	36.47650
KES431	Naiyenareng Loc 1	2.41158	36.71647
KES432	Naiyenareng Loc 1	2.41158	36.71647
KES433	Naiyenareng Loc 1	2.41158	36.71647
KES434	Naiyenareng Loc 2	2.39636	36.72939
KES435	Naiyenareng Loc 2	2.39636	36.72939
KES436	Kalossi Loc 1	0.73669	36.13150
KES437	Kalossi Loc 2	0.73867	36.13647
KES438	Kalossi Loc 2	0.73867	36.13647
KES439	Cheptumkelek Loc 1	0.80239	36.18664
KES440	Cheptumkelek Loc 1	0.80239	36.18664
KES441	Cheptumkelek Loc 2	0.79564	36.18625
KES442	Silali Loc 1	1.16747	36.15197
KES443	Silali Loc 2	1.16647	36.15581
KES444	Kibelbel Loc 1	1.47778	36.14431
KES445	Kibelbel Loc 1	1.47778	36.14431
KES446	Kibelbel Loc 1	1.47778	36.14431
KES447	Kibelbel Loc 2	1.48311	36.14272
KES448	Kibelbel Loc 2	1.48311	36.14272

Appendix 5 – continued

ANID	Source Name	Coordinates	
		°N or °S	°E
KES449	Lomi Loc 1a	1.84692	36.28567
KES450	Lomi Loc 1a	1.84692	36.28567
KES451	Lomi Loc 1b	1.84697	36.28564
KES452	Lomi Loc 1b	1.84697	36.28564
KES453	Lomi Loc 1b	1.84697	36.28564
KES454	Lomi Loc 1c	1.84714	36.28561
KES455	Lomi Loc 1c	1.84714	36.28561
KES456	Lomi Loc 1c	1.84714	36.28561
KES457	Lomi Loc 2	1.84736	36.28353
KES458	Lomi Loc 2	1.84736	36.28353
KES459	Kachalakwen	1.09603	36.19736
KES460	Kachalakwen	1.09603	36.19736
KES461	Kachalakwen	1.09603	36.19736
KES462	Kachalakwen	1.09603	36.19736
KES463	Alale Loc 1	1.13050	36.27958
KES464	Alale Loc 1	1.13050	36.27958
KES465	Alale Loc 1	1.13050	36.27958
KES466	Alale Loc 2	1.13253	36.27797
KES467	Nyakinywa Loc 1a	-0.58425	36.27667
KES468	Nyakinywa Loc 1b	-0.58425	36.27667
KES469	Nyakinywa Loc 2	-0.58597	36.27483
KES470	Nyakinywa Loc 3	-0.58647	36.27489
KES471	Jaika (Eburru Station) Loc 1a	-0.58628	36.26411
KES472	Jaika (Eburru Station) Loc 1b	-0.58628	36.26411
KES473	Jaika Loc 1c	-0.58650	36.26411
KES474	Jaika Loc 2	-0.58733	36.26394
KES475	Jaika South Loc 1	-0.58000	36.27322
KES476	Jaika South Loc 1	-0.58000	36.27322
KES477	Jaika South Loc 2	-0.57992	36.27292
KES478	Jaika South Loc 2	-0.57992	36.27292
KES479	Ole Lorkumani (ole Enkapune)	-0.61794	36.18994
KES480	Ole Polos Loc. 1 (Ol Jorai)	-0.59972	36.21133
KES481	GsJj46 Rockshelter Loc 1	-0.64764	36.32633
KES482	GsJj46 Rockshelter Loc 2	-0.64836	36.32686
KES483	GsJj46 Rockshelter Loc 3	-0.64817	36.32883
KES484	GsJj46 Rockshelter Loc 4	-0.64644	36.32961
KES485	Marula Valley NE	-0.58756	36.32050
KES486	Marula Valley NE	-0.58756	36.32050
KES487	Nagum Loc 2a	-0.57722	36.30086
KES488	Nagum Loc 2b	-0.57686	36.30058
KES489	Nagum Loc 3	-0.56533	36.30942

Appendix 5 – continued

ANID	Source Name	Coordinates	
		°N or °S	°E
KES490	GsJj84 Loc 1	-0.54561	36.31392
KES491	Nagum pipeline Loc 1	-0.54708	36.30608
KES492	Nagum pipeline Loc 2	-0.54675	36.30575
KES493	Murai loc 1	-0.54408	36.30128
KES494	Njeru Ofisini East	-0.56769	36.29978
KES495	Njeru Ofisini North	-0.57928	36.28989
KES496	Kilima Loc 1a (Kinangop)	-0.63358	36.48719
KES497	Kilima Loc 1a (Kinangop)	-0.63358	36.48719
KES498	Kilima Loc 1b (Kinangop)	-0.63353	36.48708
KES499	Kilima Loc 1b (Kinangop)	-0.63353	36.48708
KES500	Kilima Loc 1c (Kinangop)	-0.63333	36.48711
KES501	Kilima Loc 1c (Kinangop)	-0.63333	36.48711
KES502	Kilima Loc 1c (Kinangop)	-0.63333	36.48711
KES503	Lemudongo Loc 1	-1.30433	35.97869
KES504	Lemudongo Loc 1	-1.30433	35.97869
KES505	Lemudongo Loc 1	-1.30433	35.97869
KES506	Lemudongo Loc 1	-1.30433	35.97869
KES507	Lemudongo Loc 1	-1.30433	35.97869
KES508	Lemudongo Loc 1	-1.30433	35.97869
KES509	Ol Doinyo Nyokie West Loc 1	-1.81092	36.35694
KES510	Ol Doinyo Nyokie West Loc 1	-1.81092	36.35694
KES511	Ol Doinyo Nyokie West Loc 2a	-1.81506	36.35892
KES512	Ol Doinyo Nyokie West Loc 2a	-1.81506	36.35892
KES513	Ol Doinyo Nyokie West Loc 2b	-1.81553	36.35911
KES514	Ogata Rongai Loc 1	-1.39075	36.72436
KES515	Ogata Rongai Loc 1	-1.39075	36.72436
KES516	North Island Loc 1	4.05336	36.05781
KES517	North Island Loc 2	4.06472	36.04553
KES518	North Island Loc 2	4.06472	36.04553
KES519	North Island Loc 3	4.06542	36.04447
KES520	North Island Loc 4	4.06697	36.04331
KES521	North Island Loc 4	4.06697	36.04331
KES522	North Island Loc 5	4.06775	36.04458
KES523	North Island Loc 5	4.06775	36.04458
KES524	North Island Loc 6	4.06775	36.04542
KES525	North Island Loc 6	4.06775	36.04542
KES526	North Island Loc 7	4.06936	36.04569
KES527	Ol Doinyo Nyiru	-1.72064	36.62275
KES528	Ol Doinyo Nyiru	-1.72064	36.62275
KES529	Ol Doinyo Nyiru	-1.72064	36.62275
KES530	Ol Doinyo Nyiru	-1.72064	36.62275

Appendix 5 – continued

ANID	Source Name	Coordinates	
		°N or °S	°E
KES531	Ol Doinyo Nyiru	-1.72064	36.62275
KES532	Ol Doinyo Nyiru	-1.72064	36.62275
KES533	Ol Doinyo Nyiru	-1.72064	36.62275
KES534	Museum Hill Bus Stage	-1.27325	36.81383
KES535	Museum Hill Bus Stage	-1.27325	36.81383
KES536	Kalusha Loc 1c (Lukenya)	-1.44781	37.10525
KES537	Lukenya Road Loc 1	-1.46258	37.11436
KES538	Lukenya Road Loc 1	-1.46258	37.11436
KES539	Lukenya Road Loc 2b	-1.45528	37.12481
KES540	Kabazi	-0.06900	36.14786
KES541	Chepungus (Paka) Loc 1b	0.87758	36.18489
KES542	Chepungus (Paka) Loc 1b	0.87758	36.18489

Appendix 6 - Concentration data from NAA for obsidian from Kenya. All concentrations are in parts per million (ppm)

Sample ID	Al	Cl	Dy	K	Mn	Na	Ba
KES001	45718.3	1732.0	31.514	32253.8	1469.42	47281.4	0.0
KES002	46702.8	1671.8	31.641	30100.0	1463.09	46994.0	0.0
KES003	65231.8	856.9	16.288	40291.7	308.48	33476.0	0.0
KES004	58297.1	808.9	15.609	41032.3	329.37	33323.8	46.9
KES005	39670.8	2419.9	61.424	40559.7	1641.97	50158.8	0.0
KES006	43875.0	2631.3	72.075	34024.9	1841.18	56668.0	143.3
KES007	51415.2	2555.6	66.552	37538.3	1735.53	51982.8	0.0
KES008	32159.0	1564.4	42.702	37305.6	2118.47	52009.6	77.0
KES009	41756.4	1700.3	43.911	38894.5	2129.80	52392.2	0.0
KES010	41613.4	2620.1	68.255	44636.1	1729.27	51845.2	0.0
KES011	41241.4	2715.8	71.538	34333.6	1817.00	53605.4	0.0
KES012	42359.4	2020.4	54.670	40423.0	1710.06	46633.9	0.0
KES013	44079.7	1868.1	42.318	34033.8	1912.42	49868.7	152.3
KES014	37539.0	1135.7	27.787	39046.1	2169.04	38244.8	0.0
KES015	38937.4	1262.8	28.227	42509.6	2269.72	47645.1	0.0
KES016	75639.7	634.9	14.523	36943.9	1044.30	36808.4	238.6
KES017	71351.4	618.9	14.115	42795.4	1074.79	37551.1	288.5
KES018	69790.0	536.8	13.651	40691.0	1113.40	37122.9	253.4
KES019	73470.5	582.5	14.727	41953.8	1077.95	37700.7	266.7
KES020	84152.2	813.9	16.850	46228.3	2613.64	63592.6	331.2
KES021	54726.4	1866.0	31.596	36272.1	492.64	39978.4	79.3
KES022	53729.2	1734.2	32.685	39852.6	519.28	39751.2	72.2
KES023	52903.3	1808.7	33.490	33491.4	478.62	40299.2	84.9
KES024	52448.0	1804.4	31.784	34476.5	479.47	39846.8	37.2
KES025	55696.1	1956.8	34.424	42345.4	481.21	40717.7	62.4
KES026	58010.1	1888.6	34.732	37620.8	471.61	40023.6	43.9
KES027	63432.3	1884.9	34.048	37097.8	481.74	40200.2	86.5
KES028	56365.7	1850.0	35.048	36824.6	480.87	40372.4	53.3
KES029	57422.0	1855.4	34.493	39806.3	472.92	40420.7	37.5
KES030	59229.5	1809.2	33.803	35880.0	460.56	39027.5	63.4
KES031	51614.6	1905.4	34.835	36966.6	466.97	40035.1	72.0
KES032	59077.0	1861.3	34.384	35940.7	471.59	40592.4	66.4
KES033	41869.3	2097.6	44.798	35745.6	1899.03	49342.0	0.0
KES034	51611.8	1897.2	44.948	32984.8	1903.06	49802.3	0.0
KES035	39651.0	1929.5	46.765	36918.2	1888.54	48599.9	123.7
KES036	36731.0	1986.1	45.331	36599.0	1904.55	49068.3	142.7
KES037	39110.1	2010.4	45.329	40888.0	1870.07	48887.5	167.6
KES038	49170.4	1987.1	44.348	37817.6	1882.25	48726.3	64.1
KES039	44806.6	1972.7	44.551	36917.6	1888.25	48965.2	100.7
KES040	37003.9	2080.1	44.717	34232.7	1897.57	49637.3	116.9
KES042	43439.8	2329.0	44.916	35107.3	2339.91	53468.8	0.0
KES043	37605.1	1704.5	47.541	32052.2	2122.24	51716.9	0.0
KES044	34636.8	1666.6	45.995	35858.2	2150.08	52517.9	52.9
KES045	38781.7	1962.4	49.283	37950.6	2151.78	52482.2	109.1
KES046	34054.6	1679.0	45.692	42284.9	1985.61	50412.3	97.0

Appendix 6 – continued. All concentrations are in parts per million (ppm).

Sample ID	Al	Cl	Dy	K	Mn	Na	Ba
KES047	52526.5	1935.9	35.008	36734.6	471.96	39893.4	56.0
KES048	53937.9	1810.1	32.006	38865.2	458.56	38941.0	53.4
KES049	53158.3	1859.8	33.089	36856.9	465.62	39767.4	54.3
KES050	50389.3	1704.7	34.937	36063.8	439.15	38911.6	67.4
KES051	53849.1	1739.0	36.216	37814.5	443.15	39063.3	67.4
KES052	50299.0	1900.0	40.025	34242.3	519.53	40983.6	74.3
KES053	53291.3	1962.0	40.954	31740.6	521.33	40741.3	62.9
KES054	46669.3	1543.4	44.626	37611.8	2228.87	55853.8	0.0
KES055	44578.5	1457.6	44.116	39050.4	2226.31	56193.1	0.0
KES056	40082.5	1445.9	42.727	33544.5	2203.83	54424.3	0.0
KES057	60975.2	843.3	23.064	38287.1	2794.18	57212.7	0.0
KES058	43803.8	2175.8	56.755	37326.0	1586.83	47992.7	83.5
KES059	37459.9	2371.8	70.272	32766.2	1853.10	56358.9	135.8
KES060	48217.1	1474.1	47.477	38385.5	1319.50	44907.5	74.3
KES061	48097.5	1513.4	47.312	36185.6	1321.21	44837.8	71.2
KES062	37661.9	2107.8	51.933	36865.7	1685.13	45967.0	105.3
KES063	41879.5	2095.7	53.500	36544.9	1675.14	47911.6	0.0
KES064	57104.7	2036.6	54.219	39950.3	1767.06	48015.2	0.0
KES065	39805.4	2024.2	55.851	33814.3	1644.44	47780.4	0.0
KES066	67186.3	694.0	18.264	35529.9	2441.42	51363.9	62.6
KES067	49440.3	1954.1	54.598	36765.9	1555.49	47251.9	0.0
KES068	42113.9	2014.1	54.467	34216.5	1545.82	47126.8	0.0
KES069	45716.7	2062.2	54.730	39083.9	1530.45	46506.8	0.0
KES070	41395.5	2357.9	67.541	34490.5	1842.17	55586.2	0.0
KES071	37160.8	2445.7	68.083	29866.3	1827.47	55657.5	0.0
KES072	42654.3	2436.6	71.221	31538.3	1859.69	57218.4	0.0
KES073	44779.8	2435.7	66.079	34700.9	1798.68	54835.8	90.3
KES074	42779.3	2355.8	69.519	29086.9	1825.13	55783.0	0.0
KES075	56615.8	1790.6	38.528	32418.5	397.83	39818.2	85.1
KES076	69857.7	854.0	15.870	36689.0	498.04	32866.9	0.0
KES077	55401.9	805.3	15.561	36066.6	293.91	32157.5	35.4
KES078	58981.8	820.8	14.766	36439.5	302.64	32351.2	43.4
KES079	40276.3	2232.9	58.938	33294.8	1623.58	48866.9	0.0
KES080	59891.2	757.1	20.883	31512.9	2547.39	51863.3	0.0
KES081	47956.3	1632.1	45.055	35060.7	1891.95	49214.5	138.4
KES082	48842.7	1755.9	44.569	41107.3	1913.35	50405.2	133.4
KES083	53242.4	1856.4	43.826	42029.4	1908.89	49815.5	147.2
KES084	47083.3	1834.3	44.339	35852.1	1882.32	49438.7	83.5
KES085	50163.8	1716.1	45.294	35521.3	1914.23	50494.6	99.3
KES086	50421.0	1888.6	45.375	34858.2	1910.26	49816.5	100.5
KES087	43861.1	2090.1	66.180	30407.3	1654.77	49762.2	102.4
KES088	43539.5	2143.6	66.720	32675.2	1815.83	49952.9	0.0
KES089	46922.6	1265.5	28.526	37602.0	2144.13	55764.2	0.0
KES090	43213.8	1173.8	30.807	37136.3	2174.57	56669.1	0.0
KES091	44762.2	1803.5	53.198	32713.1	1679.57	45474.9	0.0

Appendix 6 – continued. All concentrations are in parts per million (ppm).

Sample ID	Al	Cl	Dy	K	Mn	Na	Ba
KES092	41491.3	1845.7	54.524	35581.5	1691.04	46302.8	0.0
KES093	49952.7	1828.5	54.086	38458.6	1709.09	46439.3	0.0
KES094	44732.4	1699.1	54.283	38117.8	1696.49	45687.4	0.0
KES095	45100.4	1806.0	53.319	38696.9	1522.74	46712.5	0.0
KES096	47213.6	1830.7	54.816	34402.9	1513.72	46025.5	0.0
KES097	44180.4	1798.4	54.428	38261.0	1526.15	46217.8	0.0
KES098	43418.9	1044.8	29.783	34104.5	2228.96	46342.0	0.0
KES099	48208.5	992.9	28.753	36790.7	2232.40	46844.1	0.0
KES100	42487.2	1139.8	27.519	33403.7	2221.26	46475.2	0.0
KES101	68631.5	675.7	19.100	38045.6	2512.42	48846.7	131.1
KES102	68669.7	720.5	18.741	37716.7	2171.96	47829.4	0.0
KES103	79001.4	704.9	19.090	37497.9	2106.95	47674.1	144.4
KES104	70034.2	1055.2	18.078	36773.4	2264.08	47773.1	0.0
KES124	63006.4	643.3	17.406	40877.8	2276.74	39976.3	91.1
KES125	63545.0	397.0	19.730	50558.1	2233.73	31566.5	104.8
KES126	71872.1	686.8	18.698	39770.3	2450.26	52459.5	99.4
KES127	64036.1	481.8	18.613	38809.3	2392.27	40717.5	0.0
KES128	62212.1	457.1	16.160	48218.0	2360.32	27059.3	0.0
KES130	69824.6	669.8	18.004	38652.6	2421.60	51460.0	102.6
KES131	68159.7	686.1	20.393	41915.9	2442.67	51515.7	0.0
KES132	65064.9	610.1	17.793	40461.3	2396.69	51837.0	100.3
KES133	92386.2	924.3	16.222	38592.6	2667.44	63948.9	329.4
KES134	84898.7	825.7	15.646	41159.4	2660.60	60886.3	310.3
KES135	75720.8	773.0	15.880	39446.8	2648.83	64148.8	388.9
KES136	84437.1	879.5	16.219	38547.2	2585.28	63392.6	338.7
KES137	75582.0	793.7	18.395	36584.2	2745.60	63823.2	0.0
KES138	75140.0	748.3	21.407	43781.9	2763.67	64145.8	67.2
KES139	83035.5	848.9	16.127	37094.8	2649.46	63709.3	304.3
KES140	83564.3	923.5	15.180	41037.5	2610.74	63927.6	313.2
KES141	71310.9	978.1	18.134	39186.5	2651.54	65377.3	302.5
KES147	52203.3	1780.9	39.865	32867.9	398.65	39953.5	76.4
KES148	57228.0	1663.1	39.741	34702.8	397.97	39770.7	80.8
KES149	56564.4	1667.4	39.110	34994.4	395.28	39930.5	58.7
KES150	54147.9	1761.8	39.221	40466.9	406.29	40482.7	67.6
KES151	56216.8	1742.6	38.925	36157.4	397.03	39994.3	65.6
KES152	53377.3	1663.6	38.757	39381.6	393.87	39560.5	85.1
KES153	52381.6	1645.8	40.472	33682.1	392.96	39697.0	0.0
KES154	55818.7	1684.3	37.721	35125.7	392.69	39633.5	64.3
KES155	55377.5	1661.1	39.382	39530.3	393.95	39623.4	86.8
KES156	59217.8	1693.3	38.648	34656.9	390.42	39205.4	0.0
KES157	53790.7	1711.5	39.783	33522.2	401.61	40413.9	0.0
KES158	55324.8	1648.0	37.500	36794.9	392.67	39580.3	67.3
KES159	58449.5	1594.2	38.747	38603.4	397.20	39811.1	0.0
KES160	51833.2	1758.7	39.389	35550.5	401.94	40489.0	45.4
KES161	54458.5	1699.6	40.812	36400.0	407.50	40745.3	0.0

Appendix 6 – continued. All concentrations are in parts per million (ppm).

Sample ID	Al	Cl	Dy	K	Mn	Na	Ba
KES162	56663.8	1643.1	37.919	34663.1	394.80	39483.0	96.7
KES163	58566.1	1747.5	39.282	35265.5	396.12	39735.0	98.1
KES164	61296.1	1723.1	40.923	36948.0	405.50	40585.9	81.7
KES165	34000.1	2234.5	41.606	31899.4	2241.82	53731.3	0.0
KES166	37804.8	2302.3	42.566	31651.6	2195.80	52399.6	0.0
KES167	34362.9	2302.1	44.795	31064.3	2276.75	53339.4	0.0
KES168	39158.4	1212.3	35.761	29331.6	2100.46	51068.7	0.0
KES169	58975.3	1138.8	26.436	36518.3	1322.91	46506.9	0.0
KES170	54507.6	833.3	28.166	38061.3	1157.84	42456.7	0.0
KES171	54380.1	904.1	28.344	39552.4	1239.71	42695.2	0.0
KES172	54515.4	899.5	28.344	36610.1	1162.33	42421.6	0.0
KES173	59547.9	825.8	28.904	42635.7	1199.49	43249.5	0.0
KES174	55322.0	832.5	28.945	41715.8	1149.14	42736.9	0.0
KES175	53549.3	846.2	28.101	37471.5	1096.43	41621.5	0.0
KES176	62597.4	899.1	15.737	39100.3	305.79	34203.7	0.0
KES177	66206.4	945.8	16.659	36913.8	305.84	33714.6	0.0
KES178	64894.2	911.4	16.378	39468.5	311.93	35143.7	70.0
KES179	66551.8	879.3	15.770	40329.7	298.96	33308.9	0.0
KES180	58940.0	840.9	15.767	41602.9	308.99	33781.9	0.0
KES181	62186.8	810.0	16.319	40650.9	314.63	34471.5	81.1
KES182	41957.2	1993.6	56.620	40091.9	1637.21	48557.3	156.0
KES183	49448.2	2058.2	57.592	37808.3	1641.38	48728.4	0.0
KES184	42188.8	1957.9	55.698	35260.2	1601.11	47148.6	0.0
KES185	40317.8	1985.8	56.977	43949.6	1630.11	48288.0	0.0
KES186	40244.9	1929.3	54.548	36227.8	1571.23	46507.4	0.0
KES187	40981.0	1974.5	54.310	35464.3	1577.76	47000.9	0.0
KES188	38498.9	1938.1	51.937	38833.9	1602.34	47433.6	0.0
KES189	41572.3	2037.2	54.514	40533.2	1593.09	47500.1	0.0
KES190	43199.7	2005.5	57.200	38492.3	1619.29	47726.9	115.6
KES191	41279.1	2005.7	55.785	39928.3	1603.07	47398.5	0.0
KES192	38737.1	1988.4	56.271	37612.6	1629.41	47333.3	0.0
KES193	42167.4	2081.0	56.293	42228.7	1638.27	47641.1	0.0
KES194	42391.2	1988.3	55.705	37640.7	1612.69	46963.3	0.0
KES195	47586.1	2076.1	57.666	45612.8	1649.98	48964.1	0.0
KES196	45727.6	1999.9	56.383	40076.4	1607.06	47415.5	0.0
KES197	43538.1	1961.4	56.152	39527.8	1592.99	47119.2	0.0
KES198	45622.0	1961.5	55.242	36561.0	1573.73	46580.4	0.0
KES199	48771.8	1944.3	54.607	38999.3	1568.71	46529.9	0.0
KES200	38036.6	2012.1	56.454	37532.5	1616.74	47684.5	0.0
KES201	37502.7	2040.7	55.925	38674.8	1593.66	47187.5	0.0
KES202	38672.1	2128.9	56.684	40935.9	1638.32	48432.9	0.0
KES203	45055.1	1977.9	54.956	36104.6	1577.57	46934.5	0.0
KES204	38605.4	1979.2	54.914	41868.2	1595.86	47286.3	0.0
KES205	40703.6	2003.4	56.269	44278.2	1629.20	47538.1	0.0
KES206	44960.8	1960.9	57.719	38206.5	1617.31	47889.1	0.0

Appendix 6 – continued. All concentrations are in parts per million (ppm).

Sample ID	Al	Cl	Dy	K	Mn	Na	Ba
KES207	43601.2	1944.4	54.483	35984.7	1577.41	46876.8	0.0
KES208	47597.6	1967.1	55.130	31270.3	1581.28	46395.5	0.0
KES209	45127.0	1985.7	50.211	36931.4	1609.28	47372.0	0.0
KES210	47285.4	1931.4	56.235	35226.1	1637.90	48055.7	0.0
KES211	43423.2	1829.7	55.182	36469.3	1594.65	46959.7	0.0
KES212	44862.9	2048.8	56.631	33985.9	1618.64	47881.2	0.0
KES213	41699.3	1985.7	56.131	39721.4	1632.97	47603.8	0.0
KES214	43520.8	1936.0	54.792	38027.8	1608.72	47336.3	0.0
KES215	44485.0	2034.5	56.080	44520.7	1625.65	47637.9	0.0
KES216	36486.7	2136.2	56.709	38285.9	1610.19	48172.4	0.0
KES217	43787.7	2096.9	57.623	40583.6	1601.49	48310.2	0.0
KES218	57605.3	1798.2	40.249	39049.6	396.30	39861.4	0.0
KES219	59171.7	1792.8	38.696	33961.6	386.79	39458.6	84.3
KES220	45426.7	2108.3	56.599	31650.2	1575.41	47668.2	0.0
KES221	43757.1	2106.3	56.672	35573.9	1606.17	47723.2	0.0
KES222	40323.0	2136.4	56.039	39978.7	1600.75	48158.7	0.0
KES223	42179.5	2125.2	53.077	32935.1	1572.76	46825.8	0.0
KES224	42589.4	2152.1	54.566	34412.0	1583.99	47463.5	0.0
KES225	43484.9	2107.2	54.829	36900.7	1584.64	47134.2	0.0
KES226	46907.1	2091.7	55.343	34173.9	1575.24	47334.4	0.0
KES227	45841.6	2094.6	53.651	42465.3	1560.47	46590.8	0.0
KES228	42118.3	2150.1	56.697	36504.8	1584.99	47704.7	0.0
KES229	42261.4	1964.8	54.295	36748.1	1535.24	46453.7	0.0
KES230	44116.6	2029.1	55.550	35642.7	1567.94	46601.0	0.0
KES231	52171.3	2315.6	59.000	42497.2	1660.56	50117.1	0.0
KES232	40533.0	2195.7	56.077	32971.9	1610.58	47729.2	0.0
KES233	39966.0	2093.4	56.399	34336.0	1608.37	48019.4	99.8
KES234	41935.5	1993.0	55.200	38379.7	1620.96	47609.2	0.0
KES235	46672.4	2118.0	56.761	34233.3	1602.55	47530.1	0.0
KES236	46255.4	2073.1	56.076	35456.0	1622.26	47537.1	0.0
KES237	47078.5	2035.6	55.419	41446.1	1614.21	47253.4	102.6
KES238	44527.3	2020.3	55.894	37022.3	1605.04	47554.2	0.0
KES239	42869.6	2095.0	56.182	37925.2	1593.75	47033.9	0.0
KES240	47192.2	2045.0	55.323	32522.0	1739.90	46914.9	0.0
KES241	41717.5	1945.7	55.480	35451.5	1600.92	47233.3	0.0
KES242	42682.9	2000.3	56.526	35643.0	1642.69	47969.6	0.0
KES243	61426.5	1884.1	34.123	40157.4	478.08	40784.1	57.5
KES244	53316.1	1853.9	33.269	36576.2	465.55	40037.8	118.7
KES245	57156.4	1789.9	30.668	41447.6	487.11	40500.5	110.3
KES246	56539.4	1927.1	33.359	38948.1	482.24	40468.6	70.0
KES247	53455.1	1749.9	33.021	35033.9	497.30	39850.5	78.7
KES248	55727.9	1765.8	34.320	38092.7	509.68	41127.4	0.0
KES249	56684.1	1864.8	33.704	37334.0	546.29	41071.3	138.7
KES250	52925.2	1775.9	32.131	38879.8	479.67	40285.0	0.0
KES251	56232.1	1650.8	30.572	38057.5	473.35	38478.3	82.6

Appendix 6 – continued. All concentrations are in parts per million (ppm).

Sample ID	Al	Cl	Dy	K	Mn	Na	Ba
KES252	49696.1	1899.3	33.048	40946.8	475.67	40268.5	100.6
KES253	51625.1	1894.4	33.656	37295.1	469.65	40680.1	77.5
KES254	55265.2	1845.0	34.078	39758.0	479.42	40943.9	0.0
KES255	67307.8	617.4	15.421	40931.5	1099.78	37841.6	235.2
KES256	74116.6	641.1	13.252	40378.0	1101.89	38187.6	225.7
KES257	71345.9	643.8	15.099	39927.4	1102.12	38597.5	219.5
KES258	59770.9	572.4	14.803	40691.2	1142.78	37530.7	261.6
KES259	72332.0	652.9	15.200	38560.8	1079.86	37875.6	300.7
KES260	66802.9	648.3	15.407	41658.1	1087.34	38079.4	254.5
KES261	67182.2	680.1	15.832	47214.0	1107.38	37818.6	287.3
KES262	66078.1	672.2	15.254	43491.5	1117.05	37903.7	275.9
KES263	75185.4	691.6	15.853	48581.4	1169.21	40306.4	286.4
KES264	72690.7	720.5	15.662	40990.9	1155.46	38512.2	243.0
KES265	71742.7	540.2	15.603	53240.9	1124.67	38750.6	286.5
KES266	68507.3	612.6	16.253	41898.4	1114.20	38801.3	305.4
KES267	68549.2	579.3	15.923	48003.9	1146.30	39154.1	295.3
KES268	74068.9	648.2	15.223	42682.3	1096.01	38596.5	249.6
KES269	66945.6	567.0	16.147	42065.2	1121.47	37257.2	264.7
KES270	65093.1	640.4	15.795	44705.8	1092.57	38063.4	290.4
KES271	74482.2	574.5	15.086	41585.6	1083.91	37381.8	322.7
KES272	74893.6	665.6	14.926	39924.5	1085.39	37683.8	276.0
KES273	69540.3	631.1	15.542	46779.5	1087.24	38240.8	261.4
KES274	70987.6	587.7	15.726	41807.8	1118.93	37979.9	313.4
KES275	69561.2	690.6	14.865	41111.6	1093.27	37215.0	245.7
KES276	71382.2	661.4	15.244	41427.4	1066.95	37565.8	217.8
KES277	72450.5	671.2	15.351	43650.8	1091.71	37199.2	201.4
KES278	55323.9	1898.6	31.948	38356.4	475.79	39573.5	107.6
KES279	59653.3	1832.4	33.410	38373.4	464.08	39680.9	0.0
KES281	54519.8	1714.1	31.947	34189.4	515.60	38657.0	131.6
KES282	56651.3	1781.7	31.382	37863.9	478.95	38810.6	0.0
KES283	60305.7	1770.1	30.709	35427.1	497.43	39430.0	0.0
KES284	54531.4	1740.1	30.457	37485.1	500.76	38709.5	0.0
KES285	72045.5	854.0	24.672	40306.7	2803.98	55296.1	0.0
KES286	67442.3	824.7	23.161	34560.1	2833.69	55469.6	0.0
KES287	69618.8	1161.4	21.722	33737.8	2919.62	61687.5	0.0
KES288	59920.7	1175.9	22.158	35496.3	2850.04	56718.7	0.0
KES289	61956.3	1331.6	21.411	40013.8	2942.94	60832.0	0.0
KES290	66838.8	1228.9	21.411	37915.8	2945.03	61785.6	0.0
KES291	67278.0	1405.7	19.443	40345.9	2858.08	59986.7	0.0
KES292	58752.1	1255.7	19.126	43155.1	2880.12	60464.3	0.0
KES293	62556.1	1336.1	20.980	39011.7	2918.54	61573.9	0.0
KES294	66043.0	1235.8	22.183	33491.0	2928.91	61693.0	0.0
KES295	63877.3	1360.0	21.979	38749.8	2913.10	61453.4	46.6
KES296	74039.7	1269.1	21.145	40606.3	2928.09	61047.6	0.0
KES297	55775.3	1872.8	41.147	38693.7	407.41	39920.0	0.0

Appendix 6 – continued. All concentrations are in parts per million (ppm).

Sample ID	Al	Cl	Dy	K	Mn	Na	Ba
KES298	59869.7	1808.4	40.858	37138.3	397.27	39360.5	60.8
KES299	56607.9	1839.1	39.764	35781.4	397.77	39953.1	89.4
KES300	55437.8	2477.0	68.205	30506.6	1670.85	49363.9	264.9
KES301	38358.8	2404.1	64.522	35761.3	1644.29	49189.8	0.0
KES302	42134.8	2412.1	64.189	28687.0	1615.72	48523.3	244.7
KES303	45983.7	2439.3	64.573	33753.3	1644.46	48631.2	209.3
KES304	40775.7	2405.0	64.093	37749.4	1650.65	48849.3	0.0
KES305	43190.6	2475.7	64.901	33993.2	1620.28	48680.4	278.9
KES306	42616.2	2325.0	65.318	42688.4	1644.83	49283.7	221.1
KES307	44173.7	2311.6	65.926	33253.9	1612.37	48930.8	170.0
KES308	43254.3	2007.0	68.086	33360.8	1660.85	49551.9	167.0
KES309	43137.5	2067.0	67.015	34294.6	1585.55	48137.2	0.0
KES310	44127.0	1984.2	68.130	30999.4	1575.09	48782.0	0.0
KES311	47643.6	2075.1	71.228	35512.3	1723.79	50596.5	0.0
KES312	39583.8	2086.2	68.493	34497.5	1671.22	49307.0	225.2
KES313	40631.6	2045.4	69.486	36028.7	1677.72	49045.4	0.0
KES314	40831.4	2083.5	70.875	35537.3	1709.51	50000.2	0.0
KES315	43148.0	2070.7	66.190	39064.5	1676.93	49082.4	0.0
KES316	41185.4	1803.7	66.086	36348.2	1555.50	47401.2	0.0
KES317	42324.0	1977.1	66.172	40875.0	1581.19	48065.4	102.2
KES318	51103.4	1016.5	31.286	38353.3	2168.90	53765.7	0.0
KES319	42173.2	1063.4	33.797	35350.1	2339.91	52111.7	0.0
KES320	33383.5	2574.8	65.856	39754.1	2317.28	58527.6	0.0
KES321	38859.5	1866.6	50.981	33610.7	1811.58	50786.2	0.0
KES322	38088.3	1225.3	36.491	31953.6	2291.76	52791.3	0.0
KES323	47066.0	1507.7	43.476	33431.0	1802.49	47159.3	0.0
KES324	42738.9	1673.6	43.342	32509.8	1829.50	47530.9	130.0
KES325	40223.3	1645.7	43.818	33839.9	1845.62	48330.4	216.7
KES326	44405.9	1652.4	43.452	37000.3	1848.12	48327.8	138.5
KES327	46287.2	1605.6	44.501	31941.2	1840.40	47919.1	0.0
KES328	44673.9	1644.6	45.499	35285.7	1889.70	49108.9	0.0
KES329	47937.2	1707.8	45.729	39372.1	1899.51	49696.8	148.5
KES330	42799.9	1603.8	43.808	32238.0	1847.61	48165.2	0.0
KES331	47659.0	1656.8	45.118	34808.0	1883.18	49003.1	0.0
KES335	45937.3	1638.1	44.316	34367.7	1882.11	48843.9	141.4
KES336	43097.0	1581.1	44.514	42995.6	1864.85	48459.5	122.9
KES337	44396.0	1708.9	43.692	35565.4	1827.80	47692.7	126.4
KES338	49151.1	1638.6	43.966	37887.5	1854.59	48432.6	0.0
KES339	45040.7	1667.7	43.667	40773.7	1835.26	47914.4	0.0
KES340	52449.0	1614.0	44.013	41159.2	1874.18	49055.1	101.2
KES341	51508.6	1088.9	32.960	34851.7	2328.57	52197.7	0.0
KES342	42808.3	1291.6	42.927	40513.3	1976.01	48890.2	138.3
KES343	42640.9	1042.1	35.004	35095.8	2338.18	52400.9	0.0
KES344	45428.5	1194.1	34.151	38220.7	2345.31	52415.4	0.0
KES345	58139.8	714.6	20.960	36089.6	2529.59	50857.2	0.0

Appendix 6 – continued. All concentrations are in parts per million (ppm).

Sample ID	Al	Cl	Dy	K	Mn	Na	Ba
KES346	61399.7	792.4	21.157	39780.2	2555.86	51636.7	0.0
KES347	47033.9	1568.4	49.139	37366.8	1288.46	44467.5	0.0
KES348	48238.8	1500.6	47.679	39083.1	1295.15	44406.7	0.0
KES349	47436.5	1665.5	50.154	35913.7	1305.89	44794.5	0.0
KES350	45443.1	2507.2	70.991	32408.2	1813.20	55962.0	0.0
KES351	41354.3	2515.2	73.882	31588.5	1835.97	56775.8	0.0
KES352	44793.1	2453.5	73.683	36146.4	1828.84	56738.2	0.0
KES353	40370.5	2461.1	71.208	34051.2	1793.78	55688.6	0.0
KES354	34947.0	2577.2	72.460	34086.9	1823.64	56306.2	0.0
KES355	42222.4	2496.0	72.956	33706.0	1786.72	55423.3	0.0
KES356	37358.3	2479.8	71.834	32605.7	1829.87	56494.5	0.0
KES357	44796.2	2580.8	72.256	35911.6	1834.77	56756.2	0.0
KES358	38519.5	2430.5	74.559	33089.0	1823.86	56303.4	0.0
KES359	45244.3	2591.7	73.577	36033.2	1853.05	56785.0	0.0
KES360	38295.8	2554.8	72.344	33903.1	1824.37	56420.8	0.0
KES361	40524.9	2364.5	71.329	40711.9	1801.95	55662.2	0.0
KES362	41818.0	2492.8	70.690	33141.0	1802.46	56129.0	0.0
KES363	42260.0	2577.6	71.869	29277.6	1822.41	57166.3	0.0
KES364	47243.2	2580.0	67.447	34647.7	1658.34	49670.7	0.0
KES365	43220.6	2474.8	67.100	32623.7	1653.08	49586.5	0.0
KES366	42511.6	2476.3	65.257	35559.2	1640.93	49029.8	0.0
KES367	45810.6	2385.7	67.223	32478.7	1630.54	48796.5	0.0
KES368	39592.5	2538.2	67.943	32712.2	1643.52	49834.4	0.0
KES369	40539.2	2485.0	67.372	34745.4	1634.28	48792.4	0.0
KES370	41252.0	1232.1	29.225	37467.1	2216.44	47124.5	0.0
KES371	43160.2	1182.1	28.456	32247.1	2291.76	45987.0	0.0
KES372	46197.3	1242.0	27.738	33350.8	2171.02	45837.0	0.0
KES373	41943.3	1285.9	27.340	38533.7	2201.59	46561.1	0.0
KES374	58238.8	1530.3	28.203	41290.9	449.09	38674.1	0.0
KES375	57545.4	1473.9	26.036	32793.6	431.10	37184.1	75.9
KES376	58156.7	1841.0	33.979	38846.0	468.89	40385.3	62.5
KES377	58870.1	1889.7	33.137	34903.8	461.10	39818.7	77.5
KES378	55789.7	1957.7	33.655	33733.0	461.20	39972.1	57.6
KES379	56930.1	1643.4	34.571	36089.3	463.48	39842.5	0.0
KES380	64425.7	1631.8	34.438	37985.4	473.11	40552.3	0.0
KES381	58081.9	1680.2	34.795	36350.5	465.37	39750.2	64.2
KES382	59609.1	1669.6	34.131	34357.4	471.11	40500.2	85.4
KES383	58766.7	1613.9	33.863	35836.5	472.10	40277.1	0.0
KES384	53354.6	1692.0	33.911	37893.0	467.80	40042.6	0.0
KES385	62633.8	1630.1	33.370	35213.2	464.64	39895.6	66.0
KES386	57755.4	1730.9	33.652	35868.4	468.93	40315.2	0.0
KES387	61915.8	1610.2	34.219	36681.2	466.30	39845.9	0.0
KES388	62539.2	1721.5	35.186	34931.5	476.22	40825.1	69.4
KES389	65379.8	1643.0	34.967	38100.9	478.87	40793.4	0.0
KES390	58879.6	1750.3	35.080	34776.3	473.95	40516.7	0.0

Appendix 6 – continued. All concentrations are in parts per million (ppm).

Sample ID	Al	Cl	Dy	K	Mn	Na	Ba
KES391	65423.5	1627.7	35.452	35050.3	486.69	41788.8	0.0
KES392	57239.8	1665.9	36.837	36269.9	485.27	40502.0	0.0
KES393	58379.7	1646.3	32.910	36604.7	462.98	40061.3	106.8
KES394	62217.7	1534.9	37.326	37005.5	452.77	39856.1	102.1
KES403	51067.7	1426.7	27.7967	35834.7	2165.31	45918.1	0.0
KES404	54166.8	1479.9	28.9645	36985.6	2320.72	46387.5	0.0
KES405	43041.0	1312.7	28.6762	38443.9	2329.30	46301.6	0.0
KES406	37256.0	1358.1	28.3368	36712.0	2232.73	46987.1	0.0
KES407	49927.1	1423.6	27.4910	39916.5	2166.31	45818.7	0.0
KES408	68703.6	2167.8	38.3726	26739.8	4041.44	92923.5	0.0
KES409	81724.2	2340.1	41.6976	40783.6	4162.81	95454.9	0.0
KES410	70461.7	2290.6	40.3164	36698.3	4107.31	94287.0	0.0
KES411	57329.7	1931.3	27.4926	41275.3	3043.57	66393.6	0.0
KES412	53162.3	3850.7	38.5651	35999.9	1451.18	50290.8	145.1
KES413	51800.1	3837.8	36.0300	34506.2	1470.70	51434.8	110.4
KES414	64779.1	1531.6	20.7193	37895.2	2951.81	61979.0	0.0
KES415	75616.3	1787.5	23.7351	36279.7	3025.65	63582.9	0.0
KES416	65858.3	1807.0	21.3926	38098.0	2965.36	61546.2	0.0
KES417	70476.0	1687.6	22.8927	34029.4	3005.91	63210.3	0.0
KES418	67399.8	918.4	22.5488	34634.6	2420.13	58865.1	0.0
KES419	86322.1	1284.8	16.8574	42822.4	2610.13	70207.5	0.0
KES420	81544.0	1192.1	17.3727	41879.6	2630.83	71557.2	0.0
KES421	88992.3	1234.0	19.1463	41266.0	2640.24	71854.4	0.0
KES422	80771.0	1479.2	18.5464	41726.8	2639.24	55806.6	0.0
KES423	77680.0	1187.1	16.6364	33947.6	2594.03	70716.8	0.0
KES424	66253.1	1752.5	25.5142	40038.1	2421.64	69536.0	0.0
KES425	72073.0	1397.8	25.6167	33452.1	2371.57	65039.7	0.0
KES426	79508.4	1516.0	24.4505	33004.5	2295.34	65168.8	129.7
KES427	84597.4	1420.8	26.4695	36199.0	2355.88	66351.7	0.0
KES428	63032.2	1405.4	23.9832	33753.3	2304.78	64781.2	0.0
KES429	82820.7	1521.8	17.4545	40656.9	2523.88	68850.6	0.0
KES430	66489.6	746.7	12.4515	48712.3	1560.33	27183.0	501.1
KES431	58377.1	977.5	16.4394	36827.9	900.55	37255.1	60.3
KES432	63466.4	1154.4	16.8257	38665.5	884.68	37432.1	95.4
KES433	50167.3	1305.0	19.3680	39215.3	1055.26	41155.0	0.0
KES434	54416.2	1113.2	15.7694	40042.9	909.01	38309.7	97.0
KES435	58856.8	1318.0	14.9229	40307.8	893.77	37043.5	114.4
KES436	69485.1	0.0	20.6529	41259.6	2634.56	44539.8	0.0
KES437	87031.7	1146.0	14.0616	43723.2	2476.65	64521.8	0.0
KES438	87970.4	1268.8	16.9153	34506.2	2571.62	68635.5	0.0
KES439	70135.4	1822.2	29.7717	39316.8	2629.01	65004.9	109.3
KES440	53990.4	1878.8	31.0821	36378.9	2596.19	64136.4	0.0
KES441	57580.9	1835.6	29.1392	34352.5	2708.35	64975.7	115.5
KES442	72050.7	664.7	25.0103	41448.1	2769.28	59467.8	200.5
KES443	69524.9	556.8	23.7235	43892.5	2804.46	60015.1	147.9

Appendix 6 – continued. All concentrations are in parts per million (ppm).

Sample ID	Al	Cl	Dy	K	Mn	Na	Ba
KES444	39249.9	2266.4	47.2820	32655.5	3004.76	53848.2	173.8
KES445	38341.9	2126.3	47.2253	29541.7	2947.23	52640.8	140.2
KES446	34682.3	3781.2	74.7878	35526.6	3098.70	60859.6	194.6
KES447	48339.0	1347.3	26.9782	34419.1	3086.75	58806.1	0.0
KES448	49354.1	1756.6	26.5260	28935.0	3080.58	59461.2	0.0
KES449	53181.5	1761.8	23.1987	34395.7	2492.54	53078.7	0.0
KES450	54748.2	1869.5	23.0573	37257.1	2471.53	54658.4	0.0
KES451	48094.5	1662.6	21.6742	35454.6	2403.57	53210.7	98.1
KES452	46731.4	1720.2	22.8476	35055.1	2423.24	53126.0	0.0
KES453	48484.2	1676.5	22.6889	35713.4	2555.84	54476.4	0.0
KES454	50764.3	1810.7	22.3791	33846.7	2402.34	53231.5	0.0
KES455	48927.9	1715.2	21.6011	36375.2	2406.12	52714.0	0.0
KES456	52271.6	1790.2	22.5125	37937.9	2416.39	53168.8	0.0
KES457	47125.3	1504.1	23.4363	33972.3	2686.73	53978.0	231.7
KES458	49289.3	1607.9	21.8285	35949.6	2664.03	54036.8	191.6
KES459	89080.2	1039.7	16.9987	39028.8	2224.62	63914.3	0.0
KES460	97550.7	922.6	14.4503	47275.5	2199.23	62454.9	0.0
KES461	83527.9	1329.1	18.3784	43146.7	2624.91	70581.7	0.0
KES462	86143.6	950.9	14.6733	39501.1	2165.62	62556.6	0.0
KES463	81789.6	1286.1	17.6753	38368.6	2355.50	61395.5	0.0
KES464	85697.6	1264.3	17.6501	48014.0	2374.79	61126.9	0.0
KES465	83587.1	1197.8	16.7552	41495.9	2360.75	61237.9	0.0
KES466	86404.8	1296.9	17.1919	46699.5	2380.14	62088.9	0.0
KES467	41657.8	3222.4	69.9159	36257.4	1754.39	51608.1	219.5
KES468	42100.6	3235.7	67.8909	33960.6	1715.60	50861.6	0.0
KES469	35429.6	3330.9	68.3281	35673.7	1838.10	51235.3	0.0
KES470	42491.2	3379.2	64.8706	35730.9	1696.76	50662.1	0.0
KES471	46545.8	2161.9	41.2161	35968.7	2074.34	51345.4	0.0
KES472	42184.7	2120.3	40.5722	34133.3	2048.93	50792.7	0.0
KES473	42617.3	2190.9	41.5700	35163.5	2076.02	51216.2	0.0
KES474	42805.1	1995.2	42.2342	30360.3	2057.91	51380.7	0.0
KES475	46683.5	3268.6	69.0423	36513.9	1753.09	51929.2	296.4
KES476	44249.3	3029.2	67.7062	39312.0	1714.81	50821.5	0.0
KES477	45767.9	2160.4	41.3468	36593.9	2089.45	51679.6	0.0
KES478	48551.8	2133.2	42.0119	33148.9	2074.10	51245.3	0.0
KES479	46540.6	2717.8	55.6296	31784.1	1656.14	48500.5	0.0
KES480	40597.3	1898.0	42.5506	35548.2	2160.82	54003.8	0.0
KES481	44953.2	1889.0	39.3153	32907.4	1992.86	49917.3	0.0
KES482	39350.0	1872.0	40.5553	28307.9	2006.47	49960.3	0.0
KES483	42981.3	3018.7	64.2946	33941.7	1687.85	50902.0	0.0
KES484	38684.6	3058.9	62.6561	35852.5	1654.21	49460.7	0.0
KES485	42784.2	2656.1	53.9359	34150.0	1695.31	47876.4	0.0
KES486	42205.5	2669.7	54.5768	39411.1	1641.00	48536.5	0.0
KES487	50328.0	2735.3	51.8981	39190.4	1528.53	47136.5	0.0
KES488	42851.3	2412.0	50.0614	40196.4	1588.51	45563.2	0.0

Appendix 6 – continued. All concentrations are in parts per million (ppm).

Sample ID	Al	Cl	Dy	K	Mn	Na	Ba
KES489	43558.3	2607.5	50.6044	33989.4	1692.20	46309.9	0.0
KES490	36981.7	2443.6	52.5111	37191.9	1745.97	47951.0	0.0
KES491	44043.4	2491.7	51.4370	40397.3	1722.91	47152.8	0.0
KES492	45811.6	2748.0	51.9067	37976.9	1717.94	47170.9	0.0
KES493	42304.0	2760.6	50.9092	31200.6	1703.92	46742.5	0.0
KES494	42680.0	2674.8	51.2331	37409.0	1727.96	47214.7	0.0
KES495	45541.5	2542.2	48.0831	36034.2	1687.82	46348.1	65.1
KES496	54856.1	2125.8	31.4480	37467.8	1392.61	46028.7	67.5
KES497	51564.8	2115.6	29.5586	38732.7	1409.05	45986.8	0.0
KES498	55697.9	2185.5	29.2988	33482.2	1412.38	45348.7	0.0
KES499	48622.2	2054.7	31.9971	38016.5	1421.29	45701.4	0.0
KES500	53484.4	2078.2	29.2661	38286.1	1438.82	45837.6	0.0
KES501	47841.2	2307.3	30.5031	34118.6	1518.38	44956.4	0.0
KES502	48695.7	2203.2	30.3878	34167.9	1401.45	45073.4	0.0
KES503	94175.4	1657.6	12.2381	44724.3	1979.48	63101.3	0.0
KES504	88877.2	1632.5	11.4647	44970.6	1831.09	63759.9	0.0
KES505	91274.4	1779.3	13.5928	39597.1	1796.51	64461.8	0.0
KES506	91246.8	1721.3	12.3369	49333.6	1769.21	63140.9	0.0
KES507	89683.8	1665.6	12.8491	42278.5	1796.26	64859.7	0.0
KES508	91636.5	1758.5	12.3822	41410.1	1778.99	63978.8	0.0
KES509	78515.6	815.3	18.7407	41091.6	2434.34	49741.2	129.5
KES510	66452.8	912.2	19.2610	43641.6	2522.34	50625.4	0.0
KES511	68420.0	961.9	19.4786	39490.0	2433.89	52138.3	102.5
KES512	73822.2	975.3	18.8814	43865.2	2370.09	51151.5	70.7
KES513	70884.7	618.3	16.3506	58683.8	2230.05	31941.8	115.7
KES514	88069.9	1235.9	14.1379	39938.1	2218.09	58918.2	269.0
KES515	81709.7	1148.0	14.2100	40256.0	2153.64	58148.2	294.6
KES516	82648.8	1112.0	15.1491	35189.4	1138.39	44064.6	678.9
KES517	79805.1	1033.3	15.3760	30474.9	1154.40	42898.2	644.9
KES518	83203.1	831.3	15.7807	33668.3	1195.68	45685.2	654.1
KES519	77858.9	1176.2	14.4376	34958.8	1125.67	43402.7	616.6
KES520	80611.8	1062.0	14.8772	31321.5	1192.57	43950.7	655.2
KES521	80931.4	1097.7	14.6717	33145.7	1122.96	43244.9	565.0
KES522	81629.8	1141.3	14.8446	33020.2	1149.48	44540.9	651.3
KES523	87588.9	1152.7	15.2361	34004.7	1145.46	44320.4	631.6
KES524	77267.3	1113.8	15.1835	28484.8	1174.45	43729.9	676.1
KES525	80517.5	985.3	15.4979	35062.3	1185.66	43859.8	615.9
KES526	76109.0	1078.5	15.0509	34994.8	1109.18	44079.8	593.6
KES527	80524.8	604.3	9.3380	41570.2	2079.82	52413.8	0.0
KES528	87962.1	569.6	10.3347	47016.2	2000.50	54143.4	0.0
KES529	78014.3	601.2	10.9268	46962.1	1966.58	53033.0	0.0
KES530	77906.3	389.3	9.7746	47249.0	1829.55	43483.9	62.0
KES531	80669.0	344.7	10.1121	44977.2	1874.49	43396.6	87.7
KES532	82312.6	509.8	10.4363	43054.1	1855.50	46047.8	57.3
KES533	82539.1	405.0	10.8257	44240.3	1908.92	45236.1	0.0

Appendix 6 – continued. All concentrations are in parts per million (ppm).

Sample ID	Al	Cl	Dy	K	Mn	Na	Ba
KES534	62418.0	2020.4	35.3839	37510.7	441.59	39239.7	72.9
KES535	56363.8	2030.9	36.2948	35445.2	441.87	39293.4	55.5
KES536	47114.2	1267.8	28.5641	35512.3	2186.03	46105.2	68.2
KES537	47868.4	1352.8	28.5459	36624.3	2190.22	46290.1	85.5
KES538	44869.6	1446.7	28.2985	37070.1	2219.15	46703.3	67.2
KES539	48381.3	1353.8	27.5955	35666.5	2195.49	46585.8	134.1
KES540	74308.6	1856.1	27.7029	37821.6	3034.93	65896.3	42.6
KES541	78424.9	1235.9	24.4409	34827.8	2233.02	62618.4	49.6
KES542	69071.3	1381.9	25.0526	34794.3	2359.17	67333.1	0.0

Appendix 6 - Concentration data from NAA for obsidian from Kenya. All concentrations are in parts per million (ppm)

Sample ID	Ce	Co	Cs	Eu	Fe	Hf	La
KES001	418.518	0.189	4.196	1.919	47950.2	39.154	215.510
KES002	420.077	0.185	4.280	1.972	48491.3	39.158	216.151
KES003	143.183	0.355	4.136	0.155	13291.3	16.442	71.697
KES004	150.857	0.523	3.930	0.179	13321.8	16.846	76.394
KES005	845.528	0.177	6.549	4.609	53752.6	77.659	438.370
KES006	918.127	0.000	7.562	4.740	56682.8	80.665	469.564
KES007	894.034	0.141	6.919	4.873	53553.7	82.869	466.748
KES008	518.614	0.241	1.893	4.321	67104.0	41.300	259.103
KES009	506.603	0.240	1.888	4.276	65503.9	40.504	256.228
KES010	971.649	0.157	7.523	5.287	57024.7	89.741	504.070
KES011	953.508	0.175	7.354	5.139	55917.4	87.599	495.179
KES012	745.535	0.164	5.729	4.213	55854.7	66.995	389.466
KES013	510.265	0.388	2.145	3.289	58312.4	43.082	258.984
KES014	495.112	0.155	2.810	5.206	60359.6	40.000	249.782
KES015	508.037	0.192	2.955	5.370	61779.0	42.249	259.304
KES016	292.733	1.513	3.284	1.808	24391.2	28.331	158.774
KES017	293.620	1.581	3.279	1.834	24763.6	28.445	159.212
KES018	294.241	1.505	3.268	1.858	24398.1	28.344	158.332
KES019	289.108	1.482	3.148	1.808	23895.4	28.017	157.362
KES020	294.901	2.600	1.964	3.209	63784.2	22.475	169.103
KES021	271.603	0.390	6.602	0.646	27305.1	41.890	130.605
KES022	267.633	0.661	6.261	0.648	27347.1	39.690	129.204
KES023	271.968	0.202	6.638	0.580	26516.2	42.077	129.313
KES024	271.751	0.213	6.569	0.583	26251.1	41.478	131.380
KES025	273.858	0.147	6.888	0.602	26794.9	43.682	129.393
KES026	267.982	0.134	6.779	0.587	26241.2	42.845	128.044
KES027	273.850	0.272	6.923	0.622	27241.3	43.522	130.810
KES028	273.647	0.226	6.888	0.604	26960.5	43.453	129.770
KES029	270.025	0.138	6.899	0.582	26356.4	43.081	128.435
KES030	257.446	0.136	6.586	0.562	25001.8	41.128	122.867
KES031	258.581	0.118	6.615	0.580	25240.7	41.184	122.792
KES032	259.019	0.145	6.679	0.560	25149.4	41.185	122.897
KES033	489.016	0.361	2.071	3.148	55792.8	40.898	246.935
KES034	494.793	0.343	2.156	3.166	55904.8	41.384	249.981
KES035	495.602	0.364	2.100	3.204	56341.9	41.583	250.978
KES036	490.599	0.364	2.063	3.163	55926.0	41.123	247.989
KES037	495.761	0.362	2.088	3.194	56256.8	41.499	249.799
KES038	495.231	0.368	1.998	3.201	56123.2	41.335	249.217
KES039	486.972	0.372	2.043	3.096	55352.7	40.796	247.591
KES040	486.445	0.401	2.046	3.133	55648.7	40.886	248.055
KES042	481.757	0.301	2.952	3.016	62421.3	39.814	253.501
KES043	493.056	0.213	1.822	4.249	63335.3	38.946	247.731
KES044	488.254	0.193	1.865	4.268	62861.5	38.868	246.691
KES045	499.234	0.204	1.877	3.989	62490.2	40.337	252.071
KES046	501.253	0.176	1.826	4.066	62614.5	40.425	253.892

Appendix 6 – continued. All concentrations are in parts per million (ppm).

Sample ID	Ce	Co	Cs	Eu	Fe	Hf	La
KES047	242.315	0.126	6.222	0.542	23797.8	38.876	116.145
KES048	258.102	0.116	6.574	0.554	24954.4	41.074	122.798
KES049	257.266	0.121	6.583	0.560	24972.5	40.904	122.955
KES050	259.607	0.102	6.361	0.572	25069.4	44.698	122.266
KES051	261.277	0.116	6.456	0.566	25141.2	44.803	122.060
KES052	330.139	0.130	8.042	0.717	28660.4	54.034	156.435
KES053	329.022	0.138	8.193	0.729	28597.5	53.931	155.410
KES054	449.587	0.210	2.088	3.435	67254.4	38.550	228.423
KES055	452.442	0.223	2.162	3.391	67784.5	38.895	229.531
KES056	453.462	0.216	2.124	3.412	67672.2	38.980	231.058
KES057	418.967	0.182	1.621	2.836	64503.2	25.906	223.556
KES058	777.255	0.142	6.086	4.151	49758.4	70.490	406.222
KES059	873.751	0.041	7.313	4.483	54166.2	77.012	452.039
KES060	595.128	0.161	4.927	3.185	45596.4	55.910	313.676
KES061	598.426	0.157	4.958	3.220	45843.3	56.129	313.574
KES062	716.337	0.216	5.487	3.992	53384.4	63.939	375.166
KES063	707.813	0.447	5.378	3.968	52255.3	63.155	374.976
KES064	707.145	0.159	5.432	3.963	52487.2	64.730	382.311
KES065	760.070	0.195	5.838	4.134	51678.0	68.672	401.338
KES066	282.568	1.055	1.617	3.055	61100.5	23.432	155.261
KES067	706.204	0.193	5.502	3.782	49228.1	64.513	375.405
KES068	712.149	0.171	5.494	3.799	49467.5	65.036	376.424
KES069	707.662	0.208	5.443	3.800	49559.3	64.805	376.439
KES070	878.221	0.421	7.289	4.503	54702.2	77.698	455.423
KES071	875.489	0.111	7.322	4.517	54392.2	77.668	460.800
KES072	872.520	0.121	7.203	4.473	54244.8	77.173	456.270
KES073	880.096	0.085	7.235	4.504	54399.7	79.001	456.228
KES074	879.421	0.110	7.126	4.498	54402.2	77.687	455.670
KES075	238.790	0.101	6.390	0.530	24391.2	51.963	106.342
KES076	147.181	0.401	4.111	0.154	14580.5	16.410	75.509
KES077	137.458	0.336	4.177	0.163	13217.2	16.652	69.220
KES078	145.733	0.634	4.027	0.175	17465.3	16.839	74.581
KES079	804.424	0.161	6.218	4.374	51005.1	74.417	433.984
KES080	216.714	0.312	0.723	2.260	68864.4	16.920	113.481
KES081	496.269	0.376	2.016	3.175	56162.5	41.580	257.378
KES082	501.019	0.416	2.064	3.203	56617.6	41.876	259.641
KES083	498.441	0.400	2.053	3.220	56815.4	42.065	259.271
KES084	503.767	0.402	2.118	3.196	56660.6	42.058	258.074
KES085	498.330	0.399	2.105	3.199	56361.0	41.753	258.166
KES086	495.210	0.411	2.190	3.177	56593.9	41.614	258.978
KES087	894.679	0.198	6.857	4.812	52732.0	82.600	468.085
KES088	868.253	0.161	6.704	4.771	51697.7	82.232	468.167
KES089	326.620	0.152	1.184	3.588	69678.1	27.066	163.052
KES090	334.117	0.136	1.250	3.645	70546.7	27.569	165.574
KES091	744.823	0.243	5.696	4.134	54978.1	66.134	359.260

Appendix 6 – continued. All concentrations are in parts per million (ppm).

Sample ID	Ce	Co	Cs	Eu	Fe	Hf	La
KES092	744.866	0.215	5.563	4.167	54935.9	66.374	366.929
KES093	724.531	0.179	5.599	4.050	53891.4	64.852	366.022
KES094	703.768	0.177	5.429	3.974	52605.8	63.450	365.940
KES095	711.735	0.184	5.619	3.877	50130.3	65.270	369.356
KES096	744.212	0.230	5.759	4.006	51942.1	67.887	382.265
KES097	726.941	0.244	5.600	3.938	50699.1	66.212	373.513
KES098	492.024	0.202	3.018	5.086	59112.3	40.555	248.619
KES099	490.562	0.416	2.962	5.107	59245.6	40.484	247.493
KES100	474.695	0.215	2.940	5.010	57837.6	39.498	244.276
KES101	282.127	1.823	1.714	2.076	55460.7	23.246	153.099
KES102	294.731	1.044	1.669	2.053	56310.9	23.461	151.747
KES103	285.732	1.422	1.718	2.110	55017.0	22.949	154.906
KES104	274.352	1.070	1.665	1.964	54707.7	22.616	148.935
KES124	261.574	1.084	1.555	2.881	57931.7	21.693	139.947
KES125	257.773	1.045	0.715	2.825	55533.3	21.200	136.247
KES126	287.501	1.060	1.687	3.101	61908.6	24.106	152.692
KES127	278.520	0.920	1.374	3.000	59777.3	23.435	148.856
KES128	260.791	0.990	1.116	2.886	57312.3	22.016	140.213
KES130	279.761	1.124	1.646	3.094	62114.5	23.284	151.402
KES131	291.603	1.094	1.668	3.147	63423.5	24.227	154.407
KES132	281.333	1.111	1.612	3.101	61472.1	23.380	148.828
KES133	287.267	2.497	1.920	3.079	61385.5	21.927	162.890
KES134	286.417	2.545	1.908	3.031	61099.2	21.723	162.389
KES135	283.765	2.476	1.902	3.017	61092.6	21.522	161.330
KES136	284.561	2.521	1.853	3.015	61241.0	21.764	162.997
KES137	354.073	1.046	2.547	2.680	55447.3	28.667	202.890
KES138	345.126	1.069	2.484	2.630	55169.3	28.407	201.321
KES139	301.534	2.484	1.964	3.125	61126.9	23.539	172.592
KES140	282.214	2.511	1.857	2.989	60797.4	21.440	158.111
KES141	310.563	2.470	2.164	3.181	60663.0	24.459	176.204
KES147	239.623	0.111	6.491	0.544	24450.7	52.150	105.067
KES148	245.396	0.259	6.498	0.537	24883.1	53.237	105.202
KES149	239.703	0.096	6.518	0.540	24478.9	52.144	106.339
KES150	241.223	0.246	6.452	0.548	24651.1	52.245	106.601
KES151	236.484	0.298	6.444	0.519	24206.3	51.624	106.194
KES152	231.432	0.259	6.440	0.515	24109.4	51.247	103.363
KES153	231.076	0.251	6.495	0.518	23963.3	50.870	103.493
KES154	230.902	0.233	6.383	0.506	23841.6	50.816	102.123
KES155	226.255	0.085	6.352	0.502	23633.7	50.217	102.947
KES156	229.557	0.128	6.340	0.512	24101.7	51.048	102.566
KES157	236.103	0.091	6.537	0.515	24433.6	51.901	104.844
KES158	232.576	0.117	6.413	0.508	24151.4	51.357	103.255
KES159	238.106	0.144	6.429	0.533	24190.7	51.595	107.398
KES160	236.764	0.102	6.427	0.531	24230.7	51.704	105.954
KES161	235.963	0.107	6.429	0.529	24231.0	51.428	106.703

Appendix 6 – continued. All concentrations are in parts per million (ppm).

Sample ID	Ce	Co	Cs	Eu	Fe	Hf	La
KES162	240.029	0.235	6.439	0.541	24301.5	52.056	106.725
KES163	234.358	0.233	6.401	0.525	24248.2	51.615	108.096
KES164	232.665	0.263	6.349	0.516	23997.1	51.008	106.591
KES165	488.312	0.294	3.208	2.487	59706.7	40.844	256.238
KES166	502.484	0.300	3.354	2.619	62165.2	42.461	266.094
KES167	507.894	0.274	3.260	2.615	62367.1	42.428	268.930
KES168	436.839	0.066	2.374	3.807	61848.6	35.913	225.710
KES169	329.666	0.090	3.285	1.808	41029.1	27.126	175.643
KES170	374.882	0.307	2.781	1.544	37163.9	31.499	193.350
KES171	371.173	0.307	2.768	1.531	37885.6	31.241	193.943
KES172	375.029	0.065	2.872	1.501	36998.3	31.597	195.043
KES173	377.597	0.051	2.829	1.505	37770.1	31.693	195.403
KES174	373.212	0.076	2.821	1.541	37034.7	31.521	193.890
KES175	381.443	0.049	2.912	1.563	37717.2	32.267	198.585
KES176	129.592	0.354	4.023	0.156	12790.5	16.261	68.522
KES177	133.351	0.470	4.091	0.162	12750.6	16.039	67.940
KES178	136.454	0.578	4.237	0.160	13140.0	16.613	67.284
KES179	139.463	0.368	4.245	0.163	13597.5	17.312	70.347
KES180	140.945	0.455	4.077	0.176	13410.9	16.444	72.931
KES181	136.691	0.639	4.061	0.182	13395.7	16.268	71.710
KES182	702.639	0.334	5.673	3.906	49958.5	66.355	395.466
KES183	718.563	0.164	5.649	3.933	50067.5	66.472	390.017
KES184	688.618	0.165	5.544	3.882	49322.7	65.727	361.165
KES185	676.920	0.384	5.429	3.870	48822.3	64.918	358.046
KES186	675.684	0.367	5.549	3.835	48646.8	64.859	354.814
KES187	674.194	0.159	5.574	3.825	48643.1	64.705	355.443
KES188	665.798	0.159	5.472	3.820	48218.6	63.979	358.201
KES189	651.812	0.169	5.429	3.757	47522.1	62.955	352.722
KES190	669.828	0.371	5.525	3.839	48519.9	64.337	358.353
KES191	664.533	0.416	5.542	3.765	48016.5	63.891	353.904
KES192	675.939	0.110	5.558	3.904	48340.5	64.287	362.865
KES193	682.794	0.342	5.642	3.886	48593.6	64.819	360.453
KES194	683.537	0.116	5.578	3.960	48821.5	65.087	364.502
KES195	667.477	0.298	5.541	3.812	48240.4	63.972	357.747
KES196	684.563	0.369	5.560	3.872	49063.9	65.439	364.058
KES197	675.593	0.317	5.504	3.887	48646.5	64.830	362.920
KES198	677.769	0.329	5.578	3.826	48470.1	64.724	357.541
KES199	668.114	0.149	5.509	3.796	48084.0	63.948	358.042
KES200	675.377	0.167	5.529	3.834	48692.5	64.881	359.730
KES201	685.342	0.178	5.661	3.923	49197.2	65.549	365.510
KES202	677.928	0.183	5.540	3.839	48457.7	64.832	361.610
KES203	682.263	0.301	5.535	3.867	49130.0	65.041	362.255
KES204	675.513	0.333	5.605	3.842	48811.9	64.707	362.648
KES205	676.376	0.206	5.672	3.906	49472.2	65.443	367.871
KES206	673.658	0.316	5.454	3.805	48309.4	64.327	360.283

Appendix 6 – continued. All concentrations are in parts per million (ppm).

Sample ID	Ce	Co	Cs	Eu	Fe	Hf	La
KES207	680.239	0.402	5.543	3.874	49085.2	65.171	367.858
KES208	677.018	0.378	5.631	3.871	48835.4	64.883	364.725
KES209	669.486	0.457	5.467	3.823	48578.6	63.208	354.401
KES210	684.004	0.299	5.546	3.979	49008.9	65.148	369.807
KES211	671.540	0.157	5.430	3.839	47877.2	63.650	361.324
KES212	676.597	0.154	5.534	3.911	48394.6	64.209	394.681
KES213	678.530	0.165	5.570	3.903	48378.1	64.430	394.838
KES214	686.287	0.190	5.613	3.970	48911.5	65.158	400.019
KES215	675.294	0.307	5.495	3.899	48157.8	64.066	394.837
KES216	673.385	0.195	5.484	3.834	47946.5	63.879	394.060
KES217	749.039	0.179	5.764	4.162	51805.4	68.223	392.723
KES218	240.664	0.117	6.655	0.527	24790.1	52.814	106.902
KES219	245.451	0.300	6.761	0.540	25280.2	53.521	108.412
KES220	755.835	0.369	5.923	4.094	51460.0	68.204	382.751
KES221	754.381	0.290	5.870	4.124	51851.9	68.401	388.254
KES222	742.925	0.377	5.708	4.069	51213.8	67.675	385.848
KES223	764.723	0.331	5.987	4.155	52225.5	68.912	391.878
KES224	743.251	0.278	5.786	4.030	50798.7	67.264	382.674
KES225	738.297	0.162	5.928	4.040	50862.1	67.028	381.820
KES226	740.866	0.366	5.788	4.007	50606.4	66.834	381.878
KES227	753.489	0.189	5.858	4.153	52214.8	68.638	390.940
KES228	734.387	0.170	5.735	4.024	50449.0	66.621	384.075
KES229	740.794	0.187	5.841	4.050	51477.1	68.076	388.751
KES230	738.206	0.197	5.773	3.966	51000.6	67.600	382.624
KES231	738.077	0.336	5.850	4.026	51463.3	67.759	385.834
KES232	736.318	0.339	5.771	4.009	50494.1	66.814	380.393
KES233	739.911	0.157	5.746	4.039	50543.6	67.014	386.282
KES234	751.554	0.314	5.881	4.127	51274.6	68.085	387.568
KES235	746.252	0.325	5.751	4.077	51005.7	67.545	388.756
KES236	769.243	0.280	6.081	4.256	52733.7	69.656	400.789
KES237	752.949	0.198	5.898	4.125	51453.5	68.135	389.994
KES238	725.855	0.307	5.659	3.974	49858.2	66.079	381.103
KES239	741.236	0.324	5.787	4.060	51200.5	67.355	389.168
KES240	742.656	0.152	5.826	4.068	51078.7	67.473	388.982
KES241	736.254	0.173	5.651	4.010	50526.4	66.657	383.552
KES242	744.737	0.342	5.852	4.113	51437.6	67.903	391.571
KES243	263.075	0.182	6.723	0.562	25312.6	41.827	125.916
KES244	269.925	0.300	6.887	0.583	26063.4	42.850	130.889
KES245	263.846	0.469	6.647	0.592	25979.9	41.947	127.761
KES246	269.589	0.318	6.819	0.607	26404.8	42.681	128.263
KES247	264.290	0.505	6.641	0.606	26695.3	41.564	128.546
KES248	267.042	0.683	6.690	0.629	26762.4	41.675	128.230
KES249	268.599	0.777	6.709	0.681	27877.7	41.843	130.045
KES250	260.988	0.521	6.509	0.598	25520.0	40.436	123.948
KES251	268.556	0.295	6.394	0.586	25589.9	39.863	127.128

Appendix 6 – continued. All concentrations are in parts per million (ppm).

Sample ID	Ce	Co	Cs	Eu	Fe	Hf	La
KES252	260.402	0.338	6.568	0.567	25050.1	41.197	122.988
KES253	266.977	0.318	6.754	0.570	25732.4	42.263	124.366
KES254	265.644	0.366	6.621	0.579	25564.3	41.485	124.373
KES255	286.418	1.557	3.181	1.781	23988.1	27.532	153.624
KES256	288.986	1.469	3.066	1.786	23719.0	27.838	157.041
KES257	293.380	1.751	3.229	1.788	24247.9	27.966	155.254
KES258	281.858	1.539	3.141	1.751	22734.4	27.358	154.267
KES259	289.978	1.484	3.194	1.751	24052.6	27.809	154.547
KES260	293.508	1.561	3.205	1.791	24492.3	28.169	157.252
KES261	277.492	1.650	3.189	1.713	23014.4	27.018	152.073
KES262	288.481	1.481	3.239	1.784	23863.8	27.916	154.373
KES263	294.293	1.670	3.205	1.787	24328.3	28.099	154.832
KES264	290.266	1.454	3.185	1.772	23584.9	27.858	155.167
KES265	293.066	1.544	3.198	1.810	24382.9	28.094	157.064
KES266	288.476	1.510	3.175	1.767	23388.2	27.753	153.921
KES267	290.353	1.467	3.196	1.787	23757.4	28.061	156.203
KES268	292.424	1.486	3.239	1.771	23942.2	28.075	156.327
KES269	286.005	1.408	3.169	1.753	23307.9	27.747	154.042
KES270	289.376	1.497	3.214	1.794	24077.0	28.046	156.970
KES271	280.832	1.527	3.093	1.761	23661.1	27.253	152.619
KES272	287.110	1.549	3.201	1.775	24307.6	27.591	154.833
KES273	285.414	1.492	3.123	1.782	23687.5	27.665	155.664
KES274	288.332	1.539	3.190	1.771	24333.9	27.813	154.293
KES275	290.256	1.667	3.234	1.782	23879.6	27.893	155.534
KES276	283.339	1.483	3.199	1.763	22912.0	27.577	153.659
KES277	287.644	1.555	3.154	1.790	23998.1	27.890	152.234
KES278	261.656	0.408	6.686	0.614	26337.7	41.735	119.822
KES279	259.445	0.373	6.722	0.591	25813.5	42.269	120.072
KES281	260.095	1.114	6.600	0.734	27696.5	40.738	122.104
KES282	256.538	0.473	6.373	0.609	26111.6	39.772	122.685
KES283	266.238	0.580	6.278	0.642	26961.2	39.822	125.316
KES284	258.363	0.704	6.144	0.660	27004.3	38.780	122.847
KES285	404.852	0.179	1.622	2.822	64204.6	25.571	206.018
KES286	412.497	0.205	1.543	2.845	64847.8	25.960	209.084
KES287	361.499	0.197	1.421	2.007	64704.8	21.431	189.892
KES288	369.520	0.235	1.584	2.011	65181.8	22.252	191.399
KES289	371.944	0.208	1.517	2.027	65532.0	21.979	192.081
KES290	365.733	0.390	1.531	2.042	64961.4	21.754	190.444
KES291	379.488	0.232	1.528	2.090	67104.2	22.382	195.502
KES292	361.139	0.170	1.486	2.007	65042.6	21.758	191.437
KES293	377.867	0.160	1.491	2.084	66712.3	22.236	192.718
KES294	373.704	0.187	1.605	2.050	66052.1	22.094	195.778
KES295	375.513	0.211	1.560	2.070	66221.0	22.196	196.823
KES296	375.905	0.398	1.572	2.053	66174.7	22.053	194.540
KES297	246.064	0.113	6.669	0.543	25149.7	53.810	106.797

Appendix 6 – continued. All concentrations are in parts per million (ppm).

Sample ID	Ce	Co	Cs	Eu	Fe	Hf	La
KES298	241.016	0.234	6.493	0.561	24723.6	52.677	106.104
KES299	246.028	0.276	6.667	0.553	25192.7	53.650	106.150
KES300	840.229	0.144	6.800	4.810	51919.4	81.414	405.028
KES301	777.581	0.123	6.374	4.543	49353.1	76.327	384.529
KES302	805.589	0.151	6.534	4.629	50384.8	78.382	398.208
KES303	809.239	0.201	6.573	4.583	50237.0	78.438	396.230
KES304	818.638	0.290	6.684	4.646	50332.7	78.687	397.558
KES305	814.410	0.345	6.597	4.675	51126.5	79.128	401.544
KES306	816.963	0.350	6.614	4.611	51115.5	78.752	397.312
KES307	801.088	0.141	6.447	4.579	49869.6	77.486	395.355
KES308	788.203	0.173	6.375	4.575	49579.8	76.372	391.841
KES309	803.767	0.346	6.405	4.613	48538.7	78.096	398.202
KES310	797.049	0.311	6.440	4.575	46690.1	78.441	391.617
KES311	891.505	0.184	7.073	4.817	52477.2	82.618	457.949
KES312	909.696	0.146	7.012	4.972	53671.5	84.067	460.665
KES313	884.522	0.182	7.069	4.828	52000.8	82.060	454.018
KES314	899.972	0.138	6.983	4.822	52840.5	83.253	456.249
KES315	912.687	0.150	7.123	4.927	53598.8	84.305	464.390
KES316	851.777	0.075	6.711	4.654	48445.4	79.975	435.181
KES317	844.497	0.097	6.749	4.609	48432.5	79.514	439.193
KES318	341.323	0.096	1.302	3.740	70582.2	27.875	174.140
KES319	360.215	0.050	1.285	4.488	71379.6	28.872	184.811
KES320	785.148	0.173	3.300	5.071	60251.2	65.100	392.674
KES321	582.984	0.135	2.553	3.503	58922.3	50.657	288.757
KES322	425.673	0.060	1.492	4.983	69628.8	33.855	210.195
KES323	487.591	0.364	2.081	3.138	55612.9	41.125	247.952
KES324	493.533	0.362	1.994	3.209	55646.2	41.494	245.593
KES325	472.316	0.352	2.048	3.127	54737.8	40.375	245.029
KES326	484.386	0.364	2.229	3.095	54935.4	40.753	245.184
KES327	477.784	0.345	2.134	3.123	55017.3	40.662	241.985
KES328	487.819	0.380	2.108	3.141	55378.4	41.020	247.956
KES329	489.514	0.350	2.196	3.215	55870.5	41.346	247.087
KES330	485.681	0.336	2.104	3.167	55402.1	40.960	245.848
KES331	490.172	0.350	2.100	3.216	55817.0	41.284	246.860
KES335	487.259	0.383	2.035	3.182	55551.9	41.327	248.798
KES336	482.928	0.393	2.042	3.139	54949.5	40.732	244.417
KES337	486.113	0.477	2.145	3.130	54984.6	40.908	245.163
KES338	475.065	0.420	2.058	3.089	54335.3	40.286	245.663
KES339	479.284	0.372	2.061	3.093	54966.5	40.592	247.596
KES340	497.724	0.403	2.130	3.173	56022.5	41.686	250.101
KES341	347.738	0.060	1.319	4.282	71862.3	27.724	178.384
KES342	431.726	0.546	3.296	3.384	58303.4	36.439	220.945
KES343	341.775	0.079	1.255	4.299	70746.1	27.354	176.276
KES344	349.839	0.074	1.247	4.366	72716.7	27.852	179.651
KES345	210.933	0.423	0.768	2.204	67102.1	16.479	107.474

Appendix 6 – continued. All concentrations are in parts per million (ppm).

Sample ID	Ce	Co	Cs	Eu	Fe	Hf	La
KES346	207.012	0.305	0.686	2.216	66794.6	16.394	106.934
KES347	589.286	0.166	4.844	3.177	45470.0	55.518	320.341
KES348	598.913	0.193	4.865	3.254	45955.9	56.222	322.161
KES349	605.057	0.175	4.869	3.290	46367.3	56.629	326.275
KES350	872.591	0.095	7.180	4.547	54379.7	77.135	464.584
KES351	871.388	0.104	7.108	4.534	54577.9	76.904	465.107
KES352	872.336	0.060	7.111	4.513	54610.1	77.033	465.999
KES353	856.781	0.030	7.104	4.507	54102.2	76.090	461.709
KES354	871.155	0.261	7.140	4.556	54434.4	76.990	458.199
KES355	858.583	0.000	7.079	4.491	54018.0	76.200	463.325
KES356	860.499	0.331	7.093	4.469	53809.1	76.113	457.264
KES357	867.187	0.321	7.210	4.535	54220.9	76.870	460.219
KES358	854.876	0.000	7.117	4.484	54192.9	76.266	464.538
KES359	851.691	0.138	7.009	4.404	53236.8	75.288	454.937
KES360	858.322	0.000	7.031	4.470	53816.9	76.103	458.660
KES361	861.206	0.070	7.080	4.463	53966.3	76.425	462.311
KES362	854.660	0.128	7.073	4.456	53695.6	75.848	459.009
KES363	867.332	0.109	7.182	4.511	54146.5	76.709	462.557
KES364	883.545	0.169	6.735	4.855	52793.6	81.883	470.838
KES365	849.226	0.144	6.637	4.659	51227.3	78.994	465.003
KES366	859.672	0.360	6.708	4.769	52164.8	80.631	473.462
KES367	854.978	0.179	6.665	4.714	51737.0	80.021	467.630
KES368	861.233	0.212	6.655	4.749	51466.7	80.246	465.639
KES369	889.347	0.343	6.830	4.856	53057.6	82.392	479.913
KES370	489.814	0.346	2.958	5.121	59472.5	40.632	253.157
KES371	488.367	0.224	2.920	5.046	59183.0	40.486	253.568
KES372	487.786	0.215	2.911	5.125	59200.0	40.612	253.865
KES373	479.139	0.333	2.920	5.039	58165.6	39.832	250.200
KES374	248.996	0.155	5.430	0.484	23749.7	33.563	128.095
KES375	252.436	0.168	5.414	0.494	23808.4	33.705	129.679
KES376	267.859	0.317	6.725	0.598	26203.4	42.863	133.407
KES377	270.092	0.173	6.833	0.594	26375.0	43.080	131.322
KES378	265.136	0.145	6.714	0.576	25853.2	42.374	128.874
KES379	258.728	0.145	6.572	0.573	25405.5	41.751	130.789
KES380	245.995	0.185	6.484	0.566	24613.8	40.529	127.610
KES381	249.863	0.151	6.612	0.563	24896.0	40.994	127.852
KES382	251.710	0.149	6.575	0.564	24831.2	40.960	128.944
KES383	251.120	0.174	6.608	0.571	24972.3	41.110	130.116
KES384	255.996	0.155	6.523	0.568	24890.6	40.941	128.123
KES385	250.210	0.311	6.524	0.578	24908.2	41.097	128.044
KES386	248.737	0.156	6.490	0.555	24643.7	40.537	126.129
KES387	251.688	0.328	6.389	0.560	24529.9	40.310	129.076
KES388	251.510	0.157	6.420	0.557	24565.0	40.409	128.488
KES389	249.310	0.335	6.470	0.563	24734.2	40.922	130.327
KES390	247.681	0.132	6.392	0.551	24403.5	40.203	127.105

Appendix 6 – continued. All concentrations are in parts per million (ppm).

Sample ID	Ce	Co	Cs	Eu	Fe	Hf	La
KES391	251.247	0.176	6.498	0.564	24741.5	40.809	128.962
KES392	253.019	0.160	6.543	0.573	25142.3	41.609	130.245
KES393	250.806	0.150	6.697	0.577	25041.5	41.073	130.019
KES394	247.225	0.104	6.176	0.577	24464.7	43.705	127.072
KES403	486.467	0.2570	2.9296	5.0011	58277.7	40.2599	244.251
KES404	492.642	0.2617	2.9216	5.1354	59019.5	40.6947	246.922
KES405	496.088	0.2489	2.8859	5.1116	59435.0	40.8493	249.392
KES406	492.921	0.2619	2.9180	5.0411	58890.6	40.6383	248.745
KES407	492.014	0.2739	2.8657	5.0631	59187.9	40.6957	248.605
KES408	726.741	0.7268	4.4897	5.3765	65959.4	45.5118	404.621
KES409	717.551	0.8110	4.3851	5.3382	65508.1	45.1032	400.764
KES410	718.281	0.7200	4.4958	5.3602	65701.8	45.4123	404.650
KES411	419.803	0.7192	2.2999	2.3044	75895.4	26.5238	223.103
KES412	643.914	0.4881	4.3307	2.2235	45636.2	43.8973	356.511
KES413	655.977	0.4898	4.4487	2.2407	46438.3	44.4313	358.820
KES414	375.897	0.2285	1.5210	2.0063	65366.0	21.9288	203.186
KES415	377.465	0.2452	1.5393	2.0058	65079.0	21.9472	199.972
KES416	372.486	0.2707	1.4929	1.9767	64507.6	21.6447	197.812
KES417	380.706	0.2823	1.5371	2.0517	66028.4	22.1768	205.057
KES418	242.806	0.3284	1.4808	3.1884	69379.8	23.5812	124.467
KES419	333.791	0.4650	1.6266	2.6826	55679.8	19.4531	182.704
KES420	324.140	0.4542	1.6311	2.5796	54017.1	18.9756	179.215
KES421	324.854	0.4877	1.5720	2.5990	54471.5	18.9129	178.740
KES422	337.012	0.5011	1.6238	2.7368	56209.4	19.6176	185.349
KES423	333.453	0.4861	1.6212	2.6984	55760.1	19.5538	182.946
KES424	260.404	1.4437	1.9724	2.3730	67802.6	31.7827	132.152
KES425	231.480	6.2314	1.5431	2.1659	65480.8	28.2157	118.214
KES426	206.892	7.2157	1.5247	2.2244	64712.0	24.8744	104.611
KES427	252.072	2.2371	1.7752	2.2798	65671.0	30.7514	127.142
KES428	247.635	3.2687	1.8807	2.3197	67415.8	30.3210	124.981
KES429	327.574	0.4274	1.6677	2.6223	54153.8	19.1471	179.479
KES430	176.507	0.5468	1.1051	2.1795	38162.7	15.8853	93.446
KES431	166.740	0.1256	0.9549	1.8907	28928.2	17.5674	82.883
KES432	169.732	0.1517	1.0811	1.9435	29415.5	17.8835	85.102
KES433	188.945	0.1299	1.1958	2.3035	35344.7	19.6021	94.921
KES434	171.244	0.1422	0.9936	1.9434	29997.8	17.8930	85.009
KES435	171.402	0.1843	1.0174	1.9358	30581.3	17.9761	84.233
KES436	259.999	0.3587	1.3618	4.2634	68373.8	21.5980	136.053
KES437	236.250	0.6242	0.9704	2.5644	52575.2	12.6514	128.775
KES438	318.438	0.4647	1.5964	2.5708	53652.0	18.7670	175.487
KES439	300.159	0.8916	2.0140	4.6251	74471.3	32.4764	154.879
KES440	303.897	0.8612	2.0430	4.6500	74852.1	32.7879	157.553
KES441	304.839	0.8724	2.1701	4.6635	74914.2	32.8523	157.504
KES442	296.800	0.8797	1.5571	3.7616	64932.8	25.5202	154.997
KES443	295.563	0.8905	1.4779	3.7199	64369.0	25.3865	153.422

Appendix 6 – continued. All concentrations are in parts per million (ppm).

Sample ID	Ce	Co	Cs	Eu	Fe	Hf	La
KES444	638.754	0.4150	3.2783	7.6139	71965.0	60.7442	329.361
KES445	625.134	0.4040	3.2382	7.3863	70795.5	59.2623	323.777
KES446	1024.936	0.3887	5.5563	11.0579	65287.8	98.2014	525.392
KES447	339.776	0.3107	1.5116	3.9984	75840.5	27.9877	177.412
KES448	337.494	0.2698	1.4794	3.9646	76220.5	27.8689	178.822
KES449	289.807	0.2924	2.4346	3.5756	67154.4	26.0329	154.839
KES450	286.185	0.2820	2.3964	3.5539	66322.6	25.6371	153.604
KES451	288.440	0.2621	2.3390	3.5972	66977.0	25.8714	153.699
KES452	296.170	0.2597	2.4933	3.6602	68425.7	26.4383	156.823
KES453	300.156	0.2723	2.4260	3.6847	68979.2	26.5120	158.635
KES454	297.421	0.2716	2.4229	3.6662	68263.7	26.2454	155.765
KES455	293.154	0.2918	2.4120	3.6221	67544.7	25.9535	154.212
KES456	297.783	0.2717	2.4240	3.6880	68519.6	26.3000	156.421
KES457	299.062	0.2654	2.3459	4.7079	75170.2	26.3715	155.576
KES458	299.921	0.2519	2.2952	4.7734	75496.5	26.5808	155.147
KES459	289.105	1.0176	2.7051	1.5747	43607.9	29.5758	156.653
KES460	266.320	1.1343	2.4694	1.6716	43303.3	26.7121	143.182
KES461	335.926	0.4114	1.6097	2.6849	55831.4	19.4527	182.233
KES462	279.218	1.0740	2.5740	1.6243	43601.5	28.4820	152.353
KES463	281.059	0.9900	2.0089	1.8088	46745.8	27.0382	150.097
KES464	283.395	1.0813	1.9940	1.8387	47074.7	27.0494	150.900
KES465	277.737	0.9772	1.9220	1.8107	46094.0	26.4905	148.219
KES466	291.685	1.0618	2.0505	1.8381	47052.7	28.2645	157.350
KES467	924.567	0.1247	7.1571	4.9938	53871.0	84.4805	481.986
KES468	932.787	0.1685	7.2548	5.0855	54315.2	85.9033	492.297
KES469	921.702	0.1717	7.0687	5.0106	53599.7	84.8702	486.175
KES470	914.554	0.1599	7.1007	4.9412	53038.8	83.9410	480.136
KES471	494.888	0.2193	1.9193	4.1314	64027.0	39.4652	252.986
KES472	498.729	0.2560	1.9551	4.1939	64330.6	39.6907	249.238
KES473	482.948	0.2429	1.8039	4.0350	62493.1	38.3971	247.270
KES474	493.894	0.2248	1.7816	4.1439	63633.7	39.2695	253.266
KES475	946.296	0.1257	7.2627	5.1176	54568.6	87.0855	502.394
KES476	930.700	0.1636	7.2705	4.9982	53645.9	85.2153	487.311
KES477	490.673	0.2437	1.8380	4.1331	63324.5	39.0499	247.745
KES478	489.457	0.2269	1.8357	4.0730	63187.9	38.9259	249.669
KES479	761.430	0.1403	6.0399	4.1014	48893.2	69.5215	406.674
KES480	444.800	0.2229	2.1767	3.3469	66467.8	38.0823	226.477
KES481	432.879	0.4856	3.1608	3.3816	58259.0	35.9463	220.013
KES482	439.321	0.4631	3.2638	3.4285	58994.5	36.3817	225.215
KES483	858.259	0.1964	6.6864	4.6758	50832.5	79.3374	458.662
KES484	869.026	0.2861	6.7826	4.7459	51527.0	80.5053	468.331
KES485	754.818	0.2683	5.8947	4.1411	51484.9	68.1427	401.768
KES486	744.204	0.2529	5.8495	4.0931	50949.0	67.5158	400.577
KES487	701.275	0.2770	5.4358	3.7615	48695.0	63.8773	373.230
KES488	687.163	0.2870	5.3880	3.7130	48104.3	62.8627	369.530

Appendix 6 – continued. All concentrations are in parts per million (ppm).

Sample ID	Ce	Co	Cs	Eu	Fe	Hf	La
KES489	713.869	0.2230	5.4407	4.0011	52517.8	63.6055	381.027
KES490	732.300	0.2386	5.7009	4.0902	53985.6	65.2457	392.363
KES491	722.012	0.2533	5.5238	4.0630	53184.8	64.4066	382.910
KES492	720.713	0.2433	5.5532	4.0393	53182.6	64.2261	385.339
KES493	717.902	0.2558	5.4753	4.0565	53012.5	63.9890	385.138
KES494	718.577	0.2198	5.4917	4.0504	53479.7	64.1610	383.422
KES495	707.907	0.2410	5.4774	3.8022	49226.4	64.4533	380.340
KES496	409.515	0.2869	4.1606	1.8791	46476.6	38.0303	214.105
KES497	431.731	0.2750	4.3024	1.9637	48497.3	39.6523	222.280
KES498	422.068	0.2964	4.2701	1.9597	48002.1	39.4352	221.547
KES499	404.380	0.2571	4.0891	1.8422	45625.9	37.5251	212.790
KES500	405.510	0.2757	4.0133	1.8892	46817.7	37.4167	210.083
KES501	421.100	0.2849	4.2412	1.9608	47954.3	39.1539	216.401
KES502	406.173	0.2722	4.0543	1.8504	45835.1	37.7360	202.273
KES503	334.261	0.8868	2.3730	1.2549	35592.4	28.3883	186.864
KES504	331.715	0.8812	2.3841	1.2361	35308.5	28.1291	186.026
KES505	336.230	0.9007	2.3898	1.2698	35795.0	28.6112	188.294
KES506	338.685	0.9395	2.4128	1.2740	35690.7	28.7538	188.469
KES507	337.276	0.9331	2.4312	1.2755	35922.4	28.7590	189.906
KES508	339.127	0.9027	2.4672	1.2702	35904.4	28.8399	189.108
KES509	289.227	1.1987	1.6381	3.1342	63153.4	23.9493	154.861
KES510	299.156	1.1077	1.7352	3.2563	64171.6	24.9823	157.620
KES511	288.954	1.1761	1.6808	3.1610	62909.5	24.1392	154.114
KES512	284.276	1.2159	1.6592	3.1049	61917.5	23.5504	152.603
KES513	278.451	1.0673	1.0979	2.9371	58894.9	22.5376	145.801
KES514	278.422	0.2370	2.2276	3.4793	36240.2	22.7990	149.203
KES515	282.312	0.2321	2.1872	3.4810	36799.8	22.9194	151.712
KES516	163.245	7.2924	1.8091	2.1223	41060.3	18.9089	84.508
KES517	166.192	7.0237	1.8843	2.0909	41132.3	19.5267	85.051
KES518	166.305	7.0816	1.8464	2.0975	41141.5	19.2126	86.125
KES519	158.407	7.7372	1.7756	2.1066	42404.7	18.1503	81.520
KES520	161.341	7.4950	1.8375	2.0666	41473.8	18.7293	83.670
KES521	157.648	7.8827	1.7883	2.0068	40569.6	18.3611	81.281
KES522	161.396	6.5254	1.8343	2.0613	39392.7	18.7367	84.250
KES523	164.136	6.6702	1.8259	2.1011	40118.8	19.1259	85.607
KES524	161.721	6.7676	1.8593	2.0301	40397.1	18.8097	85.073
KES525	163.924	7.5844	1.7826	2.0447	42297.8	19.1245	85.269
KES526	145.702	11.4491	1.5670	2.1028	47043.6	16.6627	75.931
KES527	213.709	0.5137	0.8968	2.6975	39905.3	14.5192	111.592
KES528	215.551	0.5475	0.8343	2.7013	39710.2	14.5712	112.840
KES529	210.900	0.4857	0.8240	2.6545	39135.3	14.3703	112.685
KES530	206.518	0.5778	0.7436	2.6315	37934.3	13.9760	109.309
KES531	202.354	0.6050	0.7075	2.5878	37165.0	13.7184	106.783
KES532	203.711	0.6163	0.8062	2.5870	38506.9	13.9290	107.978
KES533	205.484	0.6047	0.7410	2.6173	38046.9	13.9551	108.137

Appendix 6 – continued. All concentrations are in parts per million (ppm).

Sample ID	Ce	Co	Cs	Eu	Fe	Hf	La
KES534	269.101	0.1951	6.5472	0.6008	25816.0	46.1431	128.863
KES535	269.233	0.1853	6.5926	0.5955	25818.7	46.1793	127.236
KES536	495.813	0.2608	2.9657	5.1515	59644.4	41.1328	253.553
KES537	488.041	0.2596	2.9056	5.0264	58845.0	40.4841	250.477
KES538	485.529	0.3186	2.9006	5.0231	58578.6	40.3018	249.821
KES539	490.250	0.2684	2.9248	5.0667	59077.9	40.7099	250.841
KES540	417.321	0.7433	2.3296	2.3385	75777.5	26.4402	227.744
KES541	229.448	7.0877	1.5654	2.1750	66381.8	27.3268	115.956
KES542	249.816	5.1953	1.8824	2.2955	68982.2	30.5587	128.588

Appendix 6 - Concentration data from NAA for obsidian from Kenya. All concentrations are in parts per million (ppm)

Sample ID	Lu	Nd	Rb	Sb	Sc	Sm	Sr
KES001	2.702	153.652	259.9	0.619	0.340	31.461	0.00
KES002	2.597	158.509	260.2	0.625	0.390	31.404	0.00
KES003	1.750	48.772	282.6	0.381	0.501	11.827	0.00
KES004	1.774	51.017	269.6	0.416	0.620	12.090	0.00
KES005	5.406	296.992	431.5	0.722	0.343	56.940	0.00
KES006	6.289	326.999	461.7	0.831	0.171	64.926	0.00
KES007	5.825	318.477	450.1	0.779	0.324	60.666	0.00
KES008	4.008	203.554	219.9	0.406	0.359	41.971	0.00
KES009	3.954	203.257	213.6	0.400	0.354	41.728	0.00
KES010	6.258	335.873	480.8	0.757	0.316	65.978	0.00
KES011	5.024	334.027	472.5	0.751	0.329	65.121	0.00
KES012	4.858	274.702	390.4	0.664	0.356	51.822	0.00
KES013	3.924	202.296	228.6	0.435	0.528	40.235	0.00
KES014	2.258	190.371	216.6	0.559	1.106	35.099	0.00
KES015	2.342	195.490	220.8	0.572	1.027	36.072	0.00
KES016	1.772	94.630	210.4	0.682	2.809	16.168	47.90
KES017	1.806	95.292	212.1	0.676	2.849	16.314	55.50
KES018	1.779	93.279	213.1	0.661	2.891	16.318	60.20
KES019	1.768	95.472	209.2	0.664	2.798	16.018	50.60
KES020	2.012	97.183	173.2	0.618	3.656	16.678	0.00
KES021	2.462	101.397	399.7	0.830	0.491	24.266	0.00
KES022	2.400	97.058	383.7	0.715	0.776	23.529	0.00
KES023	2.553	101.677	403.2	0.812	0.221	24.282	0.00
KES024	2.474	101.582	400.2	0.785	0.246	24.022	0.00
KES025	2.551	105.486	417.6	0.834	0.169	24.858	0.00
KES026	2.572	103.206	410.0	0.786	0.142	24.448	0.00
KES027	2.590	103.323	410.7	0.743	0.286	24.635	0.00
KES028	2.581	103.282	410.7	0.000	0.261	24.688	0.00
KES029	3.330	102.302	411.4	0.000	0.143	24.617	0.00
KES030	2.597	91.707	395.3	0.701	0.131	23.212	0.00
KES031	2.592	89.846	394.0	0.687	0.130	23.225	0.00
KES032	2.573	87.087	394.7	0.708	0.134	23.220	0.00
KES033	3.467	180.763	213.5	0.327	0.501	37.047	0.00
KES034	3.446	185.444	214.6	0.368	0.509	37.302	0.00
KES035	3.425	180.507	217.4	0.365	0.526	37.396	0.00
KES036	3.428	181.198	219.3	0.377	0.507	37.081	0.00
KES037	3.494	185.476	216.7	0.355	0.511	37.473	0.00
KES038	3.508	182.982	215.4	0.358	0.515	37.504	0.00
KES039	3.490	182.476	216.0	0.364	0.509	36.967	0.00
KES040	3.380	185.993	214.2	0.373	0.512	36.874	0.00
KES042	3.788	176.792	272.5	0.429	0.502	35.088	0.00
KES043	3.527	194.901	209.7	0.333	0.321	39.314	0.00
KES044	3.505	192.630	207.8	0.349	0.326	39.060	0.00
KES045	3.633	193.175	217.2	0.332	0.285	39.615	0.00
KES046	3.676	195.843	217.2	0.313	0.289	39.852	0.00

Appendix 6 – continued. All concentrations are in parts per million (ppm).

Sample ID	Lu	Nd	Rb	Sb	Sc	Sm	Sr
KES047	2.438	89.670	376.7	0.664	0.132	22.045	0.00
KES048	2.663	96.161	395.7	0.723	0.130	23.606	0.00
KES049	2.625	94.631	397.9	0.688	0.132	23.567	0.00
KES050	2.832	98.715	393.1	0.661	0.122	25.128	0.00
KES051	2.827	97.124	391.1	0.681	0.121	25.123	0.00
KES052	3.374	120.712	469.0	0.832	0.145	30.164	0.00
KES053	3.366	121.209	467.0	0.857	0.153	30.229	0.00
KES054	3.778	182.861	215.3	0.330	0.164	36.517	0.00
KES055	3.804	179.480	220.3	0.315	0.156	36.786	0.00
KES056	3.809	175.392	222.2	0.321	0.165	37.076	0.00
KES057	2.266	148.328	166.3	0.290	3.282	26.239	0.00
KES058	4.578	280.083	404.7	0.571	0.295	53.928	0.00
KES059	5.580	324.638	442.1	0.726	0.163	63.825	0.00
KES060	3.873	219.239	336.0	0.424	0.355	41.078	0.00
KES061	3.785	216.552	340.5	0.441	0.363	40.905	0.00
KES062	4.138	255.970	366.7	0.504	0.338	47.781	0.00
KES063	4.383	215.762	365.6	0.507	0.329	48.358	0.00
KES064	4.404	205.067	365.3	0.511	0.324	48.765	0.00
KES065	4.762	239.094	392.7	0.571	0.315	52.005	0.00
KES066	2.014	103.378	146.9	0.300	4.707	19.525	0.00
KES067	4.518	213.575	373.1	0.514	0.382	48.028	0.00
KES068	4.522	219.087	371.9	0.545	0.350	48.499	0.00
KES069	4.652	235.911	374.3	0.528	0.404	48.657	0.00
KES070	5.991	274.205	446.9	0.735	0.164	62.714	0.00
KES071	5.955	284.512	445.6	0.693	0.163	63.182	0.00
KES072	5.873	282.029	442.1	0.679	0.159	62.472	0.00
KES073	5.883	285.825	446.5	0.735	0.165	62.185	0.00
KES074	5.865	286.036	444.3	0.696	0.160	62.698	0.00
KES075	3.488	92.979	414.4	0.487	0.106	26.230	0.00
KES076	1.430	50.802	275.7	0.349	0.496	11.708	0.00
KES077	1.720	48.498	290.8	0.370	0.473	12.002	0.00
KES078	1.450	47.066	277.5	0.370	0.604	11.753	0.00
KES079	5.263	291.479	410.3	0.578	0.327	56.151	0.00
KES080	1.782	103.629	98.3	0.135	2.320	20.010	0.00
KES081	3.810	203.516	216.4	0.351	0.509	39.960	0.00
KES082	3.872	216.011	218.9	0.350	0.510	40.648	0.00
KES083	3.825	212.566	220.0	0.351	0.515	40.138	0.00
KES084	3.861	210.376	215.8	0.378	0.514	40.331	0.00
KES085	3.858	206.341	217.8	0.357	0.509	40.114	0.00
KES086	3.884	218.951	213.9	0.359	0.519	40.659	0.00
KES087	5.749	309.200	443.2	0.647	0.322	61.493	0.00
KES088	5.673	314.314	434.4	0.613	0.316	60.723	0.00
KES089	2.321	126.563	137.2	0.226	0.273	26.077	0.00
KES090	2.390	134.783	140.1	0.232	0.268	26.060	0.00
KES091	4.245	226.588	378.3	0.525	0.427	42.480	0.00

Appendix 6 – continued. All concentrations are in parts per million (ppm).

Sample ID	Lu	Nd	Rb	Sb	Sc	Sm	Sr
KES092	4.400	251.942	378.9	0.531	0.343	44.268	0.00
KES093	4.355	247.486	374.2	0.519	0.339	44.426	0.00
KES094	4.461	252.092	366.4	0.515	0.332	44.502	0.00
KES095	4.327	240.376	378.2	0.483	0.362	48.446	0.00
KES096	4.422	244.933	392.7	0.495	0.377	49.781	0.00
KES097	4.293	244.135	383.8	0.497	0.361	49.633	0.00
KES098	2.093	177.722	212.2	0.475	0.989	35.600	0.00
KES099	2.111	185.699	209.6	0.439	0.988	35.671	0.00
KES100	2.053	182.144	212.2	0.487	0.959	34.875	0.00
KES101	1.670	96.664	149.8	0.322	4.332	18.064	0.00
KES102	1.696	99.498	158.2	0.321	4.350	18.574	0.00
KES103	1.665	98.985	151.0	0.330	4.292	18.276	0.00
KES104	1.591	98.831	153.1	0.304	4.227	17.785	0.00
KES124	1.628	92.481	129.9	0.331	4.807	17.680	108.31
KES125	1.556	89.382	124.3	0.339	4.334	17.035	209.95
KES126	1.730	99.857	152.6	0.301	4.667	19.243	0.00
KES127	1.690	96.766	140.8	0.278	4.390	18.157	0.00
KES128	1.593	97.178	129.5	0.315	4.420	17.573	40.94
KES130	1.684	107.250	148.4	0.299	4.771	18.852	0.00
KES131	1.758	106.866	153.7	0.345	4.704	19.230	0.00
KES132	1.653	101.295	145.4	0.336	4.784	18.576	0.00
KES133	1.563	90.582	165.3	0.595	3.504	16.356	0.00
KES134	1.619	89.329	169.4	0.545	3.506	16.335	87.93
KES135	1.560	87.145	168.1	0.579	3.513	16.044	52.03
KES136	1.518	88.150	166.1	0.560	3.503	16.267	0.00
KES137	2.045	112.484	200.6	0.715	1.790	19.942	0.00
KES138	1.996	109.732	203.7	0.683	1.825	19.109	0.00
KES139	1.711	96.895	168.8	0.596	3.421	17.112	50.53
KES140	1.501	85.024	167.1	0.559	3.480	15.828	0.00
KES141	1.719	96.375	175.2	0.665	3.346	17.414	0.00
KES147	3.143	96.102	420.0	0.533	0.114	26.567	0.00
KES148	3.174	95.037	427.5	0.577	0.114	26.689	0.00
KES149	3.080	96.772	418.9	0.574	0.111	27.231	0.00
KES150	3.146	99.744	418.3	0.539	0.107	27.276	0.00
KES151	3.163	98.081	414.6	0.553	0.105	26.365	0.00
KES152	3.169	96.481	411.7	0.556	0.110	26.194	0.00
KES153	3.161	92.257	410.7	0.569	0.111	26.362	0.00
KES154	3.147	91.763	412.6	0.571	0.109	25.946	0.00
KES155	3.231	91.450	408.1	0.541	0.111	26.088	0.00
KES156	3.124	93.884	411.6	0.564	0.108	25.601	0.00
KES157	3.203	94.376	416.8	0.557	0.111	26.671	0.00
KES158	3.129	93.066	411.0	0.591	0.113	26.253	0.00
KES159	3.261	94.934	413.5	0.538	0.110	26.998	0.00
KES160	3.203	100.033	410.1	0.551	0.106	26.968	0.00
KES161	3.163	98.434	410.1	0.514	0.109	26.564	0.00

Appendix 6 – continued. All concentrations are in parts per million (ppm).

Sample ID	Lu	Nd	Rb	Sb	Sc	Sm	Sr
KES162	3.234	102.016	415.1	0.517	0.104	26.676	0.00
KES163	3.255	100.782	412.9	0.546	0.111	27.262	0.00
KES164	3.244	95.395	411.1	0.512	0.109	26.448	0.00
KES165	3.887	174.367	282.0	0.463	0.430	35.513	0.00
KES166	3.915	188.755	292.1	0.474	0.444	38.387	0.00
KES167	3.953	187.695	293.3	0.438	0.456	38.352	0.00
KES168	3.181	170.841	243.6	0.322	0.209	34.744	0.00
KES169	2.094	134.304	222.6	0.285	0.226	24.658	0.00
KES170	2.252	143.660	228.5	0.314	0.096	27.645	0.00
KES171	2.256	143.168	231.4	0.303	0.112	27.364	0.00
KES172	2.245	145.182	230.7	0.322	0.091	27.515	0.00
KES173	2.241	146.721	233.2	0.321	0.094	27.672	0.00
KES174	2.249	146.261	229.4	0.352	0.092	27.339	0.00
KES175	2.299	151.524	236.3	0.312	0.092	27.896	0.00
KES176	1.377	47.636	269.2	0.388	0.465	11.410	0.00
KES177	1.375	46.068	277.6	0.379	0.451	11.669	0.00
KES178	1.406	47.566	283.0	0.402	0.474	11.771	0.00
KES179	1.474	48.373	283.2	0.403	0.467	12.291	0.00
KES180	1.415	49.448	278.6	0.387	0.592	12.262	0.00
KES181	1.392	50.176	274.9	0.353	0.583	11.941	0.00
KES182	4.389	275.300	377.5	0.577	0.355	52.104	0.00
KES183	4.349	277.449	377.6	0.565	0.340	50.716	0.00
KES184	3.490	225.382	371.7	0.543	0.333	41.020	0.00
KES185	3.904	225.850	366.1	0.537	0.337	40.163	0.00
KES186	4.014	239.897	369.5	0.558	0.334	40.165	0.00
KES187	4.051	245.308	371.7	0.540	0.329	40.588	0.00
KES188	3.552	240.899	366.6	0.531	0.318	41.435	0.00
KES189	3.896	238.717	359.9	0.535	0.319	40.044	0.00
KES190	3.908	226.516	365.6	0.557	0.328	40.735	0.00
KES191	4.067	242.398	364.4	0.534	0.337	40.566	0.00
KES192	4.046	235.335	365.9	0.564	0.294	42.069	0.00
KES193	4.105	249.748	367.2	0.545	0.289	42.012	0.00
KES194	3.940	259.460	370.0	0.560	0.296	42.351	0.00
KES195	3.931	246.391	365.1	0.514	0.325	41.518	0.00
KES196	4.085	248.741	373.4	0.545	0.332	42.691	0.00
KES197	4.118	246.080	368.6	0.548	0.329	42.167	0.00
KES198	4.093	244.633	368.3	0.584	0.328	41.686	0.00
KES199	4.031	243.655	364.8	0.531	0.319	42.156	0.00
KES200	4.099	236.650	367.9	0.555	0.328	41.751	0.00
KES201	4.081	248.617	371.2	0.553	0.334	42.713	0.00
KES202	4.068	249.395	369.6	0.551	0.332	42.944	0.00
KES203	4.057	251.603	367.4	0.544	0.328	42.516	0.00
KES204	4.088	255.215	369.4	0.539	0.332	42.948	0.00
KES205	4.035	246.497	374.0	0.553	0.357	42.466	0.00
KES206	4.066	257.156	367.6	0.523	0.327	42.785	0.00

Appendix 6 – continued. All concentrations are in parts per million (ppm).

Sample ID	Lu	Nd	Rb	Sb	Sc	Sm	Sr
KES207	4.091	269.892	369.6	0.531	0.332	43.335	0.00
KES208	4.067	256.671	372.9	0.521	0.325	42.875	0.00
KES209	3.997	250.217	358.2	0.549	0.878	42.564	0.00
KES210	4.150	259.703	373.6	0.557	0.298	43.596	0.00
KES211	4.156	254.922	365.1	0.546	0.291	43.596	0.00
KES212	4.910	298.365	367.8	0.560	0.288	50.732	0.00
KES213	4.990	296.043	369.6	0.545	0.295	50.806	0.00
KES214	4.787	312.511	368.0	0.542	0.301	51.710	0.00
KES215	4.938	313.423	365.9	0.573	0.289	51.041	0.00
KES216	4.263	315.079	365.5	0.559	0.290	51.502	0.00
KES217	4.345	254.974	388.7	0.615	0.318	50.623	0.00
KES218	3.067	97.409	430.7	0.589	0.115	28.158	0.00
KES219	3.093	97.507	430.9	0.630	0.114	28.235	0.00
KES220	4.381	255.769	394.2	0.598	0.318	51.612	0.00
KES221	4.338	255.889	399.3	0.639	0.323	51.822	0.00
KES222	4.291	235.748	389.1	0.595	0.310	51.042	0.00
KES223	4.415	256.438	396.6	0.616	0.317	51.973	0.00
KES224	4.369	253.169	391.7	0.600	0.309	51.849	0.00
KES225	4.345	245.540	382.3	0.600	0.313	53.614	0.00
KES226	4.458	256.281	384.0	0.600	0.305	52.563	0.00
KES227	4.414	259.303	393.6	0.587	0.315	52.176	0.00
KES228	4.456	258.200	384.1	0.586	0.316	51.716	0.00
KES229	4.010	253.450	390.5	0.600	0.349	52.308	0.00
KES230	4.394	249.930	387.0	0.615	0.357	52.646	0.00
KES231	4.448	258.952	388.5	0.620	0.353	52.644	0.00
KES232	4.416	256.863	382.7	0.614	0.309	52.312	0.00
KES233	4.395	256.216	385.4	0.613	0.298	53.494	0.00
KES234	4.441	262.982	384.0	0.595	0.312	52.783	0.00
KES235	4.409	262.508	386.7	0.549	0.313	53.225	0.00
KES236	4.468	265.119	396.8	0.585	0.314	54.793	0.00
KES237	4.402	259.132	390.9	0.619	0.317	53.440	0.00
KES238	4.374	253.763	383.6	0.623	0.295	52.494	0.00
KES239	4.333	255.956	389.1	0.582	0.307	52.522	0.00
KES240	4.436	264.217	391.1	0.574	0.316	53.217	0.00
KES241	4.462	258.790	381.0	0.590	0.312	52.989	0.00
KES242	4.389	266.993	386.0	0.578	0.312	53.821	0.00
KES243	2.654	102.509	406.1	0.777	0.135	24.577	0.00
KES244	3.141	101.880	411.0	0.751	0.139	25.264	0.00
KES245	2.760	102.573	398.0	0.763	0.324	24.539	0.00
KES246	2.751	105.973	408.3	0.772	0.271	24.825	0.00
KES247	2.746	100.490	399.0	0.737	0.539	24.995	0.00
KES248	2.768	100.079	399.1	0.723	0.573	24.530	0.00
KES249	2.732	100.619	400.6	0.713	0.919	24.883	0.00
KES250	2.504	91.379	390.3	0.554	0.349	22.364	0.00
KES251	2.507	92.902	381.0	0.565	0.329	22.436	0.00

Appendix 6 – continued. All concentrations are in parts per million (ppm).

Sample ID	Lu	Nd	Rb	Sb	Sc	Sm	Sr
KES252	3.186	88.548	392.8	0.567	0.144	22.073	0.00
KES253	2.709	97.916	405.5	0.584	0.147	22.937	0.00
KES254	2.575	98.564	398.2	0.623	0.173	23.030	0.00
KES255	1.792	91.297	207.7	0.479	3.029	15.641	65.00
KES256	1.840	92.626	207.4	0.497	2.699	15.661	39.20
KES257	1.833	89.352	211.1	0.481	3.028	15.952	35.50
KES258	1.821	86.395	207.0	0.469	2.620	15.538	44.34
KES259	1.841	92.112	210.0	0.490	2.773	15.921	53.79
KES260	1.499	90.254	209.8	0.500	2.815	15.995	35.80
KES261	1.799	88.812	201.9	0.456	2.713	15.442	26.54
KES262	1.772	94.642	210.4	0.503	2.748	15.956	60.66
KES263	1.862	89.796	212.5	0.500	2.785	16.024	37.68
KES264	1.535	93.057	209.9	0.489	2.774	16.183	48.89
KES265	1.498	98.733	212.0	0.478	2.782	16.330	50.70
KES266	1.834	95.828	211.2	0.479	2.698	16.139	40.22
KES267	1.382	95.083	210.2	0.512	2.691	16.337	44.44
KES268	1.874	94.399	209.7	0.505	2.764	16.319	51.28
KES269	1.868	94.089	207.0	0.482	2.723	16.273	50.58
KES270	1.405	99.284	210.9	0.468	2.786	16.890	58.27
KES271	1.814	94.058	204.8	0.487	2.860	16.408	29.49
KES272	1.940	94.569	207.2	0.497	2.873	16.794	47.55
KES273	1.881	95.360	209.9	0.494	2.793	16.906	60.77
KES274	1.332	98.949	209.6	0.474	2.742	16.790	46.60
KES275	1.868	97.607	208.0	0.484	2.744	16.876	52.91
KES276	1.332	88.091	208.2	0.493	2.666	16.256	41.74
KES277	1.444	88.641	211.0	0.518	2.785	14.803	74.10
KES278	2.655	74.457	404.6	0.647	0.439	20.018	0.00
KES279	2.696	87.132	407.6	0.656	0.147	20.351	0.00
KES281	2.628	79.960	392.1	0.629	1.016	21.220	0.00
KES282	2.600	88.403	381.9	0.624	0.525	21.238	0.00
KES283	2.259	83.550	386.4	0.612	0.652	20.924	0.00
KES284	2.495	87.869	376.6	0.610	0.830	19.793	0.00
KES285	1.965	114.862	163.6	0.234	3.506	21.928	0.00
KES286	1.988	120.124	167.7	0.237	3.311	21.557	0.00
KES287	1.769	103.077	166.3	0.174	3.108	19.313	0.00
KES288	1.821	109.304	168.6	0.184	3.112	20.013	0.00
KES289	1.697	96.263	165.3	0.181	3.062	19.495	0.00
KES290	1.728	101.205	167.3	0.210	3.022	19.525	0.00
KES291	1.723	114.449	174.0	0.197	3.167	19.853	0.00
KES292	1.610	107.005	166.7	0.187	3.042	19.783	0.00
KES293	1.745	114.534	170.5	0.187	3.154	20.920	0.00
KES294	1.722	121.986	170.8	0.179	3.103	20.303	0.00
KES295	1.821	109.693	171.6	0.170	3.088	20.965	0.00
KES296	1.717	114.530	170.3	0.190	3.124	20.920	0.00
KES297	2.845	89.700	433.8	0.511	0.114	25.386	0.00

Appendix 6 – continued. All concentrations are in parts per million (ppm).

Sample ID	Lu	Nd	Rb	Sb	Sc	Sm	Sr
KES298	3.310	97.361	423.4	0.500	0.108	25.126	0.00
KES299	3.237	96.358	430.8	0.510	0.110	24.904	0.00
KES300	3.613	168.393	439.1	0.562	0.302	41.505	0.00
KES301	3.466	173.420	415.8	0.564	0.302	38.133	0.00
KES302	3.609	177.362	425.2	0.575	0.308	41.450	0.00
KES303	3.681	166.257	422.0	0.597	0.309	41.356	0.00
KES304	3.584	180.348	427.6	0.595	0.312	41.771	0.00
KES305	3.666	179.751	428.3	0.613	0.310	42.072	0.00
KES306	3.558	187.555	430.6	0.547	0.313	42.122	0.00
KES307	3.724	175.975	420.1	0.585	0.309	41.583	0.00
KES308	3.571	183.896	416.0	0.534	0.304	41.337	0.00
KES309	3.705	201.447	423.2	0.597	0.292	42.889	0.00
KES310	3.805	195.136	420.8	0.582	0.275	43.315	0.00
KES311	4.969	284.968	443.5	0.652	0.309	57.985	0.00
KES312	4.902	284.166	448.4	0.645	0.320	55.175	0.00
KES313	4.883	280.083	444.0	0.658	0.311	55.458	0.00
KES314	4.981	285.540	449.4	0.623	0.307	56.597	0.00
KES315	5.031	292.226	452.8	0.623	0.314	59.536	0.00
KES316	4.908	285.059	433.1	0.524	0.279	56.729	0.00
KES317	4.855	285.778	430.7	0.600	0.294	56.642	0.00
KES318	2.483	137.469	151.4	0.215	0.199	29.250	0.00
KES319	2.509	143.484	148.9	0.221	0.291	31.340	0.00
KES320	5.209	285.784	309.3	0.517	0.206	61.252	0.00
KES321	3.843	206.627	244.6	0.402	0.183	42.509	0.00
KES322	2.885	153.874	182.1	0.266	0.162	33.758	0.00
KES323	3.425	180.905	215.4	0.290	0.512	37.884	0.00
KES324	3.442	187.537	215.9	0.362	0.509	37.630	0.00
KES325	3.325	178.260	215.6	0.341	0.504	36.911	0.00
KES326	3.379	180.108	216.4	0.338	0.497	37.621	0.00
KES327	3.331	177.210	214.3	0.335	0.499	36.366	0.00
KES328	3.409	187.491	213.8	0.364	0.507	38.164	0.00
KES329	3.384	185.788	219.6	0.372	0.519	37.650	0.00
KES330	3.368	190.586	213.9	0.372	0.512	37.967	0.00
KES331	3.461	189.078	214.0	0.367	0.503	38.204	0.00
KES335	3.485	185.803	213.9	0.374	0.509	38.227	0.00
KES336	3.464	185.512	212.0	0.332	0.506	37.410	0.00
KES337	3.473	186.205	210.6	0.341	0.504	37.745	0.00
KES338	3.442	187.416	211.9	0.314	0.500	38.175	0.00
KES339	3.481	186.391	219.3	0.362	0.502	38.827	0.00
KES340	3.522	197.791	220.1	0.393	0.509	39.459	0.00
KES341	2.437	143.701	145.6	0.225	0.304	29.981	0.00
KES342	3.296	171.939	245.6	0.358	0.613	36.523	0.00
KES343	2.405	139.916	147.3	0.212	0.295	28.904	0.00
KES344	2.483	149.786	151.5	0.215	0.303	30.246	0.00
KES345	1.685	92.021	94.5	0.124	2.270	19.083	0.00

Appendix 6 – continued. All concentrations are in parts per million (ppm).

Sample ID	Lu	Nd	Rb	Sb	Sc	Sm	Sr
KES346	1.694	88.938	97.0	0.128	2.263	18.473	0.00
KES347	3.855	219.002	333.1	0.474	0.359	43.769	0.00
KES348	3.794	216.110	338.7	0.468	0.353	43.810	0.00
KES349	3.795	223.683	340.7	0.490	0.360	44.698	0.00
KES350	5.560	302.912	442.4	0.727	0.160	65.915	0.00
KES351	5.447	310.168	440.5	0.738	0.170	64.734	0.00
KES352	5.507	322.429	440.1	0.740	0.165	65.755	0.00
KES353	5.355	316.022	438.1	0.748	0.164	64.867	0.00
KES354	5.410	310.033	442.8	0.717	0.165	64.128	0.00
KES355	5.345	312.773	439.2	0.785	0.166	64.943	0.00
KES356	5.459	318.434	440.4	0.778	0.162	64.812	0.00
KES357	5.517	319.521	441.9	0.745	0.171	65.108	0.00
KES358	5.513	321.352	439.4	0.704	0.163	65.665	0.00
KES359	5.296	322.736	428.5	0.756	0.163	64.760	0.00
KES360	5.420	316.916	434.6	0.758	0.162	64.416	0.00
KES361	5.426	327.164	435.9	0.711	0.172	64.934	0.00
KES362	5.358	319.989	437.5	0.709	0.165	64.079	0.00
KES363	5.401	319.447	441.1	0.752	0.164	64.930	0.00
KES364	5.124	326.442	441.6	0.689	0.326	62.824	0.00
KES365	5.085	309.548	425.7	0.668	0.316	61.718	0.00
KES366	5.162	319.687	437.2	0.647	0.319	62.630	0.00
KES367	5.115	316.883	432.9	0.677	0.322	61.102	0.00
KES368	5.091	320.597	431.1	0.723	0.319	61.989	0.00
KES369	5.286	322.970	442.7	0.682	0.320	63.606	0.00
KES370	1.801	186.627	213.4	0.499	0.994	35.525	0.00
KES371	1.820	191.513	212.5	0.515	0.991	35.639	0.00
KES372	1.763	178.681	212.9	0.533	0.981	35.463	0.00
KES373	1.761	185.912	210.6	0.512	0.970	35.101	0.00
KES374	2.244	94.694	344.4	0.575	0.126	21.397	0.00
KES375	2.268	94.672	345.2	0.600	0.124	21.715	0.00
KES376	2.820	105.125	409.3	0.698	0.138	25.337	0.00
KES377	2.747	105.465	411.7	0.703	0.138	24.851	0.00
KES378	2.716	108.560	403.1	0.701	0.139	24.646	0.00
KES379	3.322	105.717	399.5	0.703	0.129	25.717	0.00
KES380	2.795	99.418	390.0	0.695	0.127	25.058	0.00
KES381	3.297	97.534	394.2	0.698	0.129	24.893	0.00
KES382	2.845	90.609	391.3	0.670	0.129	25.096	0.00
KES383	3.189	98.524	395.8	0.688	0.125	25.665	0.00
KES384	2.831	95.440	394.8	0.713	0.124	25.410	0.00
KES385	3.268	96.210	395.3	0.673	0.129	25.351	0.00
KES386	3.135	92.832	390.0	0.690	0.126	24.737	0.00
KES387	3.174	100.635	388.4	0.671	0.127	25.617	0.00
KES388	2.881	96.269	388.4	0.671	0.126	24.841	0.00
KES389	2.875	97.477	391.5	0.698	0.130	25.666	0.00
KES390	3.184	93.108	386.1	0.669	0.124	25.444	0.00

Appendix 6 – continued. All concentrations are in parts per million (ppm).

Sample ID	Lu	Nd	Rb	Sb	Sc	Sm	Sr
KES391	3.226	99.288	391.7	0.691	0.132	25.407	0.00
KES392	2.940	100.274	396.6	0.695	0.134	25.984	0.00
KES393	3.207	99.902	396.6	0.695	0.126	25.526	0.00
KES394	3.403	109.797	382.3	0.644	0.118	26.390	0.00
KES403	1.795	176.007	208.31	0.5262	0.9721	34.469	0.00
KES404	1.803	188.940	213.59	0.5179	0.9762	34.746	0.00
KES405	1.781	179.677	218.57	0.4901	0.9927	34.980	0.00
KES406	1.786	187.735	213.92	0.5059	0.9798	35.230	0.00
KES407	1.766	175.343	210.03	0.4719	0.9915	34.882	0.00
KES408	3.464	223.852	254.31	0.5514	1.5248	39.987	0.00
KES409	3.469	226.303	249.94	0.5781	1.4936	39.563	0.00
KES410	3.440	225.216	253.69	0.5643	1.5081	39.581	0.00
KES411	2.435	151.446	199.09	0.2912	0.7535	27.716	0.00
KES412	3.051	207.550	344.03	0.6206	0.2285	35.520	0.00
KES413	3.125	215.167	348.85	0.5836	0.2288	35.776	0.00
KES414	2.020	133.650	172.24	0.2067	3.0475	23.985	0.00
KES415	2.014	130.196	171.21	0.2031	3.0518	23.667	0.00
KES416	2.027	134.836	165.87	0.1939	3.0248	23.399	0.00
KES417	1.991	133.668	174.81	0.2476	3.1078	23.741	0.00
KES418	1.915	94.594	133.55	0.2111	0.4367	20.578	0.00
KES419	1.643	106.789	166.42	0.1951	4.4994	19.560	0.00
KES420	1.623	104.998	160.79	0.1627	4.3549	19.096	0.00
KES421	1.648	112.780	162.87	0.1578	4.3886	19.091	0.00
KES422	1.670	119.333	166.02	0.2015	4.5428	19.692	0.00
KES423	1.665	108.320	164.94	0.1868	4.5128	19.512	0.00
KES424	2.357	101.892	163.32	0.2294	1.4048	22.062	0.00
KES425	2.123	95.057	144.73	0.2094	2.3727	20.022	0.00
KES426	1.948	81.093	128.24	0.2050	5.1305	17.933	61.52
KES427	2.368	97.767	160.34	0.2235	1.4820	21.686	0.00
KES428	2.285	96.211	155.94	0.2096	3.3454	21.309	0.00
KES429	1.673	107.521	169.50	0.1796	4.3808	19.366	0.00
KES430	0.870	68.535	113.55	0.2356	1.0984	13.868	0.00
KES431	1.351	71.122	118.15	0.1261	0.2684	15.303	0.00
KES432	1.376	69.742	121.73	0.1205	0.2758	15.486	0.00
KES433	1.473	76.224	129.19	0.1748	0.1324	17.198	0.00
KES434	1.345	78.281	121.06	0.1419	0.2877	15.484	0.00
KES435	1.348	76.653	122.60	0.1409	0.3068	15.365	0.00
KES436	1.750	105.851	188.91	0.2196	1.2077	21.438	0.00
KES437	1.186	84.386	129.94	0.1073	7.3702	14.671	0.00
KES438	1.620	110.723	161.42	0.1880	4.3320	18.761	0.00
KES439	2.561	120.531	159.58	0.2855	0.4937	25.760	0.00
KES440	2.573	119.342	161.11	0.2669	0.4571	26.181	0.00
KES441	2.600	117.356	163.48	0.2483	0.4589	26.176	0.00
KES442	2.052	112.189	152.56	0.1261	1.8848	22.796	0.00
KES443	2.041	115.746	145.82	0.1352	1.8687	22.882	0.00

Appendix 6 – continued. All concentrations are in parts per million (ppm).

Sample ID	Lu	Nd	Rb	Sb	Sc	Sm	Sr
KES444	3.541	239.795	277.15	0.7374	0.8876	45.997	0.00
KES445	3.532	226.667	275.08	0.6771	0.8559	45.213	0.00
KES446	5.214	367.820	386.66	1.1902	0.3903	71.124	0.00
KES447	2.369	132.945	159.82	0.3725	0.7911	25.489	0.00
KES448	2.360	134.254	171.39	0.3602	0.7811	25.495	0.00
KES449	1.842	107.069	185.45	0.4660	0.3842	21.859	0.00
KES450	1.843	105.352	182.73	0.4625	0.3740	21.693	0.00
KES451	1.842	118.070	193.27	0.4435	0.3793	21.706	0.00
KES452	1.850	115.958	189.70	0.5128	0.3935	21.957	0.00
KES453	1.988	105.003	190.17	0.5226	0.3869	22.186	0.00
KES454	2.118	115.444	188.93	0.5454	0.3772	22.518	0.00
KES455	1.966	115.490	184.91	0.5367	0.3819	22.439	0.00
KES456	2.111	109.453	189.16	0.5065	0.3879	22.638	0.00
KES457	1.986	102.117	171.35	0.5353	0.8721	22.451	0.00
KES458	1.941	111.929	172.67	0.5117	0.8750	22.486	0.00
KES459	2.165	96.398	229.93	0.2278	2.6126	16.621	0.00
KES460	1.925	87.710	210.24	0.1917	2.9672	15.651	0.00
KES461	1.749	112.460	163.99	0.1838	4.5145	19.544	0.00
KES462	2.128	85.232	223.20	0.2078	2.7586	15.958	0.00
KES463	2.128	83.504	190.54	0.2017	3.0377	17.997	0.00
KES464	2.166	103.611	190.10	0.1783	3.2413	17.998	0.00
KES465	2.169	91.173	187.82	0.1820	3.1138	17.292	0.00
KES466	2.279	104.443	198.01	0.2015	3.1599	18.263	0.00
KES467	5.651	314.381	451.37	0.7141	0.2999	63.208	0.00
KES468	5.792	305.104	462.35	0.7549	0.3018	64.416	0.00
KES469	5.653	298.345	454.85	0.7048	0.2995	63.255	0.00
KES470	5.339	297.046	453.09	0.7434	0.2897	62.739	0.00
KES471	3.666	219.673	209.13	0.3136	0.3479	41.281	0.00
KES472	3.763	201.137	212.53	0.3275	0.3445	41.222	0.00
KES473	3.734	193.947	208.15	0.3277	0.3342	40.338	0.00
KES474	3.730	211.951	212.58	0.3232	0.3425	41.558	0.00
KES475	5.853	309.894	469.57	0.7221	0.3000	64.881	0.00
KES476	5.788	323.092	460.23	0.7160	0.2893	63.560	0.00
KES477	3.754	202.467	208.90	0.3669	0.3390	40.612	0.00
KES478	3.624	200.179	209.79	0.3170	0.3395	40.901	0.00
KES479	4.959	268.175	396.56	0.6294	0.2864	53.480	0.00
KES480	3.830	178.437	216.08	0.3082	0.1521	37.968	0.00
KES481	3.471	179.312	244.26	0.4034	0.6032	36.250	0.00
KES482	3.392	177.358	247.53	0.4385	0.6172	37.012	0.00
KES483	5.574	300.629	430.12	0.6960	0.3145	59.973	0.00
KES484	5.704	304.420	439.88	0.6883	0.3163	60.776	0.00
KES485	4.770	283.569	389.90	0.6145	0.3063	53.052	0.00
KES486	4.778	272.750	389.49	0.6021	0.3062	52.497	0.00
KES487	4.648	259.121	371.80	0.5417	0.3490	49.474	0.00
KES488	4.481	262.385	364.42	0.5505	0.3815	48.973	0.00

Appendix 6 – continued. All concentrations are in parts per million (ppm).

Sample ID	Lu	Nd	Rb	Sb	Sc	Sm	Sr
KES489	4.620	274.009	373.96	0.5780	0.3289	51.000	0.00
KES490	4.635	281.406	379.70	0.5464	0.3336	52.905	0.00
KES491	4.509	276.543	374.11	0.5766	0.3274	51.351	0.00
KES492	4.713	277.243	373.93	0.6040	0.3267	51.511	0.00
KES493	4.697	285.091	369.96	0.5499	0.3328	50.714	0.00
KES494	4.600	266.563	374.86	0.5633	0.3262	50.957	0.00
KES495	4.796	258.910	374.51	0.5717	0.3541	50.856	0.00
KES496	2.625	162.965	252.22	0.5714	0.3393	31.782	0.00
KES497	2.582	178.463	262.32	0.5978	0.3466	33.123	0.00
KES498	2.621	173.003	259.92	0.5812	0.3298	33.102	0.00
KES499	2.490	157.588	252.32	0.5532	0.3189	31.663	0.00
KES500	2.501	164.918	249.78	0.5650	0.4938	32.158	0.00
KES501	2.569	160.446	261.48	0.5808	0.3727	31.686	0.00
KES502	2.345	145.517	248.55	0.5814	0.3432	29.218	0.00
KES503	1.812	99.901	200.92	0.5046	2.3831	16.889	0.00
KES504	1.815	93.540	201.46	0.5060	2.3792	16.876	0.00
KES505	0.993	102.620	203.29	0.5044	2.4021	17.077	0.00
KES506	1.877	103.297	203.18	0.5285	2.4069	17.104	0.00
KES507	1.042	107.107	203.09	0.5244	2.4207	17.126	0.00
KES508	0.996	102.824	202.74	0.5321	2.4392	17.191	0.00
KES509	1.934	104.194	151.36	0.3130	5.4101	19.966	0.00
KES510	2.004	107.083	155.85	0.3399	4.8199	20.245	0.00
KES511	1.926	103.645	150.61	0.3106	4.8050	19.675	0.00
KES512	1.906	103.987	149.12	0.2950	4.8226	19.499	0.00
KES513	1.871	99.802	129.30	0.3021	4.5025	18.809	65.31
KES514	1.551	99.470	148.46	0.4862	3.5768	17.803	0.00
KES515	1.574	101.171	148.32	0.4573	3.6912	18.241	0.00
KES516	1.522	64.439	133.83	0.3077	7.1696	13.898	77.07
KES517	1.545	62.818	136.99	0.3405	7.1684	14.038	79.46
KES518	1.434	63.291	135.65	0.3319	6.8138	14.157	58.29
KES519	1.367	62.418	130.01	0.3088	7.8086	13.697	80.00
KES520	1.520	65.226	131.65	0.3371	7.3366	13.910	79.28
KES521	1.451	61.777	129.58	0.3231	10.7172	13.493	42.61
KES522	1.495	63.935	133.15	0.3127	6.6201	13.783	83.09
KES523	1.532	65.194	136.50	0.3423	6.7818	14.027	62.90
KES524	1.511	65.073	133.57	0.3749	7.1648	13.993	67.31
KES525	1.517	65.275	135.47	0.3255	7.2273	13.995	44.84
KES526	1.385	60.774	112.99	0.2858	11.2641	12.883	142.41
KES527	1.190	81.448	105.35	0.1762	6.3291	14.308	0.00
KES528	1.161	79.887	104.58	0.1902	6.1841	14.509	0.00
KES529	0.952	79.716	102.05	0.1885	6.1018	14.382	0.00
KES530	0.897	76.548	97.46	0.2080	6.0715	13.824	208.07
KES531	0.733	75.239	95.09	0.1907	5.8173	13.534	214.12
KES532	1.134	74.821	97.11	0.1960	6.0223	13.857	103.12
KES533	0.903	76.832	95.31	0.1965	5.9447	13.754	221.10

Appendix 6 – continued. All concentrations are in parts per million (ppm).

Sample ID	Lu	Nd	Rb	Sb	Sc	Sm	Sr
KES534	3.505	112.457	410.16	0.6969	0.1268	27.372	0.00
KES535	3.437	112.443	403.02	0.6671	0.1279	26.902	0.00
KES536	2.658	190.362	215.16	0.5344	0.9950	35.912	0.00
KES537	2.594	190.703	213.23	0.5024	0.9760	35.939	0.00
KES538	1.775	190.368	210.89	0.4914	0.9764	35.575	0.00
KES539	2.715	191.088	213.16	0.5327	0.9820	36.030	0.00
KES540	2.660	161.601	196.88	0.2738	0.7513	28.454	0.00
KES541	2.132	93.352	140.36	0.1770	3.4080	19.747	76.67
KES542	2.350	105.595	155.29	0.1943	1.9454	21.747	0.00

Appendix 6 - Concentration data from NAA for obsidian from Kenya. All concentrations are in parts per million (ppm)

Sample ID	Ta	Tb	Th	U	Yb	Zn	Zr
KES001	14.926	5.090	40.191	12.762	16.972	382.90	1419.30
KES002	14.915	5.140	40.234	13.285	16.947	401.60	1484.90
KES003	12.407	2.319	39.646	14.015	10.069	158.00	448.30
KES004	12.316	2.243	39.426	13.433	10.078	146.40	468.20
KES005	30.822	9.786	82.210	26.248	38.913	628.20	2957.40
KES006	35.438	11.377	87.385	30.851	44.804	735.90	2991.90
KES007	33.036	10.400	87.663	29.851	41.136	650.00	3174.70
KES008	19.665	7.225	34.565	13.430	26.960	541.90	1510.70
KES009	19.451	7.187	34.138	13.859	26.634	525.50	1556.70
KES010	35.575	11.187	94.493	32.440	44.829	681.40	3455.30
KES011	34.491	10.975	92.805	31.289	40.148	697.80	3339.90
KES012	26.505	8.520	69.966	24.501	32.112	560.40	2554.20
KES013	20.618	6.988	38.089	16.426	26.139	468.00	1568.20
KES014	18.739	4.817	36.695	16.490	12.704	464.30	1605.20
KES015	19.445	5.060	38.425	15.744	13.781	497.90	1665.20
KES016	16.072	2.387	37.012	14.892	9.496	162.50	1075.50
KES017	16.281	2.407	37.279	14.943	9.401	164.70	1055.40
KES018	16.206	2.438	37.099	14.878	9.313	171.10	1097.30
KES019	15.909	2.333	36.683	14.886	9.432	163.80	1043.60
KES020	18.910	2.728	32.667	13.477	10.890	264.90	903.80
KES021	22.316	4.807	66.342	24.285	19.346	320.30	1460.00
KES022	21.295	4.638	63.056	22.966	18.420	305.60	1372.20
KES023	22.328	4.792	66.741	24.311	19.504	324.40	1477.80
KES024	22.104	4.778	65.917	23.616	19.735	321.10	1433.30
KES025	23.334	4.979	69.396	25.310	20.089	332.30	1518.70
KES026	22.925	4.875	68.095	24.632	19.836	328.10	1491.70
KES027	23.040	4.934	68.607	25.626	20.212	331.40	1489.80
KES028	23.130	4.936	68.812	25.695	20.384	324.90	1539.80
KES029	23.191	4.915	68.257	25.646	19.910	317.20	1493.10
KES030	21.969	4.655	65.692	23.649	18.656	271.60	1394.50
KES031	21.933	4.681	65.809	23.161	18.878	274.20	1403.10
KES032	22.008	4.648	65.941	23.262	18.619	277.90	1410.30
KES033	19.634	6.686	36.593	14.680	24.798	401.60	1437.70
KES034	19.793	6.689	36.956	15.402	24.968	400.40	1504.60
KES035	19.782	6.701	37.158	14.744	24.934	386.30	1537.60
KES036	19.717	6.678	36.557	15.683	24.666	393.30	1519.40
KES037	19.681	6.734	36.904	14.839	24.773	394.80	1529.90
KES038	19.772	6.694	36.929	15.182	25.242	390.90	1527.60
KES039	19.560	6.636	36.509	15.817	24.706	394.90	1495.30
KES040	19.639	6.692	36.396	16.233	24.560	400.80	1468.60
KES042	22.467	6.380	40.483	18.357	25.956	418.30	1472.60
KES043	18.839	7.063	33.145	15.191	25.168	442.50	1432.70
KES044	18.856	6.969	32.889	14.576	24.971	445.30	1411.00
KES045	19.440	7.071	34.337	15.471	25.633	449.30	1480.20
KES046	19.517	7.075	34.421	15.483	25.978	451.50	1534.70

Appendix 6 – continued. All concentrations are in parts per million (ppm).

Sample ID	Ta	Tb	Th	U	Yb	Zn	Zr
KES047	20.666	4.425	61.594	24.356	18.124	256.80	1346.80
KES048	22.019	4.703	65.677	25.170	19.042	270.50	1418.40
KES049	21.949	4.632	64.098	26.140	18.820	271.20	1410.50
KES050	21.900	5.060	66.004	25.785	20.406	289.70	1537.10
KES051	21.950	5.068	66.442	26.113	20.365	290.80	1532.50
KES052	27.975	6.077	82.976	32.601	24.583	348.40	1866.40
KES053	27.814	6.081	82.930	33.350	24.518	344.80	1834.60
KES054	18.399	6.753	33.220	15.830	26.300	433.90	1444.00
KES055	18.488	6.815	33.293	16.457	26.166	440.80	1421.10
KES056	18.583	6.855	33.540	16.520	26.634	440.40	1398.00
KES057	13.906	3.957	28.606	13.237	15.708	303.50	1011.50
KES058	28.047	8.819	75.028	32.710	31.974	488.70	2654.40
KES059	34.182	10.871	83.827	35.483	39.934	612.10	2795.50
KES060	22.914	7.129	59.279	25.107	26.727	411.80	2041.70
KES061	22.953	7.251	59.575	26.028	26.705	412.70	2069.90
KES062	25.482	8.121	67.237	28.820	29.476	466.50	2399.10
KES063	25.421	7.847	66.410	21.845	30.465	404.80	2362.40
KES064	25.437	7.931	66.633	22.303	30.453	408.00	2341.00
KES065	27.221	8.476	72.219	23.913	33.175	421.20	2525.30
KES066	13.624	2.968	24.730	9.374	11.933	224.20	900.90
KES067	25.747	7.886	67.987	23.329	31.132	402.60	2386.70
KES068	25.800	8.026	68.525	22.221	31.042	400.60	2401.10
KES069	25.649	7.958	68.195	24.067	31.198	401.70	2392.10
KES070	34.421	10.767	83.856	29.414	41.054	528.30	2764.50
KES071	34.439	10.691	83.788	29.586	41.323	525.20	2806.30
KES072	34.304	10.625	83.704	29.082	40.697	528.60	2785.30
KES073	34.590	10.729	84.164	28.891	40.597	534.50	2796.20
KES074	34.638	10.721	84.165	30.210	40.873	530.80	2806.60
KES075	21.304	5.546	65.910	21.705	23.117	279.90	1752.10
KES076	12.344	2.255	38.831	13.646	10.885	106.60	442.50
KES077	12.591	2.234	39.062	14.980	10.883	114.20	450.90
KES078	12.398	2.273	39.075	13.804	9.680	114.10	448.60
KES079	29.461	9.076	77.981	28.255	36.273	448.50	2736.50
KES080	8.377	3.166	12.426	6.271	12.197	228.70	627.20
KES081	19.904	6.657	36.713	17.251	25.405	348.30	1481.80
KES082	20.022	6.676	37.181	15.921	25.961	351.10	1512.70
KES083	20.146	6.796	37.093	14.976	25.565	352.90	1477.90
KES084	20.096	6.712	37.218	15.899	25.665	354.80	1504.60
KES085	20.067	6.701	36.931	16.605	25.657	352.30	1502.60
KES086	20.065	6.698	36.751	16.001	25.680	347.50	1520.60
KES087	32.734	10.063	86.999	32.723	35.643	488.60	3048.10
KES088	32.359	9.890	85.100	31.887	35.437	478.60	2975.20
KES089	12.562	4.687	20.138	10.303	16.517	310.60	987.60
KES090	12.895	4.736	20.659	10.256	16.627	317.20	1011.00
KES091	26.401	8.232	69.521	24.892	30.076	424.60	2491.70

Appendix 6 – continued. All concentrations are in parts per million (ppm).

Sample ID	Ta	Tb	Th	U	Yb	Zn	Zr
KES092	26.446	8.274	69.727	25.945	30.087	423.70	2468.20
KES093	26.009	8.123	67.967	27.373	30.122	411.70	2435.10
KES094	25.445	7.976	66.462	26.658	30.092	402.90	2351.90
KES095	25.750	7.962	68.861	22.423	30.132	476.51	2451.23
KES096	26.554	8.185	71.813	23.540	31.111	490.57	2517.05
KES097	25.922	8.079	70.148	22.010	29.884	478.04	2461.78
KES098	18.842	4.688	37.360	16.683	12.283	428.24	1530.81
KES099	18.769	4.678	37.358	15.809	13.347	430.37	1535.13
KES100	18.442	4.567	36.399	15.516	12.142	415.25	1552.62
KES101	13.448	2.907	24.825	10.369	11.446	215.81	898.28
KES102	13.815	2.926	25.433	10.565	11.924	224.43	864.86
KES103	13.409	2.956	24.716	10.910	11.250	215.61	859.52
KES104	13.042	2.727	24.088	11.148	11.078	254.25	846.44
KES124	12.589	2.750	23.084	10.875	10.854	215.04	804.66
KES125	12.210	2.727	22.815	10.483	11.033	207.71	829.71
KES126	13.893	3.003	25.441	11.404	12.060	235.36	925.44
KES127	13.570	2.873	24.713	12.083	11.272	235.60	884.79
KES128	12.686	2.729	23.100	11.227	11.100	222.70	820.36
KES130	13.606	2.983	24.735	12.074	12.141	228.84	851.45
KES131	14.059	3.028	25.523	11.978	12.365	236.43	909.36
KES132	13.398	2.974	24.399	11.238	11.641	229.97	898.91
KES133	18.683	2.635	32.077	15.425	10.777	223.86	815.38
KES134	18.337	2.589	31.725	14.842	10.743	228.00	845.59
KES135	18.254	2.597	31.339	14.783	10.422	219.00	825.56
KES136	18.315	2.525	31.571	15.699	10.869	223.17	840.34
KES137	22.702	3.195	38.784	19.658	13.930	268.31	1086.05
KES138	22.762	3.146	38.134	18.208	13.533	264.69	1097.41
KES139	19.271	2.711	34.681	16.305	11.476	229.35	925.65
KES140	18.344	2.537	31.375	14.801	10.215	219.61	857.65
KES141	20.110	2.851	36.552	17.767	11.825	233.56	960.06
KES147	21.444	5.603	66.274	24.952	22.347	316.57	1715.17
KES148	21.684	5.625	67.561	25.347	22.500	321.95	1784.51
KES149	21.508	5.581	66.306	26.489	22.511	316.21	1743.50
KES150	21.478	5.544	66.428	25.986	22.609	316.73	1750.68
KES151	21.214	5.584	65.721	22.902	22.521	311.16	1747.92
KES152	21.202	5.558	65.416	22.666	22.351	311.04	1700.45
KES153	21.069	5.485	65.030	21.456	22.467	308.81	1710.06
KES154	21.082	5.482	65.099	22.444	22.142	308.32	1718.73
KES155	20.844	5.418	64.202	22.293	22.316	302.67	1682.00
KES156	21.071	5.439	64.987	22.013	22.303	309.84	1691.42
KES157	21.358	5.540	66.442	22.707	22.613	311.22	1739.10
KES158	21.185	5.499	65.696	22.957	22.452	312.71	1721.73
KES159	21.105	5.528	64.949	22.359	22.593	308.21	1743.67
KES160	21.118	5.584	65.594	22.066	22.800	312.69	1734.27
KES161	21.149	5.530	65.393	22.189	22.671	309.77	1718.06

Appendix 6 – continued. All concentrations are in parts per million (ppm).

Sample ID	Ta	Tb	Th	U	Yb	Zn	Zr
KES162	21.311	5.643	66.298	23.054	22.628	310.99	1734.78
KES163	21.102	5.544	65.534	22.824	22.782	312.64	1760.31
KES164	20.952	5.546	64.714	23.100	22.595	307.76	1707.58
KES165	22.489	6.496	41.592	17.535	25.973	407.82	1490.41
KES166	23.140	6.681	43.134	16.621	26.923	429.03	1524.25
KES167	23.010	6.648	43.093	17.811	27.036	426.24	1497.54
KES168	16.655	5.830	33.267	13.272	22.027	441.63	1267.72
KES169	11.793	3.918	32.326	11.676	14.535	274.42	1001.09
KES170	13.687	4.230	35.612	11.985	15.283	252.15	1116.08
KES171	13.704	4.275	35.343	12.671	15.139	257.94	1106.16
KES172	13.729	4.287	35.617	11.968	15.128	251.73	1144.05
KES173	13.712	4.212	35.838	10.922	15.645	257.93	1106.66
KES174	13.771	4.261	35.545	12.473	15.591	254.52	1132.21
KES175	14.097	4.337	36.508	13.225	15.798	262.09	1150.87
KES176	12.091	2.181	37.151	14.023	9.806	108.12	438.15
KES177	12.370	2.231	38.086	14.063	9.860	110.37	427.40
KES178	12.594	2.266	38.870	14.677	9.859	113.54	443.15
KES179	12.709	2.300	39.494	14.646	10.071	117.33	457.02
KES180	12.480	2.248	38.622	15.097	10.073	112.76	437.94
KES181	12.240	2.238	37.829	14.261	9.928	113.17	450.57
KES182	26.517	8.199	69.648	29.811	31.012	467.03	2471.29
KES183	26.540	8.234	69.779	27.901	30.949	461.43	2473.10
KES184	25.809	8.151	67.446	19.883	29.187	418.42	2498.14
KES185	25.691	8.067	66.600	18.292	28.896	411.40	2454.55
KES186	25.680	8.134	66.931	20.246	29.068	412.46	2466.16
KES187	25.670	8.042	66.694	20.422	28.783	412.95	2462.29
KES188	25.507	7.930	66.186	18.401	28.342	410.07	2430.75
KES189	25.281	7.861	65.213	18.360	27.944	405.02	2398.33
KES190	25.569	8.010	66.220	17.426	29.487	414.18	2446.43
KES191	25.523	7.972	66.242	20.533	28.602	410.93	2399.85
KES192	25.720	8.167	66.966	19.995	28.783	415.12	2456.40
KES193	25.842	8.098	67.266	20.970	29.250	412.97	2474.18
KES194	26.149	8.179	67.629	21.759	29.216	417.98	2471.33
KES195	25.571	8.028	66.583	19.675	28.943	406.59	2434.57
KES196	26.045	8.153	67.314	20.589	29.287	417.37	2491.39
KES197	25.583	8.055	66.126	21.096	28.888	412.57	2454.41
KES198	25.699	8.030	66.710	19.684	28.680	412.95	2475.08
KES199	25.517	7.989	65.856	20.819	29.604	407.90	2422.61
KES200	25.889	8.078	66.757	19.706	29.265	413.58	2478.39
KES201	26.031	8.106	67.568	20.194	27.209	416.66	2465.15
KES202	25.697	8.034	66.722	20.588	29.729	414.42	2486.70
KES203	25.985	8.070	67.222	20.752	26.594	413.34	2498.88
KES204	25.724	8.050	66.544	22.494	29.695	414.79	2457.83
KES205	26.073	8.166	66.857	21.837	29.788	416.12	2517.01
KES206	25.629	7.978	66.209	21.507	29.988	408.31	2410.11

Appendix 6 – continued. All concentrations are in parts per million (ppm).

Sample ID	Ta	Tb	Th	U	Yb	Zn	Zr
KES207	25.882	8.137	67.020	22.939	29.890	416.64	2471.22
KES208	25.811	8.064	66.509	20.777	28.844	415.73	2451.25
KES209	25.029	7.853	64.897	21.638	28.981	403.88	2447.83
KES210	25.894	8.130	66.544	20.697	30.406	413.49	2470.63
KES211	25.462	7.955	65.414	22.292	29.415	404.95	2412.56
KES212	25.730	8.058	65.988	25.549	29.763	407.46	2452.35
KES213	25.657	8.078	65.993	27.378	32.335	412.66	2468.88
KES214	25.640	8.074	66.313	25.305	32.822	416.92	2478.55
KES215	25.408	8.013	65.861	23.382	32.800	408.35	2457.09
KES216	25.493	7.975	65.618	27.986	29.589	403.43	2446.01
KES217	27.119	8.525	71.489	24.908	31.116	480.60	2520.26
KES218	22.238	5.730	67.632	23.219	23.270	321.58	1759.16
KES219	22.079	5.715	68.061	24.188	23.765	328.16	1798.31
KES220	27.418	8.519	72.189	24.535	30.981	481.99	2528.94
KES221	27.424	8.554	72.106	24.587	31.780	478.57	2571.68
KES222	27.225	8.415	71.244	25.246	30.832	483.66	2546.45
KES223	27.474	8.588	72.820	25.627	31.147	483.02	2561.90
KES224	26.902	8.337	70.803	25.843	30.710	479.42	2532.24
KES225	27.007	8.347	70.711	25.111	30.613	475.64	2494.74
KES226	26.931	8.379	70.738	25.320	30.603	464.43	2501.78
KES227	27.371	8.490	71.762	26.053	31.673	487.99	2530.47
KES228	26.680	8.281	69.932	25.877	30.576	469.43	2486.66
KES229	27.299	8.457	71.750	25.982	31.233	475.94	2497.65
KES230	27.160	8.352	71.250	25.919	31.282	479.49	2518.08
KES231	27.201	8.363	71.354	25.880	31.302	480.38	2541.52
KES232	26.757	8.340	70.113	25.519	30.735	470.18	2517.46
KES233	26.986	8.363	70.579	26.490	31.513	476.37	2513.24
KES234	27.063	8.402	71.372	25.121	30.808	486.16	2523.42
KES235	27.008	8.375	70.832	26.390	31.568	476.14	2496.70
KES236	27.663	8.708	72.910	27.351	31.558	488.15	2593.29
KES237	27.020	8.462	71.186	26.229	31.490	477.27	2523.33
KES238	26.587	8.201	69.161	24.969	30.836	466.98	2460.60
KES239	27.026	8.405	70.606	25.459	30.763	472.29	2487.98
KES240	26.888	8.396	70.582	26.907	30.721	475.06	2513.00
KES241	26.546	8.376	69.865	26.710	31.520	476.18	2493.90
KES242	27.101	8.400	70.930	26.741	30.897	478.50	2539.37
KES243	22.571	4.699	66.310	28.269	19.689	277.12	1409.54
KES244	22.819	4.776	67.879	27.147	20.515	282.92	1444.56
KES245	22.393	4.708	66.139	26.231	20.242	278.71	1413.50
KES246	22.852	4.760	67.830	27.431	20.112	284.11	1435.52
KES247	22.241	4.653	65.384	27.170	19.938	278.96	1403.26
KES248	22.355	4.704	66.143	27.656	19.758	273.00	1412.07
KES249	22.405	4.707	66.418	27.386	20.304	283.90	1402.61
KES250	21.541	4.523	64.307	21.972	19.140	249.40	1382.31
KES251	21.279	4.516	63.369	21.318	18.811	245.60	1373.48

Appendix 6 – continued. All concentrations are in parts per million (ppm).

Sample ID	Ta	Tb	Th	U	Yb	Zn	Zr
KES252	21.923	4.568	66.521	22.504	19.172	252.69	1394.15
KES253	22.467	4.719	67.002	22.971	19.422	253.15	1443.29
KES254	22.078	4.625	65.967	22.773	19.435	249.86	1408.30
KES255	15.771	2.325	36.170	13.981	9.503	133.24	1021.44
KES256	15.593	2.281	36.257	13.707	9.470	134.26	1003.52
KES257	15.980	2.338	36.831	14.322	9.608	133.86	1033.19
KES258	15.602	2.256	35.845	14.143	9.389	128.44	1017.40
KES259	15.830	2.322	36.572	14.451	9.485	130.09	1022.09
KES260	16.018	2.334	36.977	14.220	9.676	133.47	1025.92
KES261	15.533	2.280	35.433	14.451	9.184	128.75	1032.70
KES262	15.843	2.303	36.505	14.444	9.521	130.37	1038.71
KES263	15.925	2.303	36.824	14.732	9.632	134.68	1037.79
KES264	15.793	2.318	36.530	14.932	9.670	132.14	1033.75
KES265	15.971	2.303	36.654	14.392	9.468	134.41	1051.70
KES266	15.824	2.315	36.447	14.942	9.274	134.76	1033.21
KES267	16.010	2.317	36.677	14.522	9.423	129.95	1050.70
KES268	15.880	2.253	36.895	14.768	9.537	130.31	1039.14
KES269	15.684	2.277	36.214	15.171	9.393	129.33	1008.37
KES270	15.899	2.272	36.543	15.733	9.606	137.34	1049.33
KES271	15.546	2.233	35.427	14.803	9.224	134.14	1003.14
KES272	15.713	2.298	36.054	14.039	9.369	131.34	1019.06
KES273	15.737	2.276	35.963	15.594	9.567	135.50	1030.19
KES274	15.953	2.272	36.294	15.266	9.361	135.01	1050.92
KES275	15.884	2.302	36.562	15.425	9.529	132.17	1041.78
KES276	15.817	2.292	36.016	15.204	9.319	131.95	1021.74
KES277	15.853	2.325	36.689	12.638	9.466	140.58	1014.71
KES278	22.199	4.742	66.079	20.069	18.861	256.46	1418.18
KES279	22.503	4.777	66.752	19.948	19.216	253.06	1427.60
KES281	21.604	4.626	64.301	20.296	18.833	250.88	1406.61
KES282	21.138	4.554	62.953	20.478	18.153	249.90	1334.26
KES283	21.182	4.521	62.992	19.409	18.547	245.42	1375.95
KES284	20.599	4.432	61.154	19.384	17.970	243.68	1313.21
KES285	13.664	3.885	27.831	7.262	14.257	295.11	962.28
KES286	13.900	3.942	28.346	8.217	14.467	299.41	982.87
KES287	12.785	3.385	27.342	7.766	12.358	267.22	841.09
KES288	13.162	3.394	28.001	8.231	12.529	267.96	856.84
KES289	13.062	3.471	28.010	7.522	12.468	269.45	815.28
KES290	12.923	3.434	27.566	7.290	12.250	266.68	816.06
KES291	13.309	3.548	28.575	7.814	12.737	273.71	868.19
KES292	12.979	3.389	27.626	7.089	12.353	268.27	818.75
KES293	13.155	3.506	28.348	7.820	12.610	272.29	827.79
KES294	13.069	3.437	28.205	9.009	12.853	268.28	841.30
KES295	13.162	3.470	28.312	8.471	12.867	271.02	865.72
KES296	13.077	3.554	28.334	8.241	12.590	266.79	826.19
KES297	21.935	5.813	68.108	22.256	23.503	296.20	1844.35

Appendix 6 – continued. All concentrations are in parts per million (ppm).

Sample ID	Ta	Tb	Th	U	Yb	Zn	Zr
KES298	21.540	5.738	66.551	21.492	23.198	290.06	1804.10
KES299	21.947	5.842	68.403	21.916	23.188	293.37	1838.15
KES300	32.286	10.058	83.385	18.635	31.520	503.84	3073.72
KES301	30.622	9.526	78.543	19.074	29.801	468.07	2868.59
KES302	31.227	9.736	80.826	21.006	30.699	482.34	2954.73
KES303	31.163	9.756	80.543	20.579	30.932	479.58	2954.66
KES304	31.407	9.744	81.276	18.886	30.757	479.03	2932.87
KES305	31.251	9.806	81.318	21.081	31.065	487.63	2986.35
KES306	31.199	9.752	81.220	20.010	31.312	486.49	2962.88
KES307	30.976	9.606	79.865	21.748	30.817	474.69	2907.20
KES308	30.518	9.552	78.623	22.203	30.916	471.53	2843.30
KES309	31.038	9.670	80.415	21.478	30.826	475.26	2949.40
KES310	31.292	9.765	80.624	20.696	31.717	472.64	2937.31
KES311	33.038	10.056	87.753	16.178	38.372	554.66	3073.56
KES312	33.197	10.149	89.196	18.564	38.451	566.79	3140.98
KES313	32.957	9.938	87.414	18.119	38.464	554.32	3025.75
KES314	33.342	10.039	88.730	17.515	38.395	556.85	3105.69
KES315	33.431	10.058	89.358	19.002	37.905	568.01	3165.78
KES316	32.144	9.602	85.301	17.099	37.740	528.43	2978.97
KES317	31.764	9.575	84.287	16.737	36.987	525.38	2953.36
KES318	13.272	4.836	21.620	4.668	18.032	382.62	1071.82
KES319	13.780	5.091	23.442	3.833	18.495	378.37	1120.73
KES320	31.565	10.436	58.373	9.902	38.893	581.43	2374.54
KES321	22.773	7.575	44.098	8.385	28.707	454.60	1844.28
KES322	16.307	5.959	28.089	5.626	20.453	429.72	1293.63
KES323	19.663	6.448	36.454	7.581	24.665	388.31	1484.77
KES324	19.834	6.468	36.841	7.073	25.316	402.28	1479.78
KES325	19.679	6.349	35.771	6.331	24.076	387.10	1460.78
KES326	19.602	6.511	36.205	6.580	24.719	389.35	1465.98
KES327	19.810	6.366	36.138	6.520	24.158	388.69	1500.61
KES328	19.838	6.431	36.580	7.396	25.188	385.51	1497.07
KES329	19.944	6.448	36.819	6.489	25.245	392.02	1529.68
KES330	19.637	6.454	36.438	7.806	25.727	392.45	1515.33
KES331	19.756	6.411	36.570	7.716	25.598	393.54	1488.17
KES335	19.746	6.387	36.374	6.240	24.831	390.60	1508.16
KES336	19.620	6.392	36.331	6.945	24.791	384.84	1489.90
KES337	19.513	6.342	36.111	7.008	25.144	390.61	1494.35
KES338	19.410	6.310	35.616	8.142	24.693	382.33	1419.51
KES339	19.635	6.355	36.118	8.093	25.193	390.98	1489.64
KES340	19.798	6.503	36.919	6.795	25.746	396.55	1505.58
KES341	13.268	4.875	22.393	11.705	18.320	362.57	1059.31
KES342	17.479	6.136	37.125	7.924	23.131	408.26	1301.71
KES343	13.295	4.875	22.116	4.655	17.439	363.39	1045.12
KES344	13.428	4.800	22.579	4.349	17.757	367.42	1063.14
KES345	8.241	2.986	12.218	2.491	11.910	255.78	601.75

Appendix 6 – continued. All concentrations are in parts per million (ppm).

Sample ID	Ta	Tb	Th	U	Yb	Zn	Zr
KES346	8.224	3.062	11.856	6.576	11.796	249.17	621.77
KES347	22.936	6.872	59.085	14.296	28.066	394.87	2056.29
KES348	23.093	6.919	59.751	14.207	28.306	394.24	2094.73
KES349	23.221	6.967	60.100	13.431	28.836	407.73	2073.34
KES350	34.178	10.379	83.811	19.628	40.965	588.31	2855.14
KES351	34.080	10.359	83.550	19.962	41.228	586.59	2848.28
KES352	34.147	10.387	83.723	20.916	41.005	590.82	2836.32
KES353	33.892	10.340	82.656	19.208	40.904	565.84	2815.99
KES354	34.210	10.373	83.587	19.927	40.608	590.06	2861.44
KES355	33.920	10.317	82.780	20.748	40.197	582.25	2827.82
KES356	33.859	10.289	82.922	18.732	40.172	573.26	2811.84
KES357	34.225	10.350	83.549	20.781	40.658	580.21	2865.36
KES358	33.895	10.319	82.384	19.128	40.891	577.33	2819.89
KES359	33.367	10.097	81.402	19.530	40.622	570.17	2790.08
KES360	33.830	10.274	82.558	19.903	40.506	578.57	2812.84
KES361	33.904	10.319	82.701	18.645	40.739	569.68	2842.64
KES362	33.917	10.273	82.434	19.817	40.645	576.76	2834.13
KES363	33.883	10.333	83.122	19.194	40.679	582.41	2850.28
KES364	32.572	9.907	86.627	19.556	38.800	536.17	3100.54
KES365	31.721	9.526	83.779	19.862	37.805	513.49	2993.74
KES366	32.157	9.661	85.045	20.705	38.285	533.29	3045.42
KES367	32.122	9.685	84.618	19.210	37.799	525.32	3048.63
KES368	32.064	9.600	84.846	18.812	38.095	527.47	3056.94
KES369	32.615	9.912	87.091	19.618	38.945	538.77	3138.90
KES370	18.868	4.650	37.378	10.469	13.057	408.55	1612.92
KES371	18.882	4.638	37.182	9.584	13.076	409.47	1586.36
KES372	18.838	4.618	37.192	9.647	13.074	410.45	1583.05
KES373	18.661	4.530	36.808	9.590	12.987	401.57	1575.62
KES374	18.411	3.797	54.827	13.961	16.656	231.75	1160.76
KES375	18.452	3.842	55.161	13.636	16.697	228.53	1159.47
KES376	22.667	4.657	69.425	16.326	20.968	277.54	1487.40
KES377	22.893	4.692	68.168	16.523	20.499	274.69	1500.84
KES378	22.549	4.638	67.252	16.032	20.179	275.41	1456.54
KES379	22.090	4.565	65.872	23.510	20.931	270.92	1423.30
KES380	21.686	4.495	64.121	22.843	20.610	270.37	1392.83
KES381	21.902	4.509	64.941	23.047	20.668	271.57	1407.17
KES382	21.733	4.483	64.780	22.398	20.853	269.25	1386.72
KES383	21.901	4.505	64.969	22.491	20.919	265.03	1404.26
KES384	21.981	4.510	65.119	23.491	20.553	270.47	1397.74
KES385	21.954	4.493	64.810	23.243	20.891	268.61	1398.79
KES386	21.759	4.457	64.144	23.465	20.343	268.17	1378.65
KES387	21.479	4.425	63.885	23.543	21.200	261.10	1368.18
KES388	21.570	4.481	63.902	23.391	20.667	271.63	1373.26
KES389	21.791	4.483	64.749	23.312	20.636	270.28	1384.20
KES390	21.505	4.408	63.647	23.264	20.452	266.94	1375.40

Appendix 6 – continued. All concentrations are in parts per million (ppm).

Sample ID	Ta	Tb	Th	U	Yb	Zn	Zr
KES391	21.783	4.464	64.502	24.330	20.659	268.99	1389.23
KES392	21.999	4.592	65.267	24.559	21.028	274.54	1424.55
KES393	22.070	4.545	65.071	24.026	20.858	272.70	1399.59
KES394	21.438	4.755	63.725	24.557	22.404	278.22	1497.80
KES403	18.6984	4.8091	36.9758	10.375	12.662	408.80	1525.15
KES404	18.9480	4.8863	37.3595	9.895	12.960	409.44	1520.82
KES405	18.8737	4.9538	37.5761	9.280	13.050	414.17	1569.33
KES406	19.0287	4.8483	37.3830	9.279	12.966	413.88	1512.42
KES407	18.9580	4.8241	37.3435	9.186	13.079	420.63	1557.80
KES408	30.5571	6.5308	73.5349	15.819	25.532	473.35	1793.56
KES409	30.4043	6.4689	72.7759	14.470	24.896	462.97	1804.22
KES410	30.4700	6.4394	72.7818	14.784	25.106	473.27	1865.11
KES411	17.1074	4.5014	31.7168	5.830	16.849	329.80	1026.57
KES412	23.4231	5.5419	65.1304	13.680	21.924	380.95	1570.32
KES413	23.6847	5.7069	66.0873	14.729	22.170	381.64	1618.76
KES414	13.0658	3.5475	28.2627	5.951	13.457	277.62	831.72
KES415	13.0111	3.4938	28.1250	4.901	13.287	277.47	845.38
KES416	13.0394	3.4563	28.0091	5.601	13.468	271.48	814.16
KES417	13.3226	3.5484	28.5445	5.448	13.455	282.36	831.63
KES418	11.0051	3.5366	18.3181	3.788	12.855	230.83	884.41
KES419	12.6294	2.8882	25.6263	5.177	11.410	230.88	733.34
KES420	12.3558	2.8395	24.9100	5.001	10.777	226.32	736.40
KES421	12.4832	2.8739	25.0549	4.951	11.431	229.79	699.31
KES422	12.7203	2.9511	25.9499	5.368	11.415	237.51	742.90
KES423	12.6512	2.9134	25.6299	5.124	11.372	237.05	760.95
KES424	12.8330	4.0405	20.2812	5.668	16.438	251.81	1187.99
KES425	11.4666	3.6696	18.0070	4.513	14.529	232.15	1052.89
KES426	10.0833	3.2777	15.8362	3.828	12.910	207.28	922.36
KES427	12.4422	3.9487	19.6770	4.713	15.722	244.87	1119.19
KES428	12.1851	3.9112	19.3025	4.853	15.659	245.13	1128.06
KES429	12.5124	2.8587	25.2505	4.951	11.163	234.61	715.84
KES430	7.7707	1.9881	14.4559	3.478	5.888	143.87	601.03
KES431	5.5919	2.5009	11.8372	2.390	9.230	177.93	655.08
KES432	5.6446	2.5569	12.0490	2.699	9.287	179.05	625.76
KES433	6.9221	2.9082	13.8670	3.414	10.468	214.65	726.75
KES434	5.7180	2.5524	12.0568	2.555	9.389	179.99	664.77
KES435	5.6564	2.5498	12.1754	2.604	9.181	183.72	651.85
KES436	10.8734	3.4761	17.3976	2.307	12.020	230.14	847.68
KES437	8.2991	2.1110	15.6869	3.244	7.856	190.40	473.21
KES438	12.2593	2.8025	24.6844	5.297	10.991	226.64	722.96
KES439	13.5886	4.6369	24.2311	4.586	17.157	291.24	1198.14
KES440	13.7891	4.7886	24.5952	5.526	18.188	291.23	1224.65
KES441	13.9377	4.8021	24.4982	5.524	17.541	287.16	1242.32
KES442	14.4518	3.8135	22.2916	6.388	13.840	253.86	966.03
KES443	14.1689	3.7149	22.2344	5.224	13.849	247.33	974.86

Appendix 6 – continued. All concentrations are in parts per million (ppm).

Sample ID	Ta	Tb	Th	U	Yb	Zn	Zr
KES444	31.9521	7.4218	51.4894	11.620	24.794	509.00	2280.09
KES445	31.3272	7.3637	50.2538	11.349	24.443	491.43	2287.27
KES446	52.0942	11.7920	85.0438	18.957	37.924	667.11	3825.44
KES447	15.6869	4.2114	25.3297	5.003	15.978	332.07	1096.17
KES448	15.6193	4.2039	25.0959	5.877	16.123	333.92	1078.09
KES449	14.9088	3.5524	29.0341	5.740	12.614	270.52	953.64
KES450	14.7921	3.5618	28.5882	6.524	12.554	267.11	1009.66
KES451	14.8386	3.6122	28.8970	6.785	12.709	269.77	1025.96
KES452	15.2213	3.6240	29.5846	6.652	12.980	277.35	1011.58
KES453	15.2858	3.6429	30.0362	8.753	12.788	276.17	1060.26
KES454	15.2715	3.6437	29.8304	9.907	12.610	271.78	1056.56
KES455	14.9732	3.5987	29.3933	11.328	12.522	264.65	1051.81
KES456	15.2884	3.6011	29.9440	9.901	12.864	268.41	1068.75
KES457	14.9262	3.6880	28.7628	11.027	12.799	284.63	1067.93
KES458	15.0130	3.7183	28.8994	10.979	12.471	288.51	1074.79
KES459	20.4488	2.5622	32.0187	14.742	11.456	223.17	1223.73
KES460	18.3899	2.4081	28.3265	13.275	10.224	211.26	1075.56
KES461	12.7344	2.8528	25.7944	8.515	10.795	260.73	811.65
KES462	19.5437	2.4576	30.5184	13.498	10.615	216.58	1157.28
KES463	17.2947	2.7668	26.5172	12.120	11.777	223.83	1087.92
KES464	17.3617	2.7838	26.6021	11.385	11.733	223.00	1079.44
KES465	16.9720	2.6915	26.0407	12.273	11.738	219.82	1057.36
KES466	18.0331	2.8725	27.8690	12.480	12.123	228.63	1105.06
KES467	33.4856	10.5001	89.2249	30.097	38.646	557.67	3259.10
KES468	33.9262	10.6576	90.6396	31.513	39.560	562.23	3272.39
KES469	33.5991	10.5507	89.7581	28.830	39.251	563.95	3249.68
KES470	33.5406	10.4743	89.0426	27.957	38.794	558.85	3243.18
KES471	19.1968	6.9301	33.2873	14.379	25.262	437.83	1511.53
KES472	19.4300	7.0734	33.8885	14.674	25.044	439.30	1523.04
KES473	18.8389	6.8508	32.6907	13.692	24.767	429.27	1471.49
KES474	19.2682	7.0055	33.4866	11.968	24.874	431.74	1474.78
KES475	34.5761	10.8432	91.8300	33.606	40.533	586.13	3345.93
KES476	33.9473	10.7312	90.2319	32.318	39.218	569.62	3294.62
KES477	19.0227	6.9006	33.1809	13.518	24.870	431.02	1475.18
KES478	19.0305	6.9214	32.9596	14.090	24.429	432.91	1475.08
KES479	27.8277	8.6740	73.6901	26.611	31.993	460.74	2697.21
KES480	18.2562	6.7306	32.7622	13.269	25.699	414.71	1409.48
KES481	17.5128	6.2818	37.0268	14.838	22.579	405.26	1353.44
KES482	17.6275	6.2780	37.2931	15.264	23.253	405.02	1351.30
KES483	31.5741	9.9270	83.9185	29.259	36.878	525.00	3070.40
KES484	32.0131	10.0249	84.9341	29.328	37.336	538.90	3058.71
KES485	27.1371	8.5562	72.1399	26.565	33.179	479.63	2636.71
KES486	26.9037	8.4799	71.3702	27.824	31.016	469.69	2599.88
KES487	25.4494	7.9996	67.8920	25.761	30.316	440.53	2461.66
KES488	25.1949	7.8689	66.6994	25.775	31.562	432.95	2431.95

Appendix 6 – continued. All concentrations are in parts per million (ppm).

Sample ID	Ta	Tb	Th	U	Yb	Zn	Zr
KES489	25.3886	8.0584	67.0920	25.146	30.120	449.83	2468.07
KES490	26.1316	8.3212	69.0131	26.619	31.030	469.60	2555.18
KES491	25.8937	8.2130	68.0719	26.447	30.229	451.68	2501.19
KES492	25.5945	8.2047	67.6049	25.184	31.032	458.30	2482.05
KES493	25.7404	8.1446	67.8549	26.071	31.576	451.04	2498.88
KES494	25.8512	8.1788	67.6767	25.935	30.194	456.29	2472.39
KES495	25.6351	8.0126	68.3588	26.774	30.651	445.63	2486.46
KES496	14.6327	4.9248	39.0874	15.507	16.260	320.49	1451.74
KES497	15.1105	5.1436	40.8512	16.558	17.119	332.03	1465.95
KES498	15.0265	5.1718	40.2508	15.464	17.103	336.66	1460.82
KES499	14.5524	4.8570	38.8110	15.207	17.196	325.84	1410.93
KES500	14.3165	4.8720	38.4643	13.725	17.257	318.44	1406.70
KES501	14.9112	5.0999	40.0343	15.788	16.603	335.03	1466.53
KES502	14.4998	4.8862	38.7148	13.582	15.703	323.69	1388.65
KES503	16.9261	2.1264	37.8922	14.720	7.392	178.28	1118.33
KES504	16.8651	2.1202	37.6090	13.808	7.329	176.38	1093.95
KES505	16.9863	2.1825	38.2973	14.154	7.623	178.29	1122.62
KES506	17.0636	2.1561	38.4002	14.790	7.490	181.08	1122.77
KES507	17.0939	2.1675	38.3852	14.676	7.560	176.79	1138.64
KES508	17.0532	2.1523	38.4218	14.692	7.554	179.14	1127.77
KES509	13.7880	3.0769	25.4609	10.252	11.904	242.26	946.24
KES510	14.2432	3.2129	26.4590	11.037	12.022	252.18	953.88
KES511	13.7991	3.0634	25.4913	10.401	11.800	244.62	928.03
KES512	13.5129	2.9906	24.9500	10.230	11.758	236.30	901.45
KES513	13.0226	2.9157	23.8222	8.986	11.327	227.33	858.56
KES514	12.5167	2.2871	26.5513	11.782	6.892	207.60	940.05
KES515	12.5917	2.3378	26.6433	10.942	7.001	211.24	913.69
KES516	7.9307	2.4290	16.2118	7.183	9.909	151.46	731.00
KES517	8.0900	2.4522	16.5633	7.154	9.725	156.10	769.59
KES518	8.1271	2.4376	16.6350	7.308	10.101	152.88	742.74
KES519	7.6571	2.3641	15.5750	6.551	9.599	150.42	706.88
KES520	7.8731	2.3895	16.0689	6.991	9.540	150.96	743.26
KES521	7.6946	2.3446	15.6697	6.803	9.581	150.57	742.42
KES522	7.9215	2.4113	16.1880	6.664	9.757	150.04	743.56
KES523	8.1047	2.4159	16.5592	7.795	9.995	149.48	773.45
KES524	7.9134	2.3657	16.1576	7.925	9.638	152.53	735.93
KES525	7.9728	2.4185	16.2512	6.915	9.847	156.91	756.99
KES526	7.0457	2.2014	13.8876	6.055	8.941	152.63	662.00
KES527	8.3865	1.8372	14.5878	7.427	5.558	183.97	583.75
KES528	8.3574	1.8951	14.6689	6.891	5.485	182.30	591.95
KES529	8.2102	1.8421	14.4299	6.618	5.665	175.63	573.73
KES530	7.9375	1.7758	14.0328	6.803	5.239	174.87	561.14
KES531	7.8446	1.7780	13.7940	6.235	5.283	171.51	542.89
KES532	7.9364	1.7679	13.8743	6.689	5.322	174.22	568.52
KES533	7.9706	1.7908	13.9677	7.015	5.387	175.00	579.31

Appendix 6 – continued. All concentrations are in parts per million (ppm).

Sample ID	Ta	Tb	Th	U	Yb	Zn	Zr
KES534	22.5647	5.1553	68.2553	28.082	21.777	309.33	1571.82
KES535	22.3827	5.0858	68.0606	27.401	21.634	309.96	1563.87
KES536	18.9083	4.8288	37.6299	19.020	13.168	432.97	1575.45
KES537	18.7959	4.8041	37.2496	19.408	12.829	427.45	1558.47
KES538	18.7759	4.7718	36.9414	19.009	12.770	429.08	1556.03
KES539	18.8399	4.7714	37.3189	19.604	12.936	435.20	1565.90
KES540	16.9828	4.3436	31.5709	14.657	17.000	345.74	989.14
KES541	11.0307	3.4767	17.5919	9.879	13.911	229.32	1029.82
KES542	12.3366	3.9216	19.5630	10.657	15.647	262.00	1149.18

Appendix 7 – Results of concentration calculations for the standards analyzed for both the standard INAA procedure and the new ENAA procedure for titanium. NIST SRM 278 (obsidian) was used as a primary standard.

A. Standard INAA procedure (Ti-50(n,γ)Ti-51)

Sample ID	Mass (mg)	Counts (320 keV)	Calculated Concentration	Average	Standard Deviation
AGV-1a	200.61	7842	6680	6790	290
AGV-1b	200.15	8370	7120		
AGV-1c	200.75	7724	6560		
JA-1a	200.03	6015	6090	6210	270
JA-1b	200.37	6471	6510		
JA-1c	200.70	5983	6010		
JB-2a	200.47	7487	718	6390	803.
JB-2b	200.37	6703	643		
JB-2c	200.64	5818	5570		
JR-1a	200.80	--	--	610.	539.
JR-1b	200.66	1135	1030		
JR-1c	200.40	889	804.		
SRM 1633 381	100.29	7156	9210	10400	1330
SRM 1633 382	99.99	7078	9140		
SRM 1633 383	99.43	7026	9110		
SRM 1633 393	99.77	9137	11900		
SRM 1633 394	99.73	8484	11100		
SRM 1633 395	99.98	8926	11600		

B. Epithermal INAA procedure (Ti-47(n,γ)Sc-47)

Sample ID	Mass (mg)	Counts (159 keV)	Calculated Concentration	Average	Standard Deviation
FA7257	99.56	28067	7960	7970	23
FA7258	99.21	22443	7990		
AGV-1a	200.26	45165	6350	6460	94
AGV-1b	201.62	42209	6520		
AGV-1c	201.58	38098	6510		
JA-1a	200.51	37117	5160	5240	71
JA-1b	200.91	34486	5290		
JA-1c	200.58	30917	5260		
JB-2a	199.79	52295	7380	7480	118
JB-2b	199.90	48686	7610		
JB-2c	200.45	43233	7460		
JR-1a	200.22	4905	705.	678.	57
JR-1b	200.80	3873	613.		
JR-1c	200.55	4088	717.		

Appendix 8 – Results of concentration calculations for the standards analyzed for both the standard INAA procedure and the new ENAA procedure for barium. NIST SRM 278 (obsidian) was used as a primary standard.

A. Standard INAA procedure (Ba-138(n,γ)Ba-139)

Sample ID	Mass (mg)	Counts (165 keV)	Calculated Concentration	Average	Standard Deviation
AGV-1a	200.61	14166	1060	1020	38
AGV-1b	200.15	13544	1010		
AGV-1c	200.75	13186	981		
JA-1a	200.03	2804	249	226	31
JA-1b	200.37	2165	191		
JA-1c	200.70	2703	238		
JB-2a	200.47	1870	157	129	31
JB-2b	200.37	1603	135		
JB-2c	200.64	1136	95.2		
JR-1a	200.80	--	--	--	--
JR-1b	200.66	--	--		
JR-1c	200.40	--	--		
FA 381	100.29	11015	1240	1360	136
FA 382	99.99	11416	1290		
FA 383	99.43	10446	1190		
FA 393	99.77	13221	1511		
FA 394	99.73	13018	1490		
FA 395	99.98	12520	1430		

B. Epithermal INAA procedure (Ba-130(n,γ)Ba-131)

Sample ID	Mass (mg)	Counts (496 keV)	Calculated Concentration	Average	Standard Deviation
FA7257	99.56	18441	1290	1280	19
FA7258	99.21	16968	1270		
AGV-1a	200.26	34511	1190	1190	8
AGV-1b	201.62	33647	1190		
AGV-1c	201.58	33175	1200		
JA-1a	200.51	8561	291	294	2
JA-1b	200.91	8473	296		
JA-1c	200.58	8154	294		
JB-2a	199.79	6151	212	216	6
JB-2b	199.90	6289	223		
JB-2c	200.45	5890	214		
JR-1a	200.22	1552	54.2	53.8	0.4
JR-1b	200.80	1502	53.7		
JR-1c	200.55	1453	53.5		

Appendix 9 – Results of concentration calculations for the standards analyzed for the new ENAA procedure for arsenic after both a 7-day and 5-day decay. NIST SRM 278 (obsidian) was used as a primary standard.

A. ENAA procedure, 7-day decay

Sample ID	Mass (mg)	Counts (496 keV)	Calculated Concentration	Average	Standard Deviation
FA7257	99.56	61412	152	150	2
FA7258	99.21	29754	149		
AGV-1a	200.26	873	1.09	1.22	0.28
AGV-1b	201.62	609	1.03		
AGV-1c	201.58	664	1.54		
JA-1a	200.51	2501	3.11	3.09	0.17
JA-1b	200.91	1713	2.91		
JA-1c	200.58	1397	3.26		
JB-2a	199.79	2648	3.38	3.63	0.37
JB-2b	199.90	1985	3.47		
JB-2c	200.45	1701	4.06		
JR-1a	200.22	11949	15.7	15.9	0.4
JR-1b	200.80	8891	15.9		
JR-1c	200.55	6677	16.3		

B. ENAA procedure, 5-day decay

Sample ID	Mass (mg)	Counts (496 keV)	Calculated Concentration	Average	Standard Deviation
FA 1633 A	200.75	294126	141	142	2
FA 1633 B	201.50	218575	141		
FA 1633 C	201.5	161765	143		
JR-1d	199.36	34167	16.3	16.4	0.2
JR-1e	199.72	25461	16.3		
JR-1f	200.30	19044	16.7		

VITA

Magen Elizabeth Coleman was born to Charles and Patricia Coleman on October 25, 1984, in Bergenfield, New Jersey. Interested in ancient history, science, and art from an early age, she attended the Academy of the Holy Angels in Demarest, NJ for high school, where she was able to pursue those interests, especially in taking AP courses in Latin and Chemistry. After swearing off chemistry, she attended the University of Mary Washington, in Fredericksbug, VA, with the goal of majoring in Classics/Latin, and was re-inspired in science after taking analytical chemistry. Under the guidance of her advisors, Dr. Liane Houghtalin of the Classics Department and Dr. Raymond Scott of the Chemistry Department, she graduated in May 2006 with a double major in Chemistry and Classics. Not quite willing to give up either of her two majors, she discovered the field of archaeometry through Dr. Michael Glascock of the University of Missouri Research Reactor. In August 2006, she began the journey toward a Ph.D. in chemistry with Dr. J. David Robertson as her advisor. After receiving her doctorate in May 2010, she will be headed to Los Alamos National Laboratory, in Los Alamos, NM for a postdoctoral position under Dr. Lav Tandon.